SCHOOL OF MECHANICAL, INDUSTRIAL & AERONAUTICAL ENGINEERING

RESEARCH PROJECT

Masters project report

Project title:	**The Effect of Cylinder Pressure on Spray Penetration; in Common Rail Diesel Injection**
Project supervisor:	**Prof. D. Cipolat**
Date:	**May 2018**
Student:	**Andran Naicker**
Student number:	**317465**

A dissertation submitted to the Faculty of Engineering and the Built Environment, University of the Witwatersrand, Johannesburg, in fulfilment of the requirements for the degree of Master of Science in Engineering.

DECLARATION

University of the Witwatersrand, Johannesburg
School of Mechanical, Industrial and Aeronautical Engineering

Name: Andran Naicker	Student no: 317465
Course no: MECN 8000	Course Name: MSc (Engineering)
Submission Date: May 2018	Project Title: The effect of cylinder pressure on spray penetration; in common rail diesel injection.

I hereby declare the following:

- I am aware that plagiarism (the use of someone else's work without their permission and/or without acknowledging the original source) is wrong;
- I confirm that the work submitted herewith for assessment in the above course is my own unaided work except where the I have explicitly indicated otherwise;
- This task has not been submitted before, either individually or jointly, for any course requirement, examination or degree at this or any other tertiary education institution;
- I have followed the required conventions in referencing the thoughts and ideas of others;
- I understand that the University of the Witwatersrand may take disciplinary action against me if it can be shown that this task is not my own unaided work or that I have failed to acknowledge the sources of the ideas or words in my writing in this task.

Signature: ____________________________ Date: 16/05/2018

ACKNOWLEDGEMENTS

This dissertation is dedicated to Ayah, the personification of strength. We love you.

I would like to sincerely thank the following people for their support and assistance during the process of completing this research:

- Prof. D. Cipolat, supervisor for this project for his assistance during consultations.
- David Valentim for his advice regarding the setup of the equipment.

ABSTRACT

The aim of this research was to determine the effect of injection pressure, cylinder pressure and cylinder gas density on the spray penetration of diesel with a common rail injection system. A spray chamber capable of holding 20 bar was retrofitted to the Inov8 Test Stand in the Barloworld laboratories at The University of the Witwatersrand, Johannesburg. The data capturing system of the test stand was unmatched in quality and accuracy and the modification allowed the effects of cylinder gas pressure and density to be tested using the MIE-Scattering technique. Tests were conducted with a 1-hole injector with various injection and cylinder gas pressures. To assess the effects of injection pressure, the cylinder pressure was kept constant at 5 bar with injection pressures ranging from 700 bar to 780 bar. To investigate the effect of cylinder pressure, the injection pressure was kept constant at 780 bar and the cylinder pressure was varied between atmospheric pressure and 20 bar. Tests to determine if either the injection pressure or cylinder pressure have a greater effect on the spray were conducted by maintaining a constant 755 bar pressure difference across the nozzle. This was done by varying both the injection pressure (between 755 bar and 775 bar) and the cylinder pressure (between atmospheric pressure and 20 bar). All the experiments were repeated with nitrogen and then carbon dioxide in the spray chamber. The Akribis section of the test stand was used for flow measurements to verify the spray analysis results where necessary. The results were compared to models developed by Hiroyasu and Dent to determine their accuracy. The tests showed that the spray penetration increased with increasing injection pressure and decreased with increasing cylinder pressure. In all cases, changes in pressure had a greater impact on the spray penetration later in the injection, after the spray had broken up. The earlier phase of the injection was mostly dependent on the pressure difference across the nozzle. For the pressure ranges used in this study, changes in the cylinder pressure had a greater effect on the spray penetration than changes in injection pressure. The changes were attributed to the changes in gas density that occurs with pressure changes and had a diminishing effect as the pressure increased. It was found that the injection pressure was more important during the initial phases of the injection (before break up) and the cylinder pressure was more important later on in the injection. Carbon dioxide gave smaller spray penetrations than nitrogen at equivalent pressures due to its larger molecular mass resulting in a greater gas density. Spray penetration decreased at a decreasing rate with increasing cylinder gas density.

TABLE OF CONTENTS

DECLARATION i

ACKNOWLEDGEMENTS ii

ABSTRACT iii

TABLE OF CONTENTS iv

LIST OF FIGURES viii

LIST OF TABLES xviii

NOMENCLATURE xix

LIST OF ABBREVIATIONS xx

1. INTRODUCTION 1

1.1. Background 1

1.1.1. Diesel engines 1

1.1.2. Fuel injection 3

1.2. Literature Review 3

1.2.1. Types of fuel injection 3

1.2.2. Common rail fuel injection 4

1.2.3. Fuel injectors 8

1.2.4. Injection strategies 10

1.2.5. New, used and reconditioned fuel injectors 10

1.2.6. Spray structure 11

1.2.7. Atomisation 13

1.2.8. Break-up length 13

1.2.9. Cone angle 14

1.2.10. Spray penetration 15

1.2.11. Flow rate 17

1.2.12. Previous work 18

1.3. Motivation 26

1.4. Objectives 27
2. APPARATUS 28
2.1. Test Stand 29
2.1.1. Spray analysis system 37
2.1.2. Flow measurement system 40
2.2. Power enclosure 42
2.3. Control Enclosure 44
2.4. Fuel Injector 45
2.5. Pressurized Spray Chamber 47
2.5.1. Spray chamber 47
2.5.2. Spray chamber set-up 49
2.5.3. Spray chamber design 51
2.6. Experimental Facility Set-up 53
2.7. Experimental Facility Risk Analysis 55
3. METHODOLOGY 58
3.1. Experimental Planning 58
3.2. Experimental Procedure 59
3.3. Start up 60
3.3.1. Procedure 60
3.3.2. Precautions 61
3.4. Stopping 61
3.4.1. Procedure 62
3.4.2. Precautions 62
3.5. Injector Spray Analysis 62
3.4.1. Procedure 62
3.4.2. Precautions 64
3.6. Image Processing 65

3.7. Geometry Analysis 66
3.8. Flow Measurement 67
3.8.1. Procedure 68
3.8.2. Precautions 69
3.9. Connecting an Injector 70
3.9.1. Akribis procedure 70
3.9.2. Spray analysis procedure 71
3.9.3. Precautions 72
4. OBSERVATIONS 73
4.1. Spray Analysis 73
4.2. Flow Measurement 76
5. DATA PROCESSING 78
5.1. Spray Analysis 78
5.2. Flow Measurement 87
6. RESULTS AND DISCUSSION 88
6.1. Injection Pressure 89
6.2. Cylinder Pressure 110
6.3. Pressure Difference 119
6.4. Nitrogen vs. Carbon Dioxide 123
7. CONCLUSIONS 136
8. RECOMMENDATIONS 141
BIBLIOGRAPHY 142
REFERENCES 143
APPENDIX A – DATA CD 148
APPENDIX B – EXPORTING AKRIBIS DATA 149
APPENDIX C – DATA COLLECTION CODES 151
APPENDIX D – RESULTS 158

Injection Pressure 158
Cylinder Pressure 165
Pressure Difference 171
Nitrogen Compared to Carbon Dioxide 173
APPENDIX E – SPRAY CHAMBER DESIGN 186

LIST OF FIGURES

Figure 1: Four Stroke Compression Ignition Engine [22] 2
Figure 2: Pressure Variation in Combustion Chamber [22] 3
Figure 3: Common rail injection system [10] 5
Figure 4: Radial piston pump [10] 6
Figure 5: Common rail [9] 7
Figure 6: Fuel Injector [6] 8
Figure 7: Injected fuel jet [2] 12
Figure 8: Variation of cone angle with injection pressure [23] 15
Figure 9: Test apparatus [25] 19
Figure 10: Spray penetration results vs. Hiroyasu [25] 20
Figure 11: Delacourt et al. vs Hiroyasu and Arai, spray penetration [26] 21
Figure 12: Spray tip velocity vs. spray penetration [26] 22
Figure 13: Valentim diesel spray penetration [30] 24
Figure 14: Karimi experimental apparatus set-up [23] 25
Figure 15: Karimi observations [23] 26
Figure 16: Lab layout 29
Figure 17: Spray pattern analysis and flow measurement test stand 29
Figure 18: Air and Nitrogen Panel Assembly [15] 31
Figure 19: Supply connections 32
Figure 20: Cooling fluid and test fluid tanks 36
Figure 21: Test stand controls 37
Figure 22: Front View of Spray Analysis Section [15] 38
Figure 23: Side View of Spray Analysis Section [15] 38
Figure 24: Schlieren imaging apparatus [29] 40
Figure 25: Expo Purge Control System 41
Figure 26: Akribis unit [16] 42
Figure 27: Power enclosure control panel [15] 43
Figure 28: Control enclosure 45
Figure 29: Fuel Injector 45
Figure 30: Valentim spray chamber 48
Figure 31: Injector mounting 48

Figure 32: Injector location [30] 49
Figure 33: Table extension..50
Figure 34: Camera bracket 50
Figure 35: Spray chamber 52
Figure 36: Spray chamber with connections...52
Figure 37: Experimental facility set-up 54
Figure 38: Lab danger zones..56
Figure 39: Test stand status..61
Figure 40: Spray Analysis Computer Power Button..64
Figure 41: Set pump speed...68
Figure 42: Injector firing and pressure control 68
Figure 43: Akribis PC 69
Figure 44: Akribis Injector Connections..70
Figure 45: Flow Analysis Injector Connections 71
Figure 46: 720 bar injection pressure. 5 bar chamber pressure using nitrogen. 0.35ms – 0.4ms 73
Figure 47: 720 bar injection pressure. 5 bar chamber pressure using nitrogen. 0.45ms – 0.5ms 73
Figure 48: 720 bar injection pressure. 5 bar chamber pressure using nitrogen. 0.55ms – 0.6ms 74
Figure 49: 720 bar injection pressure. 5 bar chamber pressure using nitrogen. 0.65ms – 0.7ms 74
Figure 50: 720 bar injection pressure. 5 bar chamber pressure using nitrogen. 0.75ms – 0.8ms 74
Figure 51: 720 bar injection pressure. 5 bar chamber pressure using nitrogen. 0.85ms – 0.9ms 75
Figure 52: 720 bar injection pressure. 5 bar chamber pressure using nitrogen. 0.95ms – 1.0ms 75
Figure 53: 720 bar injection pressure. 5 bar chamber pressure using nitrogen. 1.05ms – 1.10ms 75
Figure 54: 720 bar injection pressure. 5 bar chamber pressure using nitrogen. 1.15ms..........76
Figure 55: 0.35ms to 0.4ms averaged and background removed. 720 bar injection pressure. 5 bar cylinder pressure using nitrogen. 78

Figure 56: 0.45ms to 0.5ms averaged and background removed. 720 bar injection pressure. 5 bar cylinder pressure using nitrogen. 79
Figure 57: 0.55ms to 0.6ms averaged and background removed. 720 bar injection pressure. 5 bar cylinder pressure using nitrogen. 79
Figure 58: 0.65ms to 0.7ms averaged and background removed. 720 bar injection pressure. 5 bar cylinder pressure using nitrogen. 79
Figure 59: 0.75ms to 0.8ms averaged and background removed. 720 bar injection pressure. 5 bar cylinder pressure using nitrogen. 80
Figure 60: 0.85ms to 0.9ms averaged and background removed. 720 bar injection pressure. 5 bar cylinder pressure using nitrogen. 80
Figure 61: 0.95ms to 1ms averaged and background removed. 720 bar injection pressure. 5 bar cylinder pressure using nitrogen. 80
Figure 62: 1.05ms to 1.1ms averaged and background removed. 720 bar injection pressure. 5 bar cylinder pressure using nitrogen. 81
Figure 63: 1.15ms averaged and background removed. 720 bar injection pressure. 5 bar cylinder pressure using nitrogen. 81
Figure 64: Processed Average Picture 82
Figure 65: Sheet/front lighting processed image 83
Figure 66: Manual Processing 84
Figure 67: Spray penetration vs time. 5 bar cylinder pressure. 700 – 780 bar injection pressure using nitrogen 90
Figure 68: Effect of injection pressure on spray penetration at different stages of injection ..91
Figure 69: Spray penetration test results compared to theory. 760 bar injection pressure. 5 bar cylinder pressure using nitrogen 93
Figure 70: Valentim spray penetration area of interest......93
Figure 71: Mean tip velocity. 700 – 780 bar injection pressure. 5 bar cylinder pressure using nitrogen 94
Figure 72: Fishbone structure. 720 bar injection pressure. 5 bar cylinder pressure using nitrogen. 1ms after signal sent 95
Figure 73: Mean tip velocity compared to theory. 700 bar injection pressure. 5 bar cylinder pressure using nitrogen. 97
Figure 74: Mean tip acceleration 0.35ms to 0.55ms. 700 – 780 bar injection pressure. 5 bar cylinder pressure using nitrogen 97

Figure 75: Average mean tip acceleration. 700 – 780 bar injection pressure. 5 bar cylinder pressure using nitrogen. ...98
Figure 76: Percentage difference between theoretical and actual results. 760 bar injection pressure. 5 bar cylinder pressure using nitrogen. ...99
Figure 77: Atomized test fluid at 0.6ms and 1.15ms ...100
Figure 78: Spray penetration vs time. 5 bar cylinder pressure. 770 bar to 780 bar injection pressure using nitrogen. 0.02ms time step ...101
Figure 79: Time at 0.5mm penetration. 700 – 780 bar injection pressure. 5 bar cylinder pressure using nitrogen ...102
Figure 80: Spray penetration compared to theoretical results. 720 bar injection pressure. 5 bar cylinder pressure using nitrogen. 0.02ms time step. ...103
Figure 81: Cone angle vs time. 5 bar cylinder pressure. 700 – 780 bar injection pressure using nitrogen ...105
Figure 82: Cone angle test results compared to theory. 740 bar injection pressure. 5 bar cylinder pressure using nitrogen ...105
Figure 83: Injection delivery, rate and firing pulse vs time. 700 bar injection pressure. 5 bar cylinder pressure using nitrogen ...106
Figure 84: Firing pulse vs time. 700 – 780 bar injection pressure. 5 bar cylinder pressure using nitrogen. ...107
Figure 85: Injection rate vs time. 700 – 780 bar injection pressure. 5 bar cylinder pressure using nitrogen. ...108
Figure 86: Time to 1mm^3/s rate vs injection pressure. 5 bar cylinder pressure using nitrogen ...108
Figure 87: Injection delivery vs time. 700 – 780 bar injection pressure. 5 bar cylinder pressure using nitrogen ...109
Figure 88: Spray penetration vs time. 780 bar injection pressure. 0 – 20 bar cylinder pressure using nitrogen. ...110
Figure 89: Average spray penetration vs cylinder pressure. 780 bar injection pressure. 5 bar to 20 bar cylinder pressure using nitrogen. ...111
Figure 90: Comparison of spray with 5 bar (left) and 20 bar (right) cylinder pressure at 1ms. ...112
Figure 91 Percentage difference between theoretical Dent and Hiroyasu spray penetration; and test results. 780 bar injection pressure. 15 bar cylinder pressure using nitrogen. ...113

Figure 92: Cone angle vs time. 750 bar injection pressure. 0 – 20 bar cylinder pressure using nitrogen 115
Figure 93: Average cone angle compared to theoretical cone angle. 780 bar injection pressure. Atmospheric – 20 bar cylinder pressure using nitrogen 115
Figure 94: Firing pulse vs time. 780 bar injection pressure. Atmospheric - 20 bar cylinder pressure using nitrogen 116
Figure 95: Injection rate vs time. 780 bar injection pressure. Atmospheric – 20 bar cylinder pressure using nitrogen 117
Figure 96: Average mean tip velocity vs cylinder pressure. 780 bar injection pressure. Atmospheric – 20 bar cylinder pressure using nitrogen 118
Figure 97: Duration of hesitation vs cylinder pressure. 780 bar injection pressure. Atmospheric – 20 bar cylinder pressure using nitrogen 118
Figure 98: Time at end of injection vs cylinder pressure. 780 bar injection pressure. Atmospheric – 20 bar cylinder pressure using nitrogen 119
Figure 99: Spray penetration vs. time. 755 – 775 bar injection pressure. 0 – 20 bar cylinder pressure using nitrogen. 120
Figure 100: Spray penetration test results compared to theory. 760 bar injection pressure. 5 bar cylinder pressure using nitrogen 121
Figure 101: Cone angle vs. time. 755 – 775 bar injection pressure. 0 – 20 bar cylinder pressure using nitrogen. 122
Figure 102: Spray penetration comparison. 755 bar injection pressure atmospheric cylinder pressure and 760 bar injection pressure 5 bar cylinder pressure using nitrogen 123
Figure 103: Spray penetration vs time. 5 bar Cylinder pressure. 700 – 780 bar injection pressure using carbon dioxide....124
Figure 104: Spray penetration. Nitrogen compared to carbon dioxide. 760 bar injection pressure. 5 bar cylinder pressure....125
Figure 105: Percentage difference between nitrogen and carbon dioxide spray penetration. Average 0.35ms to 0.75ms....126
Figure 106: Cone angle vs time. 7 bar Cylinder pressure. 700 – 780 bar injection pressure using carbon dioxide 127
Figure 107: Spray penetration vs time. 780 bar injection pressure. Atmospheric – 20 bar cylinder pressure using carbon dioxide....128
Figure 108: Spray penetration. Nitrogen compared to carbon dioxide. 780 bar injection pressure. 10 bar nitrogen 5 bar carbon dioxide cylinder pressure. 129

Figure 109: Percentage difference between nitrogen and carbon dioxide spray penetration. Average 130
Figure 110: Spray penetration vs time. 780 bar injection pressure. 15 bar nitrogen. 10 bar carbon dioxide 131
Figure 111: Average spray penetration vs. gas density. 780 bar injection pressure. Atmospheric – 20 bar cylinder pressure. Nitrogen and carbon dioxide 131
Figure 112: Cone angle vs time. 780 bar injection pressure. Atmospheric – 20 bar cylinder pressure using carbon dioxide 132
Figure 113: Average cone angle vs cylinder pressure. 780 bar injection pressure. Atmospheric – 20 bar cylinder pressure. Nitrogen and carbon dioxide. 133
Figure 114: Spray penetration vs. time. 755- 775 bar injection pressure. Atmospheric – 20 bar cylinder pressure using carbon dioxide 133
Figure 115: Average spray penetration vs cylinder pressure. Nitrogen and Carbon dioxide. 755 – 775 bar injection pressure. Atmospheric – 20 bar cylinder pressure 135
Figure 116: Test Scope 149
Figure 117: Export data 150
Figure 118: Export wave forms 150
Figure 119: Spray penetration test results compared to theory. 700 bar injection pressure. 5 bar cylinder pressure using nitrogen 159
Figure 120: Spray penetration test results vs theory. 720 bar injection pressure. 5 bar cylinder pressure using nitrogen 159
Figure 121: Spray penetration test results compared to theory. 740 bar injection pressure. 5 bar cylinder pressure using nitrogen 159
Figure 122: Spray penetration test results compared to theory. 780 bar injection pressure. 5 bar cylinder pressure using nitrogen 160
Figure 123: Percentage difference between Dent and actual results. 700 - 780 bar injection pressure. 5 bar cylinder pressure using nitrogen. 160
Figure 124: Percentage difference between Hiroyasu and actual results. 700 - 780 bar injection pressure. 5 bar cylinder pressure using nitrogen. 161
Figure 125: Mean tip acceleration. 700-780 bar injection pressure. 5 bar cylinder pressure using nitrogen 161
Figure 126: Cone angle test results compared to theory. 700 bar injection pressure. 5 bar cylinder pressure using nitrogen 162

Figure 127: Cone angle test results compared to theory. 720 bar injection pressure. 5 bar cylinder pressure using nitrogen 162
Figure 128: Cone angle test results compared to theory. 760 bar injection pressure. 5 bar cylinder pressure using nitrogen 162
Figure 129: Cone angle test results compared to theory. 780 bar injection pressure. 5 bar cylinder pressure using nitrogen 163
Figure 130: Spray penetration test results compared to theory. 780 bar injection pressure. Atmospheric cylinder pressure using nitrogen 166
Figure 131: Spray penetration test results compared to theory. 780 bar injection pressure. 5 bar cylinder pressure using nitrogen 166
Figure 132: Spray penetration test results compared to theory. 780 bar injection pressure. 10 bar cylinder pressure using nitrogen 166
Figure 133: Spray penetration test results compared to theory. 780 bar injection pressure. 15 bar cylinder pressure using nitrogen 167
Figure 134: Spray penetration test results compared to theory. 780 bar injection pressure. 20 bar cylinder pressure using nitrogen 167
Figure 135: Percentage difference between theoretical Dent and actual results. 780 bar injection pressure. Atmospheric - 20 bar cylinder pressure using nitrogen...........................167
Figure 136 Percentage difference between theoretical Hiroyasu and actual results. 780 bar injection pressure. Atmospheric - 20 bar cylinder pressure using nitrogen...........................168
Figure 137: Cone angle test results compared to theory. 780 bar injection pressure. Atmospheric cylinder pressure using nitrogen 168
Figure 138: Cone angle test results compared to theory. 780 bar injection pressure. 5 bar cylinder pressure using nitrogen 169
Figure 139: Cone angle test results compared to theory. 780 bar injection pressure. 10 bar cylinder pressure using nitrogen 169
Figure 140: Cone angle test results compared to theory. 780 bar injection pressure. 15 bar cylinder pressure using nitrogen 169
Figure 141: Cone angle test results compared to theory. 780 bar injection pressure. 20 bar cylinder pressure using nitrogen 170
Figure 142: Test results compared to theory. 755 bar injection pressure. atmospheric cylinder pressure using nitrogen 172
Figure 143: Test results compared to theory. 765 bar injection pressure. 10 bar cylinder pressure using nitrogen 172

Figure 144: Test results compared to theory. 770 bar injection pressure. 15 bar cylinder pressure using nitrogen 172
Figure 145: Test results compared to theory. 775 bar injection pressure. 20 bar cylinder pressure using nitrogen 173
Figure 146: Spray penetration test results compared to theory. 700 bar injection pressure. 5 bar cylinder pressure using carbon dioxide 174
Figure 147: Spray penetration test results compared to theory. 720 bar injection pressure. 5 bar cylinder pressure using carbon dioxide 174
Figure 148: Spray penetration test results compared to theory. 740 bar injection pressure. 5 bar cylinder pressure using carbon dioxide 174
Figure 149: Spray penetration test results compared to theory. 760 bar injection pressure. 5 bar cylinder pressure using carbon dioxide 175
Figure 150: Spray penetration test results compared to theory. 780 bar injection pressure. 5 bar cylinder pressure using carbon dioxide 175
Figure 151: Spray penetration. Nitrogen compared to carbon dioxide. 700 bar injection pressure. 5 bar cylinder pressure. 175
Figure 152: Spray penetration. Nitrogen compared to carbon dioxide. 720 bar injection pressure. 5 bar cylinder pressure. 176
Figure 153: Spray penetration. Nitrogen compared to carbon dioxide. 740 bar injection pressure. 5 bar cylinder pressure. 176
Figure 154: Spray penetration. Nitrogen compared to carbon dioxide. 780 bar injection pressure. 5 bar cylinder pressure. 176
Figure 155: Spray penetration test results compared to theory. 780 bar injection pressure. Atmospheric cylinder pressure using carbon dioxide. 178
Figure 156: Spray penetration test results compared to theory. 780 bar injection pressure. 5 bar cylinder pressure using carbon dioxide 178
Figure 157: Spray penetration test results compared to theory. 780 bar injection pressure. 10 bar cylinder pressure using carbon dioxide 178
Figure 158: Spray penetration test results compared to theory. 780 bar injection pressure. 15 bar cylinder pressure using carbon dioxide 179
Figure 159: Spray penetration test results compared to theory. 780 bar injection pressure. 20 bar cylinder pressure using carbon dioxide 179
Figure 160: Spray penetration. Nitrogen compared to carbon dioxide. 780 bar injection pressure. Atmospheric cylinder pressure. 179

Figure 161: Spray penetration. Nitrogen compared to carbon dioxide. 780 bar injection pressure. 5 bar cylinder pressure....180
Figure 162: Spray penetration. Nitrogen compared to carbon dioxide. 780 bar injection pressure. 15 bar cylinder pressure....180
Figure 163: Spray penetration. Nitrogen compared to carbon dioxide. 780 bar injection pressure. 20 bar cylinder pressure....180
Figure 164: Test results compared to theory. 755 bar injection pressure. Atmospheric cylinder pressure using carbon dioxide....182
Figure 165: Test results compared to theory. 760 bar injection pressure. 5 bar cylinder pressure using carbon dioxide....182
Figure 166: Test results compared to theory. 765 bar injection pressure. 10 bar cylinder pressure using carbon dioxide....182
Figure 167: Test results compared to theory. 770 bar injection pressure. 15 bar cylinder pressure using carbon dioxide....183
Figure 168: Test results compared to theory. 775 bar injection pressure. 20 bar cylinder pressure using carbon dioxide....183
Figure 169: Spray penetration. Nitrogen compared to carbon dioxide. 755 bar injection pressure. Atmospheric cylinder pressure. 183
Figure 170: Spray penetration. Nitrogen compared to carbon dioxide. 760 bar injection pressure. 5 bar cylinder pressure....184
Figure 171: Spray penetration. Nitrogen compared to carbon dioxide. 765 bar injection pressure. 10 bar cylinder pressure....184
Figure 172: Spray penetration. Nitrogen compared to carbon dioxide. 770 bar injection pressure. 15 bar cylinder pressure....184
Figure 173: Spray penetration. Nitrogen compared to carbon dioxide. 775 bar injection pressure. 20 bar cylinder pressure....185
Figure 174: Pressure vessel side walls [2]....199
Figure 175: Single wall of pressure vessel [2]....199
Figure 176: Spray box....206
Figure 177: Lid....206
Figure 178: Stress 30mm....207
Figure 179: Stress 25mm....207
Figure 180: Stress 20mm....208
Figure 181: Box with window holes....208

Figure 182: Box with window flange 209
Figure 183: Injector holder 210
Figure 184: Lid flange welds 211
Figure 185: Butt weld on box 214
Figure 186: Position of butt weld on box.. 214
Figure 187: Geometry and notation of a bolted joint [7] 216

LIST OF TABLES

Table 1: Risk analysis 57
Table 2: 700 – 780 bar injection pressure, 5 bar cylinder pressure maxima 110
Table 3: Injection pressure results. 5 bar cylinder pressure. 700 – 780 bar injection pressure. Nitrogen 158
Table 4: Injection pressure results. 5 bar cylinder pressure. 700 – 780 bar injection pressure. Nitrogen. 0.02ms time step 164
Table 5: Cylinder pressure results. 0 bar to 20 bar cylinder pressure. 780 bar injection pressure. Nitrogen 165
Table 6: Constant pressure difference results. 0 bar to 20 bar cylinder pressure. 755 bar to 775 bar injection pressure. Nitrogen 171
Table 7: Injection pressure results. 5 bar cylinder pressure. 700 – 780 bar injection pressure. Carbon dioxide 173
Table 8: Cylinder pressure results. 0 bar to 20 bar cylinder pressure. 780 bar injection pressure. Carbon dioxide 177
Table 9: Constant pressure difference results. 0 bar to 20 bar cylinder pressure. 755 bar to 775 bar injection pressure. Carbon dioxide 181
Table 10: Spray chamber concept selection 194
Table 11: Concept evaluation 196
Table 12: Spray chamber material properties [9] 204
Table 13: Maximum allowable stresses on fillet welds [8] 213
Table 14: Bolt grade properties [7] 215
Table 15: Standard bolt dimensions [7] 216
Table 16: Washer dimensions [7] 218
Table 17: Bolt stress concentration factor [7] 219
Table 18: Bolt condition [7] 220

NOMENCLATURE

Symbol	Definition	Unit
ρ_g	Gas density	Kg/m^3
P_l	Liquid density	Kg/m^3
A_n	Constant for a given nozzle geometry	-
θ	Cone angle	º
d_n	Nozzle diameter	m
Δp	Pressure drop across the nozzle	Pa
μ	Dynamic viscosity of air	Pa.s
S	Spray penetration	m
t	Time after the start of injection	s
T_g	Temperature of the gas	K
t_{break}	Time at which the jet will breakup	s
Q	Volumetric flow rate	m^3/s
C_d	Discharge coefficient of the injector	-
A	Nozzle flow area	m^2
P	Pressure difference across injector orifice	Pa

LIST OF ABBREVIATIONS

Abbreviation	Meaning
CO_2	Carbon Dioxide
N_2	Nitrogen
Vel	Velocity
Inj	Injection
Cyl	Cylinder

1. INTRODUCTION

Optimisation of fuel injection systems could significantly improve the performance and efficiency of engines.

1.1.Background

The following is a background on compression ignition engines and fuel injection.

1.1.1. Diesel engines

In a diesel engine there are four strokes (only in a four stroke engine) viz. intake, compression, power and exhaust; these four strokes are shown in Figure 1. During the intake stroke, air is inducted into the combustion chamber. The downward motion of the piston draws clean air into the combustion chamber; represented by the blue arrows in Figure 1. The air is then compressed during the compression stroke The compression ratio for diesel engines ranges from 12 to 24 [2]. The diesel fuel is then injected by a fuel injector into the compressed air when the piston is near top dead centre (TDC), just before combustion is required to take place. This is represented by the green arrows in Figure 1. Engine knocking is reduced by injecting the fuel into the combustion chamber just before combustion takes place. This allows compression ignition engines to use a higher compression ratio and thereby improve the fuel conversion efficiency [2]. As the diesel in injected it becomes atomised; it then evaporates and the fuel vapour mixes with the air in the combustion chamber [2].

After the compression stroke, the air in the combustion chamber is at a higher temperature than the ignition temperature of the diesel; the mixture therefore combusts [2]. The expanding gasses force the piston down and produce power (the gasses do work on the piston). Diesel engines are also known as compression ignition engines because unlike petrol engines which use a spark plug to ignite the fuel, ignition is achieved by compressing the air to a temperature and pressure at which the injected fuel spontaneously ignites.

As the air/fuel mixture burns and expands, the piston is forced down (power stroke). The power output is controlled by varying the amount of fuel that is introduced to the combustion chamber as the amount of air inducted at any given engine speed is constant [2]. Due to the fact that the engine’s output is determined by the amount of fuel introduced to the combustion process, the engine can be operated unthrottled. As a result, engine requires less pumping work to be done and therefore, the part-load mechanical efficiency is superior to that of a spark ignition engine [2]. After the power stroke, the burnt mixture is expelled from the combustion chamber during the exhaust stroke. This is represented by the orange arrows in Figure 1. The process then begins again.

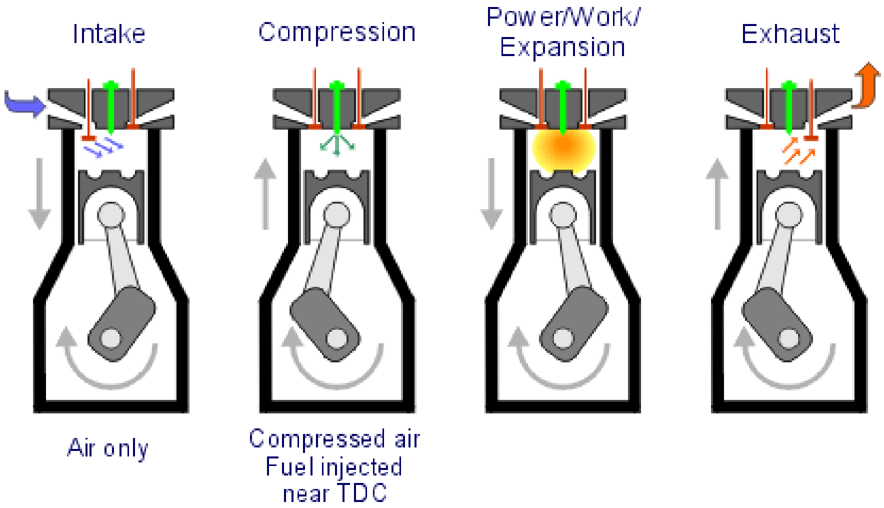

Figure 1: Four Stroke Compression Ignition Engine [22]

Figure 2 below shows the pressure variation in the combustion chamber with changing crank angle. From the figure, it can be seen that when the intake stroke starts (point 2), the exhaust valve closes (EVC). The clean air is inducted into the combustion chamber at a constant pressure. The momentum of the incoming air results in air flowing into the combustion chamber even after the piston has reached bottom dead centre (BDC). The intake valve closes at point 2 and the piston continues upward during the compression stroke. This causes a pressure rise in the combustion chamber. The diesel is injected and compression continues. Ignition of the fuel air mixture occurs just before the piston is at TDC. The onset of combustion results in a large pressure rise. This forces the piston down to BDC and therefore the pressure begins to drop. Just before BDC, the exhaust valve opens. The piston then returns to TDC and expels the burnt air fuel mixture.

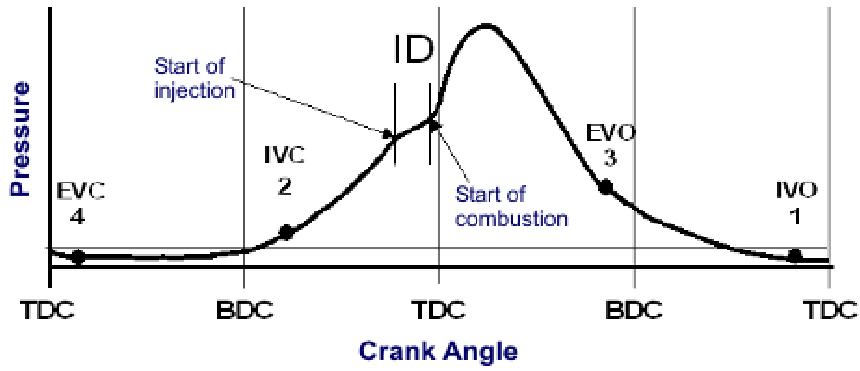

Figure 2: Pressure Variation in Combustion Chamber [22]

1.1.2. Fuel injection

The purpose of the fuel injection system in a compression ignition engine is to introduce the required amount of fuel to each cylinder, for each cycle, for various load requirements and at various engine speeds. The fuel must be introduced to the combustion chamber at the correct time, and at the correct rate. Errors in the amount of fuel injected could have an adverse effect on the engine performance and lead to poor efficiency and harmful emissions. The fuel should be injected into the combustion chamber with a high enough velocity to fully atomise the fuel so that it completely evaporates, thus allowing proper mixing of the fuel and air. [3]

1.2. Literature Review

The following literature review focuses on fuel injection systems and previous work done.

1.2.1. Types of fuel injection

Compression ignition engines employ one of two major methods of fuel injection. The first is direct-injection; these engines have a single opening to the combustion chamber through which the fuel is injected. The second type is indirect-injection. The combustion chamber is divided into two sections and the fuel is injected into a prechamber before being introduced to the combustion chamber.[2]

Direct injection allows finer control, with the use of electronics, and so knocking and rattling can be eliminated more easily [14]. One form of direct injection is common rail injection; a pressure accumulator (common rail) is used to achieve much higher pressures that other forms of fuel injection are able to achieve [14]. The high pressures are needed to counter to high back pressures in the combustion chamber, thus allowing proper mixing and atomisation of the fuel for more efficient combustion [14].

1.2.2. Common rail fuel injection

The common rail diesel injection system separates the two main functions (generating the required pressure and injection) of a fuel injection system into two separate processes. This is done by using an accumulator (the common rail) to generate the required pressure, and then injecting the fuel into the combustion chamber with the individual injectors. This allows the common rail set up to achieve very high injection pressures. [5] The system can be divided into two parts; a low pressure circuit and a high pressure circuit. The low pressure circuit will include the fuel tank and the low pressure fuel pump as well as low pressure fuel lines. The high pressure circuit will include the high pressure fuel pump, high pressure fuel lines, the common rail and the fuel injectors. The low pressure pump is used to deliver fuel from the tank, where the fuel is stored at a low pressure, to the high pressure fuel pump via a fuel filter [6]. The high pressure fuel pump raises the pressure of the fuel to the injection pressure and delivers it to the common rail; this is controlled by the engine control unit (ECU) [7]. The ECU monitors the pressure of the fuel in the common rail by means of a pressure sensor and varies the pressure of the fuel to suit the operating conditions and requirements [6]. With this arrangement, the injection pressure is independent of the engine speed [6]. The common rail has an electro-hydraulic valve, which is controlled by the ECU. It returns fuel to the fuel tank when it is necessary to reduce the pressure it the common rail in order to maintain the injection pressure [7]. The fuel injectors are connected to the common rail and are fed the high pressure fuel via rigid metal fuel lines that are capable of handling the high pressures. These fuel lines are usually of equal lengths and sharp bends are avoided so that fuel flow is not restricted [6]. This setup is less complicated and therefore proves to me more reliable than more complicated systems [8]. The common rail setup can be seen in Figure 3 below.

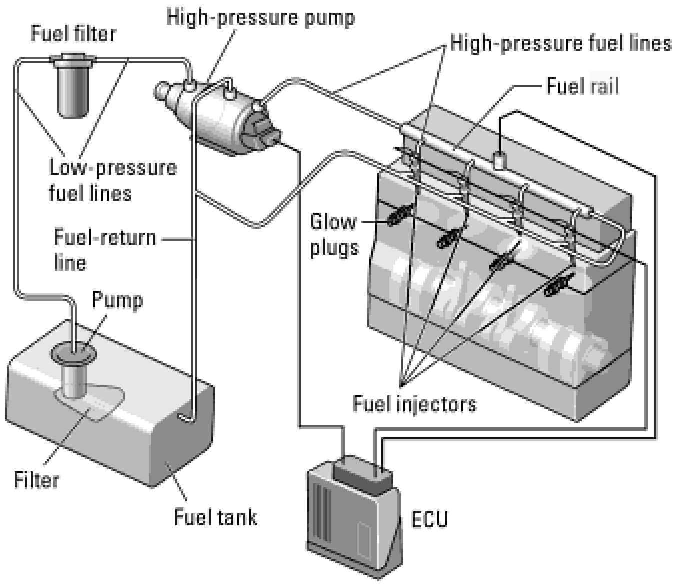

Figure 3: Common rail injection system [10]

The fuel injectors used on the common rail setup are known as electro-hydraulic injectors. The needle valve at the tip of the injector is held in the closed position by a combination of hydraulic forces generated by the high pressure in the rail and a force generated by the spring in the injector. [9]

There are two main types of fuel injectors, solenoid operated injectors and piezo-electric injectors. They differ from each other in the way in which they open the valve to allow the fuel to be injected into the combustion chamber. With a solenoid operated actuator, when fuel is to be injected, the ECU sends a pulse of about 100V to the coil of the solenoid. The coil then creates a magnetic field which pulls a plunger into it and opens the valve. Newer generation injectors make use of piezo-electric actuators. When injection is required, the ECU sends a pulse of about 100V to the piezo crystals which expand rapidly resulting in injection. The piezo-electric actuator has the benefit of a faster response as it does not have the delay associated with the solenoid operated actuator, which is caused by the self-inductance of the coil. [9] The way in which the fuel injector is actuated means that it is unable to regulate the flow. It is either on or off.

The high pressure pump pumps the fuel into the common rail which acts as an accumulator; it holds the fuel at the injection pressure. When the engine is started, the pump pressurizes the common rail to the required pressure in seconds. While the engine is running, the pump continuously pressurizes the common rail so that there is a constant reserve of high pressure fuel. It is generally made of forged steel with an internal diameter of about 10 mm and lengths that range from 280 mm to 600 mm. The rail should have a relatively large volume to prevent pressure fluctuations caused by the high pressure fuel pump and when fuel leaves the rail through the injector. The volume of the rail should be much larger than the volume of fuel being injected (in each injection) so that the amount of fuel leaving the rail per injection is regarded as being negligible. It should also have a volume small enough to allow the pressure to increase to injection pressure quickly after start up. [6][10][14]

The high pressure pump used is a reciprocating radial piston type pump as seen in Figure 4 below. This pump consists of three cylinders with a piston in each, spaced 120° apart. The pump is actuated by an eccentric camshaft, located in the centre of the pump. The pump is powered by the vehicles gear train; the pump performance is therefore dependent on the engine speed. The cylinders of the pump are connected to the low pressure circuit by a small orifice and to the high pressure circuit by a delivery valve (outlet valve). When the piston is at the bottom of the cylinder (lower dead centre), fuel flows into the cylinder via the inlet valve (small orifice), and the outlet valve is held closed. The piston is then forced up due to the action of the camshaft, this action closes the inlet valve, as the pressure in the cylinder increases with the compression of the fuel, the outlet valve is opened by the unbalanced forces and the pressurizedfuel flows to the common rail. [7]

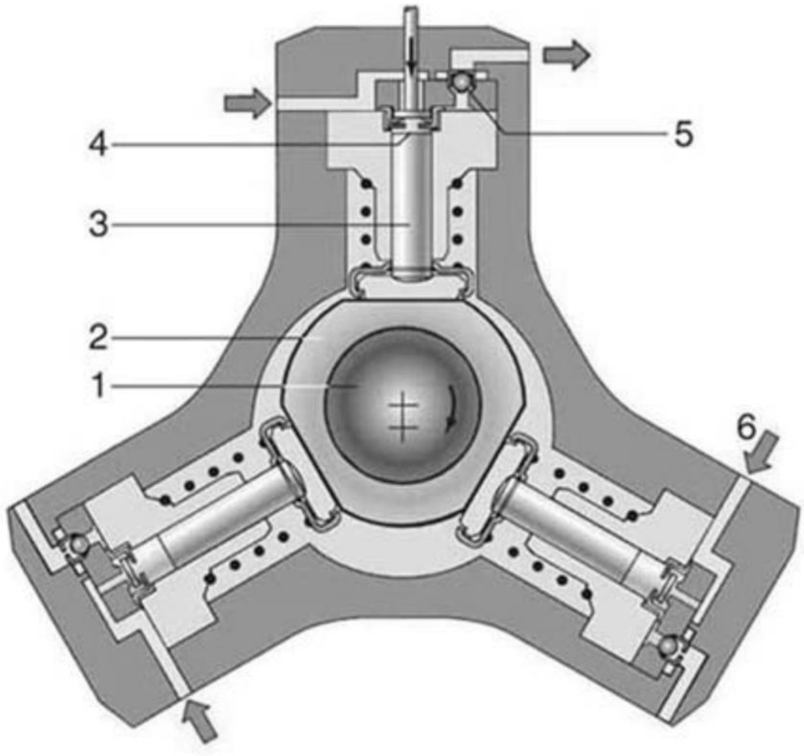

Figure 4: Radial piston pump [10]

Where:

1. Driveshaft
2. Eccentric cam
3. Pumping element
4. Inlet valve
5. Outlet valve
6. Fuel inlet

The common rail distributes the fuel to the injectors by means of rigid tubes that are capable of handling the high pressure of the fuel. A rail pressure sensor is attached to the common rail. It tells the ECU the pressure in the rail thus allowing the ECU to control this pressure (closed loop system). Also attached to the common rail is a pressure limiter valve. The pressure limiter valve prevents the pressure in the rail from reaching dangerous levels which could damage the components or have a negative impact on the injections. When the pressure is too high, the fuel passes through this valve and is returned to the fuel tank.[6] A common rail can be seen in Figure 5 below.

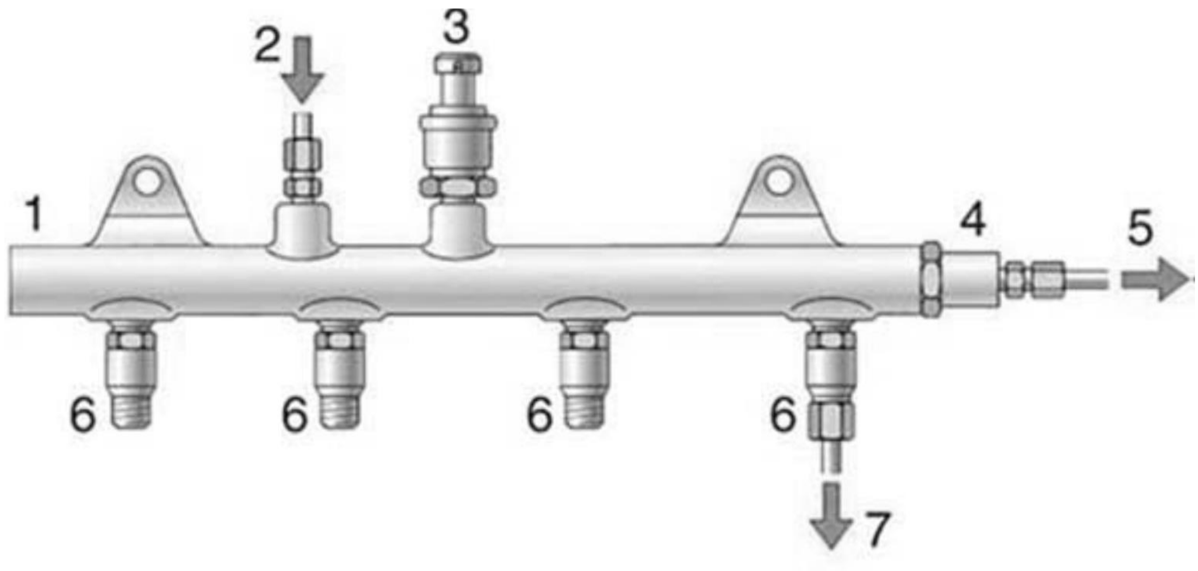

Figure 5: Common rail [9]

Where:

1. Rail
2. Inlet from high pressure pump
3. Rail pressure sensor
4. Pressure limiter valve
5. Return from rail to fuel tank
6. Connection for fuel injector
7. High pressure line to injector

1.2.3. Fuel injectors

Figure 6 below shows the components of a typical fuel injector used on a common rail injection system. Figure 6-a shows the injector in the closed position, Figure 6-b shows the injector as it is beginning to open to begin the injection process and Figure 6-c shows the injector as it is closing to stop the injecting.

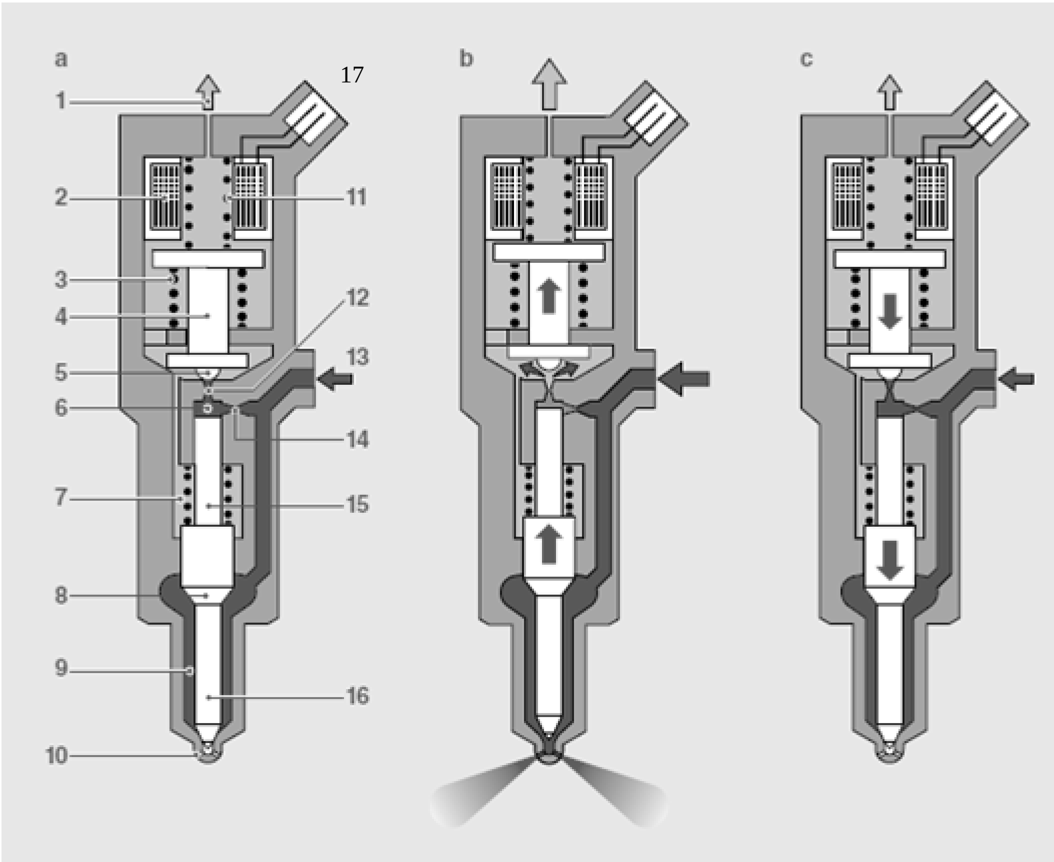

Figure 6: Fuel Injector [6]

Where:

1- Fuel-return
2- Solenoid coil
3- Overstroke spring
4- Solenoid armature
5- Valve ball
6- Valve-control chamber
7- Nozzle spring
8- Pressure shoulder of nozzle needle
9- Chamber volume

10- Injection orifice
11- Solenoid-valve spring
12- Outlet restrictor
13- High-pressure connection
14- Inlet restrictor
15- Valve plunger
16- Nozzle needle
17- Connection to ECU

When the injector is closed (Figure 6-a), the nozzle needle is held in its seat and the injection orifice is closed so that no fuel can pass. High pressure fuel from the common rail enters the injector through the high pressure connection and flows down to the chamber volume where the fuel is at almost the same pressure as in the common rail. This fuel exerts a pressure on the pressure shoulder of the nozzle needle which results in a force that tries to lift the nozzle needle out of its seat. This force is balanced by a combination of the force generated by the nozzle spring and the force acing in the top of the valve plunger. This force is created by high pressure fuel from the common rail that enters the injector through the high-pressure connection and enters the valve-control chamber through the inlet restrictor. This fuel (at a pressure close to rail pressure) is contained in the valve-control chamber by the valve ball which keeps the outlet restrictor sealed. This is achieved by forcing the solenoid armature closed with the force generated by the solenoid valve spring. [6]

For injection to occur the ECU sends a high voltage signal to the solenoid coil, this causes the solenoid armature to move up towards the coil and overcoming the force of the solenoid-valve spring (Figure 6-b). When the solenoid armature moves up, the valve ball opens the outlet restrictor and the fuel in the valve-control chamber flows up and out of the outlet restrictor, then out through the fuel-return and back to the fuel tank. This results in a drop in pressure in the valve control chamber (the inlet restrictor prevents a complete pressure equalization) and therefore a decrease in the force acting on the top of the valve plunger. The force created by the nozzle spring is not large enough to balance the force created by the high pressure fuel in the chamber volume acting on the pressure shoulder of the nozzle needle and the nozzle needle and the valve plunger move up. This opens the injection orifice. The rate at which the injector opens is dependent of the difference in flow rates through the inlet restrictor and the outlet restrictor. [6]

When the injector is open (open injection orifice), the fuel leaves the injector and enters the combustion chamber at a pressure very close to the rail pressure. The amount of fuel that is injected into the combustion chamber is proportional to the time that the injector is open and therefore independent of the engine/pump speed. [6]

When the injection needs to stop, the injector must close (Figure 6-c). The signal to the solenoid coil is cut and the solenoid armature moves down due to the unbalanced force acting on it created by the solenoid-valve spring. This puts the valve ball back in its seat and the outlet restrictor closes. The pressure in the valve-control chamber increases (to close to the rail pressure) and the force acting on the top of the valve plunger along with the force created by the nozzle spring becomes larger than the pressure acting on the pressure shoulder of the nozzle needle, this moves the valve plunger along with the nozzle needle down and the nozzle needle is returned to its seat which closes the injection orifice. The rate at which the injector closes is dependent on the flow rate of the inlet restrictor. [6]

1.2.4. Injection strategies

In the modern diesel engine, the fuel is delivered to the combustion chamber with multiple injections and not just a single injection. The injection process could consist of multiple pilot injections, the main injection and post injections. Pilot injections are primarily used for noise control. A small amount of fuel is injected into the combustion chamber before the main injection; the combustion of this small amount of fuel before the main combustion increases the temperature in the combustion chamber more gradually. This removes the sudden combustion which would occur with only the main injection by itself; this is what causes the decrease in engine noise [14]. The post injections are used to regulate the emissions of the engine. It has been found that a higher injection pressure results in a lower specific fuel consumption, higher performance (higher heat output) and decreased emissions [18].To meet the requirements of Euro 3 emissions levels, three or more injections are required per combustion cycle; to meet Euro 4 and Euro 5 emissions levels, four or more injections are required per combustion cycle. A typical pilot injection is 260 µs long while the main injection is around 500 µs long. A typical delay between the end of the last pilot injection and the beginning of the main injection is 500 µs. [1]

1.2.5. New, used and reconditioned fuel injectors

The purpose of the fuel injector is to introduce fuel to the combustion chamber and ensuring accurate metering and sufficient atomisation of the fuel. Over a period of time, continuous use of the fuel injector leads to wear which adversely affects the performance of the injector. The main cause of injector wear is due to moisture in the fuel, which causes corrosion, and wear due to contaminants in the fuel [11]. Contaminants as small as 10 microns can cause injector wear [11].

Often the worn injectors are reconditioned in an attempt to restore the original spray pattern and improve the mixing of the fuel and air which will improve performance of the engine [11]. The used injector is cleaned in an ultrasonic bath and a new strainer and o-ring are fitted [11]. The cost of reconditioning a fuel injector is comparable to the price of a brand new modern injector. Reconditioning the injector does not restore it to its original condition. The ultrasonic cleaning only cleans the nozzle tip and not the inside of the injector; it does not remove any corrosion from within the injector, this could lead to premature injector failure [11].

1.2.6. Spray structure

Diesel is introduced to the combustion chamber via a nozzle. There are various nozzle designs such a single orifice, multiorifice, throttle and pintle and the chosen nozzle depends on the needs of the engine [2]. When injection occurs, the pressure in the combustion chamber is between 50 bar and 100 bar [2]. The pressure of the fuel being injected can range from 200 bar to around 1700 bar [2]. The large pressure difference ensures that the fuel is injected with enough velocity to ensure sufficient atomisation and mixing with the compressed air in the combustion chamber.

When an injection occurs, the liquid fuel leaves the nozzle with a velocity greater than 100 m/s [2]. As the fuel leaves the nozzle of the fuel injector, the large pressure difference is converted to kinetic energy. A very large pressure drop occurs at the nozzle, this large pressure drop leads to cavitation of the fuel. The cavitation occurs as the pressure of the fuel suddenly decreases to below the saturation pressure of the liquid fuel and vapour bubbles form. The cavitation can damage the internal surfaces of the nozzle. [17] The jet of fuel becomes turbulent as it mixes with the compressed air in the combustion chamber [2]. The outer layer of the jet, near the nozzle exit, breaks up into droplets with a diameter of about 10 µm [2]. The rest of the jet disintegrates within the combustion chamber. The length over which the jet disintegrates is known as the breakup length [2]. Cavitation in the nozzle results in better spray characteristics and results in better fuel breakup due to the turbulence created in the nozzle [17].

At points further away from the nozzle, the width of the jet increases and the velocity decreases [2]. The mass of air within the jet increases as the fuel mixes with the air further away from the nozzle [2]. As the fuel mixes with the hot compressed air, it begins to evaporate. The penetration of the tip of the jet increases at a decreasing rate as the injection continues [2]. Figure 7 below shows a fuel jet.

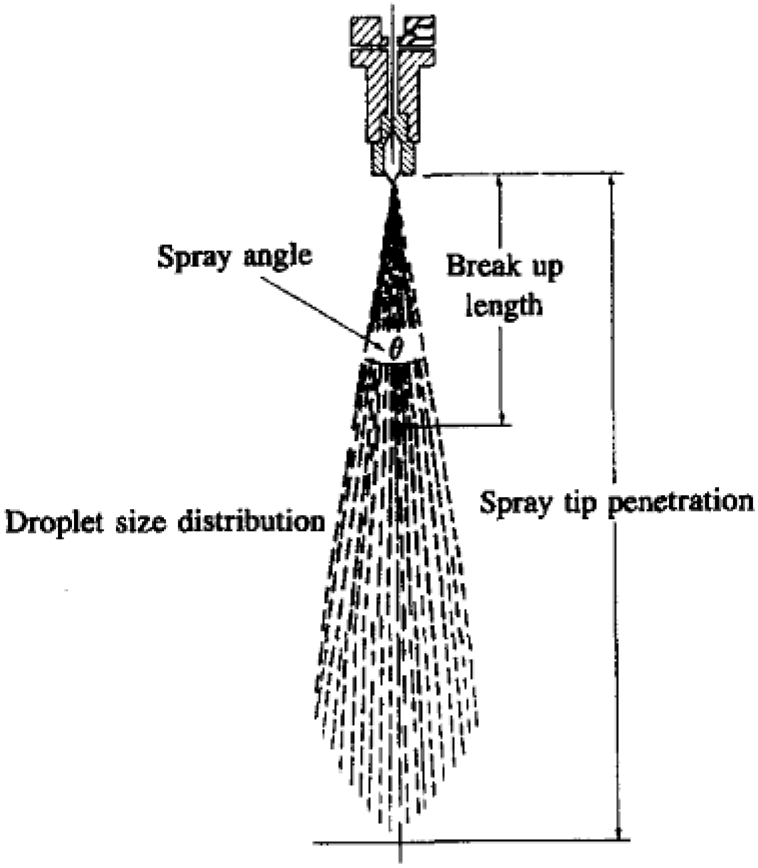

Figure 7: Injected fuel jet [2]

As the fuel on the outside of the jet evaporates and mixes with the air in the combustion chamber, it forms a vapour-air sheath around the jet which has a liquid core [2]. The highest velocities occur at the liquid core along the axis of the nozzle [2]. This explains the shape of the tip of the jet. The fuel/ air ratio decreases as one moves radially outwards from the axis of the nozzle. The highest ratio will occur at the centre of the jet where there is no air and will be a minimum at the boundary of the jet (unmixed air). As the spray reaches the combustion chamber walls, it begins to interact with them; the spray has to move tangentially along these walls. The spray from the holes on multiorifice injectors eventually interacts with each other. [2]

When the jet velocity is relatively low, the primary cause of the breakup of the spray is the unstable growth of surface wave that are caused by the surface tension. The resulting droplets are larger in diameter than the diameter of the jet. Increasing the jet velocity increases the surface tension force. The larger surface tension force is a result of the relative motion between the jet and the air. This results in droplets that have a diameter similar to that of the jet. Increasing the velocity further will give droplets with a diameter smaller than that of the jet. When the velocity of the jet is high enough, the fuel will breakup at or before the exit plane of the nozzle, this leads to atomization of the fuel and the resulting droplets have diameters that are much smaller than the nozzle diameter. [2]

1.2.7. Atomisation

The injected fuel is subjected to both internal and external forces that lead to different droplet sizes, shapes and concentrations within the spray. The spray can form into thin jets or liquid sheets. There are three different types of mechanisms for atomisation; aerodynamically-induced atomisation, jet turbulence-induced atomisation and cavitation-induced atomisation. Aerodynamically-induced atomisation is caused by waves forming in liquid jets due to the relative motion between the fuel and air. Jet turbulence-induced atomisation is caused by turbulence in the nozzle. The turbulence results in spray velocity having radial components and this causes atomisation once the fuel leaves the nozzle. Cavitation-induced atomisation is caused by the formation and collapse of vapour bubbles at the nozzle exit. When the fuel is accelerated to high velocities in the nozzle, the sudden drop in pressure causes the cavitation to occur. [23]

1.2.8. Break-up length

When the fuel leaves the nozzle, it does not all break up instantly and there is a liquid core in the centre. The length of the liquid core is referred to as the break up length. The break-up length is dependent on parameters such as injection velocity, surface tension, viscosity and aerodynamic forces. It was found that increasing the ambient gas pressure results in a decrease in the break-up length. The break-up length therefore varies inversely with ambient gas pressure. Increasing the injection pressure also has the effect of decreasing the break-up length. [23]

1.2.9. Cone angle

Researchers have not come to an agreement on the method used to measure the cone angle of a spray. There are currently a few prevailing methods; the first makes use of an equivalent isosceles triangle. The triangle will have the same area and height as the spray and the acute angle of the triangle will be the cone angle. Other methods measure the width at a certain position along the length of the spray, eg. 50% along the length of the spray or a distance that is a set number of times larger than the nozzle diameter; the acute angle then gives the cone angle. A common method involves fitting lines tangent to each side of the spray and measuring the angle between them. It can be argued that this method gives the best representation of the macroscopic cone angle. [24]

If a jet has a velocity high enough to cause atomisation, the spray angle (cone angle) (seen in Figure 7) can be found using Equation 1 [2].

$$tan\frac{\theta}{2} = \frac{1}{A}4\pi\left(\frac{\rho_g}{\rho_l}\right)^{\frac{1}{2}}\frac{\sqrt{3}}{6} \qquad \text{Eqn 1}$$

Where:

ρ_g Density of the gas (kg/m^3)

ρ_l Density of the liquid (kg/m^3)

A Constant for a given nozzle geometry

Equation 2 was used by Hiroyasu [19].

$$\theta = 0.05\left(\frac{d_n^2\rho_g\Delta p}{\mu^2}\right)^{0.25} \qquad \text{Eqn 2}$$

Where:

θ Cone angle (˚)

d_n Nozzle diameter (m)

ρ_g Density of the gas (kg/m^3)

Δp Pressure drop across the nozzle (Pa)

μ Dynamic viscosity of gas (Pa.s)

Figure 8 below shows the variation of cone angle with injection pressure. It was also noted by Hiroyasu that a decrease in the kinematic viscosity of the fuel led to an increase in the cone angle.

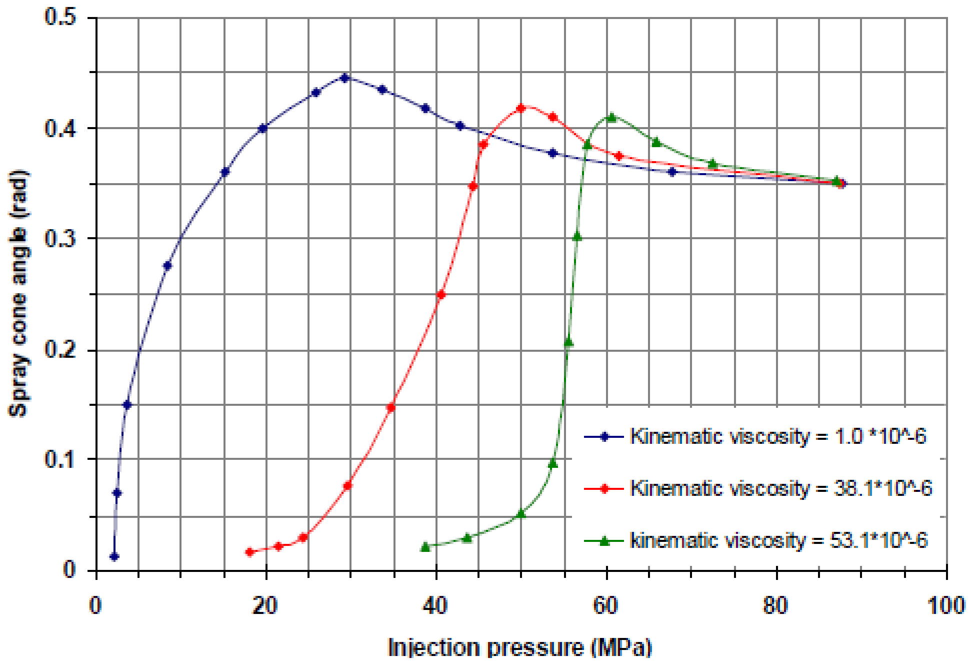

Figure 8: Variation of cone angle with injection pressure [23]

Cavitation in the nozzle has the effect of increasing the cone angle; this is due to the formation of vapour in the nozzle [17].

1.2.10. Spray penetration

The depth to which the jet penetrates and the speed at which it penetrates into the air in the combustion chamber has a direct impact on the performance of the engine. The spray penetration will determine how well the fuel mixes with the air and how well the fuel will be atomized. This will determine how efficiently combustion will take place. If the penetration is too great (overpenetration) the impingement of liquid fuel on the cold surfaces of the combustion chamber will lead to poor mixing which will result in higher emissions and unburnt species. Underpenetration will lead to poor utilization of the air in the combustion chamber and therefore this will not produce optimum results. The spray penetration (seen in Figure 7) can be calculated using Equation 3 which was developed by Dent [42].

$$S = 3.07\left(\frac{\Delta p}{\rho_g}\right)^{\frac{1}{4}}(td_n)^{\frac{1}{2}}\left(\frac{294}{T_g}\right)^{\frac{1}{4}} \quad \text{Eqn 3}$$

Where:

S Spray penetration (m)

Δp Pressure drop across the nozzle (Pa)

t Time after the start of injection (s)

d_n Nozzle diameter(m)

ρ_g Density of the gas (kg/m^3)

T_g Temperature of the gas (K)

Dent determined that his equation modelled experimental data very closely. However, there were deviations in the spray penetration for injection times < 0.5ms. The experimental spray penetrations were smaller than those predicted by the model. The model therefore over predicts the spray penetrations at the beginning of the injection. [23]

Work done by Hiroyasu shows that initially, a short time after injection has begun, the spray penetration increases linearly with time; and as a function of $\sqrt{t}$ after the jet begins to break up. The work also showed that the injection pressure significantly affects the spray penetration before the jet begins to breakup, and that the back pressure has a more significant impact after the jet begins to break up. The time at which the jet is expected to breakup can be predicted using Equation 4 below [43]:

$$t_{break} = \frac{29\rho_l d_n}{(\rho_g \Delta p)^{\frac{1}{2}}} \quad \text{Eqn 4}$$

Where:

t_{break} Time at which the jet will breakup (s)

ρ_g Density of the gas (kg/m^3)

ρ_l Density of the liquid (kg/m^3)

Δp Pressure drop across the nozzle (Pa)

d_n Nozzle diameter(m)

With this, according to Hiroyasu, the spray penetration can be calculated using Equations 5 and 6 [43]:

$$t < t_{break}: \quad S = 0.39\left(\frac{2\Delta p}{\rho_l}\right)^{\frac{1}{2}} t \qquad \text{Eqn 5}$$

$$t > t_{break}: \quad S = 2.95\left(\frac{\Delta p}{\rho_g}\right)^{\frac{1}{4}} (d_n t)^{\frac{1}{2}} \qquad \text{Eqn 6}$$

Where:

t Time after the start of injection (s)

t_{break} Time at which the jet will breakup (s)

S Spray penetration (m)

ρ_g Density of the gas (kg/m^3)

ρ_l Density of the liquid (kg/m^3)

Δp Pressure drop across the nozzle (Pa)

d_n Nozzle diameter(m)

1.2.11. Flow rate

The flow rate through the fuel injector can be modelled as the flow through a nozzle; this model can be described by Equation 7 below [12].

$$Q = C_d A\sqrt{\frac{2P}{\rho}} \qquad \text{Eqn 7}$$

Where:

Q volumetric flow rate (m^3/s)

C_d discharge coefficient of the injector

A nozzle flow area (m^2)

P Pressure difference across injector orifice (Pa)

ρ fuel density (Kg/m^3)

The nozzle flow area is the sum of the cross sectional areas of all the holes in the injector. The calibration fluid used has a density of 830 Kg/m^3 [13]. A higher flow rate during the pre-combustion phase has been found to result in a higher heat output [18].

1.2.12. Previous work

Klein-Douwel, Frijters, Somers, de Boer, Baert

Klein-Douwel et al. [24] investigated the evolution of the shape of sprays with time, produced by a modern, heavy-duty common rail injector. The emphasis was on synchronising the spray images with time, dynamic phenomena and on relating spray growth to time (i.e. Spray penetration).

The apparatus used included a constant volume test cell that could withstand pressures of up to 10 MPa. Quartz glass windows allowed for the spray to be monitored. Tests were conducted at room temperature; this has the added benefit of simulating more realistic engine gas densities. The fuel pump used could deliver rail pressures of up to 200 MPa.

The injector used was a 8 hole Bosch injector with all but 1 hole blocked. This reduces interference from multiple jets and makes the spray easier to analyse. Variations of up to 4% were seen in the rail pressure and signal sent to the injector.

Experiments were conducted with a rail pressure of 150 MPa; the gas in the chamber was nitrogen at room temperature with a pressure of 2.9 MPa. The data capturing system had uncertainties of ±0.25mm for the nozzle axis and position where the spray exits and ±0.05 ms with the timing of the pictures. Due to the speed of the camera used (too slow to capture clear images), assumptions are made for regions in which the images are blurred. These assumptions are only valid from 0.5 ms after the start of the injection when the spray has slowed down enough.

There were a lot of anomalies noticed in the results; these were attributed to changes in momentum. As the spray gained lateral momentum, the axial momentum was reduced. It was expected that the momentum transfer would show up when correlating the spray penetration to the cone angle. A plot of these results however showed a weak correlation as the variations were too large to show a relationship. It was noticed that the effect of the density of the gas in the chamber became greater as the spray progressed and slowed down.

It is generally assumed that the spray velocity is constant before the spray breaks up and the spray penetration increases linearly with time. Interpolation of the results showed that the first point measured was after the spray velocity had reduced ie. after the spray had broken up. The apparatus used was unable to observe any data before the spray broke up. The set up used does not measure the early phases of the injection and the assumptions made due to the limitations of the equipment make the accuracy of the results for the early parts of the injection questionable.

Seneschal, Ducottet, Schon, Champoussin, Gucher

Seneschal et al. [25] conducted experiments and developed data processing software to investigate the spray characteristics of a common rail diesel injection system. Figure 9 below shows the apparatus used for their tests. The fuel was pressurized and delivered to a common rail via a fuel pump. The fuel was then fed through the injector and injections were controlled by the computer. A delay was specified between the camera and the injection signal so that images could be captured at different points of injection. The spray was illuminated with halogen lights and injection took place into atmospheric pressure.

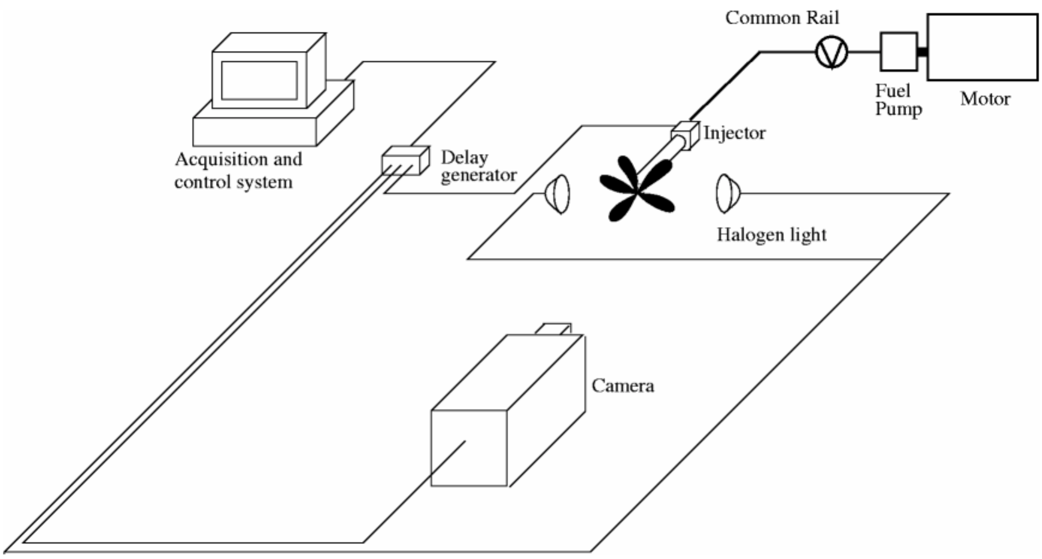

Figure 9: Test apparatus [25]

The camera was capable of taking 2 pictures a second, so only one picture was taken per injection. The injection process was divided into 18 equal time frames and 5 pictures were taken at each interval for a total of 90 pictures. These pictures were the input for the software developed. The software analysed the pictures and averaged the data to minimize anomalies. The spray penetration, cone angle and spray velocity were the outputs of the software.

The results, as seen in Figure 10 below, for spray penetration were compared to Hiroyasu's model.

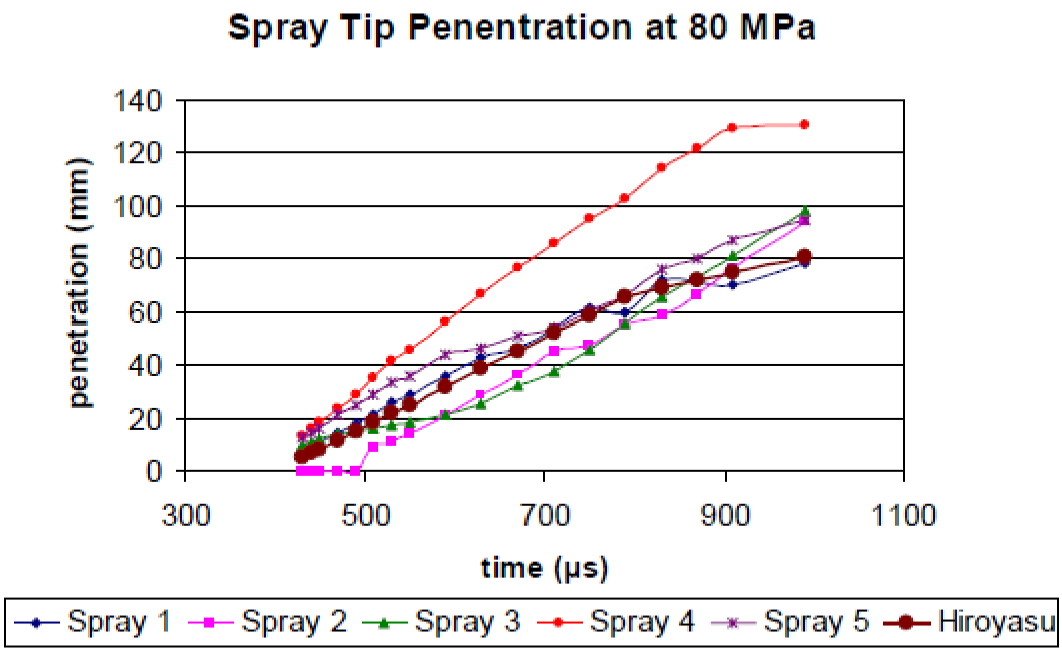

Figure 10: Spray penetration results vs. Hiroyasu [25]

It was concluded that Hiroyasu's model predicts the spray penetration closely and the two phases are clearly evident.

Delacourt, Desmet, Besson

Delacourt et al. [26] carried out a study with the objective to investigate the effect of injection pressure on the macroscopic spray characteristics for a wide pressure range.

The rig used consisted of a pressurized chamber filled with CO_2 at ambient temperature so as to minimize evaporation of droplets. The CO_2 was pressurized to replicate real world cylinder gas densities. The fuel delivery system was a common rail diesel injection system, the fuel was delivered to the injector via a pressure accumulator by a high pressure fuel pump. The spray was constantly illuminated and images were captured using a “fast video camera”. The camera was triggered with a delay from the time the injector was triggered.

The camera used posed some problems as it was not able to capture the spray in a high enough resolution to be analysed. To overcome this, the spray images were composed of various pictures taken at different points of multiple injections under the same conditions. The images are then processed using custom software. The software distinguishes the spray from the background and noise using a set luminance threshold. It then identifies the axis of the nozzle and measures the distance of the spray from the nozzle along this axis.

The spray penetration results were compared to theoretical models developed by Hiroyasu and Arai. It was concluded that Hiroyasu’s model predicts the spray penetration very closely, even for pressures much higher than those used in real world applications. The results are plotted in Figure 11 below.

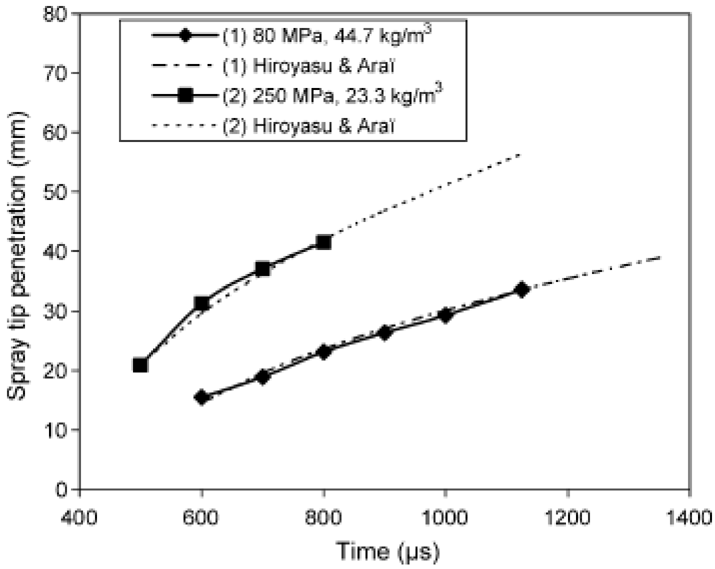

Figure 11: Delacourt et al. vs Hiroyasu and Arai, spray penetration [26]

It was also found that the spray tip velocity decreases very quickly with time regardless of the injection pressure. It was also found that at any given spray penetration; the injection pressure has a diminishing effect on the spray tip velocity as it is increased. This can be seen in Figure 12 below.

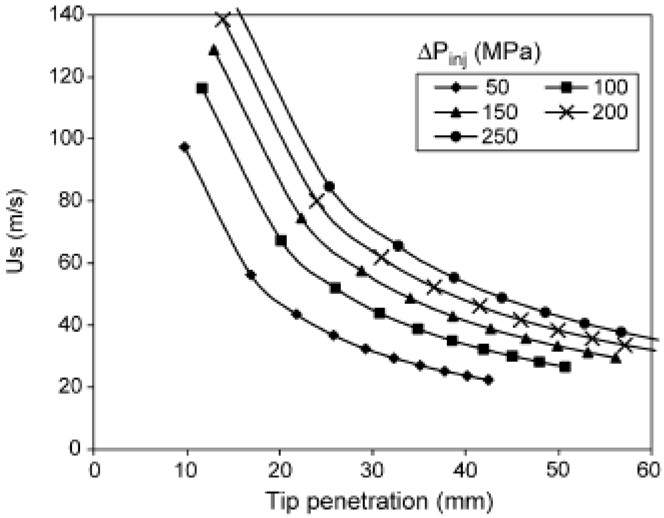

Figure 12: Spray tip velocity vs. spray penetration [26]

Payri, Salvador, Gimeno, Soare

Payri et al. [27] investigated the relationship between the spray structure and the ambient gas density, nozzle hole diameter and injection pressure. Two test rigs were used; one that simulated in-cylinder gas density and another that simulated both the in-cylinder gas density and pressure.

The first rig used a chamber filled with sulphur hexafluoride, an inert gas with a high density. This allowed in-cylinder gas densities (20-50 kg/m^3) to be simulated with relatively low pressures (0.2-0.7 MPa). The second rig used a nitrogen filled chamber that was pressurized up to 6 MPa. The temperature in both rigs was kept constant at 25°C. The gas densities were calculated using the ideal gas equation for nitrogen and Van der Waals equation for real gas was used for the sulphur hexafluoride.

The images were captured by a high resolution camera and illuminated with a flash. The experiments were controlled, and everything was synchronised by a purpose built system that included an ECU to manage the injections. The same injection and data capturing system was used for both rigs. The injection system was composed of commercially available components similar to the other experiments described in this section.

Payri et al. clearly noted two phases in the spray penetration as described by Hiroyasu. At first the spray penetration increase linearly with time until a transition point where the spray breaks up; thereafter, the spray penetration increases as a function of the square root of time. Naber and Siebers [28] attribute this transition to the point at which the spray changes from being dominated by the injected liquid to being dominated by the entrained gas.

This study found a correlation between the transition time and the time at which the injector is fully open. It was then concluded that the spray increases linearly with time as the needle in the injector is still lifting after the injection signal is received. While the needle is lifting, the mass flow rate is increasing until time t at which point the mass flow rate is constant. The time t was found to be the exact time at which the spray penetration starts to increase as a function of the square root of time.

It was found that the spray penetration in the sulphur hexafluoride was 6% higher than in the nitrogen. Cavitation and small pressure differences were disregarded as possible reasons and the difference was attributed to the formation of shock waves, however the extent to which shock waves affect the macroscopic properties of the spray are unknown and were suggested as a topic for future study. A direct comparison of the results from the two rigs showed that the results obtained with the nitrogen test rig are closer to the expected theoretical values than those obtained with the sulphur hexafluoride test.

Previous work done in the field of interest made use of equipment that lacks the accuracy of the Inov8 test stand. The data capturing methods used were unable to record the first phase of the injections correctly and numerous assumptions were made for the results of the second phase to be considered. Using the technology of the Inov8 test stand to investigate the effects of cylinder pressure will give new insights into the behaviour of fuel sprays that were previously not obtainable.

Valentim [30]

Valentim conducted research to investigate the parameters that affect the spray characteristics of both diesel and Dimethyl ether (DME). The results obtained for diesel are of interest for the purposes of the current research. Valentim used a common rail system to inject diesel into a constant volume pressure chamber with injection pressures ranging from 300 bar to 500 bar and cylinder pressures of up to 17.7 bar (carbon dioxide). Data capturing was achieved with a z-shaped schlieren system and a high speed camera operating at 20 000 fps, it was illuminated with a high power LED. A controller was used to control the triggering of the injector and high speed camera as well as data capturing. [30]

Valentim found that the spray penetration increased with increasing injection pressure and decreased with increasing cylinder pressure. It was discovered that the theoretical models over predicted the spray penetration for the initial 0.5ms. The author also found an increase in cone angle with increasing cylinder pressure (except at atmospheric pressure). There was no correlation found between cone angle and injection pressure. Valentim noted a hesitation after the first 0.2ms of the injection, which was attributed to the characteristics of the single hole injector used. [30]

Figure 13 shows Valentim's results for spray penetration compared to various theoretical models. The spray hesitation the author noted can be seen in the red circle. It can also be seen that the theoretical models over predict the spray penetration for the first 0.5ms. Valentim attempted to get a better understanding of this region by increasing the camera frame rate to 100 000fps to get a time resolution of 0.01ms, however the equipment used was unable to obtain clear images at this speed.

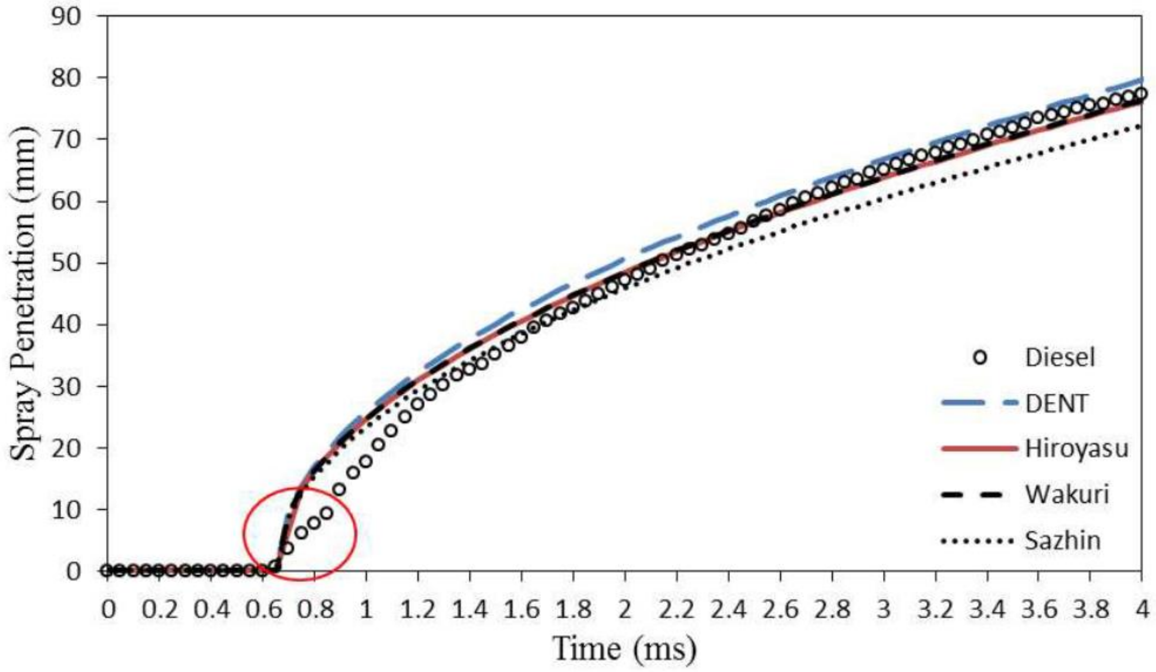

Figure 13: Valentim diesel spray penetration [30]

Karimi [23]

Karimi conducted research to determine the effect of injection pressure and cylinder pressure and in-cylinder gas density on spray patterns (spray penetration and cone angle). Karimi made use of a pressure chaber fitted with a modern common rail injection system. Tests were conducted on a variety of injectors, including single and multi-hole injectors. The experiments made use of a high speed visualization technique. The image acquisition system had a Phantom V7.1 high-speed- camera that was able to capture images at 150000 frames per second. A compromise had to be found between camera speed and image resolution and this meant a camera speed of 34300 frames per second was used for the experiments. This resulted in a time step of approximately 0.03ms between successive images. Two 125W halogen flood lights with a diffuser were used for illumination. Figure 14 below is a schematic of the experimental set-up Karimi used.

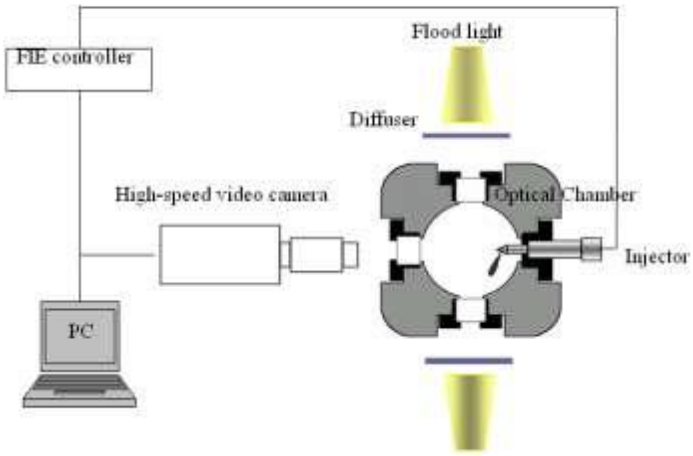

Figure 14: Karimi experimental apparatus set-up [23]

Custom software was used to analyse the images captured by the camera. A threshold was set for each test and the software picked up and measured the boundaries of the spray. Karimi found variations of ±4.6% in the spray penetration for tests done with the same parameters. The tests on a single hole injector showed that a hesitation exists at the start of the injection. It was determined that this was due to the lateral oscillation of the injector needle due to an asymmetric pressure distribution around the needle as it lefts and exposes the nozzle. It was also discovered that the delay in the start of the injection was related to the injection pressure with a higher injection pressure resulting in a shorter delay. Some of Karimi's observations can be seen in Figure 15 below with varying injection pressures and a 20 bar cylinder pressure.

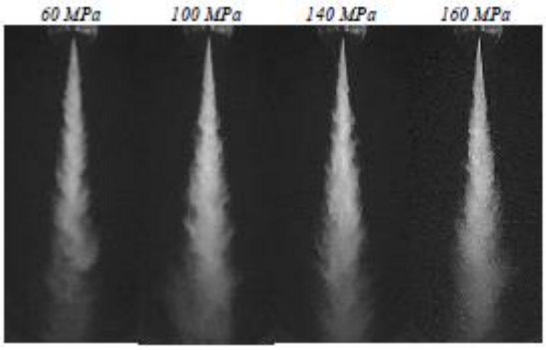

Figure 15: Karimi observations [23]

Tests were conducted with atmospheric cylinder pressure, 20 bar, 40 bar, and 60 bar; the injection pressures were 600 bar, 1000 bar, 1400 bar and 1600 bar. Karimi noticed that the spray penetration increased with increasing injection pressure and decreased with increasing cylinder pressure. The author also noted that the spray penetration tended to fluctuate after the initial stages and attributed this to cluster shedding; clusters of fuel vapour/ gas mixture breaking off from the main spray structure.

1.3.Motivation

In the past few decades, diesel engines have been used primarily in the transportation industry in both light and heavy duty applications. In the last few years, there has been a significant improvement in diesel engine technology and diesel engines now have more applications in the passenger vehicle industry. [4] This improvement in technology has led to diesel engines showing a considerable increase in market share; comparable to that of petrol engines in some countries. The popularity of combustion engines however has a negative impact on the environment and is believed to be a major contributor to global warming; a phenomenon that has received worldwide attention in recent times. Due to the connection between the emissions from combustion engines and global warming, governments have imposed strict regulations on the emissions of these engines. Engine manufacturers must now produce engines which are able to meet these requirements and at the same time be as efficient and economical to run as possible while maintaining fairly high specific power outputs. Superior efficiency and economy are required due to the global shortage of fossil fuels which have led to a drastic increase in fuel prices. The price of diesel in South Africa increased by 13.2% from January 2017 (R11.45) to December 2017 (R12.96). In order to achieve this, every component of the engine must be optimized. The fuel injection system of an engine plays a vital role in its overall performance and emissions. This research is required in order to gain a better understanding and hence optimise the fuel injection system of a diesel engine. [4]

1.4.Objectives

The objectives of this research are based on the effect of the cylinder pressure on the spray penetration. They are:

1. Modify the Inov8 Test Stand with a spray chamber that will allow it to be used to analyse spray patterns with a cylinder pressure of up to 20 bar.
2. Investigate the sensitivity of spray penetration and velocity to changes in injection pressure.
3. Investigate the sensitivity of spray penetration and velocity to changes in cylinder pressure.
4. Determine effect of cylinder gas density on spray penetration (distance and velocity).
5. Investigate the relationship between spray penetration and the injection-cylinder pressure difference.
6. Compare experimental results of spray penetration to theoretical models of Hiroyasu and Dent.
7. Investigate the accuracy of Hiroyasu's equation for the time at which the spray will break up.
8. Investigate Hiroyasu's theory that the injection pressure has a greater effect on spray penetration before the jet begins to breakup, and that the back pressure has a more significant impact after the jet begins to break up.

2. APPARATUS

The experiments were conducted with the use of the Spray Analysis and Flow Measurement test stand in the Barlow world laboratories at The University of the Witwatersrand, Johannesburg. Figure 16 below shows the layout of the lab. The equipment was prepares specially for the university by Inov8 Technologies Ltd. The test stand is able to perform spray pattern analysis and flow measurement from diesel or gasoline GDI injectors, however, it can only conduct one experiment at a time [15]. The pressures are generated by a high pressure fuel pump that operates between 100 rpm and 1000 rpm and is capable of generating rail pressures of up to 1800 bar [15]. The stand is controlled by three remote PCs. The fuel injectors must be loaded and unloaded manually i.e. all physical and electronic connections must be done manually [15]. The test stand requires a 3-phase power supply [15]. The test stand can be seen in Figure 17 below.

The Inov8 test stand uses cutting edge technology to measure spray penetration. It makes use of a high quality Imager Compact camera to take pictures of the fuel jet. The user defines the start and end point, as well as the intervals between pictures. Once the user defines the injection pressure and the injection duration, the camera will take a user defined number of pictures. The pictures are taken over multiple injections. The software then averages the pictures from different injections with the same inputs so that a better representation of the spray penetration is obtained. The effect of outliers and anomalies are significantly reduced. The software also allows the background to be removed by taking a picture before the injection and then removing that image from the experimental images. There is therefore no chance of the background affecting the results.

This test stand allows spray penetration to be analysed while injecting into atmospheric pressure. The spray chamber will be replaced by a spray chamber that can be pressurized up to 20 bar. The spray chamber will not interfere with the normal operation of the test stand. The experiments will then be run using the standard software of the test stand.

When using the test stand to measure the spray penetration, it returns a set of data points that represent the length of the jet from the nozzle to the tip of the spray at the user defined time intervals. This also allows for the velocity of the spray tip for any given interval to be calculated. The quality of the images taken and therefore the results produced will be unmatched in accuracy than previously possible due to the nature of the equipment used.

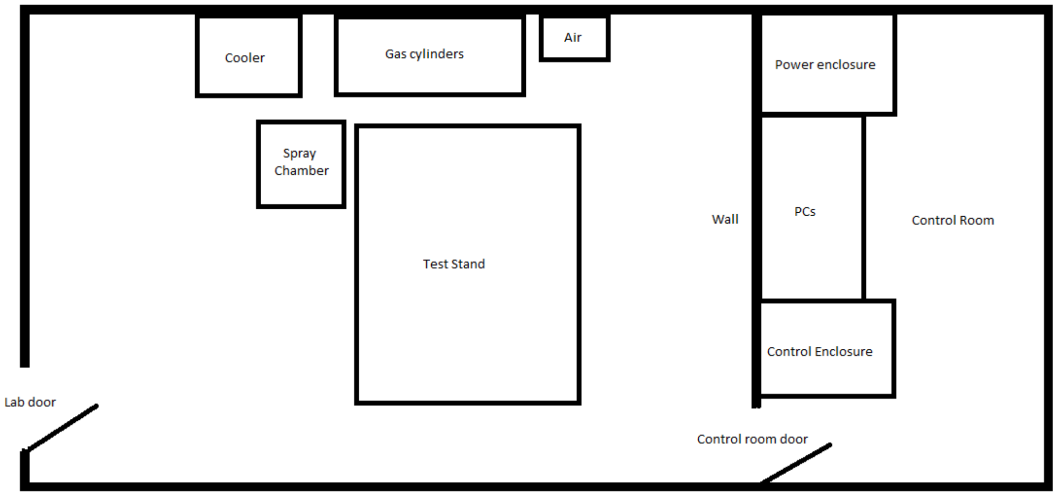

Figure 16: Lab layout

Figure 17: Spray pattern analysis and flow measurement test stand

2.1.Test Stand

The test stand requires a nitrogen supply (from a high pressure bottle regulated between 6.5 and 8MPa) and a compressed air supply (regulated between 5.5 and 8 bar) [15]. The nitrogen is piped to a manually operated shut off valve on the main Air and Nitrogen Panel Assembly [15] It is then used to simulate a back pressure in the Akribis test section and to purge the test stand so that ignition is less likely to occur. The air supply is piped to a safety relief valve and a manually operated shut off valve; it is then piped to the test stand [15]. The compressed air is used for the spray chamber lower shield actuator and the air knives (discussed later), it is also used for purging [15]. There are also connection points for cooling water inlet and outlet (cooler set to 12°C). The cooling water from the external cooler is distributed from the cooling water inlet through the machine and returned to the cooler via the cooling water outlet. The specifications of the required cold water supply are as follows [15]:

Flow capacity	50 litres/min peak (20 litres/min mean)
Max. temperature	15°C
Min. Temperature	10°C
Min. Supply pressure	3.0 bar

Figure 18 shows the Air and Nitrogen Panel Assembly. Figure 19 below shows the supply connections.

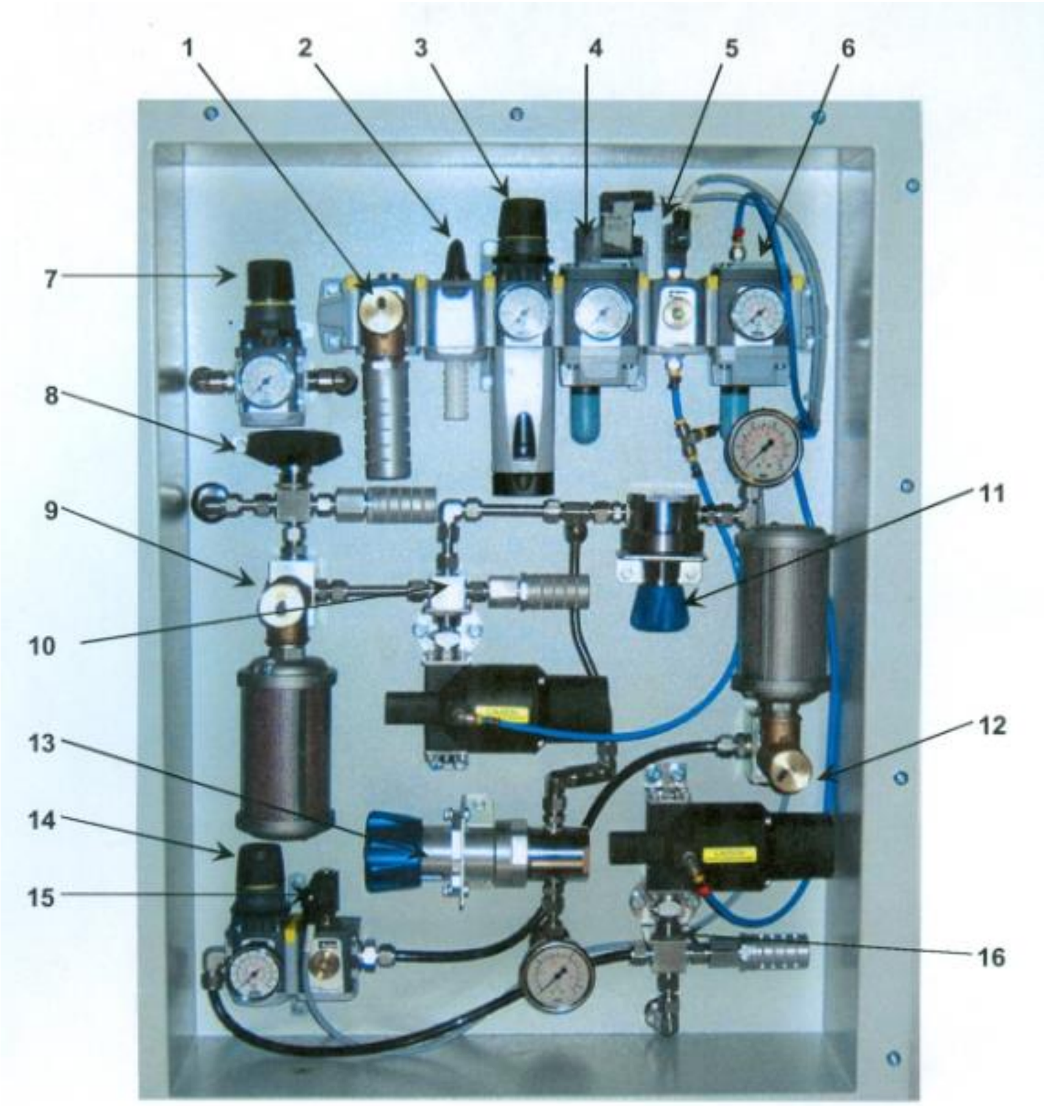

Figure 18: Air and Nitrogen Panel Assembly [15]

Where:

1. Main air safety relief valve (pre-set to 10 bar)

2. Main air shut-off valve

3. Main air pressure regulator

4. Main air solenoid soft start/dump valve

5. Main air pressure switch

6. Air purge and air knives dump valve

7. Air purge supply pressure regulator

8. Main nitrogen shut-off valve

9. Nitrogen high pressure safety relief valve

10. Main nitrogen interlock valve

11. Nitrogen low pressure regulator

12. Nitrogen low pressure safety relief valve

13. Nitrogen high pressure regulator

14. Nitrogen purge pressure regulator

15. Nitrogen low pressure switch

16. Nitrogen purge supply interlock valve

Figure 19: Supply connections

There are two fluid systems on the test stand – the cooling fluid system and the test fluid system. The cooling fluid system has the cooling fluid, the cooling fluid tank, temperature and level monitoring devices, a pump, a fluid filtration system and a pressure control system [15]. This system re-circulates cooling fluid through the test stand in order to maintain acceptable temperatures. The fluid temperature is constantly monitored by a thermostat and the test stand is set to trip when the cooling fluid temperature reaches 37°C [15]. Normal operation can continue once the cooling fluid temperature has dropped to below 37°C. In a similar manner, the cooling fluid level is also continuously monitored and the test stand will trip if the cooling fluid level drops below an acceptable level [15].The cooling system specifications are as follows [15]:

Tank	Capacity	22 litres
	System capacity	24 litres
	Low fluid level alarm setting	12 litres approx.
	Low fluid level shut-down setting	10 litres approx.
Tank accessories	Level switch	low level shut down
	Thermostat	Over temperature shut-down
	Sight gauge	Fluid level
	Temperature sensor (RTD)	Fluid temperature control
	Access cover	Cleaning empty tank
	Drain valve	
Flow Rates	Low pressure pump delivery	8.5 litres/min
	Akribis flow transducer cooling	1.5 litres/min
	Re-circulating tank cooling	7.0 litres/min
Pressure settings	Pump safety relief valve	10 bar
	Akribis flow transducer cooling	2 - 6 bar

Temperature control	20 to 25°C ±2°C using water/oil heat exchanger

The test fluid system comprises of the test fluid, the test fluid tank, temperature and level monitoring devices, a pump, a fluid filtration system and a pressure control system. This system delivers test fluid to either the spray analysis section or the Akribis section when it is required for testing. The fluid temperature is constantly monitored by a thermostat and the test stand is set to trip when the cooling fluid temperature reaches 30°C [15]. Normal operation can continue once the cooling fluid temperature has dropped to below 30°C. In a similar manner, the cooling fluid level is also continuously monitored and the test stand will trip if the cooling fluid level drops below an acceptable level [15]. The test fluid system specifications are as follows [15]:

Tank	Capacity	22 litres
	System capacity	24 litres
	Low fluid level alarm warning	12 litres approx.
	Low fluid level shut-down setting	10 litres approx.
Tank accessories	Level switch	low level shut-down
	Thermostat	Over temperature shut-down
	Sight gauge	Fluid level
	Temperature sensor (RTD)	Fluid temperature control
	Access cover	Cleaning empty tank
	Drain valve	
Flow rates	Low pressure delivery	8.5 litres/min
	Re-circulating tank cooling	7.0 litres/min

Pressure settings	Low pressure pump safety relief valve	10 bar
	High pressure pump supply	1 – 6 bar

Temperature control	20 to 25°C ±2°C using water/oil heat exchanger

Test fluid	Shell Calibration Fluid S-9365 or equivalent ISO4113
	Diesel
	Bio-diesel

Methanol or Ethanol may also be used, but only with gasoline (GDI) type injectors. The pressure may not exceed 200 bar. If used for extended periods of time, the high pressure pump may be damaged due to the poor lubricity properties of these fuels.

The test fluid used had the following specifications [13]:

Appearance	Clear, amber, mobile, fluid
Density @ 15°C	830kg/m^3
Kinematic viscosity at 40°C	2.55mm^2/s
Flash point	85°C

The tanks and pumps for the cooling fluid and the test fluid can be seen in Figure 20 below.

Figure 20: Cooling fluid and test fluid tanks

The test fluid in the common rail is raised to the injection pressure by a high pressure pump. The high pressure pump is driven by a motor with the following specifications [15]:

Motor	Leroy-Somer FLSD 132M EEXd IIB T4
Power	5.4 kW
Speed Range	300 – 3000 rpm
Speed Control	Full closed loop control
Controller	Control Techniques – Unidrive

There is an emergency stop button located on the test stand. There is also a purge control selector switch – aux control enclosure and a purge control selector switch for the Akribis enclosure. These test stand controls can be seen in Figure 21 below. [15]

Figure 21: Test stand controls

2.1.1. Spray analysis system

The spray analysis system is comprised of a chamber; two pulsed flash light sheets with a mechanism to move it up and down; a back light, cameras and a fixture to hold the injector that is being tested. [15]

The chamber is used to contain the injected fluid. It is constructed from sheet steel and has glazed and sealed windows so that the cameras are able to capture images of the spray inside. It is matt black in order to minimise reflected light. [15]

The pulsed flash light sheets are used to illuminate the spray so that a camera can capture an image of an axial view. The back light is used to illuminate the spray so that the second camera can capture an image of a radial view. [15]

The air knives (mentioned earlier) are high velocity sheets of air which flow across these windows. The air knives prevent a build-up of test fluid on the windows which would result in the cameras capturing distorted images of the spray. [15] There is also an extraction fan connected to the chamber. The extraction fan removes the vaporized test fluid from the air inside the chamber. The extraction system had the following specifications:

Model	Vortice Lineo 200-VO
Type	Inline tube fan
Motor Power	0.145 kW

Volume Flow Rate   0.260 m^3/s

The injector fixture has been designed to hold a single injector. It is adjustable and can therefore accommodate various injector geometries with ease. There is a high pressure connection as well as a connection for drainage and an electronic connection for signals to be sent to, in order to initiate an injection (Figure 44: Akribis Injector Connections). Figure 22 below shows the front view of the apparatus. Figure 23 shows a side view of the apparatus.

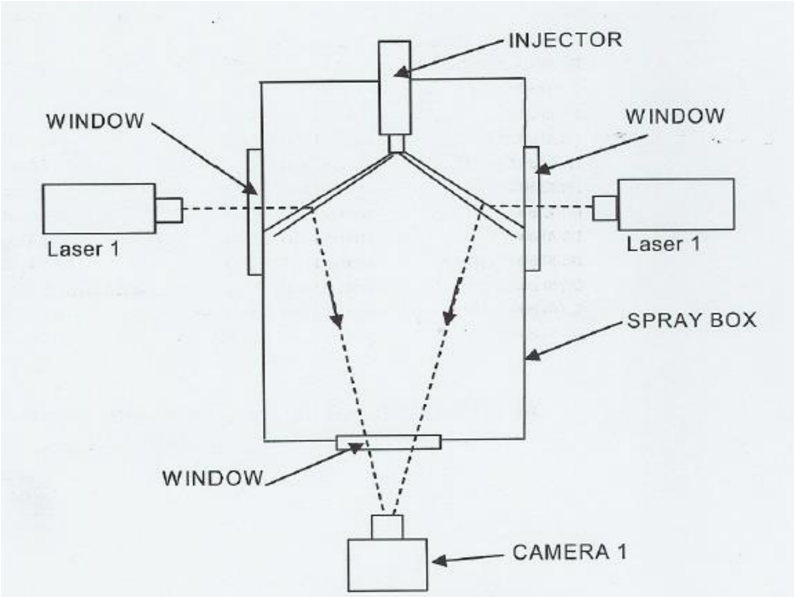

Figure 22: Front View of Spray Analysis Section [15]

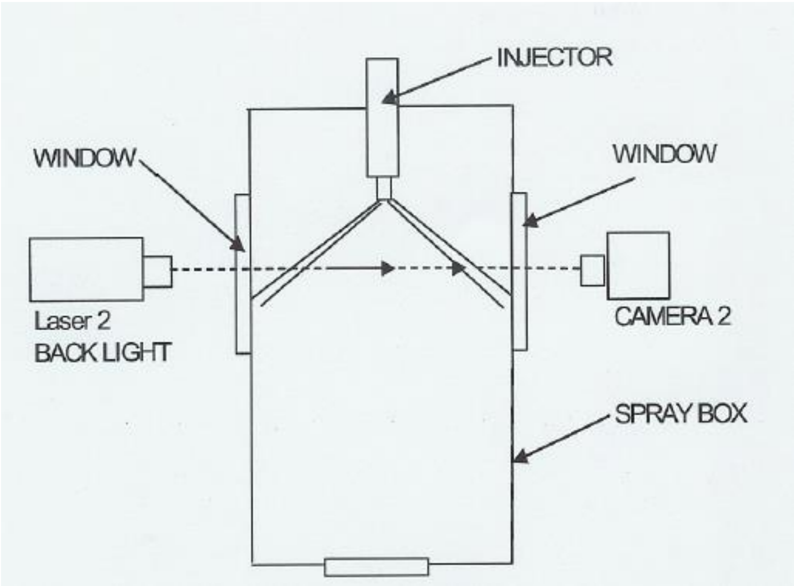

Figure 23: Side View of Spray Analysis Section [15]

For the purposes of this study, Camera 2 will be used in conjunction with the back light. Camera 2 is an Imager Compact camera and is supplied by La Vision. It is fitted with a 28mm 1:2.8 aperture Nikkor Lens. The camera is mounted under a shroud to reduce the effect of external light sources.

DaVis software

The camera is controlled via the La Vision PC with the use of the DaVis software, developed by La Vision. DaVis is also used for data capturing and data processing. The accuracy of the test stand is due to the DaVis software. It uses a method known as strobing to capture the data. Strobing involves taking images at predetermined times during the injection. Images are taken over multiple injections. A user defined number of images may be taken at a user defined time interval across the duration of the injection. The images at each time step are averaged and combined to form a single sequence of images to represent a single injection event. This has the advantage of removing anomalies and gives the researcher a more general idea of the behaviour of the spray. The software also allows for the background to be removed. A set of images are captured and averaged before injection occurs, the averaged image is then removed from the experimental images and all that is left is the spray.

Schlieren imaging vs. Mie-scattering

Schlieren photography is a popular method of imaging used in this field of study. This method has been used by various researchers including Klein-Douwel et al. [24], Valentim [29] and Alimia [30]. It is an effective method of visualising differences in density in a clear medium. Schlieren imaging is a form of shadowgraphy, the most common used visualisation technique used in spray analysis [32]. It relies on the refraction of light as it enters and leaves mediums of varying densities. A representation of the Schlieren imaging system can be seen in Figure 24 below. Light from a light source is focused with a lens past a knife edge. The knife edge stops any stray light from passing. The light that passes the through the knife edge lands on a parabolic mirror and is reflected through the area of interest. The light reflected off the mirror forms parallel rays of light. Any rays that pass through an area of different density will be refracted and its path will change. The light then reflects off a second mirror past another knife edge. The refracted rays are stopped by the knife edge and the remaining light is focused through the lens of some image capturing equipment. The light that was refracted and stopped by the second knife edge appear as shadows/darker areas in the resulting images. [33]

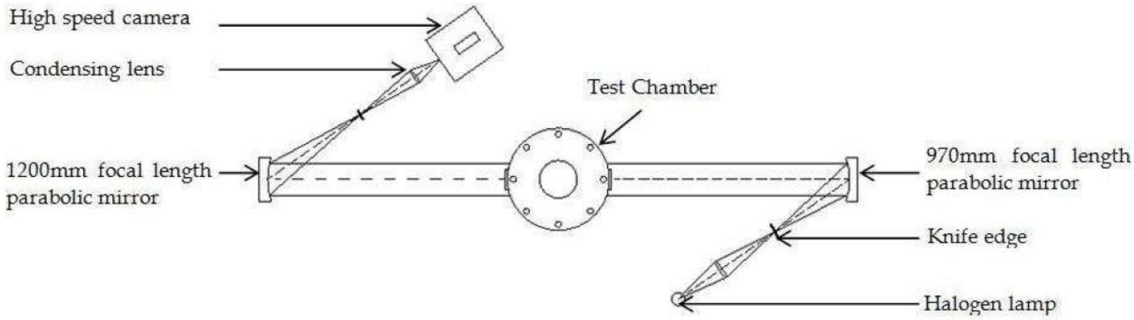

Figure 24: Schlieren imaging apparatus [29]

The La Vision system makes use of Mie-scattering method. When light hits a spherical particle, such as a fuel droplet from an injector, it is scattered. This scattering causes strong oscillations; the position and angular spacing of these oscillations are dependent on the properties of the particle that scattered the light. The number of oscillations per degree is directly related to the size of the particle using the Lorenz-Mie theory. The imaging method that was created using this theory became known as Mie- Scattering Imaging and it allows for measurements of very high accuracy. [34]

2.1.2. Flow measurement system

Due to the extremely high pressures at which this system operates, most of the components are housed in the Akribis flow enclosure. The high pressures mean that the test fluid is raised to temperatures higher than its flash temperature. High pressures also mean that if there is a mechanical failure, there is a possibility that components will be projected at extremely high velocities; escaping gasses at temperatures above their flash point could lead to explosions. [15]

For these reasons, the Akribis flow enclosure is constructed from sheet stainless steel. The window, used for visual access, is constructed from a double skin of impact resistant polycarbonate. The door is held closed by three manually operated latches, and seals the enclosure when closed. [15]

The internal volume of the enclosure is purged with nitrogen in an attempt to remove enough oxygen so that ignition will not be possible. [15] This is achieved with the Expo Size 1 001/XCF/ss/PA purge control system. This system can be seen in Figure 25 below.

Figure 25: Expo Purge Control System

Inside the Akribis flow enclosure is the Akribis flow measuring unit, on top of which, a fuel injector is mounted. The common rail is also situated inside the enclosure; the pressure is monitored with the use of a pressure transducer. There is also a pressure gauge which indicates the back pressure being applied to the Akribis unit. [15]

The injector fixture in the Akribis section of the test stand is as described above for that of the Spray Analysis section. A schematic of the Akribis unit can be seen in Figure 26 below.

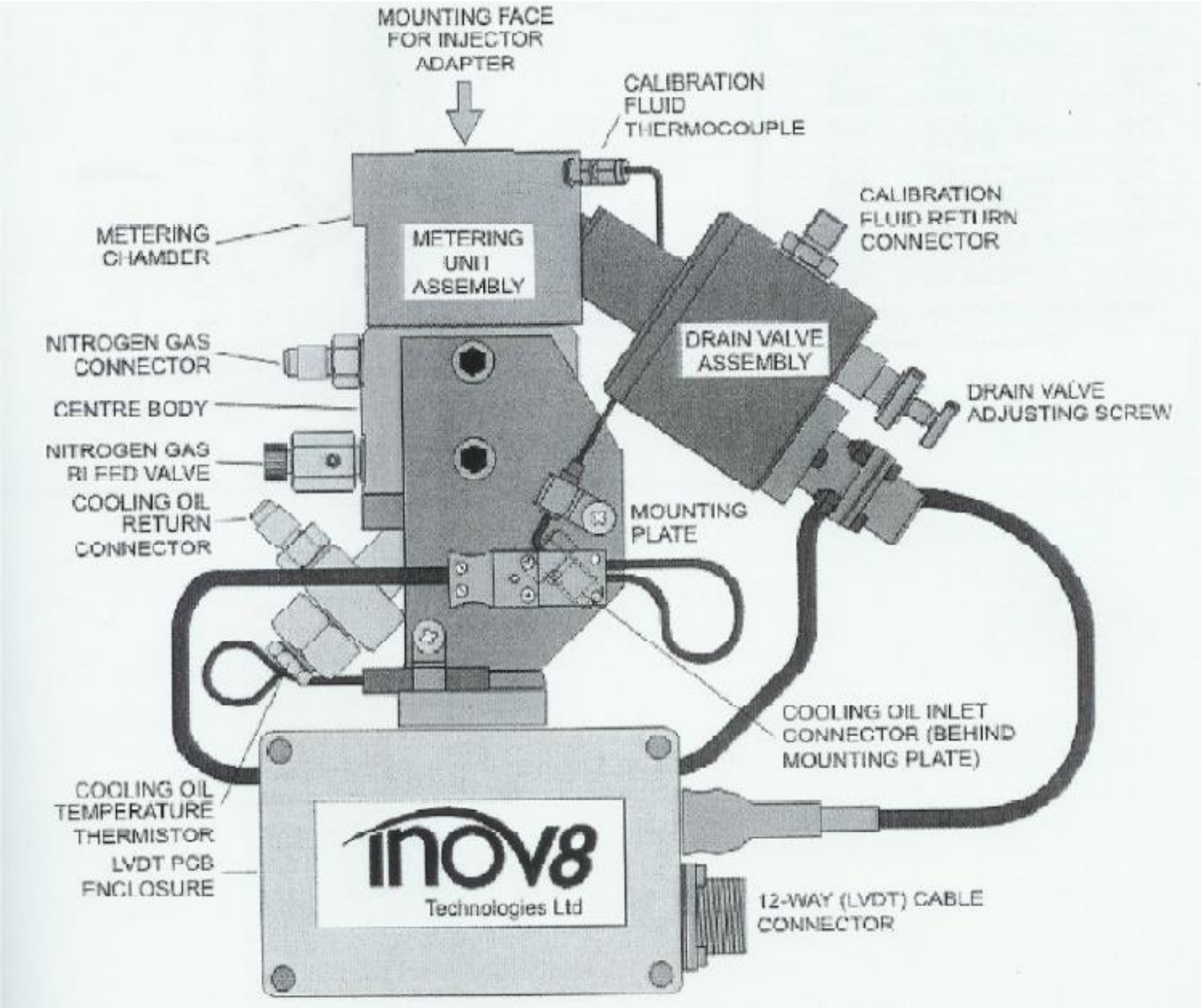

Figure 26: Akribis unit [16]

2.2.Power enclosure

The power enclose hoses various buttons that control the test stand. It has an emergency stop button which will turn off the common rail pump drive motor and the fuel pump motors when pressed [15]. It also has an isolator which turns on the power enclosure and the computers (Test Stand and Akribis computers). There is a control panel which is used to turn on the test stand and various pumps. Figure 27 shows the power enclosure control panel.

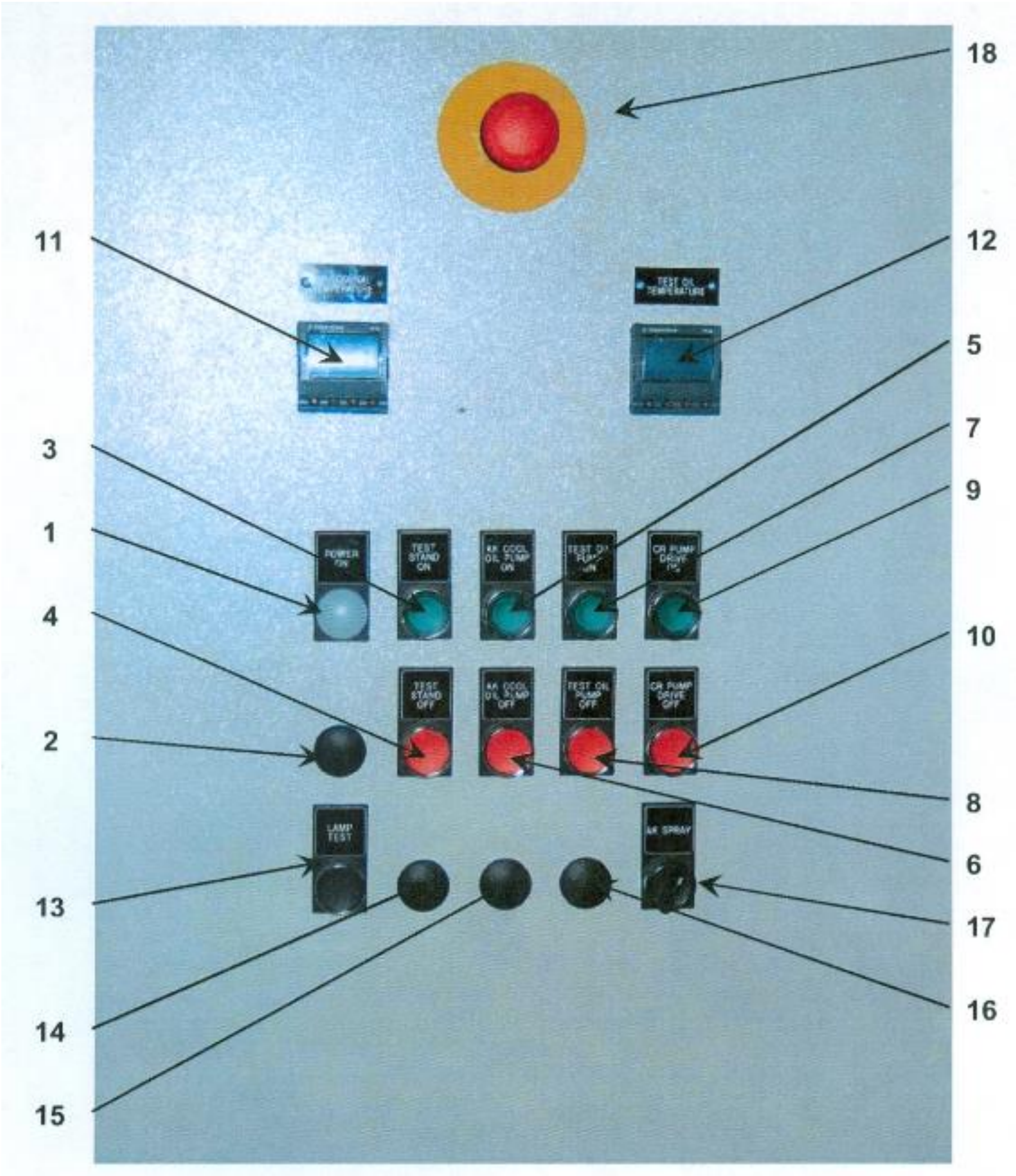

Figure 27: Power enclosure control panel [15]

Where:

1. Power on lamp

2. Spare

3. Test stand on button

4. Test stand off button

5. Akribis cooling fluid pump on button

6. Akribis cooling fluid pump off button

7. Test fluid pump on button

8. Test fluid pump off button

9. Common rail pump drive on button

10. Common rail pump drive off button

11. Akribis cooling tank temperature controller

12. Test fluid tank temperature controller

13. Lamp test pushbutton

15. Emergency stop button

2.3. Control Enclosure

The control enclosure is a free standing cubicle and holds various components of the system. The most important components in the control enclosure are the test stand computer, the Akribis system computer and the spray analysis computer. These computers are used to operate the test stand and perform the various functions. The test stand computer controls the pump, the fuel pressure and performs various other functions. The pump speed and fuel pressure can be controlled with this computer. The signals sent to the fuel injector can also be controlled from this computer and the injections are turned on and off from here. The air knives for the spray analysis experiment are controlled from this computer. The test stand computer shows the user general information about the test stand and shows the user if anything is wrong. Warnings are displayed if the test fluid or cooling fluid levels are too low or too hot; if doors are open, or if the air supply or nitrogen supply are not acceptable.

The Akribis and the spray analysis computers are primarily used to capture and process data obtained from the respective experiments. The data, once processed can then be exported for further analysis. The control enclosure can be seen in Figure 28 below.

Figure 28: Control enclosure

2.4.Fuel Injector

The injector used for the study was a 6 hole Bosch injector as used on a Mercedes Benz Vito. An example of the type of injector used can be seen in Figure 29 below.

Figure 29: Fuel Injector

The specifications of the injector are as follows:

Type:	6 hole solenoid actuated diesel injector
Model:	Robert Bosch 1St/Pc
Serial No.:	0445110 181
Nozzle No.:	060 1320
Orifice diameter:	0.170 mm
Injection pressure:	1400 bar

All but one of the holes on the injector was sealed with solder by Alimia [30]. This was done to ensure clearer images and less interference, thus allowing the software to more accurately analyse the results.

2.5. Pressurized Spray Chamber

A spray chamber was required so that the spray analysis could be done with a pressurized environment. The spray chamber would need to handle a pressure of up to 20 bar without affecting the normal operation of the Inov8 Test Stand.

2.5.1. Spray chamber

The spray chamber used was that used by Valentim [29] (Figure 30). Unlike the spray chamber in the test stand, the spray chamber used by Valentim was round. The chamber was made of steel with 2 round windows that were made of NBK-7 glass (used for optical components eg. lenses). As in the case with the spray chamber in section 2.5.3 of this report, these windows were optically pure and would not distort the images taken.

The chamber had a 3rd port which was sealed with a 12mm thick steel blank that was machined for an o-ring. This port allowed the operator access to the inside of the spray chamber by undoing a few bolts. The injector was fitted on the top cover of the spray chamber at an angle (Figure 31) so that the portion of the spray exposed to the camera was maximized as seen in Figure 32 below. The modification was made by Alimia [30]. Figure 32 (a) shows the original configuration and Figure 32 (b) shows how the injector is currently positioned. The original hole on the top lid was sealed and a new hole was drilled at a 20° angle. The angle θ is typically between 140° and 160° and so most of the spray is not visible through the window. The chamber was fitted with a pressure gauge to monitor the internal pressure and the chamber was capable of holding 25 bar.

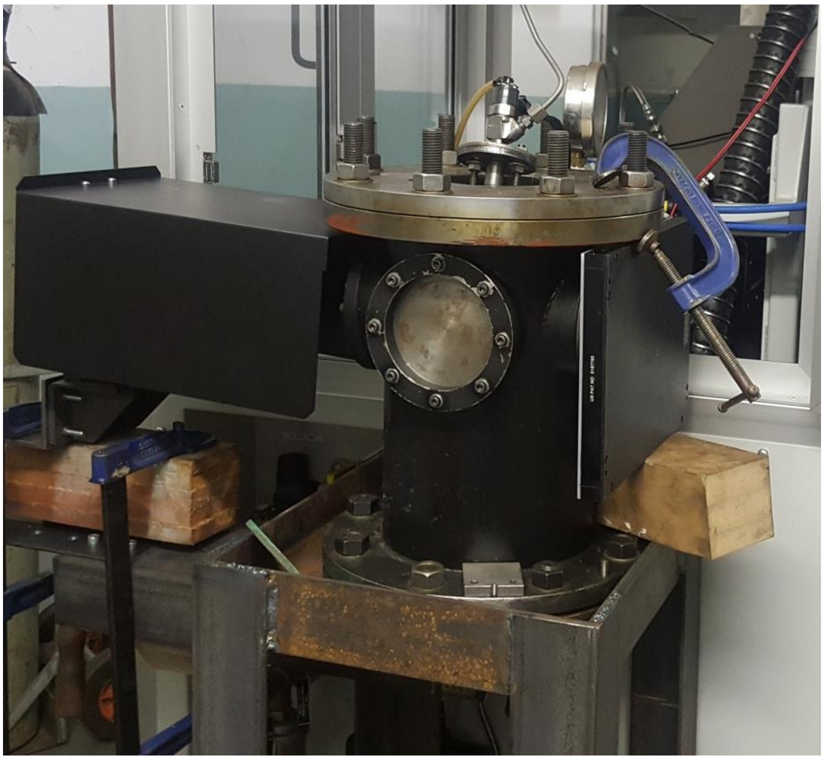

Figure 30: Valentim spray chamber

Figure 31: Injector mounting

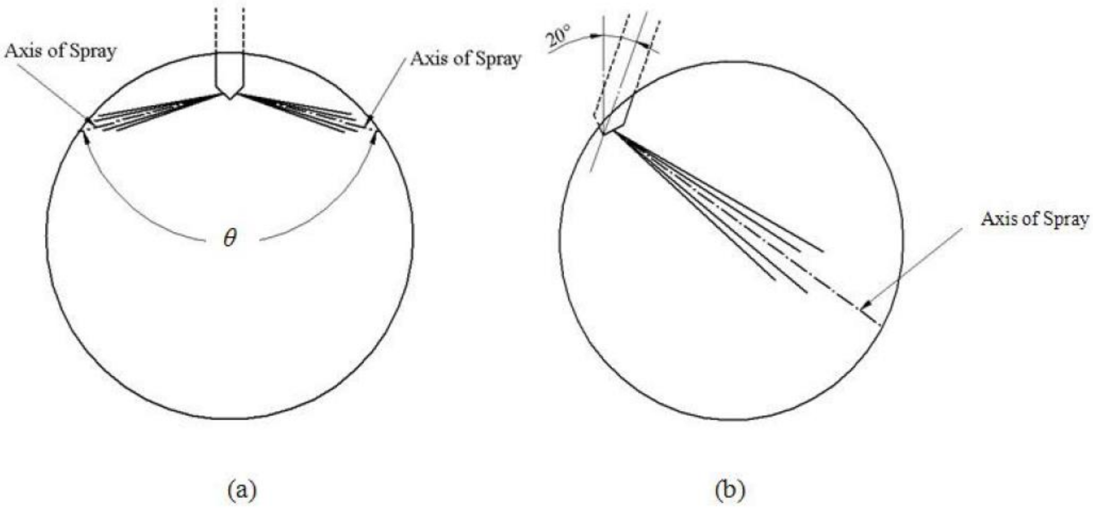

Figure 32: Injector location [30]

2.5.2. Spray chamber set-up

The original intention was to mount the spray chamber in the same location as the existing spray chamber. This proved to be unfeasible due to the size and weight of the spray chamber and the restricted space inside the test stand.

It was then decided that the spray chamber would sit outside the test stand and all the connections (electrical and fuel) would be rerouted to the new location as seen in Figure 30.

A stand was fabricated to hold the spray chamber with an adjustable bracket for the camera. The camera was relocated to the new stand and the distance between the camera and the tip of the injector were kept the same as the original set up. This was done by extending the table as seen in

Figure 33. The camera with the original bracket from the Inov8 test stand were bolted to the camera bracket in Figure 34 and then to the table extension. The bracket that the camera was mounted on allowed for fine adjustments in the vertical and horizontal direction. Even finer control of the frame of the camera was possible through the DaVis software. The original cover for the camera was used to reduce interference from outside light sources. New high pressure and return fuel lines were fabricated and connected to the test stand. The injector signal wire was extended and the original plug was used.

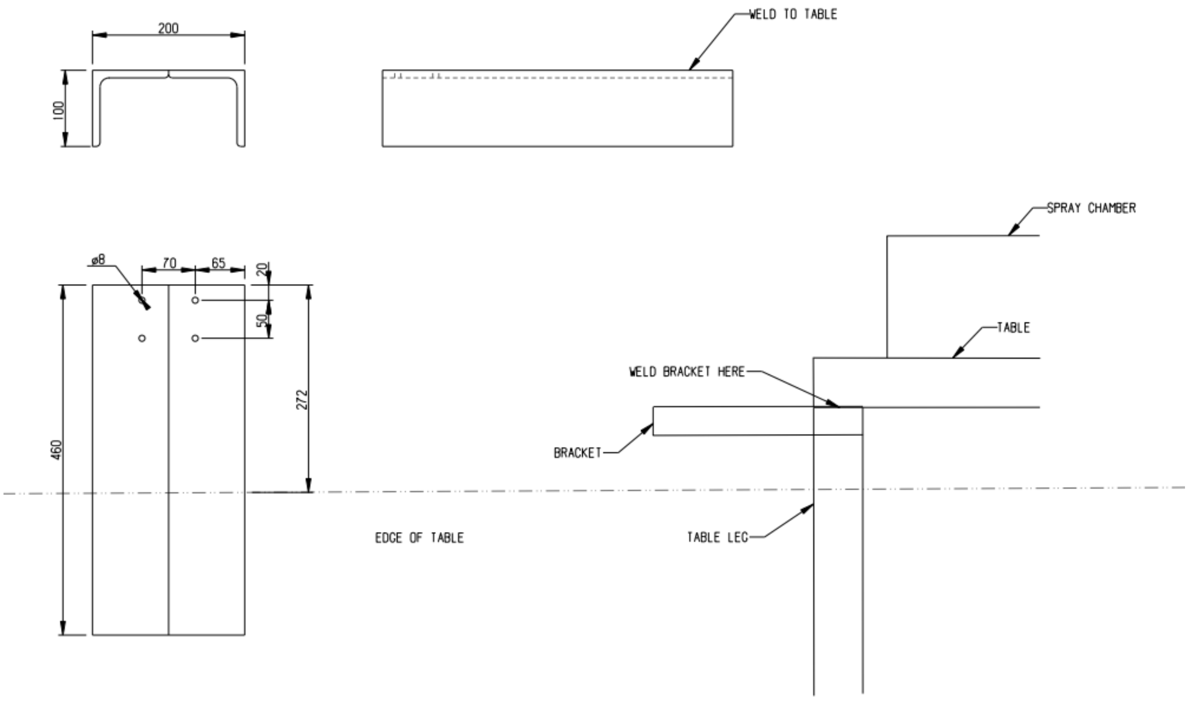

Figure 33: Table extension

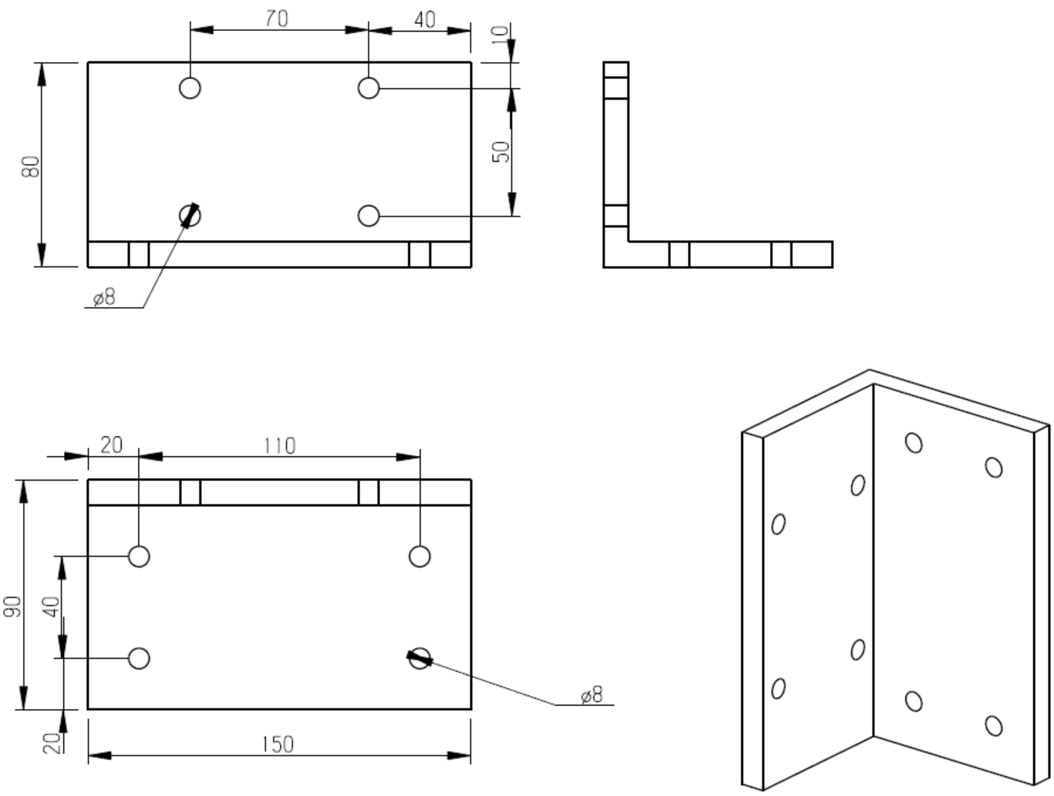

Figure 34: Camera bracket

2.5.3. Spray chamber design

A second spray chamber was designed to optimise the data capturing of the Inov8 Test Stand. The spray chamber was designed to contain a pressure of 20 bar while maintaining the critical dimensions of the existing spray chamber. It had a larger internal volume than the chamber described in Section 2.5.1 to better dissipate the atomized fluid, allowing for clearer pictures. The location of the injector and the design of the windows was optimized to allow the camera and software to work as they did before the modifications. It would also be possible to test multi-hole injectors with this set-up.

The analysis involved the superposition of the rigid frame model and plate model. A Finite Element Analysis was also conducted to verify the calculations. The details of the design of the spray chamber can be found in the design report, "Spray Chamber Design" in APPENDIX E – SPRAY CHAMBER DESIGN of this report.

A model of the designed spray chamber can be seen in Figure 35 below. The top and bottom covers as well as the window flanges were secured with M12 and M8 bolts respectively. The quartz glass windows specified ensure no distortion of the images while retaining 20 bar of pressure.

A piece of steel round bar, machined in the negative of the injector is positioned in the middle of the top lid. This ensures that the tip of the injector is located at the correct position so that the entire spray can be captured through the window. It also allows a seal to form around the injector so that the gasses inside do not escape and the pressure inside the chamber can be maintained.

On the top lid, to the side of the injector hole is another hole. This hole allows for the attachment of an inlet valve. The compressed gasses will be introduced to the chamber via this hole. There is a ball valve to regulate the flow of gas as well as a pressure relief valve set to 20 bar (the limit of the windows) and a pressure gauge to monitor internal pressure.

Figure 36 shows the completed chamber set up for testing with all the required connections.

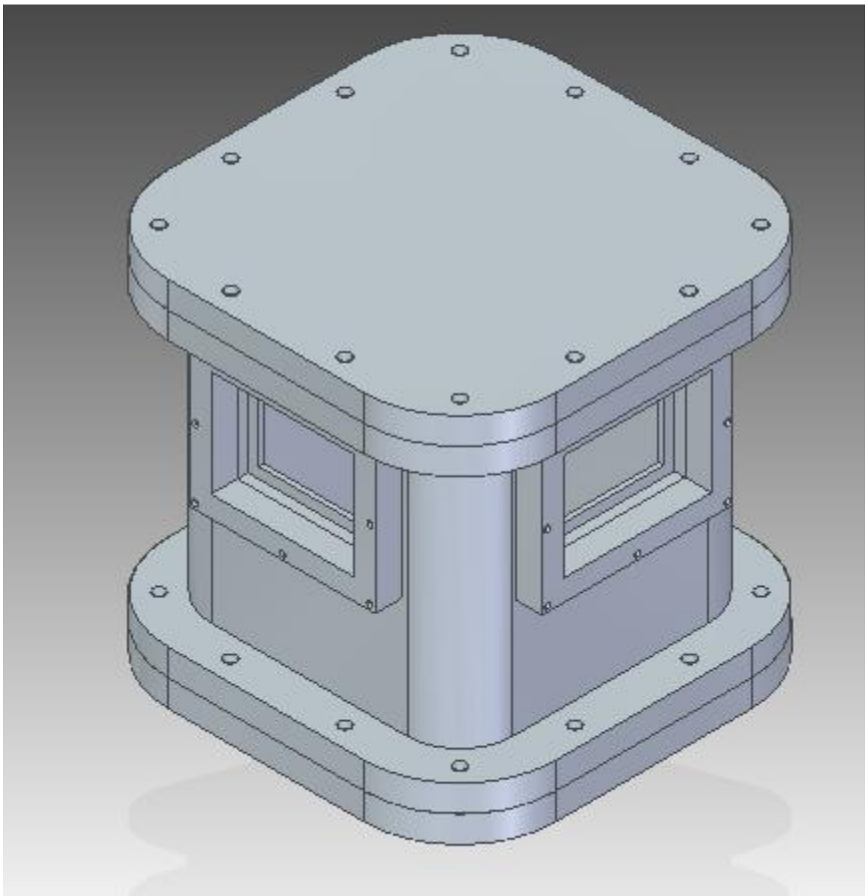

Figure 35: Spray chamber

Figure 36: Spray chamber with connections

2.6. Experimental Facility Set-up

Figure 37 below shows how the components of the experimental facility described in the previous sections were connected to each other for the purposes of this study. The figure shows the flow of power, test fluid, signals, cooling fluid and test gases as they were setup for the study.

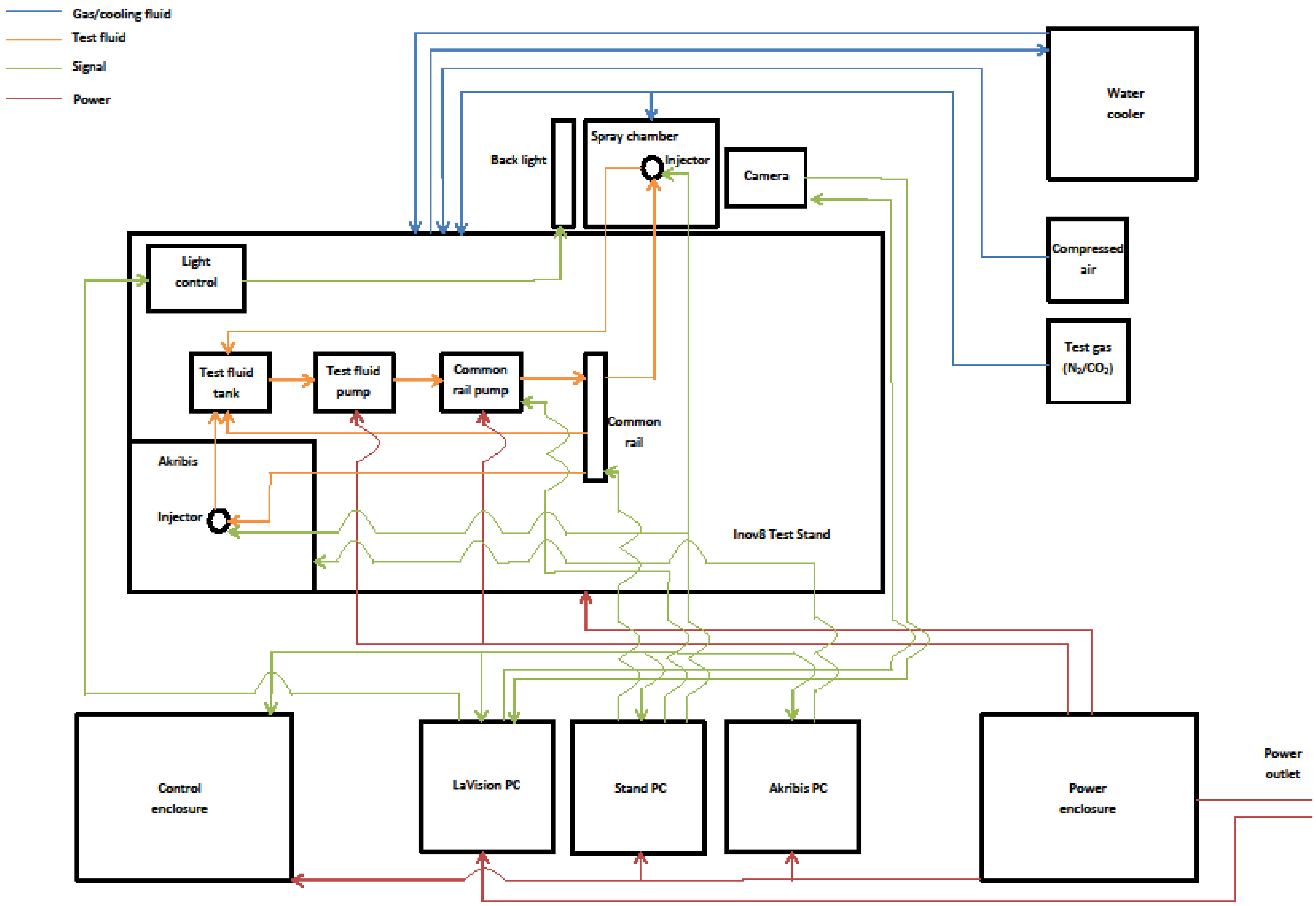

Figure 37: Experimental facility set-up

2.7. Experimental Facility Risk Analysis

The hazards associated with the operation of the test stand are identified in this section, and measures are suggested to reduce the risk of injury to the operator or damage to the equipment.

There are two pressurized systems involved in the experiments. These are the pressurized spray chamber, which can be up to 20 bar; and the common rail system which will go up to 1400 bar (limit of the injector to be used). These two systems pose the greatest risk to the safety of the operator and the equipment.

Figure 38 below shows the areas of the lab that may be hazardous. The test stand is controlled remotely from the PCs in the Control room. The operator will have to be in the control room to enable injections, control the injection pressure and perform data capturing. There is a brick wall separating the equipment from the operator. There is a window to allow the operator to monitor the equipment while testing.

The spray chamber will be pressurized using a regulator on the gas cylinder in use. The spray chamber is fitted with a pressure relief valve to prevent over pressurization. The pressure relief valve is set to 20 bar which is the maximum pressure allowable on the windows. There is also a pressure gauge on the spray chamber to monitor the pressure of the gas inside.

In Figure 38, red represents potentially very hazardous areas of the lab, orange represents areas that are potentially moderately hazardous, and green represents safe areas. From the figure, we can see that the operator is safe while conducting tests in the control room.

The operator must stay out of the red areas when the spray chamber or common rail is pressurized. The orange area should only be entered to operate the gas cylinders with the pump speed set to 0 rpm.

The door to the lab should be shut and locked when testing is in progress to prevent anyone entering the red area unexpectedly.

The gasses used to pressurize the chamber (nitrogen and carbon dioxide) would cause asphyxiation should the operator be exposed. The operator should monitor the system for gas leaks. The spray chamber is purged via a ball valve on the gas cylinder. The purged gasses are routed out the lab and into a closed off courtyard adjacent to the lab.

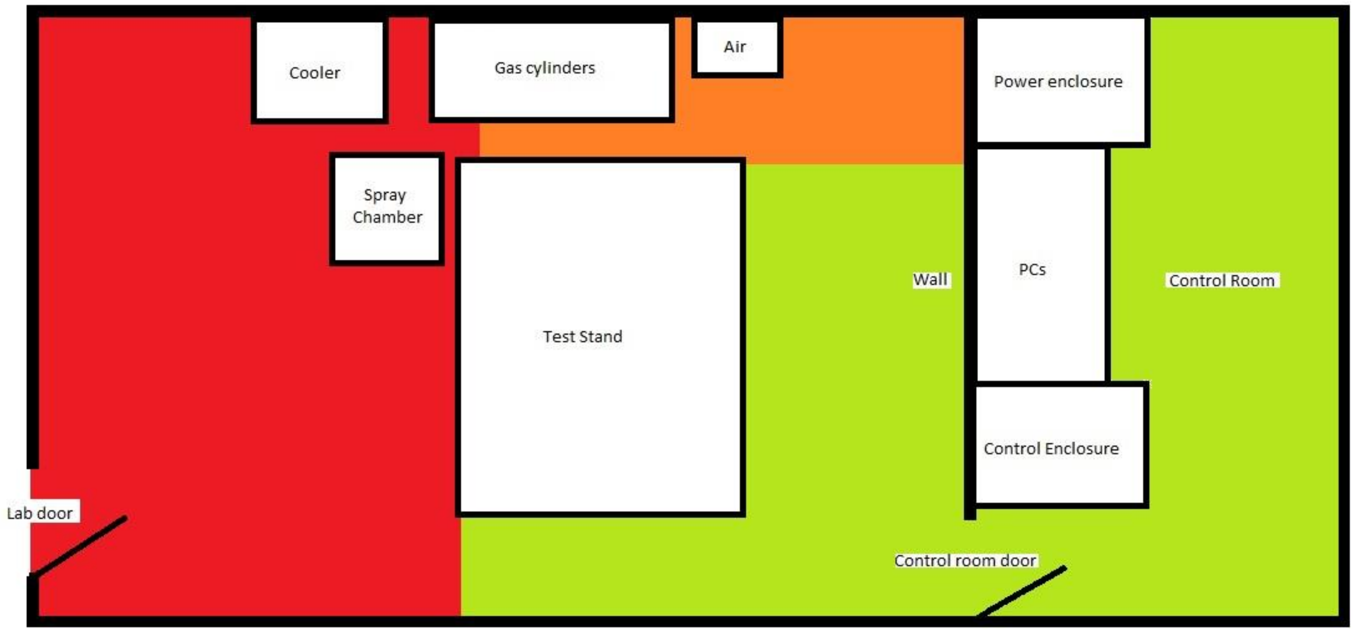

Figure 38: Lab danger zones

Table 1 below shows the identified hazards and safety measures to be taken to minimize risk to the operator and equipment.

Table 1: Risk analysis

Hazard	**Consequence**	**Severity (1-10)**	**Likelihood (1-10)**	**Safety measure**	**Notes**
Spray chamber failure	Windows blow out	10	2	Stay out of red zone when chamber is pressurized. Inspect pressure relief valve regularly.	Pressurize chamber in small increments and monitor pressure gauge. Stay under 20 bar.
Common rail system failure	Common rail/high pressure line explodes	8	1	Stay in the control room when the system is pressurized. Set rail pressure and pump speed to 0 when leaving the control room. Ensure test stand doors are closed.	Do not exceed 1400 bar rail pressure. Increase pump speed and rail pressure incrementally.
Test fluid leaks	Oil spillage.	2	5	Ensure all connections are made properly. All connections to the fuel injector must be tightened with a spanner.	Monitor the system through the window while incrementally increasing the rail pressure.
Oil spill on floor	Slipping hazard	4	7	Wear proper, closed safety shoes in the lab at all times to prevent slipping.	
Gas leak	Asphyxiation	10	3	Ensure gas cylinders are closed tightly when not in use. Ensure all connections are made tightly. Open lab door when purging/emptying spray chamber	The chamber is purged remotely and the purged gasses are routed outside.

3. METHODOLOGY

3.1. Experimental Planning

The main objective of this study is to determine the effects of cylinder pressure and cylinder gas density on spray penetration; more accurately that previously possible. This will be achieved by using the state of the art technology of the Inov8 Test Stand as described in Section 2 of this report. The data capturing equipment of the test stand is unmatched by equipment used in previous studies with similar objectives as discussed in Section 1.2.12 of this report.

The Inov8 Test Stand was designed to analyse spray patterns with atmospheric back pressures, so some modifications to the stand were necessary without affecting the accuracy of the equipment. This was achieved by retrofitting a pressurized spray chamber to the test stand.

The spray chamber used by Valentim [29] was fitted to the test stand and the necessary modifications to the camera and light position were made. Using the Valentim chamber allowed for the experimental results (diesel) obtained by Valentim to be verified by the current study. It allowed a direct comparison to be made between the tests with the only major variable being the data capturing system.

A custom spray chamber was designed for the experiments and fitted to the test stand with the intention of optimising the data capturing. During the initial set up of the spray chamber, the tip of the injector which was in the same plane as the top of the window was not visible. This was due to the perspective of the camera. The solution was to modify the injector holder on the top lid of the chamber so that the injector would sit 25mm lower. This required sending the chamber back to the manufacturer and recertification.

The spray chamber of the test stand has an extraction system to remove the vapour from the air while an injection is occurring. Due to the fact that the new spray chamber would have to be pressurized, it was not possible to retain the extraction system. If too much fluid is introduced to the chamber, it would become ‘misty’ inside and this would obscure the images. It was therefore necessary to minimise the amount of fluid injected per test. This was accomplished with the use of a ‘1 hole injector’; all but 1 hole of the Bosch injector use was seal with solder. The injection pressures were then limited to a maximum of 800 bar. This was to ensure that the solder remained on the tip of the injector, keeping the holes sealed.

Testing involved measuring the spray penetration with different combinations of injection pressure and chamber pressure (back pressure). The injection pressure was varied between 700 and 780 bar and the chamber pressure was varied between 0 (atmospheric pressure) and 20 bar. First the injection pressure was varied with a constant (5 bar) back pressure. Then the back pressure was varied with a constant injection pressure (760 bar). Finally, both the injection pressure and the back pressure were varied while maintaining a constant (5 bar) difference between them. All the experiments were conducted first with nitrogen in the chamber and then repeated with carbon dioxide in the chamber due to their different densities.

The results were processed both manually and with the use of the functions built into the DaVis software. All results were compared to the theoretical models of Dent and Hiroyasu to determine their accuracy in predicting the spray penetration as well as break up time. The flow measurement facilities of the Inov8 Test Stand (Akribis) were used to give clarity on the behaviour of the spray.

3.2. Experimental Procedure

The apparatus allows for only one experiment (either flow measurement or injector spray analysis) to be performed at a time. The start-up and stopping procedures described should be followed for both the flow measurement experiment and the spray pattern analysis experiment.

Before following the methodology outlined below, ensure the following: [15]

1. Water, oil and electrical supplies are connected
2. Cooling fluid in the cooling fluid tank is at the correct level
3. Test fluid in the test fluid tank is at the correct level
4. The Akribis door has been closed and the three door clamps are securely closed
5. All access panels and fixed covers are fitted
6. All emergency stop buttons have been reset
7. Both the Akribis section and Spray Analysis section have injectors fitted.

Before beginning with the start-up process, the experiment that is to be performed must be selected i.e. Flow measurement or spray analysis. This is done by ensuring that the correct plug is inserted into the socket in the top right hand side of the control enclosure and by selecting the experiment using the switch on the power enclosure [16].

3.3. Start up

The following start up procedure and precautions should be followed for both flow measurement and injector spray analysis.

3.3.1. Procedure

1. Switch on external heat exchanger and set it to 12° C
2. Open the nitrogen tank (set pressure to 50 bar using pressure regulator)
3. Turn on compressed air supply (open valve and set to 6.5 bar)
4. Turn on extraction fan
5. Turn on main isolator on power enclosure
6. Wait for computers to start (computers will start automatically)
7. Turn on test stand on power enclosure
8. Launch software (stand computer)
9. Turn on purge control valves (on test stand)
10. Turn off purge control valve (after allowing a few minutes to purge)
11. Check test stand status on stand computer (F10, see Figure 39)(at this stage there will be one red light; ‘Doors Closed & Locked OK)
12. Turn on cooling fluid pump (button on power enclosure)
13. Turn on test fluid pump (button on power enclosure)
14. Wait for all lights to turn green (see Figure 39)

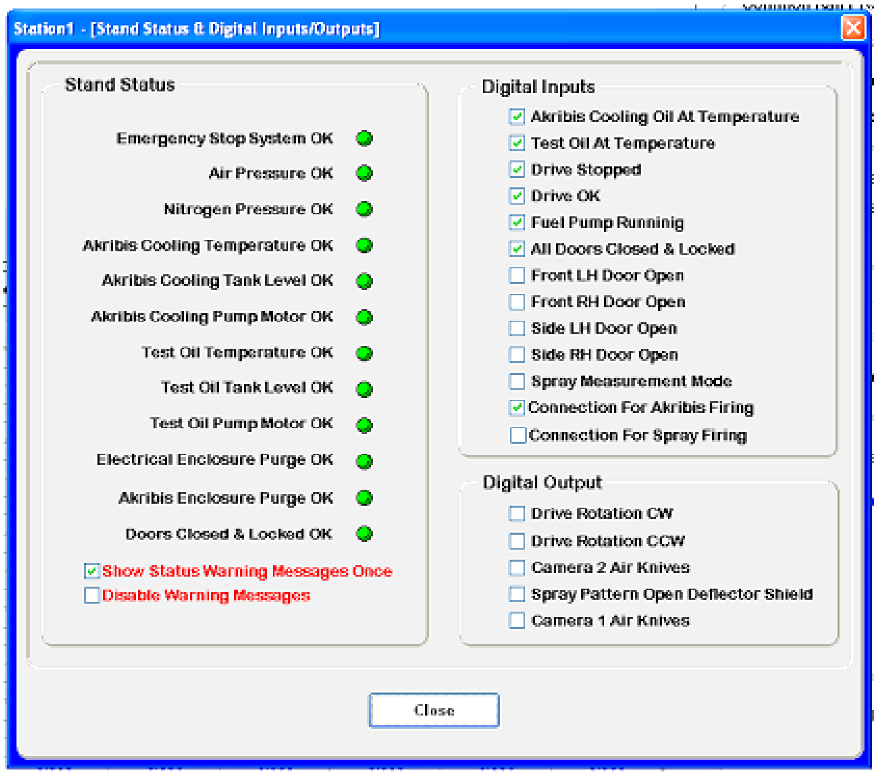

Figure 39: Test stand status

15. Turn on common rail pump (button on power enclosure)

3.3.2. Precautions

1. Ensure test stand has been switched on before pumps are switched on.
2. The common rail pump, test fluid pump and cooling fluid pump must be turned on in the order listed above.
3. Ensure that the cooling fluid level and temperature are acceptable (correct level and no warning messages).
4. Ensure that the test fluid level and temperature are acceptable (correct level and no warning messages).
5. Ensure that the Akribis door is closed securely.
6. Ensure the Akribis enclosure has been purged properly (filled with nitrogen) to prevent ignition.
7. Ensure extraction system is functional.

3.4. Stopping

The following stopping procedure and precautions should be followed for both flow measurement and injector spray analysis.

3.4.1. Procedure

1. Set pressure to 0 bar (on computer, Figure 42)
2. Turn off pump drive (Figure 41)
3. Close software
4. Shut down computers
5. Turn off common rail pump (button on power enclosure)
6. Turn off test fluid pump (button on power enclosure)
7. Turn off cooling fluid pump (button on power enclosure)
8. Turn off test stand (button on power enclosure)
9. Turn off main isolator
10. Turn off extraction fan
11. Turn off compressed air supply
12. Close nitrogen tank
13. Switch off heat exchanger

3.4.2. Precautions

1. The common rail pump, test fluid pump and cooling fluid pump must be turned off in the order listed above
2. Wait for common rail pump to turn off before turning off the test stand
3. Ensure the computers have shut down before turning off the main isolator

3.5.Injector Spray Analysis

The following procedure and precautions should be followed for the injector spray analysis experiment. [21]

3.4.1. Procedure

1. Turn on Spray Analysis computer by pressing the black power button on the control enclosure (Refer to Figure 40). The PC will turn on, no password is required, press enter.
2. Launch the LA Vision Software by double clicking the ‘DaVis” icon on the desktop.
3. Select ‘Expert User’ and login
4. Select ‘Project’, then select ‘<New Project>’ from the drop down menu.
5. Name the project; select ‘SprayMaster’ from the drop down menu, click ‘Ok’

Background image

6. Click ‘New’
7. Select ‘Background Images’ from the Recording mode drop down menu
8. Click ‘Device’
9. Click ‘Recording’ in the cascade menu. Select lights and camera to be used
10. Click ‘On’
11. Click ‘Acquisit’
12. Click ‘Recording Sequence’ in cascade menu. Tick ‘Use RAM’ and ‘Store immediately after each scan loop’
13. Click ‘Image Acquisition’ in cascade menu. Set number of images to 10. Tick ‘Start immediately’
14. Select ‘Device’. Click ‘Timing’ in the cascade menu
15. Set Trigger source to ‘Internal trigger’
16. Click ‘Start Recording’ to start recording data
17. Click ‘Close’
18. Select the background image from the cascade menu. Click ‘Batch’
19. Select ‘Statistics’ from the operation group drop down menu
20. Select ‘Parameter’ from operation list
21. Tick ‘Average’ and select ‘Camera 1’. Click ‘Start Processing’

Experimental image

The same steps (6 to 12) should be followed to obtain experimental images that were followed to obtain the background image. At step 7, ‘Experimental Images’ should be selected instead of ‘Background Images’. From step 12:

22. Ensure ‘Store in folder’ is set to operating folder and ‘Store immediately after recording’ is ticked
23. Click ‘Image Acquisition’ in cascade menu. Click ‘Delete’
24. Click ‘Recording sequence’ in cascade menu. Click ‘Insert Acquisition’
25. Select ‘Scanning’. Select ‘Reference time 1’. Click ‘Ok’
26. Repeat step 22
27. Select ‘Image Acquisition’. Select ‘Image Acquisition’ from drop down menu. Click ‘Ok’
28. Click ‘Reference time 1’in cascade menu.

29. Select ‘Scan’. Enter start time of 0.35ms. Set end time to 0.35ms + user defined pulse length. This is the time frame in which the data will be recorded. Set increment to 0.05ms.
30. Click ‘Image Acquisition’ in the cascade menu.
31. Set number of images to 10.
32. Select ‘Device’. Click ‘Timing’ in the cascade menu
33. Set Trigger source to ‘External cyclic trigger’ and ensure ‘Don’t allow external pretrigger’ is ticked.
34. Adjust the chamber pressure using the regulator on the gas cylinder as required.
35. Set pump speed, rail pressure, injection duration and enable injections as outline in Section 3.8.1 of this report.
36. Click ‘Start Recording’ to begin recording data.

Figure 40: Spray Analysis Computer Power Button

3.4.2. Precautions

1. Pressure is set to increase sequentially so problems can be found before the equipment is damaged.
2. Ensure injection has been stopped before adjusting the pressure or firing pulse
3. Ensure lights are on and correct camera has been selected as the computer will return to default settings when the recording screen is closed.
4. Rail pressure must not exceed 1800 bar
5. Ensure air knives are turned on

3.6. Image Processing

The images collected using the methodology described in Section 3.5 should be processed using the following steps using the DaVis software on the Spray Analysis computer. [21]

1. Highlight the first of the experimental images
2. Right click and select ‘Hyperloop’
3. Select ‘Current folder’
4. The filter drop down menu is used to filter images the user wishes to process. The operation drop down menu is used to select the processing the user would like to perform.

Experimental image averaging

5. Select ‘batch processing’ from the operation drop down menu.
6. Click the ‘Parameter’ button
7. Set it to averaging as done with background images.
8. Click ‘Close’ (top left)
9. Click ‘Execute’

Background subtraction

10. Repeat step 5
11. Right click ‘Averaging’. Select ‘Disable’
12. Select a new operation.
13. Select ‘Project’ when the group menu appears
14. Select ‘Background subtraction’ in the operation menu
15. Select ‘Back lighting’ for camera 2
16. Select ‘Default Background file’ in the background file menu. Tick ‘Use last result file from “Background” postprocessing’
17. Close the batch processing menu
18. Click ‘Execute’ in the Hyperloop menu

Rearrange data

19. Select ‘Rearrange’ from the operation drop down menu
20. Click ‘Parameter’
21. Ignore Time and set variable parameter to ‘T1’

Export data

22. Select ‘Export’ on the toolbar
23. Set Export type to JPG
24. Specify export path
25. Click ‘Export”

3.7. Geometry Analysis

Once the images have been processed following the steps in the previous section, the DaVis Geometry Package can be used to analyse them. The Geometry Package is only available when using the ‘Spray Master’ option as mentioned previously. The Geometry Package is accessed via the Batch Processing menu and the Hyperloop function can be used to analyse all the data at once.

The following steps should be followed to analyse the processed images.

1. Select the Geometry Package via the ‘Load” button above the operations list.
2. Select ‘SPM Inspex Evaluation’ from the ‘Load Image operation list’ selection box
3. From the Operations list, disable options 1-3.
4. Expand option 4; ‘Geometry’
5. Select ‘Maximized Parameter Dialog’
6. Select ‘Setup Parameters’ icon
7. In the Parameter box, tick the following:
    - Spray angle
    - Diameter at distance
    - Maximum diameter
    - Tip penetration
    - Arc profile
    - Tracer profile
    - Spray front
8. Set ‘Spray Type’ to Multispray
9. Expand the ‘Functions’ menu and set the parameters as follows:
    - Direction of angles: Clockwise
    - Scale Display: Buffer scale (mm)
    - Decimal Places of length values: 123.4mm

- Decimal “Point” character: Dot (.)
- Colours may be set as desired.

10. Expand the ‘Postprocessing’ menu and set the parameters as follows:
    - Use dynamic mask: Off
    - Use rectangle: Off
    - Rotation angle (°): 0
    - Percentage: Checked, set to 5
    - Filter mode: Off
11. In the radial parameter menu set the parameters as follows
    - Mode: Counting
    - Limit: 95
    - Use lines as diameters: Checked
12. Set up the submenus as follows:
    - Injector – leave unchanged
    - Penetration:
        - Mode: Pixel
        - Limit: 95
    - General:
        - Arc profile mode: Integral
        - Width of arc segment: 1
        - Stepwidth of tracer profile: 1 pixel
13. Return to the Functions menu and select ‘Define Segments of Multispray’ icon
14. Click ‘Set’ for the injector and click on the nozzle in the spray image.
15. Define the segments by selecting point through which the lines should pass
16. Two points along the length of the spray may be selected at which the spray will be analysed. (areas of interest)
17. Select the ‘Test Processing’ button.
18. Exit the batch processing menu and select ‘Execute’ from the hyperloop menu

3.8.Flow Measurement

The following procedure and precautions should be followed for the flow measurement experiment.

3.8.1. Procedure

1. Test drain valve by checking for flashing light (INJ CURRENT) when Manual Drain Control button is pressed (on control enclosure)
2. Set number of injections to 20 injections (Akribis PC, F4, setup)
3. Set pump speed to 1000 rpm (Stand PC, F7, See Figure 41)

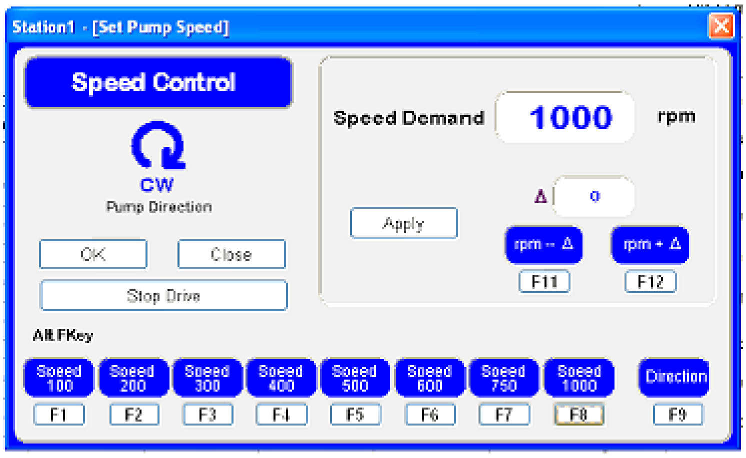

Figure 41: Set pump speed

4. Set firing pulse lengths and delays (Stand PC, F8, See Figure 42)

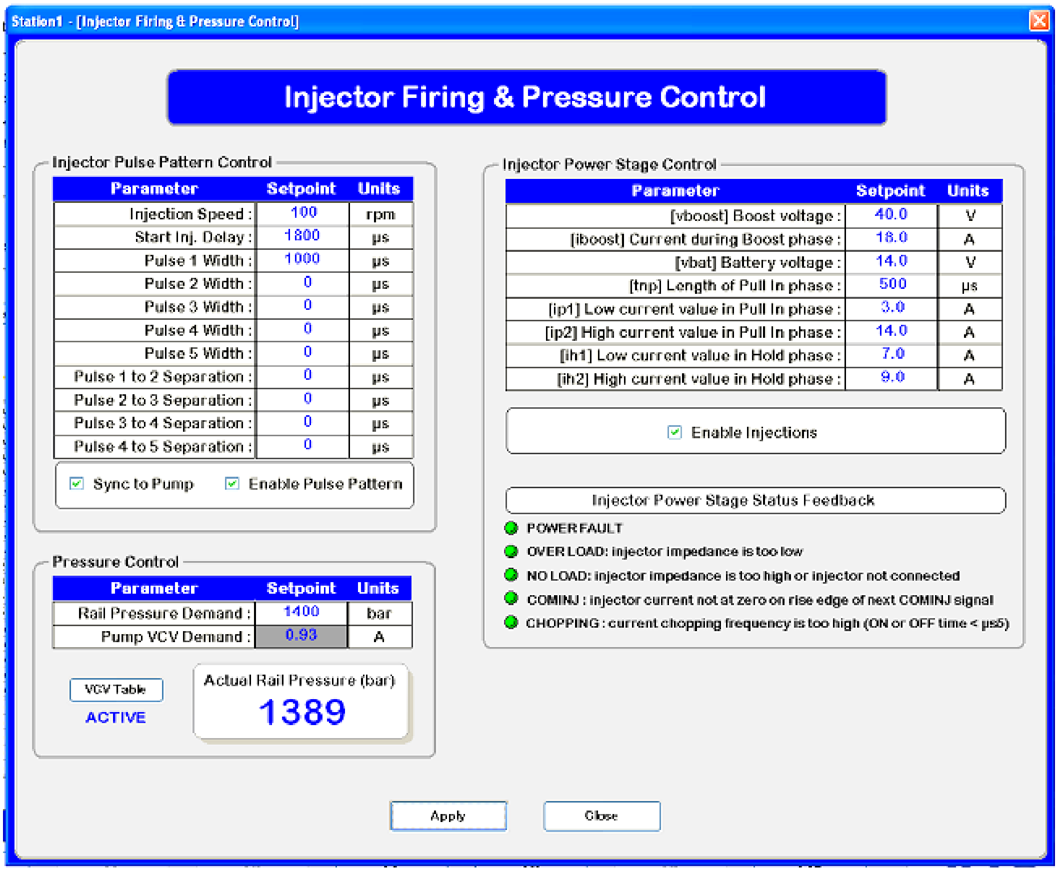

Figure 42: Injector firing and pressure control

5. Set rail pressure (Stand PC, F8, See Figure 42)
6. Enable injections (Stand PC, F8, See Figure 42)
7. Select location to save data (Akribis PC, F4, setup)
8. Run free test (Akribis PC, F9, See Figure 43)

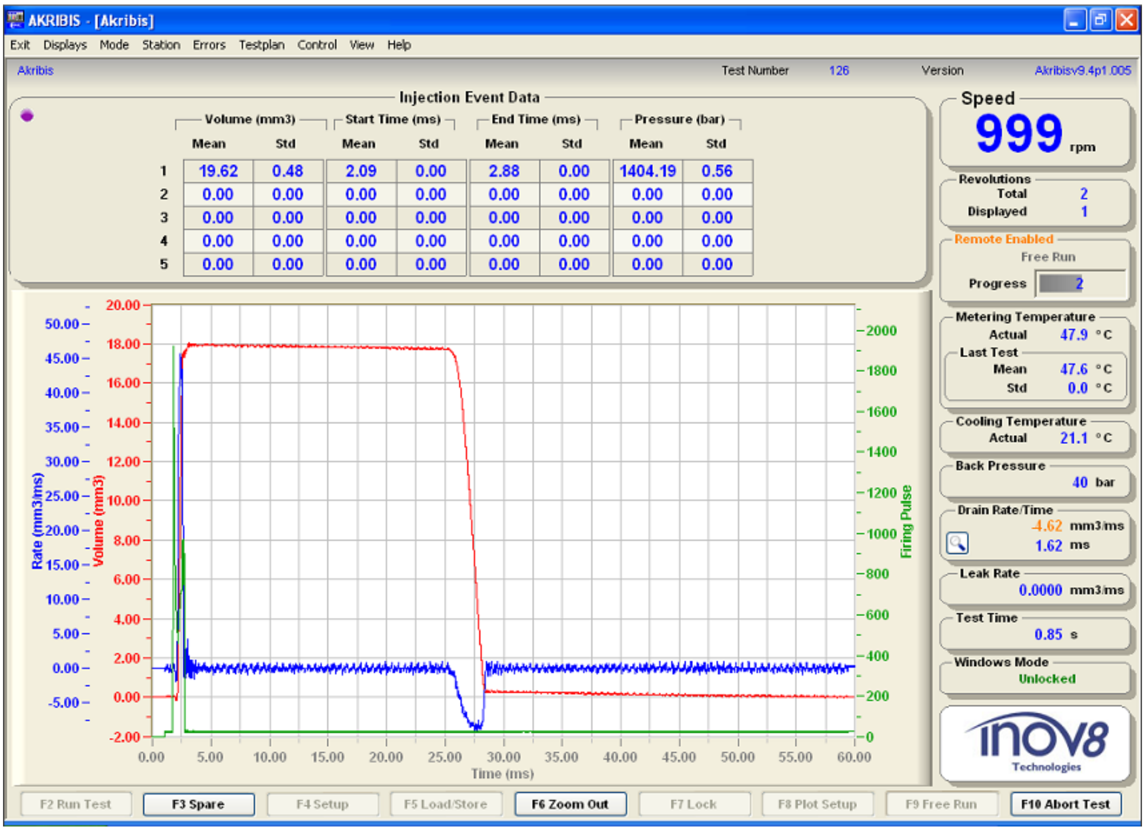

Figure 43: Akribis PC

9. If displayed results are acceptable, abort test (F10) and run test (F2)
10. Disable injections (Stand PC, F8, See Figure 42)
11. Export data (Refer to Appendix B)

3.8.2. Precautions

1. Pressure is set to increase sequentially so problems can be found before the equipment is damaged.
2. Ensure injection has been stopped before adjusting the pressure or firing pulse.
3. Ensure drain valve is working by checking if light is flashing on control enclosure.
4. When opening the Akribis enclosure door, allow enough time for the nitrogen to disperse. (risk of asphyxiation)
5. Rail pressure must not exceed 1800 bar

3.9. Connecting an Injector

The following procedure should be followed when fitting an injector to either the Spray Analysis section or the Akribis section of the test stand. Figure 44 and Figure 45 below shows the connections that must be made to the injector.

3.9.1. Akribis procedure

1. Insert the nozzle of the injector into the hole at the top of the Akribis unit while positioning the flat section of the injector in the clamp.
2. Tighten the bolt on the clamp to hold the injector securely in place (5N.m + 90° with a torque wrench).
3. Attach the high pressure test fluid connection to the high pressure connection of the injector. Note: Small connector must be used.
4. Tighten the bolt on the high pressure test fluid connection using a No. 17 spanner.
5. Insert the drainage connection into the top of the injector. Fasten using circlip.
6. Plug electronic connection into electronic connection point on injector.

To remove an injector from the test stand, follow the above mentioned procedure in reverse.

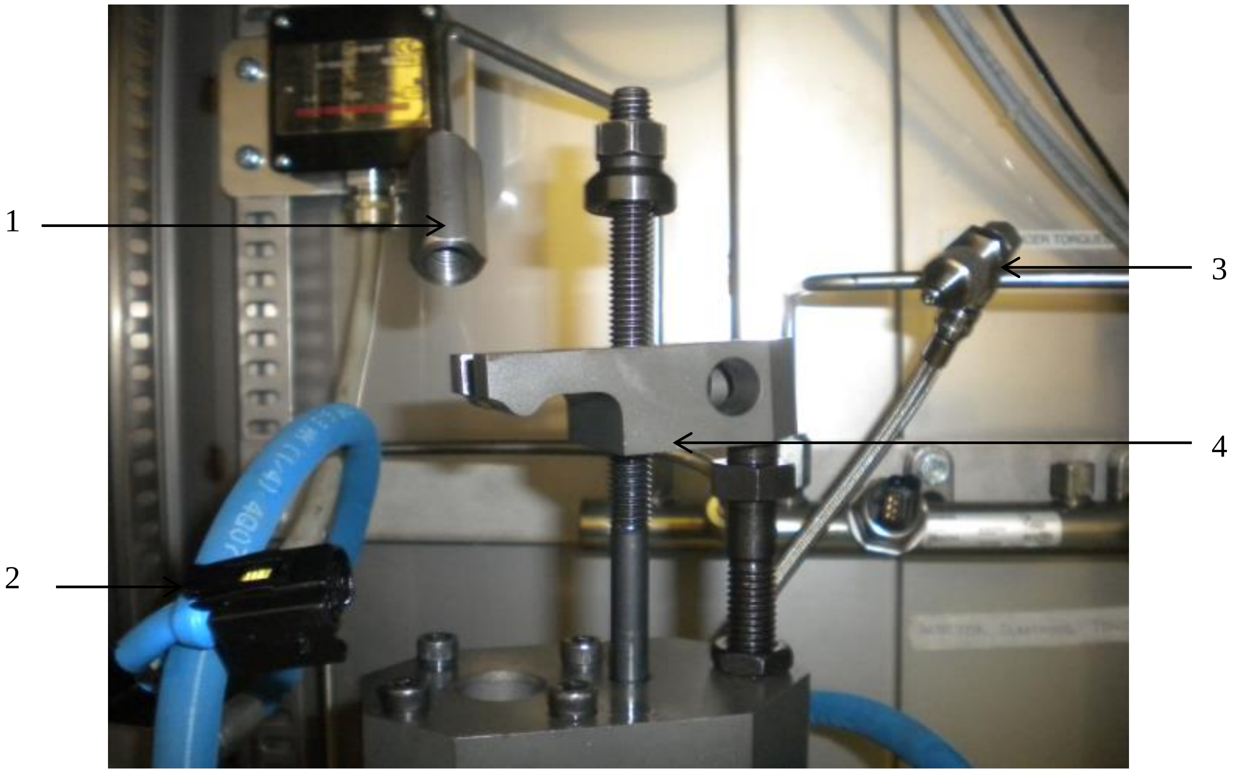

Figure 44: Akribis Injector Connections

Where:

1. High pressure test fluid connection
2. Electronic connection
3. Drainage connection
4. Clamp

3.9.2. Spray analysis procedure

1. The injector must be placed into the hole on the top of the spray chamber with a copper washer.
2. The flat section of the injector goes into the slot in the clamp and the fulcrum is placed under the clamp.
3. The weight disks are placed on the clamp.
4. Follow steps 3 – 6 as in Section 3.9.1 of this report.

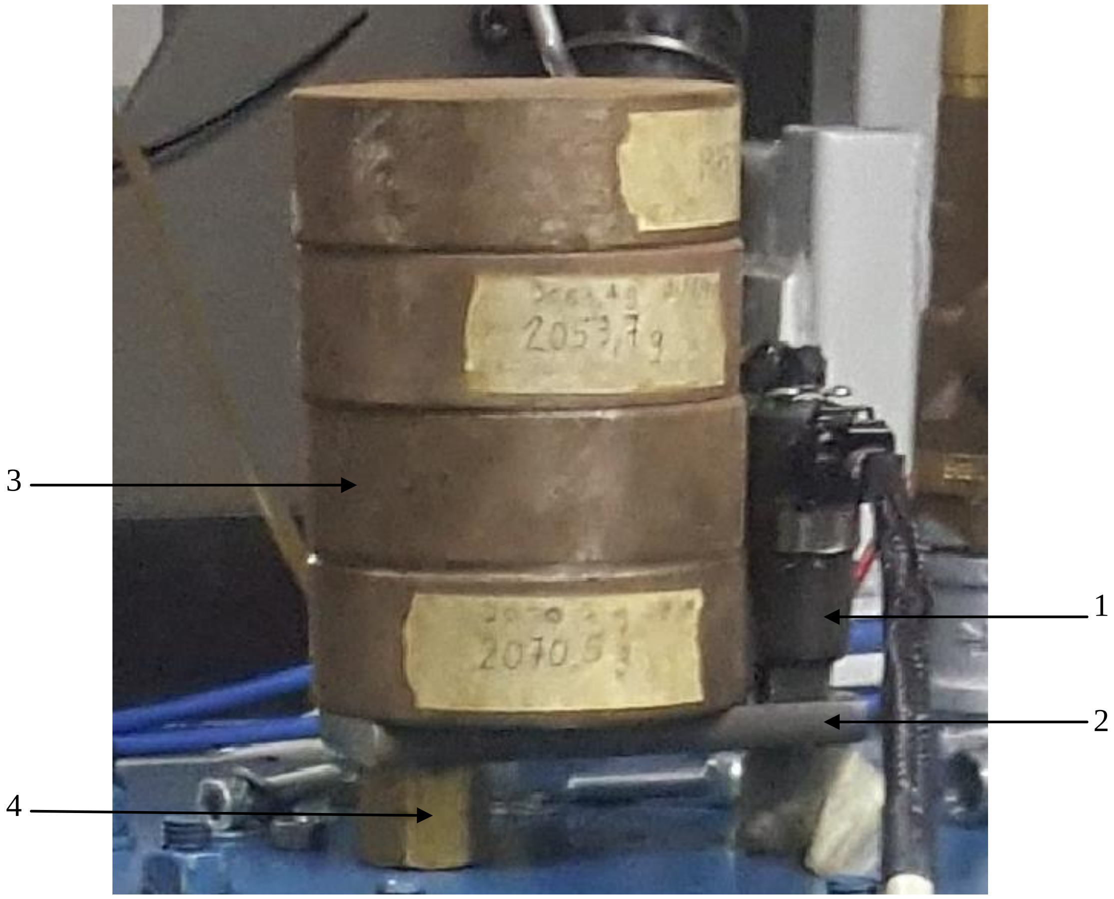

Figure 45: Flow Analysis Injector Connections

Where:

1. Injector
2. Clamp
3. Weight disk
4. Fulcrum

3.9.3. Precautions

1. Do not over tighten the clamp. This may damage the test stand and the injector
2. Ensure the test fluid connections are tight as loose connections may result in leakage
3. Ensure electronic connection is made correctly. Incorrect connection may result in injector not firing

4. OBSERVATIONS

The tests were run as described in the previous sections and the observations are presented below.

4.1. Spray Analysis

The output of the DaVis software is a set of pictures of the spray at each time step for the range specified.

Figure 46 to Figure 54 below show the images captures with an injection pressure of 720 bar and a chamber pressure of 5 bar (nitrogen).

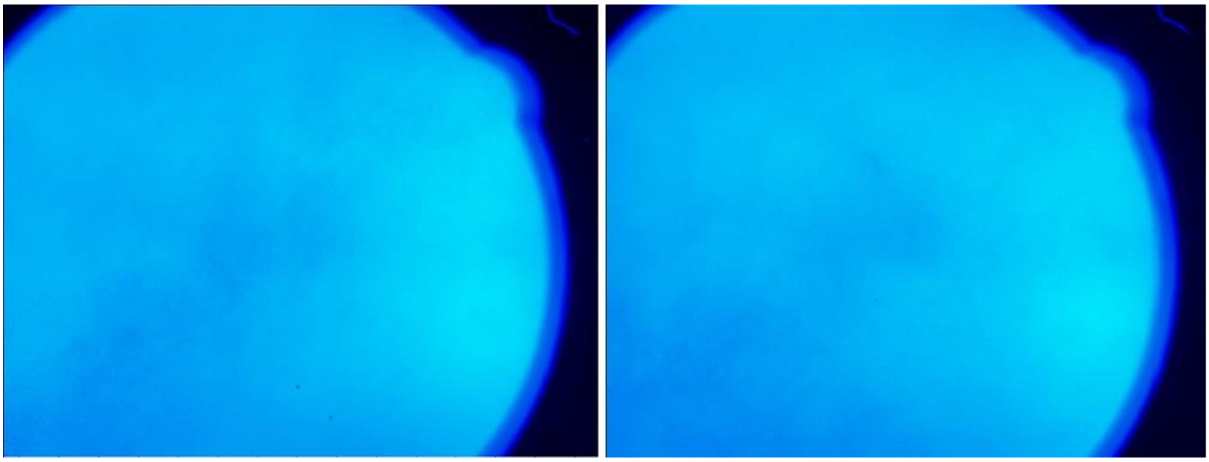

Figure 46: 720 bar injection pressure. 5 bar chamber pressure using nitrogen. 0.35ms – 0.4ms

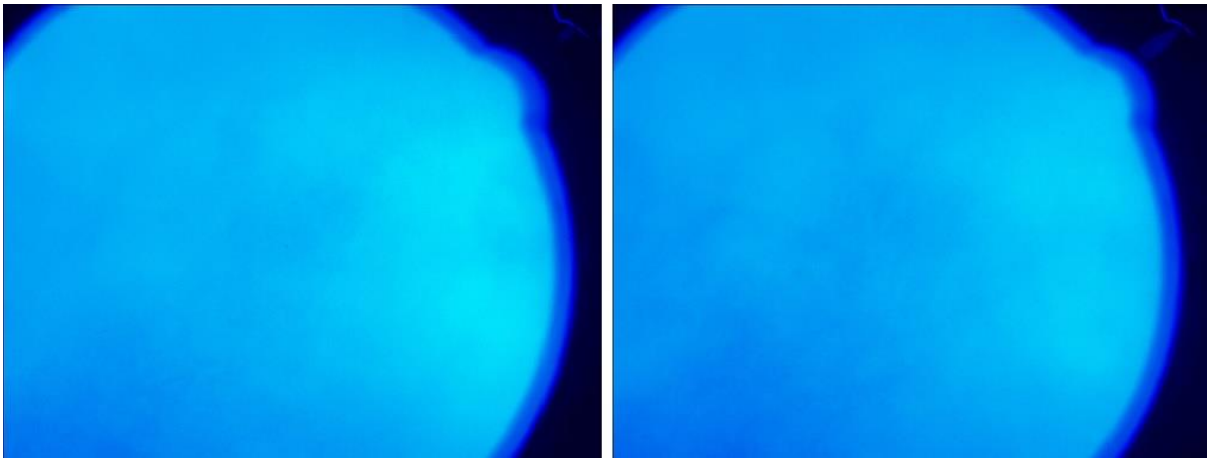

Figure 47: 720 bar injection pressure. 5 bar chamber pressure using nitrogen. 0.45ms – 0.5ms

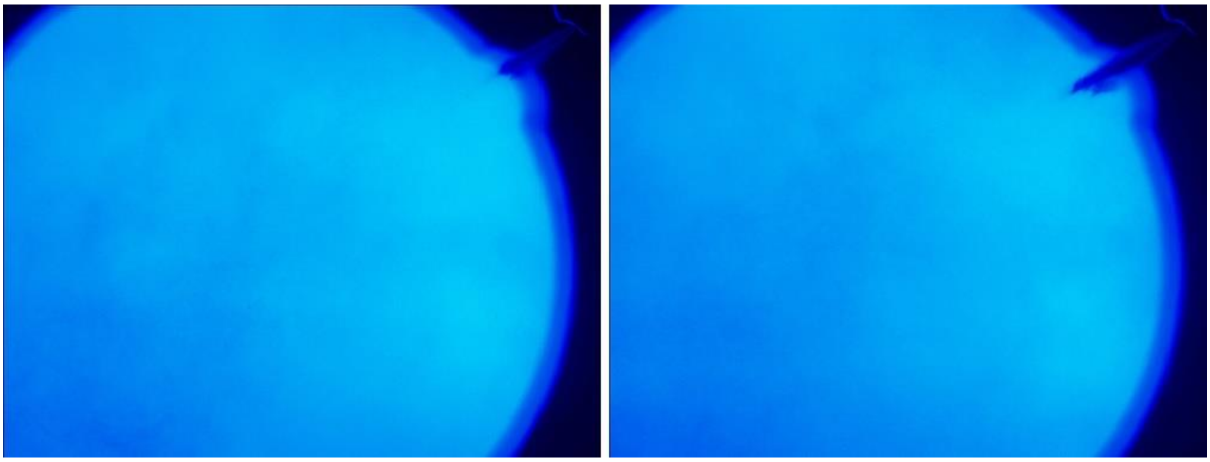

Figure 48: 720 bar injection pressure. 5 bar chamber pressure using nitrogen. 0.55ms – 0.6ms

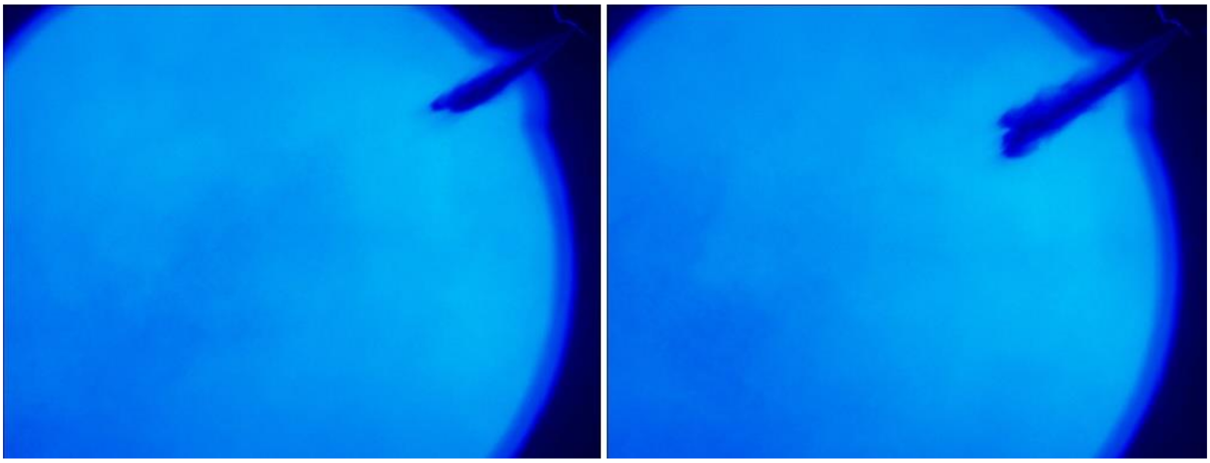

Figure 49: 720 bar injection pressure. 5 bar chamber pressure using nitrogen. 0.65ms – 0.7ms

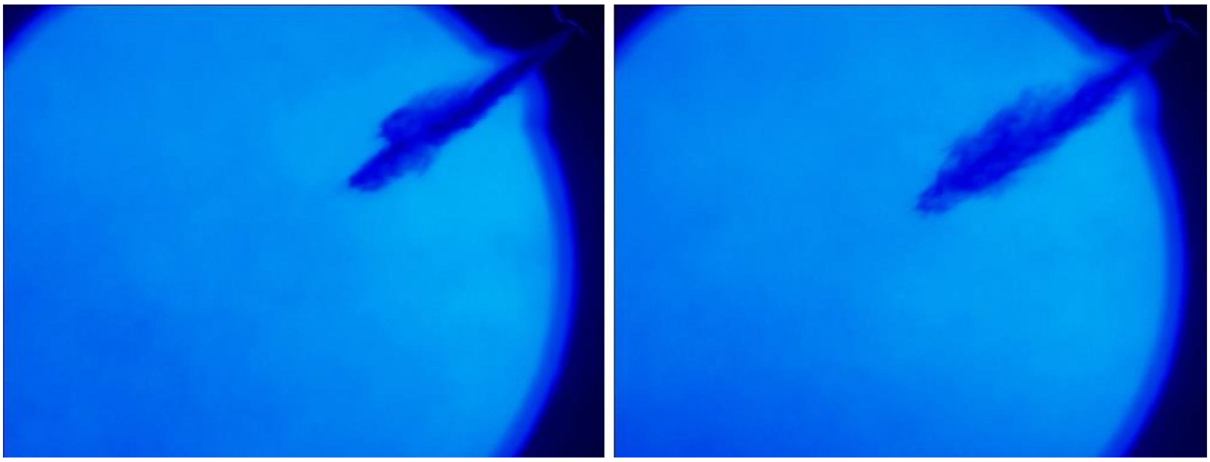

Figure 50: 720 bar injection pressure. 5 bar chamber pressure using nitrogen. 0.75ms – 0.8ms

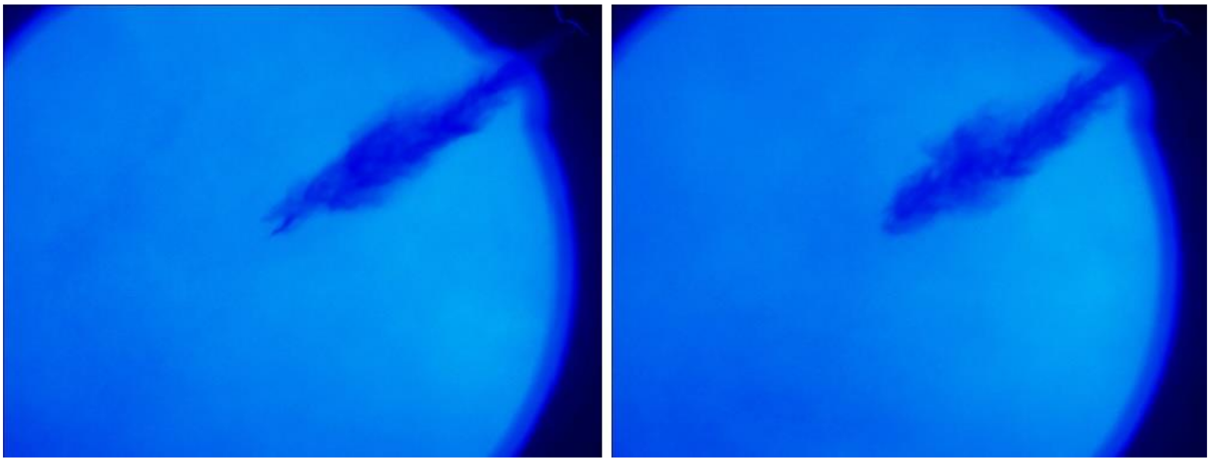

Figure 51: 720 bar injection pressure. 5 bar chamber pressure using nitrogen. 0.85ms – 0.9ms

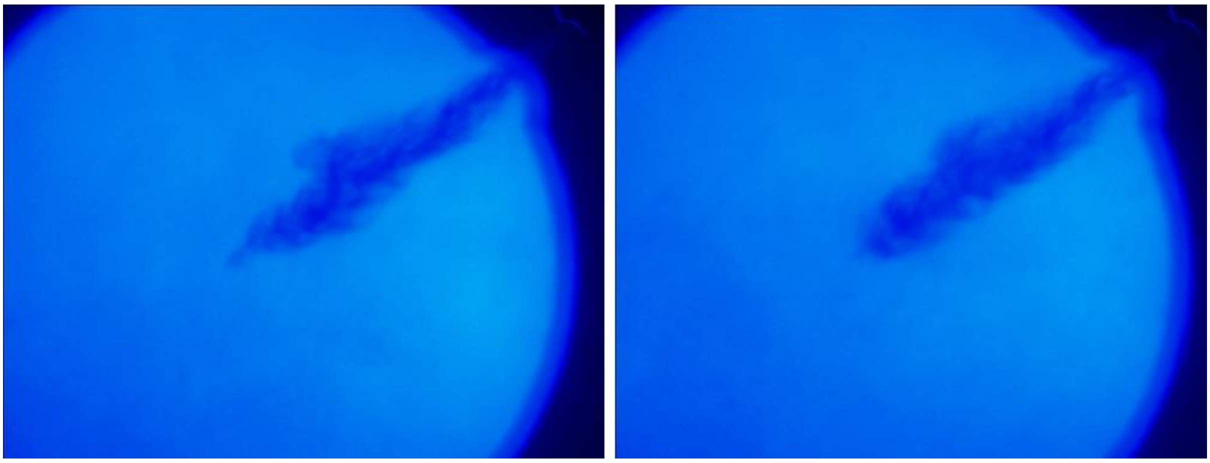

Figure 52: 720 bar injection pressure. 5 bar chamber pressure using nitrogen. 0.95ms – 1.0ms

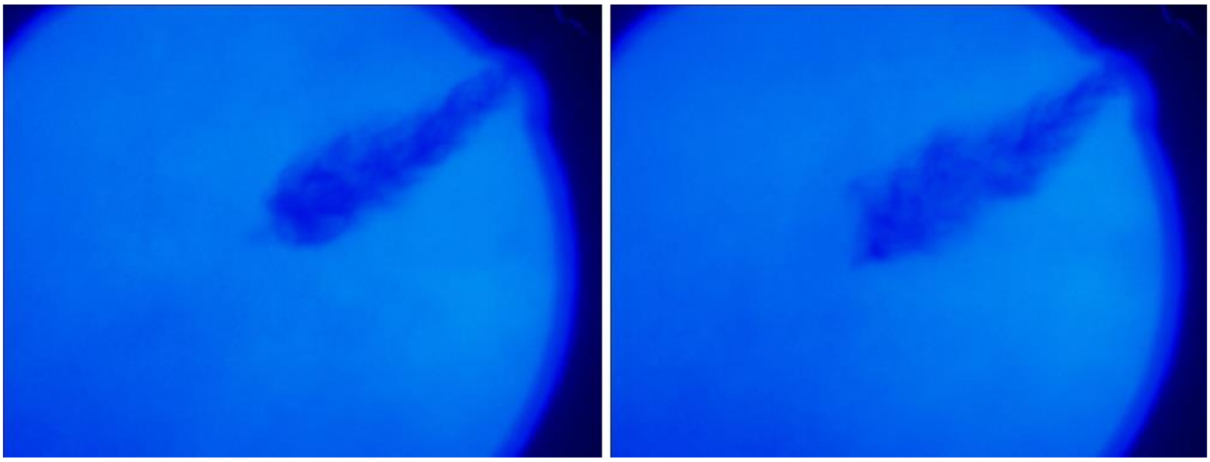

Figure 53: 720 bar injection pressure. 5 bar chamber pressure using nitrogen. 1.05ms – 1.10ms

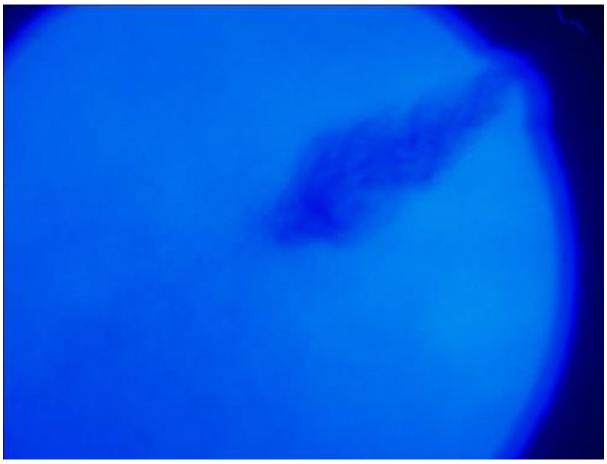

Figure 54: 720 bar injection pressure. 5 bar chamber pressure using nitrogen. 1.15ms

4.2. Flow Measurement

The Akribis section of the Inov8 Test Stand was used to measure the fuel injection rate and delivery. The software measures these parameters which are then exported to a text file. A sample is presented below and the full set of observations can be found in APPENDIX A – DATA CD.

1.0
Delivery
mm3/st
ms
0.000000
0.005000
12000
0.000
0.000
0.000
0.000

…

0.034
0.034
0.034
0.034

…

3.626
3.586
3.586
3.626

The raw data shown is for the injector delivery in mm^3. The start time is 0 and the increments are 0.005ms with 12000 data points (not shown). This is from a single injection and only shows the measurements at the beginning, middle and end of the injection. There are 20 sets of data like this for each test for each measured parameter (injection rate, injection delivery and firing pulse).

5. DATA PROCESSING

All the raw was processed using the methods described below.

5.1.Spray Analysis

The pictures taken at each increment during the test are averaged by the DaVis Software on the Spray Analysis computer. Averaging the data reduces the effect of any outliners on the final results. Individual injections have slight variations from each other; averaging the data therefore gives a more general representation of the injections. The averaged pictures with background removed for a test done with a one hole injector, 720 bar injection pressure, 5 bar cylinder pressure (nitrogen) and a 800µs injection duration are presented below.

Figure 55 shows the spray between 0.35ms and 0.4ms. Figure 56 shows the spray between 0.45ms and 0.5ms. Figure 57 shows the spray between 0.55ms and 0.6ms. Figure 58 shows the spray between 0.65ms and 0.7ms. Figure 59 shows the spray between 0.75ms and 0.8ms. Figure 60 shows the spray between 0.85ms and 0.9ms. Figure 61 shows the spray between 0.95ms and 1ms. Figure 62 shows the spray between 1.05ms and 1.1ms. Figure 63 shows the spray at 1.15ms. The times mentioned refer to the time after the signal was sent to the injector.

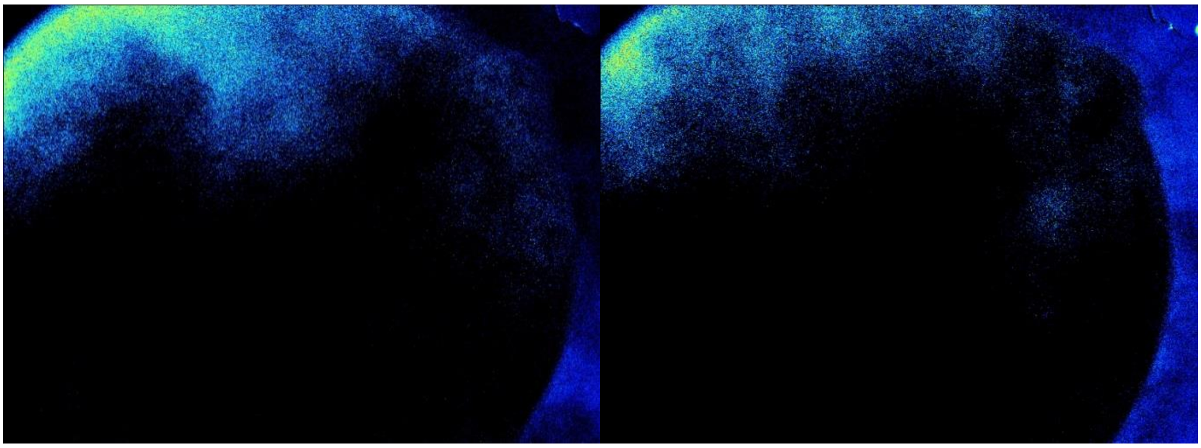

Figure 55: 0.35ms to 0.4ms averaged and background removed. 720 bar injection pressure. 5 bar cylinder pressure using nitrogen.

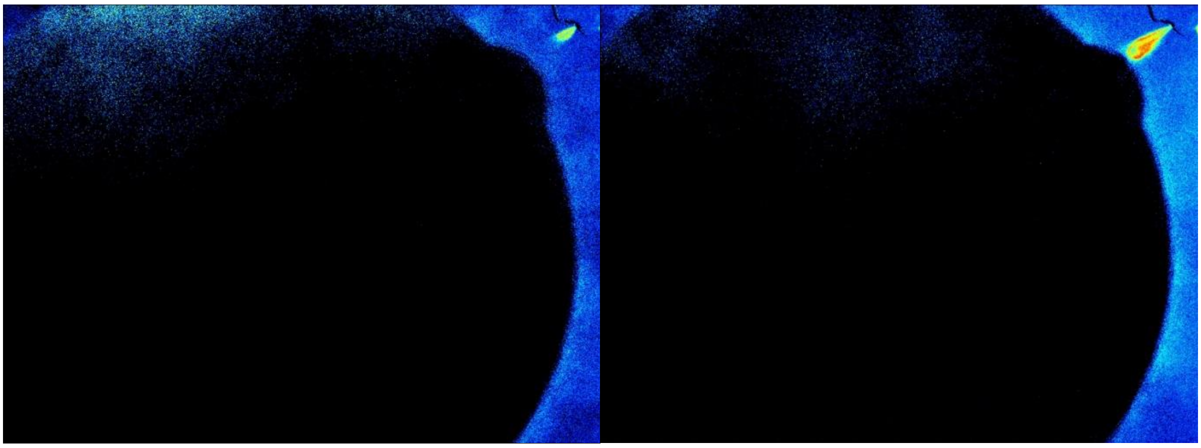

Figure 56: 0.45ms to 0.5ms averaged and background removed. 720 bar injection pressure. 5 bar cylinder pressure using nitrogen.

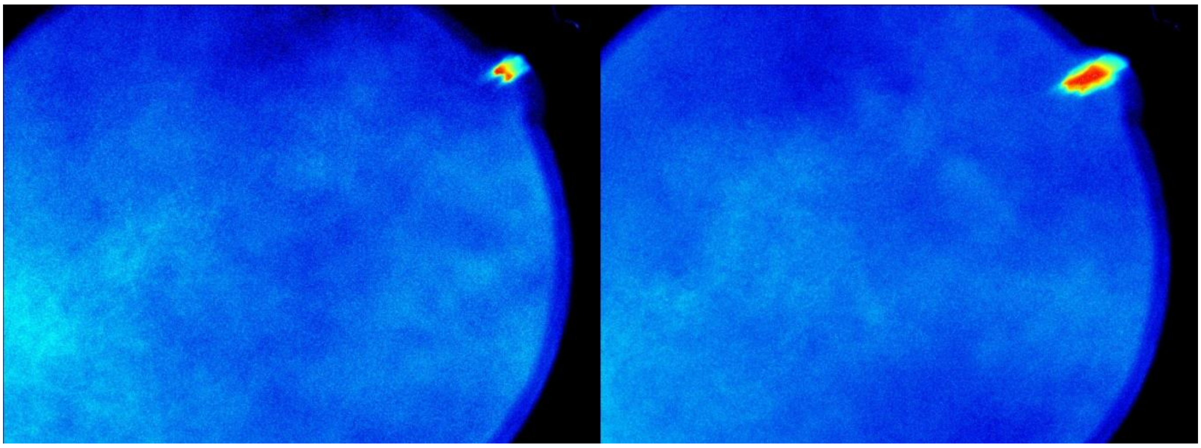

Figure 57: 0.55ms to 0.6ms averaged and background removed. 720 bar injection pressure. 5 bar cylinder pressure using nitrogen.

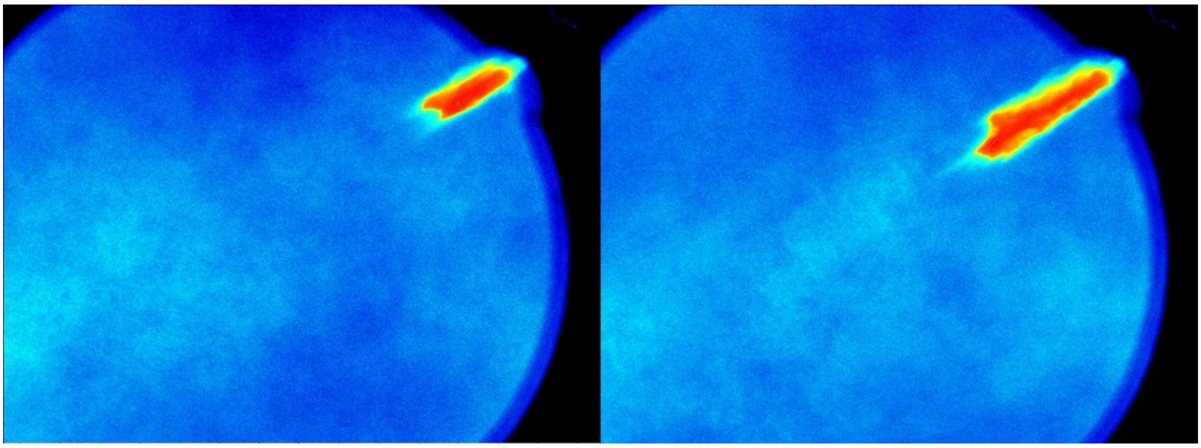

Figure 58: 0.65ms to 0.7ms averaged and background removed. 720 bar injection pressure. 5 bar cylinder pressure using nitrogen.

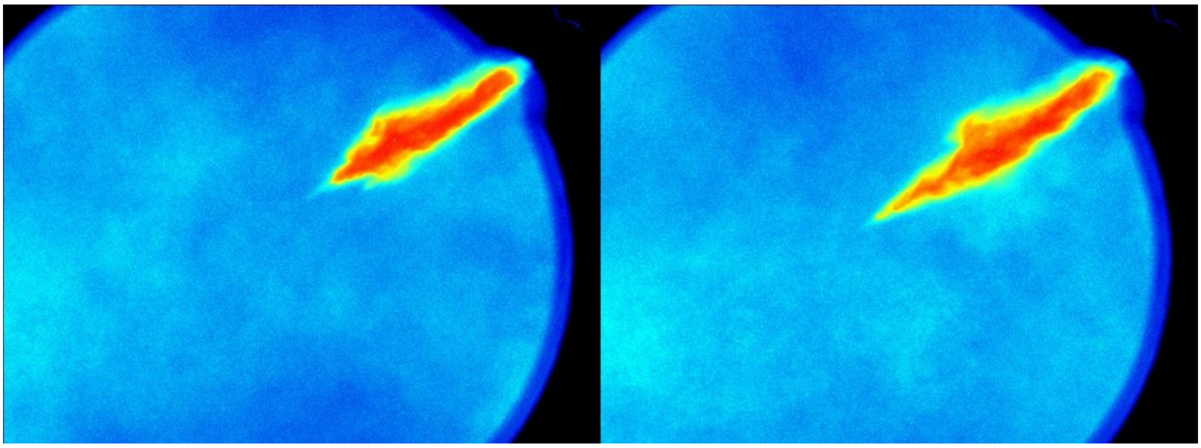

Figure 59: 0.75ms to 0.8ms averaged and background removed. 720 bar injection pressure. 5 bar cylinder pressure using nitrogen.

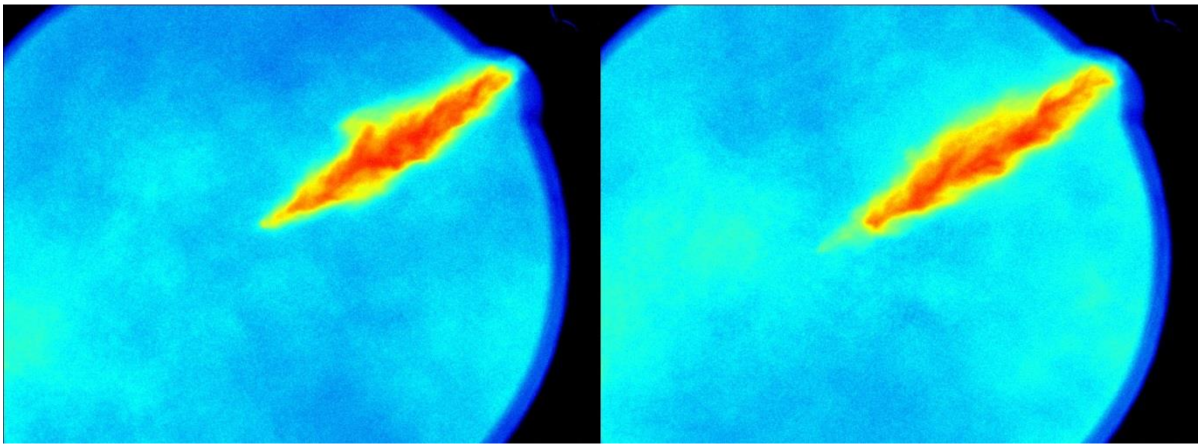

Figure 60: 0.85ms to 0.9ms averaged and background removed. 720 bar injection pressure. 5 bar cylinder pressure using nitrogen.

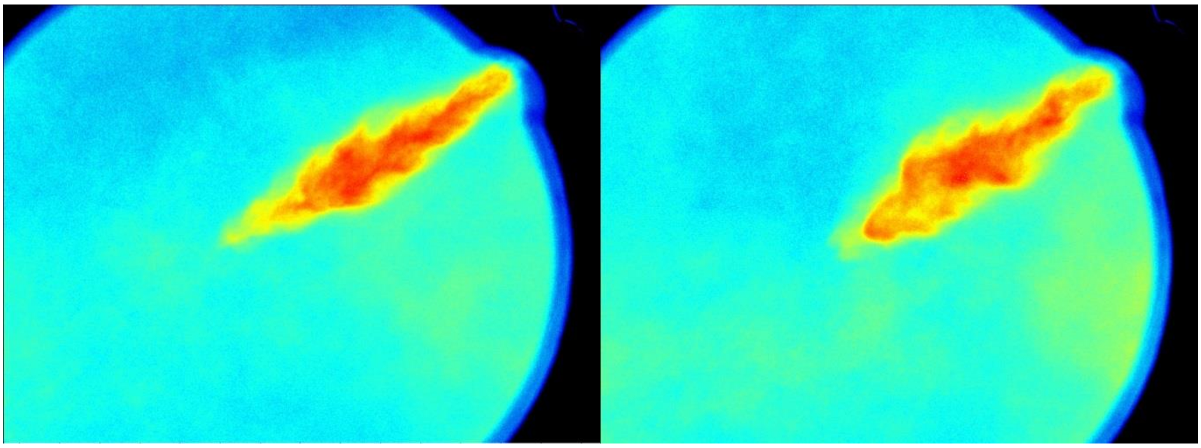

Figure 61: 0.95ms to 1ms averaged and background removed. 720 bar injection pressure. 5 bar cylinder pressure using nitrogen.

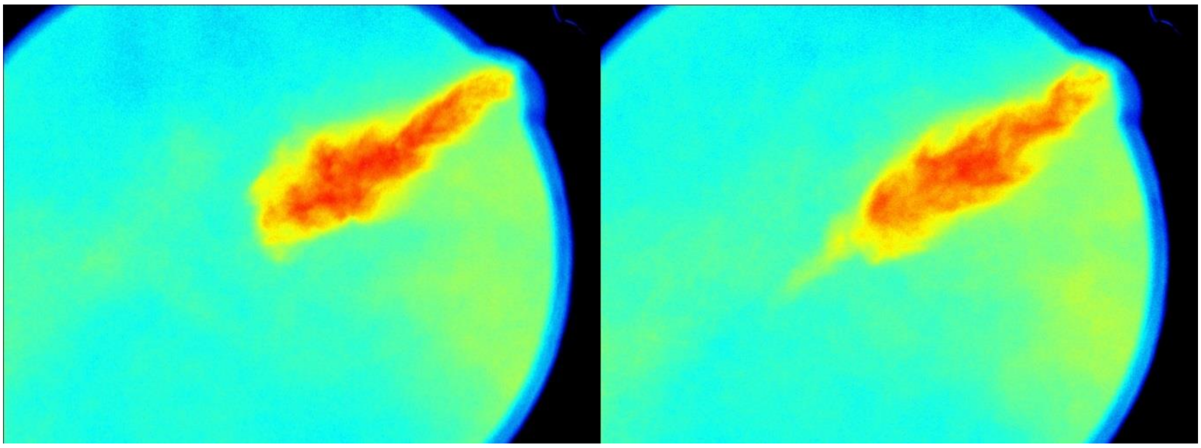

Figure 62: 1.05ms to 1.1ms averaged and background removed. 720 bar injection pressure. 5 bar cylinder pressure using nitrogen.

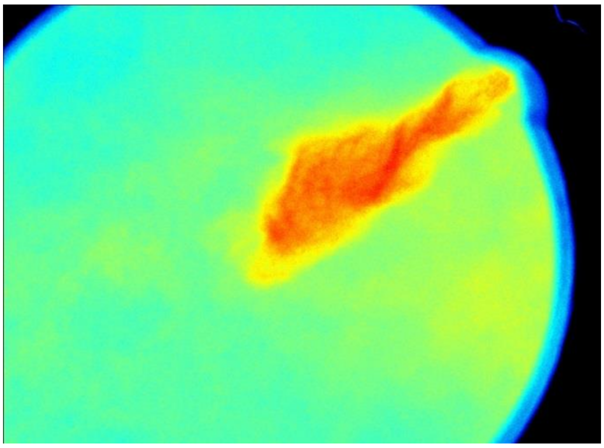

Figure 63: 1.15ms averaged and background removed. 720 bar injection pressure. 5 bar cylinder pressure using nitrogen.

Once the data has been averaged and the background removed, the images are analysed by the DaVis Software's Geometry package to determine the cone angle and spray penetration at each increment. Figure 64 below shows an averaged picture that has been processed by the DaVis Software. This image represents the processed results for an injection with a 700 bar injection pressure and 5 bar of nitrogen in the spray chamber; 0.75ms after the signal was sent to the injector.

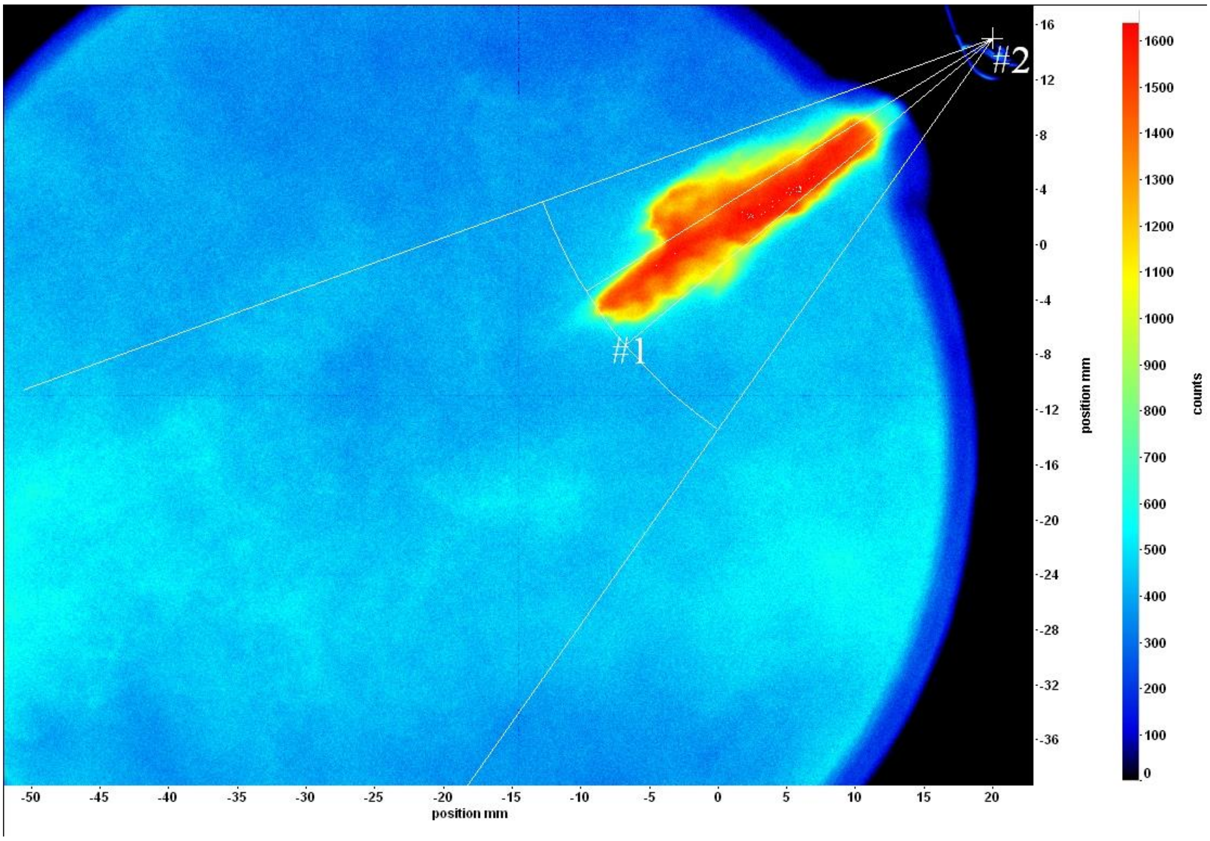

Figure 64: Processed Average Picture

The user specifies the location of the nozzle of the injector and the boundaries of the spray (the outer set of white lines in the image). The threshold must be adjusted so that the software is properly able to pick up the spray. The software then located the boundaries of the spray and calculates the spray penetration and cone angle. In Figure 64 the inner set of white lines, drawn parallel to the boundary of the spray, is used to measure the cone angle. The arc represents the tip of the spray and the software measures the distance of this arc to the nozzle location to determine the spray penetration. In this instance, the spray penetration was determined to be 32.8mm and the cone angle was 8.8º.

The Inov8 Test Stand has two options for lighting and thus two methods of analysis. The first, as seen in Figure 64 is a back light. A sheet of light is positioned behind the spray and the spray is analysed against a light background. In the figure, "#1" is the tip of the spray and "#2" is the tip of the nozzle (origin of the spray). The second is sheet/front lighting. This method illuminates the spray and not the background. For the first 0.15ms of the injection, the spray is not in front of the backlight and so this portion is analysed using the sheet/front lighting setting on the software as seen in Figure 65.

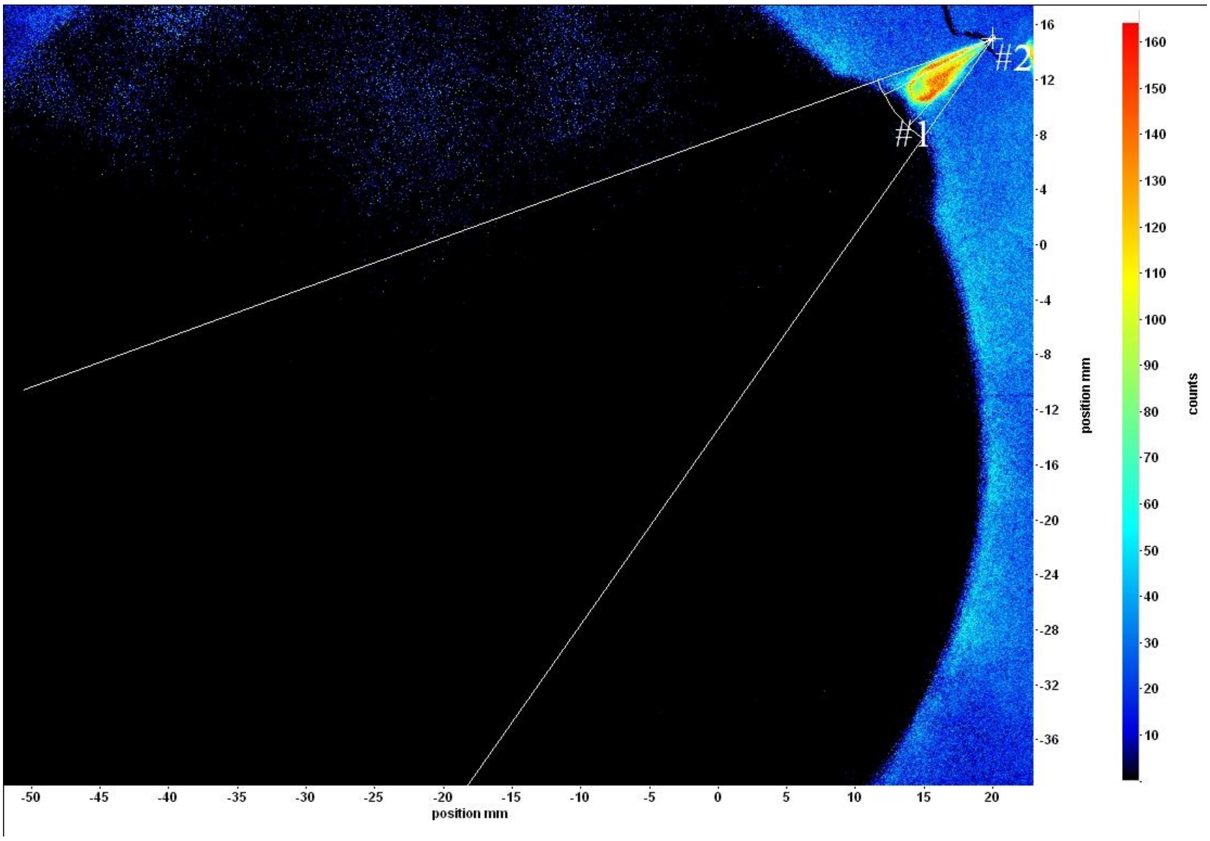

Figure 65: Sheet/front lighting processed image

The results of the measurements are saved in text files. A separate text file is created for every time step of every test and a new set of text files is created for each analysis (each time a parameter is changed in the geometry package to optimize the results eg. Threshold). The researcher has to navigate through approximately 5 subfolders to access each of these text files. The data must then be manually captured in an excel file for each instance. Research of this scope results in hundreds of text files and it would be very time consuming to manually collect all the data. Software was created by a previous student, however this researched involved a lot of optimization with the geometry package and this software was unable to extract data from multiple sets of analyses. For this reason, software was developed by the author in Python to collect the data. The code for the DataCollect software can be found in APPENDIX C – DATA COLLECTION CODES.

Manual data processing

The data can also be processed using CAD software. The unprocessed image used in Figure 64 was processed using Solidworks 2017 to illustrate this. The results can be seen in Figure 66 below. The image is imported into a Solidworks drawing and the scale on the bottom of the image is used to set the scale of the drawing to 1:1. Lines are then drawn from the nozzle, tangent to the boundary of the spray. An arc is then drawn between these lines tangent to the tip of the spray. The angle between the lines is measured to give the cone angle and the radius of the arc is measured to give the spray penetration. The manual data processing gives a spray penetration of 33.1mm and a cone angle of 8.9º.

Comparing the results obtained from the geometry package to that obtained by manually processing, there is a difference of approximately 1%.

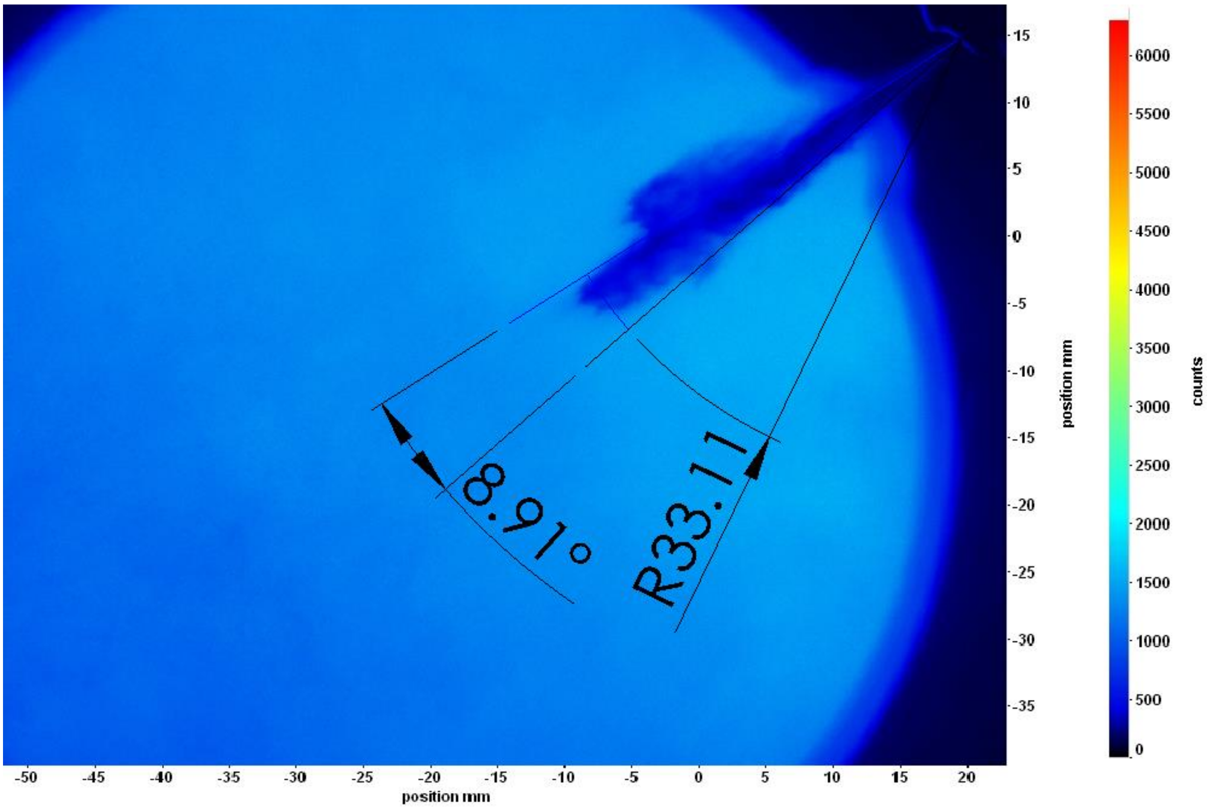

Figure 66: Manual Processing

Theoretical calculations

Before the theoretical cone angle and spray penetration can be calculated, the density of the gas in the chamber must be calculated. This can be calculated using the ideal gas equation.

$$\rho_g = \frac{P}{RT_g}$$

Where:

ρ_g	Density of the gas (kg/m^3)
P	Gas pressure (Pa)
R	Universal gas constant (Pa.m^3/kg.K)
T_g	Temperature of the gas (K)

Using a temperature of 15˚ C and a cylinder pressure of 500 KPa, the density of the nitrogen is calculated as:

$$\rho_g = \frac{500 \times 10^3}{\frac{8314}{28.013} \times 293}$$

$= 5.75$ kg/m^3

Cone angle

The theoretical cone angle can be calculated using Equation 2.

$$\theta = 0.05\left(\frac{d_n^2 \rho_g \Delta p}{\mu^2}\right)^{0.25} \qquad \text{Eqn 2}$$

Using a dynamic viscosity of 17.997 × 10^{-6} Pa.s and an injection pressure of 700bar, the cone angle can be calculated as:

$$\theta = 0.05\left(\frac{(0.17 \times 10^{-3})^2 \times 5.85 \times \left((700 \times 10^5) - 500 \times 10^3\right)}{(17.997 \times 10^{-6})^2}\right)^{0.25}$$

$$= 21.4°$$

Spray penetration

The theoretical spray penetration can be calculated using Equations 3, 4, 5 and 6. Where Equation 3 gives results that follow Dent’s theory and Equations 4, 5 and 6 are used to obtain results that follow Hiroyasu’s theory.

Dent

Using Dents theory [42] and an injection pressure of 700 bar, the spray penetration at 0.75ms after the start of the injection can be calculated as (injection only starts 0.35ms after the signal is sent, so t = 0.4ms):

$$S = 3.07\left(\frac{\Delta p}{\rho_g}\right)^{\frac{1}{4}}(td_n)^{\frac{1}{2}}\left(\frac{294}{T_g}\right)^{\frac{1}{4}} \qquad \text{Eqn 3}$$

$$= 3.07\left(\frac{(700 \times 10^5) - 500 \times 10^3}{5.75}\right)^{\frac{1}{4}}(0.4 \times 10^{-3} \times 0.17 \times 10^{-3})^{\frac{1}{2}}\left(\frac{294}{293}\right)^{\frac{1}{4}}$$

$$= 46.4mm$$

Hiroyasu

Using the same data, the spray penetration can be calculated using Hiroyasu's theory [38][43] as follows:

The time at which the spray is expected to break up can be calculated using Equation 4 as follows:

$$t_{break} = \frac{29\rho_l d_n}{(\rho_g \Delta p)^{\frac{1}{2}}} \qquad \text{Eqn 4}$$

$$= \frac{29 \times 830 \times 0.17 \times 10^{-3}}{(5.75 \times ((720 \times 10^5) - 500) \times 10^3)^{\frac{1}{2}}}$$

$$= 0.000201 \text{ s}$$

From the calculated break up time, it can be seen that at 0.75 ms, the spray would have broken up. After the spray has broken up, the spray penetration can be calculated using Equation 6. At 0.4ms after the start of injection, the spray penetration can be calculated as:

$$t > t_{break}: \qquad S = 2.95\left(\frac{\Delta p}{\rho_g}\right)^{\frac{1}{4}}(d_n t)^{\frac{1}{2}} \qquad \text{Eqn 6}$$

$$= 2.95\left(\frac{(700 \times 10^5) - 500 \times 10^3}{5.75}\right)^{\frac{1}{4}}(0.17 \times 10^{-3} \times 0.4 \times 10^{-3})^{\frac{1}{2}}$$

$$= 44.4 \text{ mm}$$

5.2. Flow Measurement

All results obtained while conducting the Flow Measurement experiments must be exported to text files using the method outlined in Appendix B of this report. Once the data has been exported to text files, it was imported to Excel spreadsheets using a VBA code developed by the author, which can be found in APPENDIX C.

The data obtained over the 20 injections is then averaged in order to obtain a more accurate representation of the experiments. Averaging the data removes the influence of outliners and other incorrect data which in inevitable in these experiments. There are also slight variations between the individual injections and the rail pressure showed fluctuations of up to ±12 bar. The impact of these variations on the data is reduced by averaging the 20 injections.

The averaged data for the firing pulse, rate and delivery is then plotted against time in order to show its variation. Multiple sets of data are plotted on the same set of axes in order to clearly show the difference between the varied parameters. The theoretical flow rates can be calculated using Equation 7 as follows;

$$Q = C_d A \sqrt{\frac{2P}{\rho}} \qquad \text{Eqn 7}$$

The nozzle area can be calculated as follows:

The area of one of the holes is:

$$A = \pi r^2$$

$$= \pi \frac{0.00017^2}{2}$$

$$= 22.698 \times 10^{-9} \text{ m}^2$$

Using a coefficient of discharge of 0.8, an injection pressure of 700 bar and a back pressure of 5 bar, the flow rate can be calculated as:

$$Q = C_d A \sqrt{\frac{2P}{\rho}}$$

$$= 0.8 \times 22.698 \times 10^{-9} \times \sqrt{\frac{2(1000 - 40) \times 10^5}{830}}$$

$$= 8.84 \text{ mm}^3/\text{ms}$$

6. RESULTS AND DISCUSSION

A study was conducted to determine the sensitivity of spray penetration with variations in back pressure and cylinder gas density. The equipment used was able to gather data with a higher level of accuracy than equipment used previously conducted research (Section 1.2.12). The DaVis software is able to control the camera very precisely and images are captured over multiple injections. These images are then averaged and put in order to form a single sequence. The triggering system is what contributes to the accuracy of the test stand as it allows for very small time steps (0.02ms) between successive images. The fact that a user defined number of images are averaged for every time step means that the effect of anomalies on the results is reduced.

The test stand was designed to analyse spray patterns with an atmospheric back pressure. This meant that a new spray chamber needed to be fitted to the test stand that could be pressurized. The new spray chamber would have to have no impact on the normal operation or accuracy of the test stand. The spray chamber used by Valentim [29] was retrofitted to the test stand for the purposes of the study. This spray chamber was sealed to hold pressure, so the extraction system could not be used. This imposed a few restrictions on testing as the amount of fluid introduced to the chamber per injection had to be minimized in order to obtain clear images.

The fuel injector used had all but one hole sealed to reduce its flow rate. This also prevented fluid build-up on the windows which would distort the images. Having multiple jets in the spray chamber could also cause interference as they interact with each other. It would also be difficult to distinguish the individual jets if one sits behind the other when viewed radially. A single jet would therefore make it easier for the software to identify the spray penetration and cone angle and thus produce more accurate results. The injection pressures were also kept below 800 bar, this was to reduce the amount of fluid injected as well as to preserve the solder used to seal the holes on the tip of the injector.

Multiple sets of tests were done in order to obtain results to meet the objectives of this study. The first set of tests involved keeping a constant cylinder pressure while varying the injection pressure. Thereafter the injection pressure was kept constant with varying cylinder pressure. The next set of tests involved varying both the injection pressure and cylinder pressure while maintaining a constant difference between them. These tests were repeated with nitrogen and carbon dioxide in the spray chamber to determine the effect of cylinder gas density on the spray penetration.

During initial testing, the tip of the injector was visible using the setup described above. This meant that the first phase of the injection would be captured sufficiently, however the tip of the injector still sat in a shadow inside the spray chamber. This was due to the nature of the camera used in the Inov8 test stand. The imaging system used by Valentim with this spray chamber used parallel light [29] and therefore the tip of the injector was illuminated. The superior DaVis software used by the Inov8 Test Stand was able to mitigate this issue.

A spray chamber was designed with the exact same internal dimensions as the original spray chamber. The windows were also kept the same size and their original position relative to the camera and back light were maintained to optimize the data capturing. The larger internal volume would also reduce the density of vapour in the air as an injection occurred and would result in clearer pictures.

After initially setting up the spray chamber it was discovered that the camera was not able to pick up the tip of the injector. This would affect the results and so the spray chamber was sent out for some minor modifications as described in Section 3.1. At the time of completing the study, the modification to the spray chamber was still in progress.

The observations in Section 4 were processed as described in Section 5 and are presented below.

6.1. Injection Pressure

In order to determine the effect of injection pressure on the spray penetration, the cylinder pressure was kept constant at 5 bar with nitrogen. The injection pressure was varied between 700 bar and 780 bar with a duration of 800 µs. The injection pressure was limited to 780 bar to ensure that the solder used to seal the holes on the tip of the injector remained in place. It also kept the amount of fluid introduced to the spray chamber per injection low enough to obtain clear pictures without the use of an extraction system. If too much vapour built up in the spray chamber, the camera would not be able to pick up the spray clearly and therefore the results would not be accurate. A plot of the spray penetration vs time for various injection pressures can be seen in Figure 67 below. The full set of tabulated results can be found in Table 3 - APPENDIX D – RESULTS.

From Figure 67 it can be seen that the spray penetration increases with increasing injection pressure as predicted by theoretical models and observed by previous researchers [2][23]. Figure 69 shows a plot of the results obtained with a 760 bar injection pressure and 5 bar cylinder pressure compared to the theoretical spray penetration with the same parameters (the results for the other injection pressures can be found in APPENDIX D – RESULTS). The spray penetration starts at 0mm at the time the signal is received by the injector (0.35ms after it is sent). As the needle lifts, the test fluid is forced through the nozzle of the injector by the large pressure difference (695 – 775 bar). The spray penetration increases almost linearly at a slightly increasing rate until the spray breaks up approximately 0.5ms after the start of the injection (0.85ms after the signal was sent). Thereafter, it continues to increase, however at a slower rate than before break up.

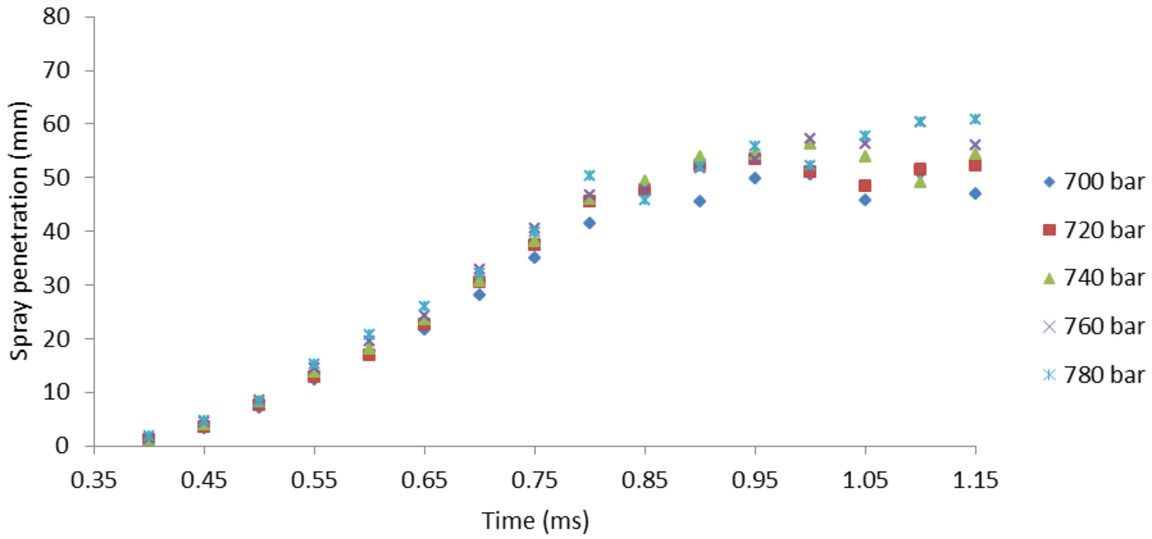

Figure 67: Spray penetration vs time. 5 bar cylinder pressure. 700 – 780 bar injection pressure using nitrogen

For the current set of tests, Hiroyasu's model predicted that the spray would break up between 0.54ms and 0.55ms. The sudden change in the gradient in Figure 67 (resulting from a sudden decrease in velocity) indicating the spray has broken up occurs at around 0.85ms. The model therefore predicts that the spray would break up around 0.3ms before it actually did. The difference is due to assumptions made when the models were developed. The injection pressures used for the development of the models was lower than those tested here and constants were built into the models to account for the experimental set up used, which differs from the set up used in the current study. [41]

For all of the injection pressures tested, the initial stages of the injections (approx. 0.5ms after the start of injection) are very similar to each other. After approximately 0.5ms, the difference in penetration resulting from each of the injection pressures tested becomes greater. This is demonstrated in Figure 68 which shows the average spray penetration at different injection pressures, for two periods during the injection. Between 0 and 75ms, the average spray penetration was closer than between 0.8ms and 1.15ms. The difference in average penetration (between 700 bar and 780 bar injection pressure) was 2.6mm between 0ms and 0.75ms. Between 0.8ms and 1.15ms, this difference increased to 7mm. This means that the injection pressure has a bigger influence on the penetration in the later stages of the injection than it does in the initial stages. In the later stages of the injection, the spray penetration more closely matches the theoretical predictions of both Hiroyasu and Dent as seen in Figure 69 below. A higher injection pressure resulted in a larger spray penetration.

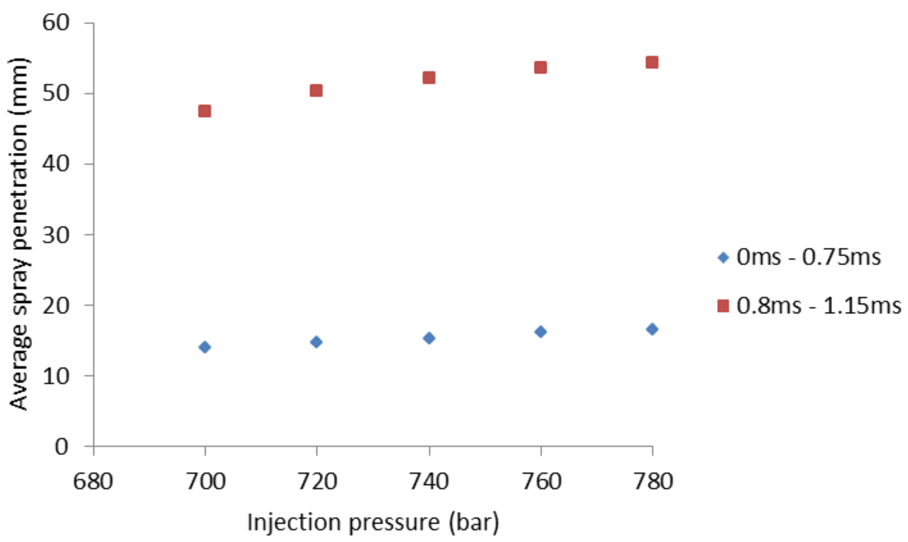

Figure 68: Effect of injection pressure on spray penetration at different stages of injection

Figure 70 below shows the results obtained by Valentim [30] for spray penetration for the time frame tested in this research ie. injection duration of 800µs (0.35ms – 1.15ms). The hesitation noted by Valentim can be seen as a discontinuity in the data points between 0.8ms and 1ms.

Figure 71 shows the mean tip velocity for this set of tests. The mean tip velocity is the average velocity of the tip of the spray for the interval between measurements (0.05ms in this case). It is calculated by dividing the difference in spray penetration between two data points by the duration of that interval. The results show that the velocity of the tip of the spray increases linearly until 0.55ms (0.2ms after the start of the injection), thereafter, the mean tip velocity suddenly decreases before beginning to increase again with another drop.

The sudden drop in the mean tip velocity coincides with results obtained by Valentim [30] and Karimi [23]. Karimi discovered that this was due to a pressure imbalance in the tip of the injector. The pressure imbalance is due to the fact that 5 of the 6 holes on the injector have been sealed to effectively make it a '1 hole injector'. The 6 holes on the injector are spaced evenly, radially, around the needle of the injector. During normal operation, there is an even pressure around the needle whether the injector is open or closed. With 5 of the holes closed, as soon as the needle starts to lift and fluid leaves through the open hole, that side of the needle experiences a pressure drop which moves the needle towards the hole and restricts flow until the needle is fully retracted, at which point, normal flow continues. This issue could possibly be alleviated by opening up another of the holes opposite to the open one to balance the pressure distribution on the needle.

The interruption in the flow of fluid out of the single hole has the effect of creating a second jet just behind the first one. This second jet was discovered by Valentim [30]. When the needle begins lifting and the fluid starts to flow out of the nozzle, the mean tip velocity increases steadily due to the pressure difference across the nozzle. The lateral movement of the needle then obstructs the flow causing it to dramatically slow down. As the needle continues its upward movement, it uncovers the hole again and a second jet leaves the injector just behind the initial one.

When the injection begins, the fluid is forced into the stationary gas that is in the cylinder as a liquid jet. The liquid jet decelerates and at the same time accelerates the gas particles it makes contact with. As the flow progresses, the liquid jet mixes with the gas in the cylinder and the jet becomes shrouded by a fluid/gas mix. The density of fluid in this mix decreases further away from the liquid core. Towards the tip of the spray, the vaporized fluid and gas mixture form clusters and these clusters tend to break away from the main spray structure. This phenomenon is known as cluster shedding [23]. This explains the fluctuations in the penetration as seen between 0.9ms and 1.15ms in Figure 67. The fluctuations are more evident when analysing the time derivative of the penetration (velocity) as seen in Figure 71. There are larger fluctuations in both the spray penetration and mean tip velocity at higher injection pressures. At higher injection pressures, the fuel is better atomized (smaller droplets) [23], this means there is a greater liquid surface area and therefore a greater interaction between the test fluid and gas. This increases the effect of cluster shedding.

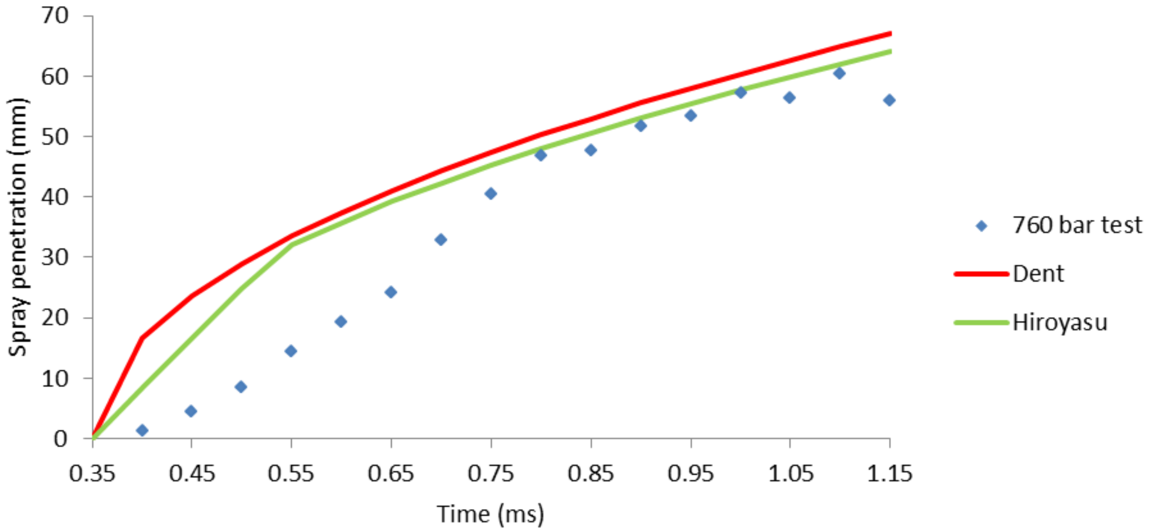

Figure 69: Spray penetration test results compared to theory. 760 bar injection pressure. 5 bar cylinder pressure using nitrogen

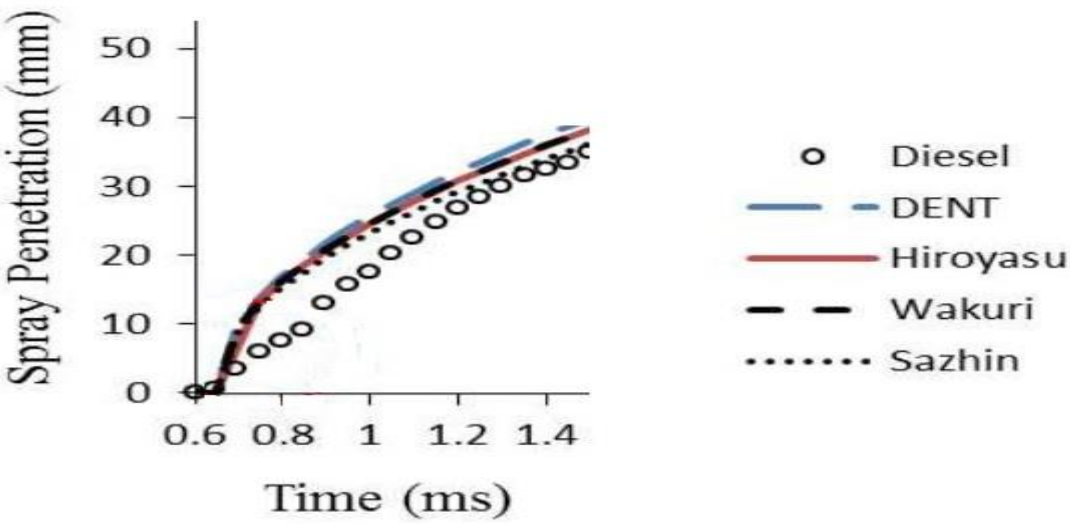

Figure 70: Valentim spray penetration area of interest

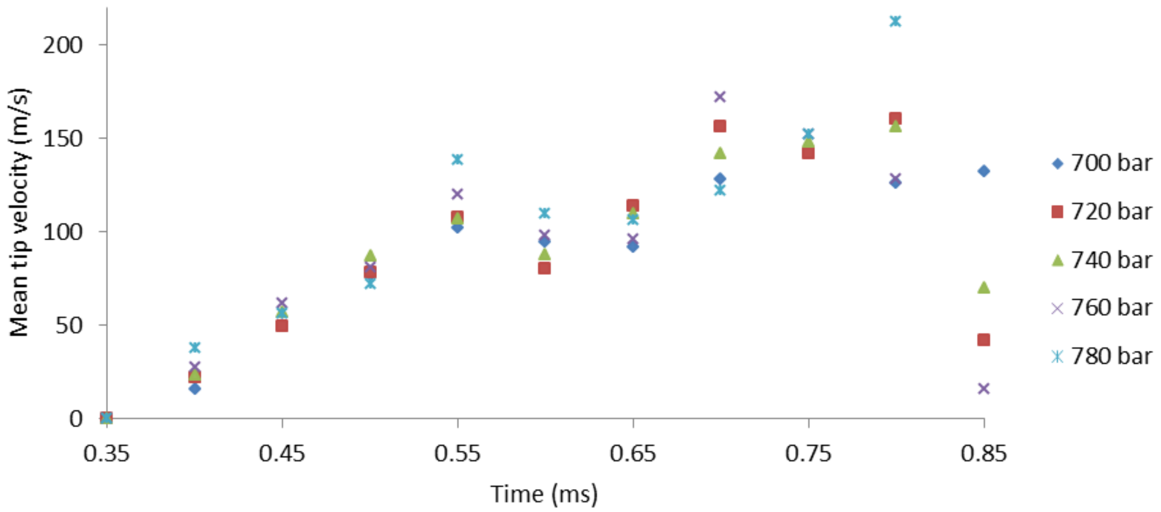

Figure 71: Mean tip velocity. 700 – 780 bar injection pressure. 5 bar cylinder pressure using nitrogen

Another structure noticed in the spray was the fish bone structure as seen in Figure 72 below. The structures are due to surface waves on the boundary of the spray caused by the inertaction of the fluid with the gas in the cylinder. The structures are closer together near the nozzle of the injector and further apart closer to the tip of the spray. These structures were also noticed by Karimi [23], Tsue et al [35], Koo and Martin [36], and Yule and Salters [37]. Karimi [23] attributed the structure to harmonic resonance that could be brought about by any of the components of the fuel delivery system or the fluid pressure or actions of the solenoid of the injector. Karimi also discovered no relation between the injection pressure and these structures and the distance between them appeared to be random.

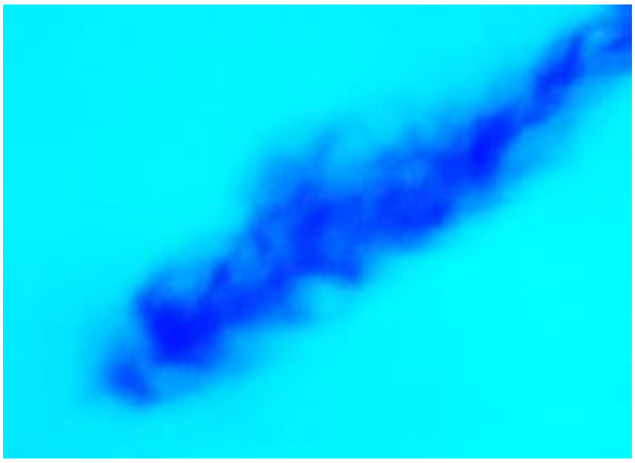

Figure 72: Fishbone structure. 720 bar injection pressure. 5 bar cylinder pressure using nitrogen. 1ms after signal sent

Figure 73 shows a comparison of the mean tip velocity with an injection pressure of 700 bar, and 5 bar nitrogen in the spray chamber; and the theoretical velocities with these parameters. The theoretical velocities were obtained by taking the time derivative of the Dent and Hiroyasu models for spray penetration respectively. From the figure, it can be seen that Dent's model predicts a sudden increase in the velocity when the injector opens, the velocity decreases thereafter at a decreasing rate with time. The initial velocity tends to infinity as the time tends to the time of the injector opening (0.35ms). Hiroyasu's model predicts a constant velocity, also with a sudden increase, until the spray breaks up. When it breaks up, it is predicted that there would be a sudden deceleration. Thereafter, the deceleration decreases at a decreasing rate.

These models seem unrealistic in predicting a sudden, instantaneous increase in velocity when the needle lifts. They do not take into account the effects of the viscosity of the fluid, the inertia of the fluid and the effects of friction. The experimental results show that the velocity of the spray increases linearly with time until the injection is interrupted by the hesitation, at which point it begins to decrease. When the secondary injection starts, the velocity increases again.

Figure 74 shows the average mean tip acceleration for each injection pressure tested, for the first 0.2ms of the injection (before breakup or hesitation). From the figure, it can be seen that the acceleration increases at an increasing rate with increasing injection pressure. The acceleration for this period increases from 512m/s^2 with 700 bar injection pressure to

691m/s^2. This represents a 35% increase in acceleration with an 11.4% increase in the injection pressure. During this phase of the injection, the spray is mostly dependent on the pressure difference across the nozzle. Increasing the injection pressure while keeping the cylinder pressure constant increases this pressure difference. More energy is transferred to the fluid and since the other parameters are kept constant, there is a larger net energy to accelerate the fluid.

Figure 75 shows the average mean tip acceleration of the spray. This was obtained by determining the change in velocity between consecutive time steps and dividing by the length of the time step; and then averaging the results for the various injection pressures. The full set of mean tip accelerations can be found in Figure 125, APPENDIX D – RESULTS. From the figure, it can be seen that the acceleration starts at 0 when the injection starts and increases to a constant value within the first time step (0.35ms to 0.4ms). This increase in acceleration is due to the pressure difference across the nozzle overcoming the inertia of the fluid. During this time, there are also viscous effects as the fluid passes through the nozzle as well as frictional losses. The acceleration remains constant from here until the hesitation. This constant acceleration is due to the constant pressure applied to the fluid. The spray suddenly decelerates as the injection is interrupted as seen by the dip in acceleration at 0.6ms (average acceleration between 0.55 and 0.6ms).

The acceleration then picks up again as the secondary spray starts. The acceleration then suddenly decreases again when the spray breaks up at around 0.85ms. The acceleration between the hesitation and the break-up of the spray is very irregular. This is due to the interactions between the spray and the gas in the cylinder.

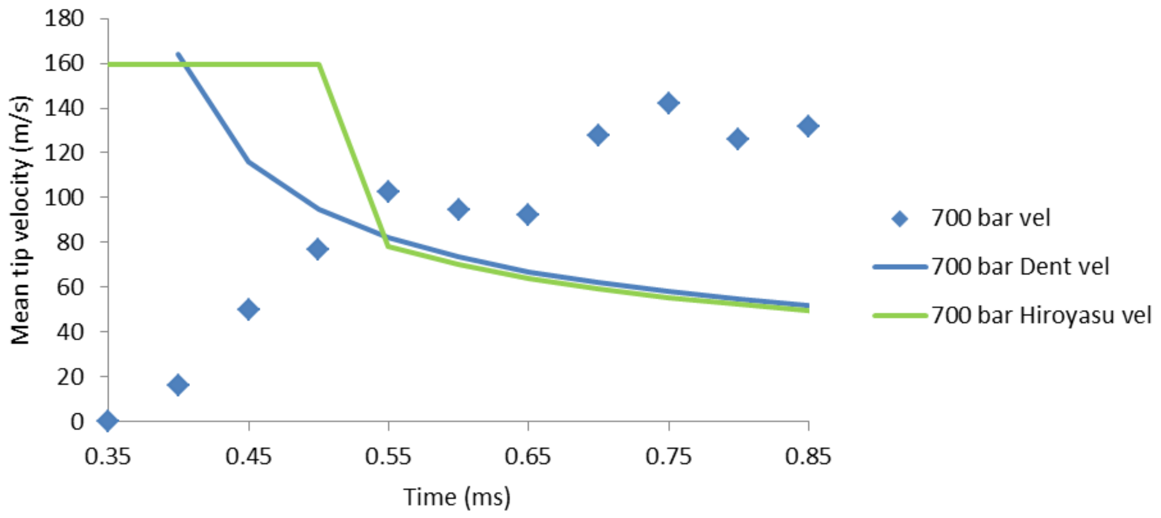

Figure 73: Mean tip velocity compared to theory. 700 bar injection pressure. 5 bar cylinder pressure using nitrogen.

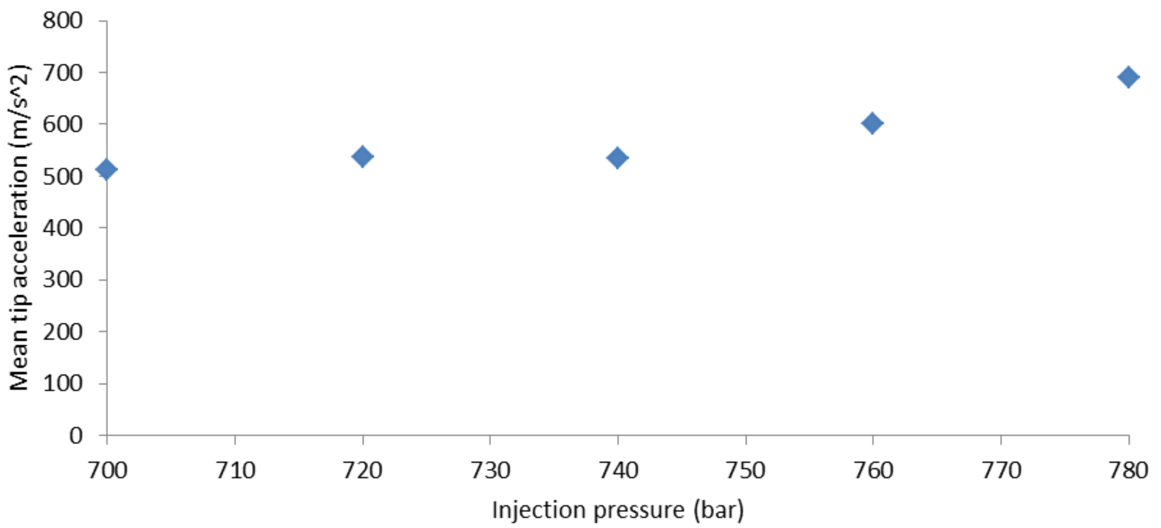

Figure 74: Mean tip acceleration 0.35ms to 0.55ms. 700 – 780 bar injection pressure. 5 bar cylinder pressure using nitrogen

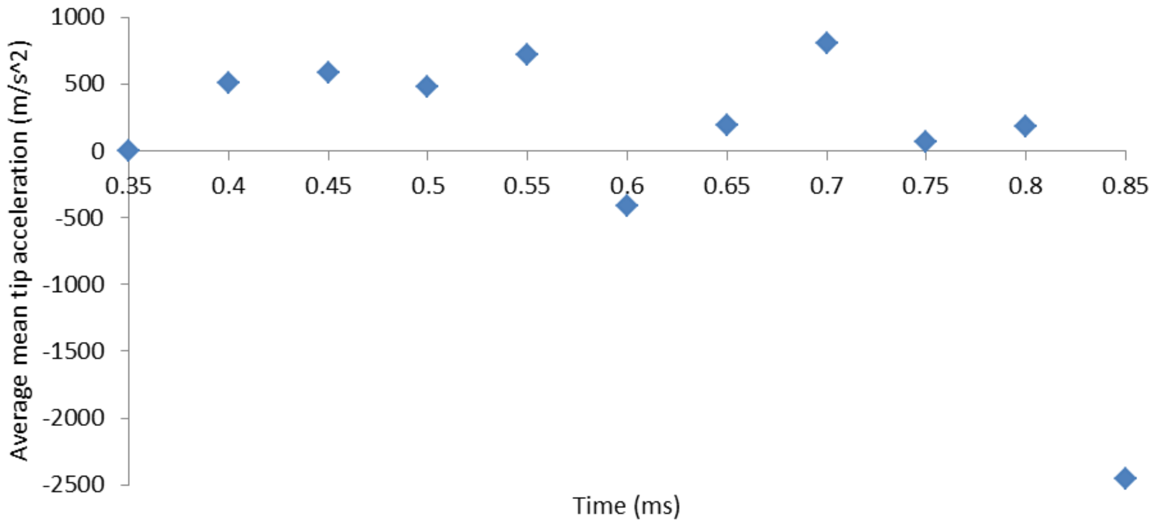

Figure 75: Average mean tip acceleration. 700 – 780 bar injection pressure. 5 bar cylinder pressure using nitrogen.

The change in acceleration (deceleration) from 0.55ms to 0.6ms is 157.8m/s, whereas the corresponding change from 0.8ms to 0.85ms is 1432.6m/s. The first deceleration is due to the hesitation (caused by the upward moving needle blocking the nozzle and interrupting the spray) whereas the second deceleration is due to the injector closing and ending the injection.

Comparing Figure 69 and Figure 70, a similar pattern can be seen in terms of the relationship between the test results and theoretical results even though different test parameters were used. In both cases, the theoretical models overestimated the spray penetration for the initial stages (the initial 0.4ms – 0.5ms after injection began). The same trend can be seen with all the injection pressures tested. After this initial period, the theoretical models predicted the spray penetration fairly well. Figure 76 shows the percentage difference between the actual and predicted spray penetration (Hiroyasu and Dent) with an injection pressure of 760 bar (5 bar nitrogen). From the graph, it can be seen that the difference between the predicted and actual results decreases rapidly from the start of the injection until about 0.45ms after the start of injection (0.8ms after the signal is sent). Hiroyasu predicts the spray penetration within 1% at 1ms (0.65ms after injection began).

Comparing the predictions of Hiroyasu and Dent, it can be seen that Hiroyasu predicts the penetration more accurately throughout the entire injection process. This is the case for all the injection pressures tested and the percentage differences for both Hiroyasu and Dent can be found in APPENDIX D – RESULTS. The theoretical predictions are closer to the test results at higher injection pressures. Considering the average difference for the whole timeframe, Dent's model goes from a 38.6% difference at 700 bar injection pressure to 30.5% at 780 bar, with the difference decreasing almost linearly. Similarly, Hiroyasu's model goes from 34.9% to 26.0%.

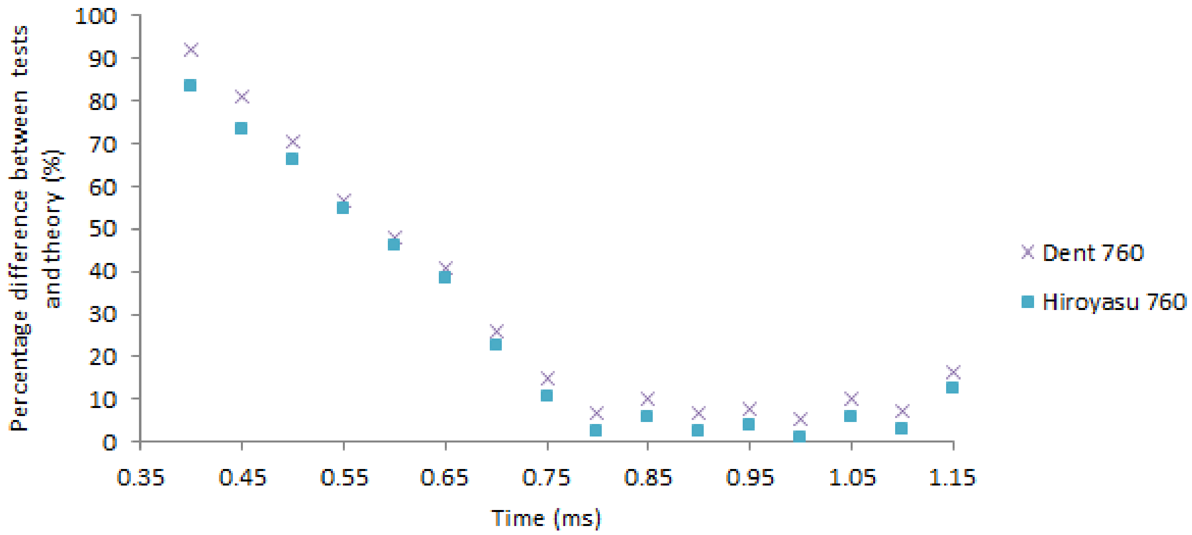

Figure 76: Percentage difference between theoretical and actual results. 760 bar injection pressure. 5 bar cylinder pressure using nitrogen.

The difference tends to increase slightly towards the end of the injection. This is as a result of the theoretical models not taking into account the effect of cluster shedding.

As the injection progresses and the spray atomized, there are more fluid particles in the gas further away from the liquid jet. The imaging system picks up the presence of a particle by the light it scatters. The particles present in the gas are picked up by the imaging system and the resolution of the spray is reduced due to this. The boundaries of the spray become less defined and therefore it becomes increasingly difficult to measure the spray. This can be seen when looking at Figure 77. The image on the left was captured at 0.6ms and the image on the right was captured at 1.15ms during the same test. The earlier image has much more contrast and the edges of the spray are very clear and defined. The image on the right has some atomized test fluid in the gas. Using the scale on the right of each of the pictures, it can be seen that the colour change represents an increase in the count of particles in the gas. The background in the later image is the same colour as the boundary of the spray in the earlier picture. Due to this phenomenon, the threshold on the analysis software needed to be changed and optimized for each progressive image. This is so that the edge of the spray would be accurately identified for measurements. It proved to be time consuming and so the results were analysed manually using CAD software and scaling the images correctly as described in the previous section.

This issue would be resolved if an extraction system was fitted to the spray chamber. The extraction system would have to remove the vapour from the chamber while maintaining a constant cylinder pressure. This system should work by passing the gas in the spray chamber through a filter so as to not waste the gases being tested.

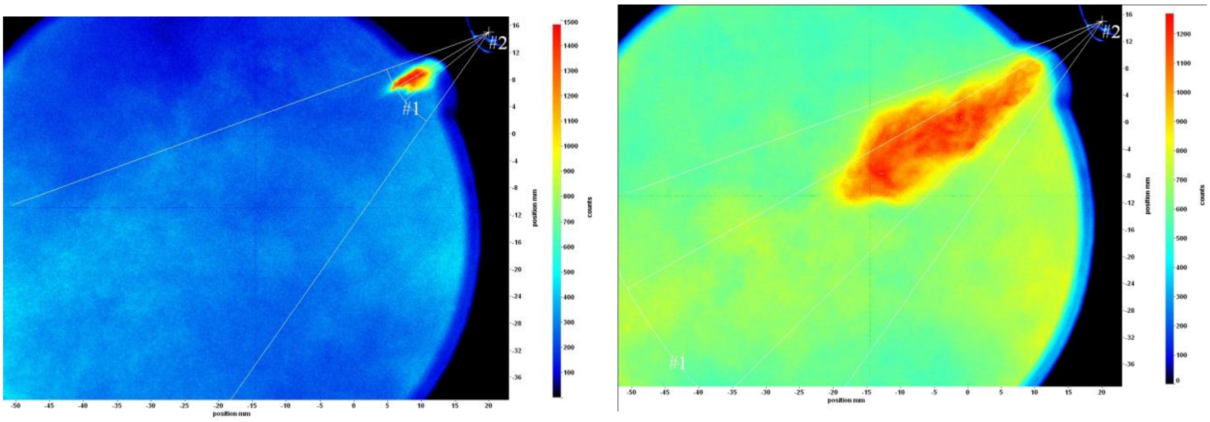

Figure 77: Atomized test fluid at 0.6ms and 1.15ms

The area of interest is the first 0.5ms of the injection. Prior to this study, there had not been any research conducted to accurately analyse the spray for this time period. Valentim [30] attempted to gain a better understanding of this portion of the spray; however his equipment was not able to accurately capture the spray in smaller time steps. The Inov8 Test Stand was able to capture images 0.01ms apart, however the limiting factor was the amount of fluid that can be injected per test.

If the test ran for too long, the spray chamber would fill up with vapour and the images captured would not be clear. Tests were run using the same parameters as above, and the time step was reduced to 0.02ms. The results are plotted in Figure 78 below.

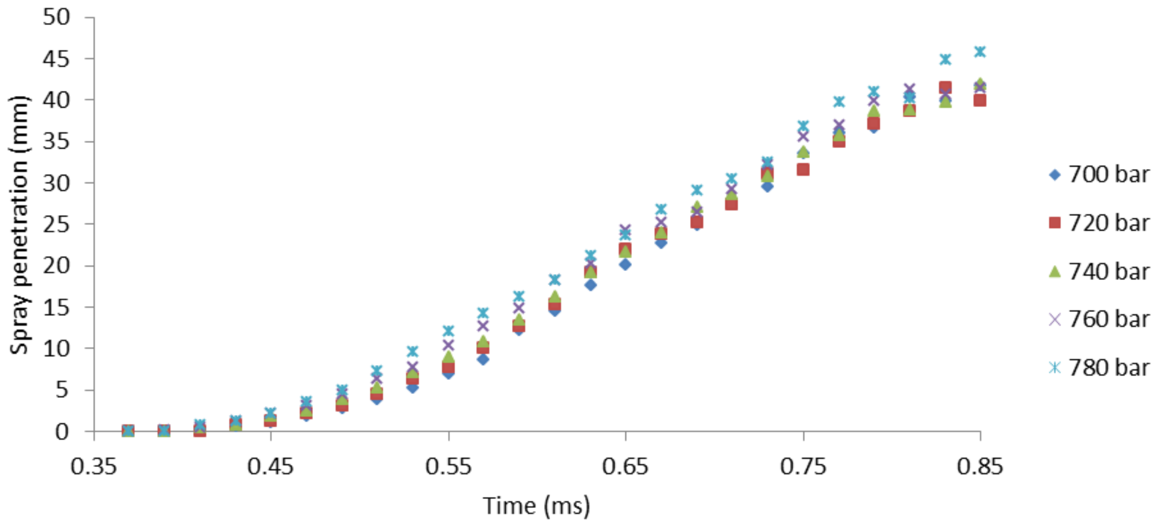

Figure 78: Spray penetration vs time. 5 bar cylinder pressure. 770 bar to 780 bar injection pressure using nitrogen. 0.02ms time step

Figure 78 shows the area of interest in higher resolution (more data points). From the figure, it can be seen that at higher injection pressure, the fluid is visible earlier. The injection pressure therefor has an influence on the opening of the injector. Referring to Figure 6, the pressurized fluid acts on the pressure shoulder at the top of the needle. This force pushes the needle up, assisting with opening the injector. The higher the injection pressure, the larger this force will be and therefore the faster the injector will open. Figure 79 shows the time at which the penetration reached 0.5mm for each of the injection pressures tested. This gives an indication of the time at which the fuel leaves the injector. From the figure, it can be seen that the time decreases at an increasing rate as the injection pressure is increased. The spray penetration reaches 0.5mm approximately 0.02ms earlier with a 780 bar injection pressure than it does with a 700 bar injection pressure. When the injector has to close, the opposite is true. The needle (spring) will have to act against this force to close the injector.

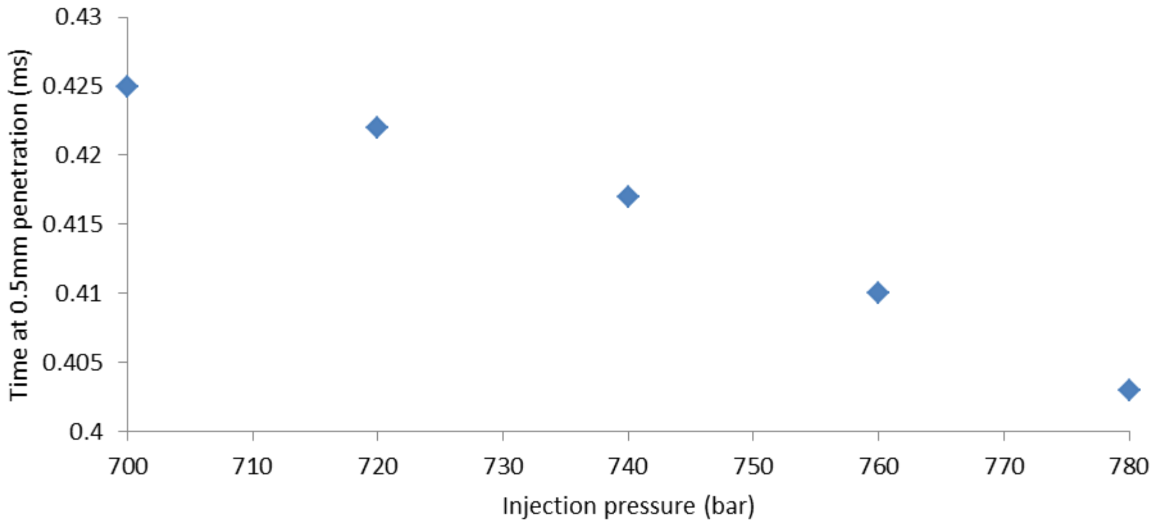

Figure 79: Time at 0.5mm penetration. 700 – 780 bar injection pressure. 5 bar cylinder pressure using nitrogen

Figure 80 shows the spray penetration with an injection pressure of 720 bar compared to the theoretical penetration. The delay between the signal being sent to the injector and the injector opening is known to be 0.35ms (a property of the injector). The figure shows that the fluid only starts to leave the injector between 0.41ms and 0.43ms after the signal is sent. This can be attributed to the relatively low injection pressure. As discussed, the start of injection is earlier with a higher injection pressure. The injector used was designed to operate with an injection pressure of 1400 bar and the test pressure was only reduced to preserve the solder on the tip (due to the modification made to make it a '1 hole injector'). According to the trend identified in Figure 79, at 1400 bar injection pressure, the start of injection would be closer to 0.35ms.

Reseach done by Karimi [23] found a discontinuity in the spray caused by lateral movements of the needle. Karimi measured the stop in the spray at approximately 0.15ms after the first sighting of fluid from the injector. The delay between the end of the first injection and the start of secondary injection was approximately 0.075ms. These points are represented by the vertical dotted lines on Figure 80. The black lines represent the range in which the injection starts (0.41ms – 0.43ms). According to Karimi, the stop in injection occurs between the purple lines (0.56ms – 0.58ms) and the start of the secondary injection occurs between the orange lines (0.635ms – 0.655ms).

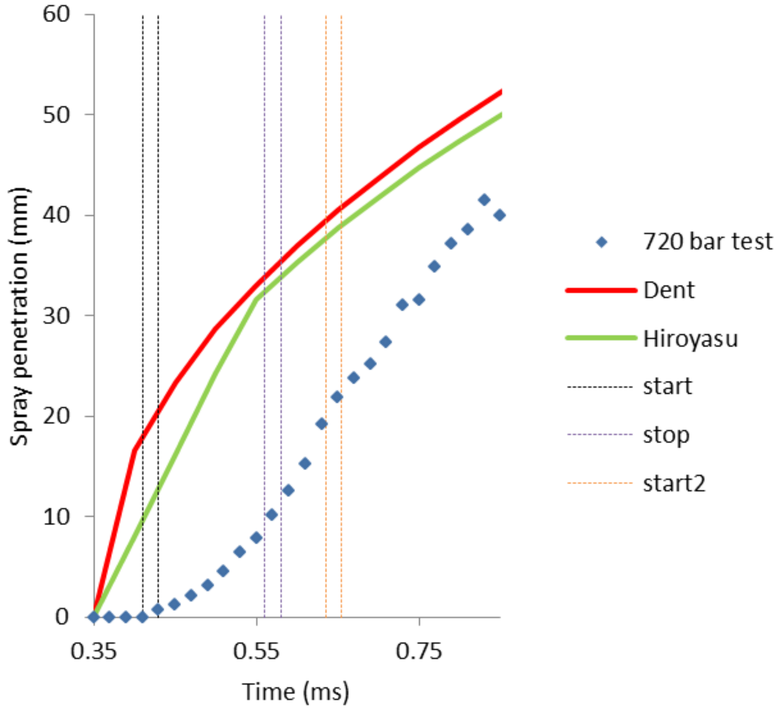

Figure 80: Spray penetration compared to theoretical results. 720 bar injection pressure. 5 bar cylinder pressure using nitrogen. 0.02ms time step.

From the figure, it can be seen that after the injection begins, the penetration increases at an increasing rate. There is a discontinuity in the spray at 0.57ms and the penetration increases linearly until 0.61ms where there is another discontinuity (between 0.61ms and 0.63ms). The first discontinuity falls within the range determined by Karimi; the rate of penetration slows down indicating that the injection has stopped. The second discontinuity occurs just before the predicted range. There is a jump in the penetration and it continues as normal thereafter, this indicates that the injection has begun again. The difference in the delay between Karimi and the experimental results could be due to differences in the injectors used and differences in the experimental setup.

Figure 81 below shows the variation of the cone angle with injection pressure for the same tests discussed above. The tests showed that the cone angle increases with increasing injection pressure. From the figure, it can be seen that the initial cone angles show no relationship with the injection pressure used; it reaches a maximum early in the injection and slowly decreases and settles down before increasing again towards the end of the injection.

When the fluid initially leaves the tip of the injector, it has a mushroom shape. This results in the cone angle being measured to be either very large or very small and does not fit in with the trend noticed with the rest of the data points. Between 0.45ms and 0.5ms, all the tests reached a maximum cone angle. This is due to the fact that the spray leaving the nozzle has not yet fully developed. As the spray progresses and the tip interacts with the air in the spray chamber, the spray takes on a conical shape and the cone angle starts to reduce.

Variations in the cone angle are due to variations in the boundary on the spray, caused by interactions with the spray chamber gas. Towards the end of the injection, as the spray starts to slow down; slow circulatory gas motion [24] causes a slight increase in the cone angle.

Typical values obtained from previous experiments for cone angle are between 25° and 30° which are higher than the range measured for this set of tests. Variations could be due to a number of reasons such as test fluid properties, nozzle geometries, gas densities and temperatures. It was noted by Klein-Douwel et. al that Mie-Scattering measured cone angles smaller than other methods such as Shadowgraphy. Actual cone angles vary broadly between 8° and 22° [24]

Figure 82 shows a comparison of the measured cone angle with an injection pressure of 760 bar and a cylinder pressure of 5 bar (nitrogen), and the theoretical cone angle. It can be seen that the measured values are very similar to the predicted cone angle with an average difference of 2.2% (21.7˚ theoretical, 21.3 ˚ test). The results for the other injection pressures can be found in APPENDIX D – RESULTS.

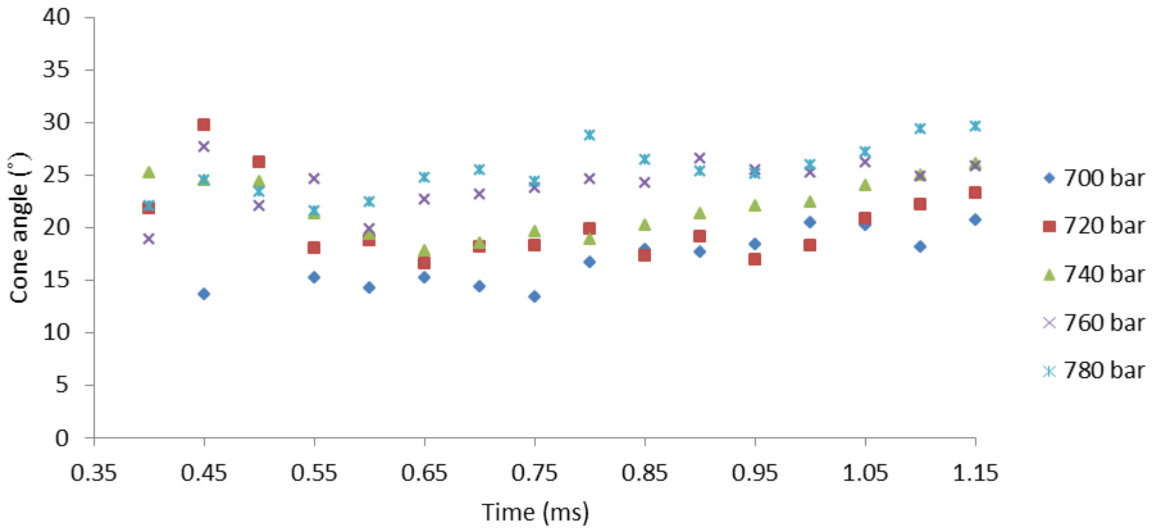

Figure 81: Cone angle vs time. 5 bar cylinder pressure. 700 – 780 bar injection pressure using nitrogen

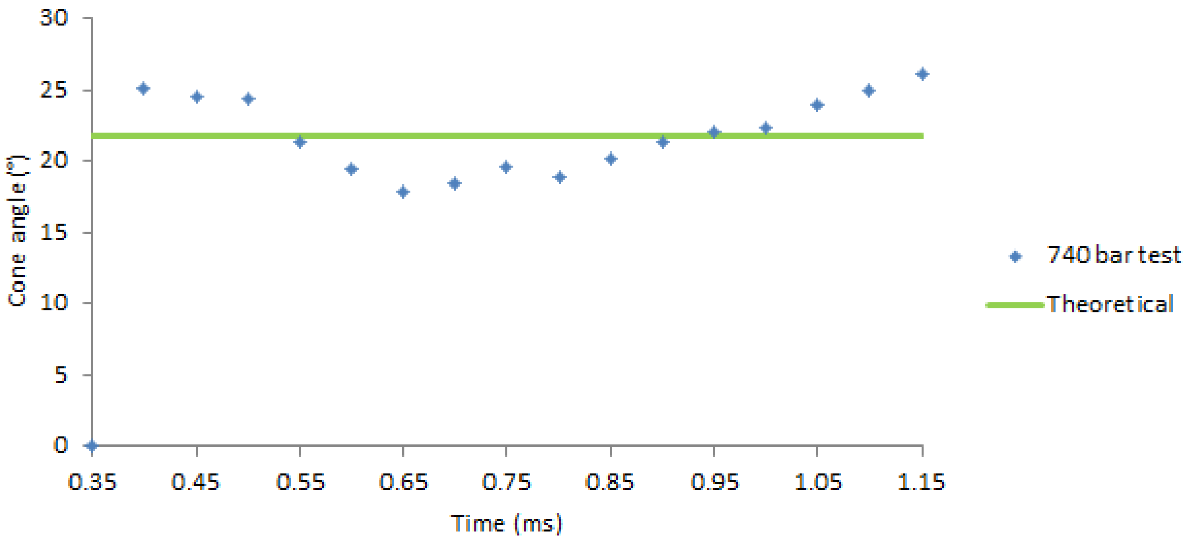

Figure 82: Cone angle test results compared to theory. 740 bar injection pressure. 5 bar cylinder pressure using nitrogen

Figure 83 below shows the injection delivery, injection rate and firing pulse (/100) vs time as measured by the Akribis with an injection pressure of 700 bar and a back pressure of 5 bar nitrogen. There was an injector delay specified when the tests were run and this explains the higher times on the graph when compared to the previous results discussed. The 0.35ms delay discussed earlier and attributed to the properties of the injector can be seen. The firing pulse starts at 1.73ms, there is no significant change in the injection rate until approximately

0.43ms later. The injector opens and the rate begins to increase quickly. The firing pulse is initially very large in order to overcome the inertia of the stationary needle. Once the injection rate begins to increase, a smaller injection pulse is applied to the injector in order to keep it open for the full duration of the injection. 0.8ms (user defined injection duration) after the start of the firing pulse, it suddenly reduces to 0 in order to close the injector and stop the injection process.

The hesitation in the injection that was noticed earlier is evident in the injection rate. After the injection rate begins to increase, it suddenly drops again between 2.265ms and 2.325ms. It then increases again. This is a delay of 0.06ms which is very close to the 0.075ms predicted by Karimi. When the firing pulse suddenly falls, the injection rate also starts to drop as the needle is forced closed by the spring. The delivery represents the volume of fluid injected by the injector as this process occurs; it is the integral of the injection rate with respect to time. It increases as the firing pulse increases and remains constant when the firing pulse stops and the injection rate goes back to 0.

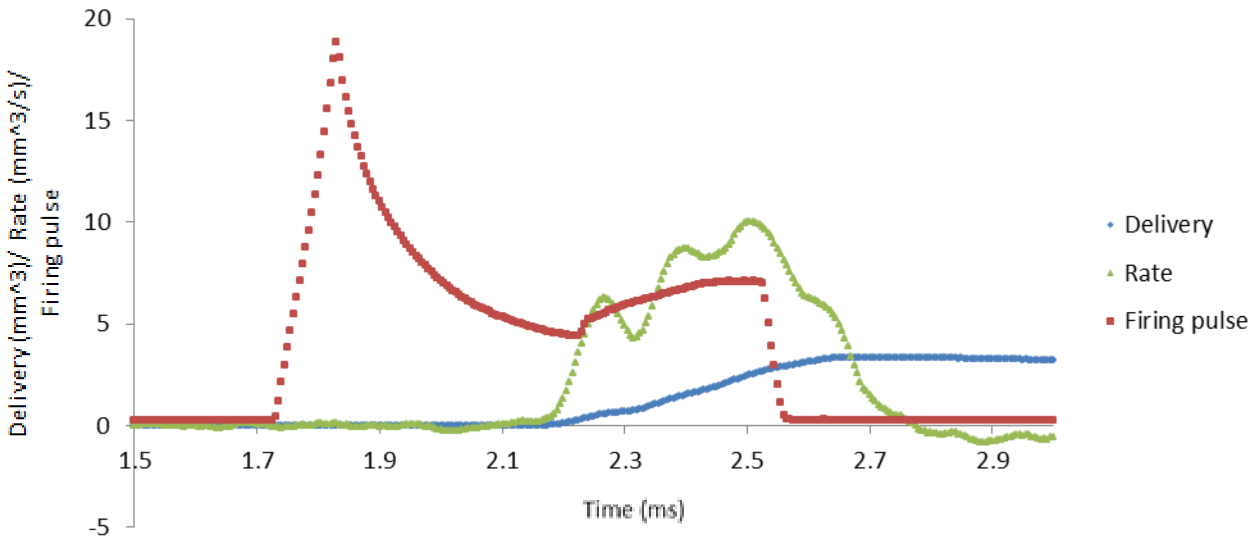

Figure 83: Injection delivery, rate and firing pulse vs time. 700 bar injection pressure. 5 bar cylinder pressure using nitrogen

Figure 84 shows the average firing pulse used for each of the tests (injection pressures). It can be seen that the firing pulses used were almost identical and were within 2.6% of each other. Figure 85 shows the injection rates for the tests. It can be seen that all of the injection rates follow the same trend. The hesitation is clearly evident in all the tests conducted. It can also be seen that an increase in injection pressure results in a higher injection rate. Another effect of a higher injection pressure was an injector that opened earlier, as previously discussed. It can be seen in Figure 85 that the injection rate begins to increase sooner with higher injection pressures; there is a 0.01ms difference between the start of the injection with injection pressures of 700 bar and 780 bar (time at which first measurement is recorded). The 0.02ms difference discussed earlier is influenced slightly by the acceleration of the fluid as well as the opening time of the injector. Figure 86 below shows the time at which each of the tests reached an injection rate of $1mm^3/s$. At higher pressures, the $1mm^3/s$ injection rate is achieved sooner. This again shows that the injection pressure definitely assists the needle in lifting.

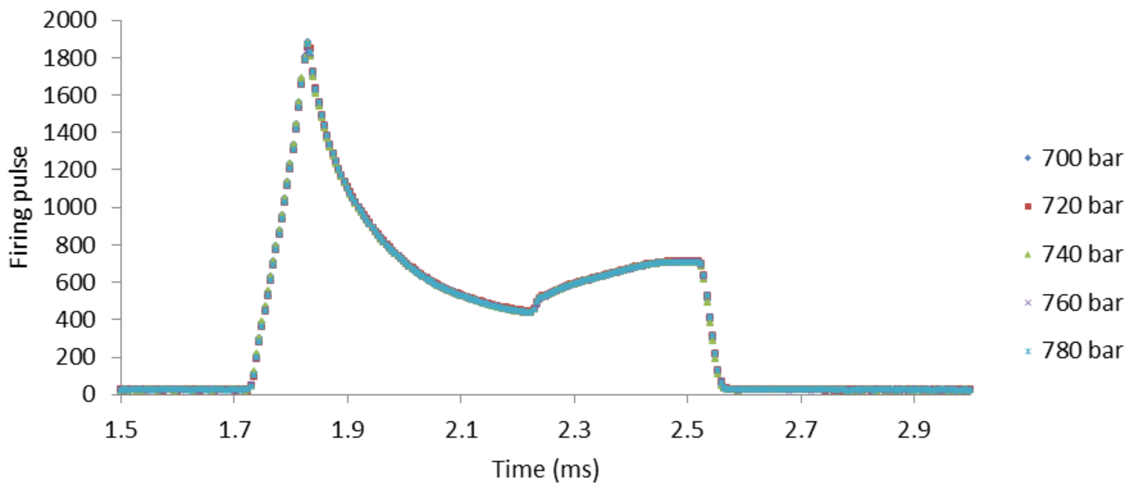

Figure 84: Firing pulse vs time. 700 – 780 bar injection pressure. 5 bar cylinder pressure using nitrogen.

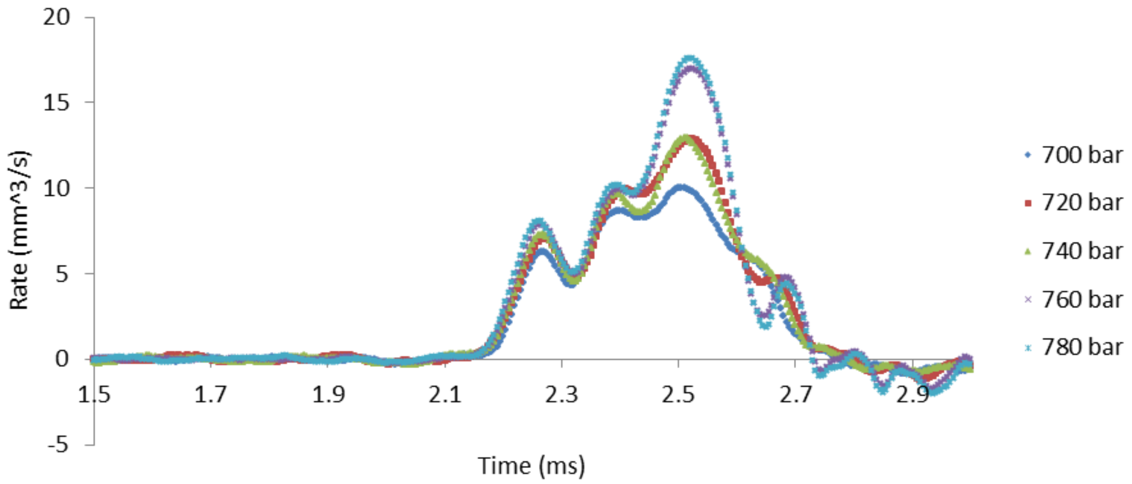

Figure 85: Injection rate vs time. 700 – 780 bar injection pressure. 5 bar cylinder pressure using nitrogen

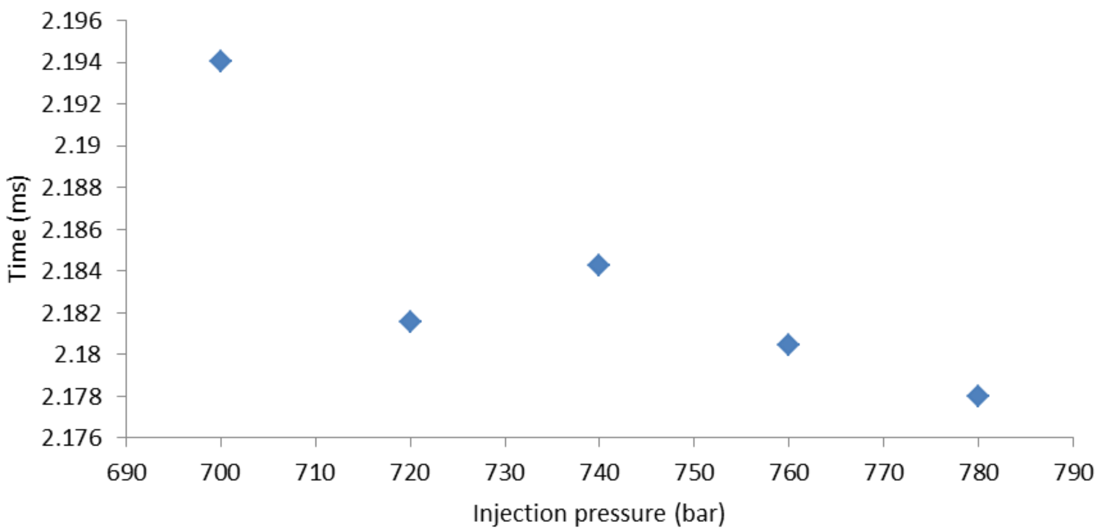

Figure 86: Time to 1mm^3/s rate vs injection pressure. 5 bar cylinder pressure using nitrogen

Figure 87 shows the injection delivery vs time for the injection pressures tested. The delivery is the time integral of the injection rate. As noted earlier, an increase in the injection pressure resulted in an increase in the injection rate; this explains why there is also an increase in the injection delivery with an increase in the injection pressure. The difference in the delivery between the tests with 720 bar and 740 bar, and 760 bar and 780 bar were very small; 2.3% and 3.7% respectively (the maxima of the firing pulse, injection rate and delivery can be found in

Table 2 below). This could be due to the fact that the pressure difference between consecutive tests was relatively small and fluctuations of ±12 bar were seen in the rail pressure during these tests.

Previous work by the author [40] compared new, used and reconditioned injectors and attributed small differences in injection rate and delivery with injection pressure changes to a faulty/worn out injector. Previous work used similar injectors that were not modified (6 hole injectors) and found that as the injection pressure approached 1400 bar injection pressure, the difference between the theoretical injection rates and the experimental injection rates reduced. This is due to the fact that the injectors were designed to operate at 1400 bar and worked optimally in those conditions. The current tests show that the difference between experimental and theoretical results grew larger as the injection pressure increased (25.7% at 700 bar to 55.4% at 780 bar). This is due to the fact that the nozzle was used and modified for these experiments and the theoretical values no longer apply. The experimental injection rates were higher than the theoretical predictions; this could indicate that the nozzle is worn and now larger than it originally was.

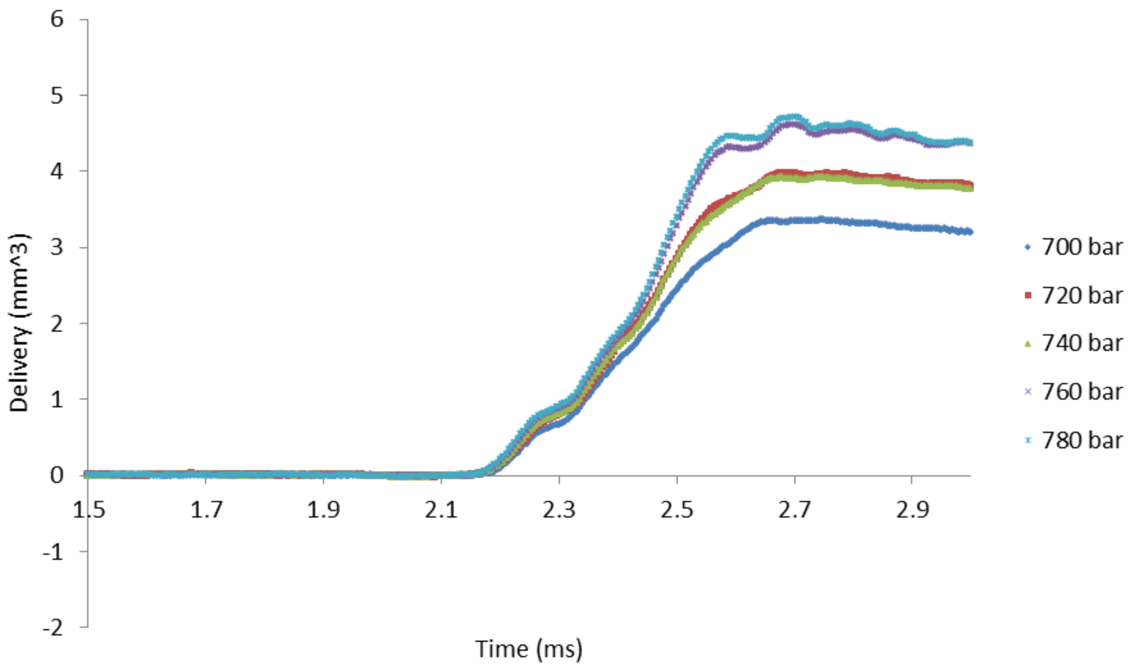

Figure 87: Injection delivery vs time. 700 – 780 bar injection pressure. 5 bar cylinder pressure using nitrogen

Table 2: 700 – 780 bar injection pressure, 5 bar cylinder pressure maxima

Injection pressure	700 bar	720 bar	740 bar	760 bar	780 bar
Injection Rate (mm^3/ms)	10.0	12.9	13.0	17.0	17.6
Firing pluse (bits)	1882.3	1851.6	1877.5	1833.9	1865.6
Delivery (mm^3)	3.8	4.4	4.3	5.2	5.4

6.2. Cylinder Pressure

To determine the sensitivity of spray penetration to variations in the cylinder pressure, the injection pressure was kept constant at 780 bar and the cylinder pressure was varied. This was done with nitrogen. The pressure was increased from 0 to 20 bar with the use of a pressure regulator on the cylinder. The cylinder pressure was verified by the pressure gauge mounted on the spray chamber. At each increment (5 bar), the test was repeated and the results were plotted as seen in Figure 88 below. The full set of results can be found in Table 5 in APPENDIX D – RESULTS.

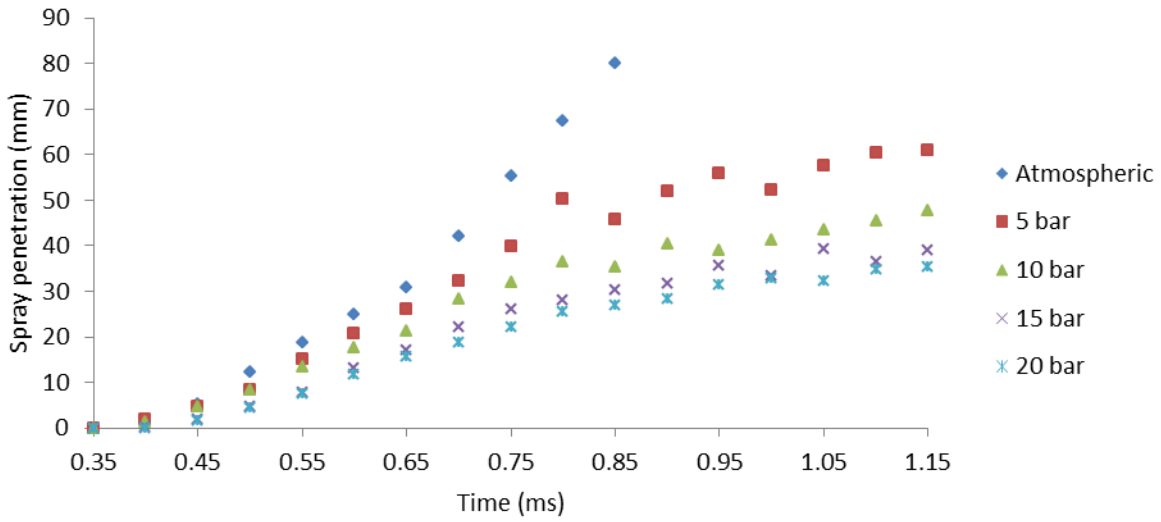

Figure 88: Spray penetration vs time. 780 bar injection pressure. 0 – 20 bar cylinder pressure using nitrogen

From the figure it can be seen that an increase in cylinder pressure results in a decrease in spray penetration. After the injection has begun, the effect of the change in cylinder pressure is noticeable earlier in the injection than with a variation in the injection pressure. The same general shape of the graph was noticed when compared to Figure 67 with the exception of the atmospheric test.

With atmospheric pressure in the cylinder (0 bar gauge pressure, 0.84 bar actual pressure) the spray penetration increased rapidly with the same hesitation as discussed in Section 6.1. At 0.9ms, the spray penetration was out of the frame of the camera and was too large to measure. The effect of the cylinder pressure on the spray penetration seems to decrease with increasing cylinder pressure. This can be seen in the trend shown in Figure 89 below. Figure 89 shows the average spray penetration at each cylinder pressure tested from 0.35ms to 1.15ms. The results for the test at atmospheric pressure were left out as a full set of results was not obtainable. The spray penetration was longer than the window and therefore out of the frame of the camera. Considering the average spray penetration across the test, the difference between 5 bar and 10 bar is 21.8% (8mm); between 10 bar and 15 bar the difference is 19.6% (5.6mm), and the difference between 15 bar and 20 bar is 10.5% (2.4mm).

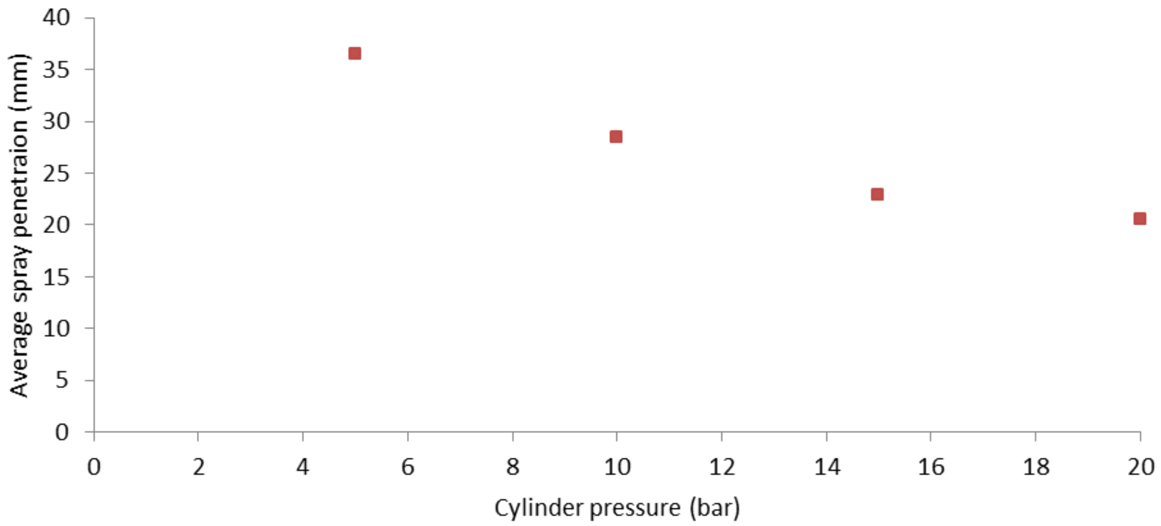

Figure 89: Average spray penetration vs cylinder pressure. 780 bar injection pressure. 5 bar to 20 bar cylinder pressure using nitrogen.

Hiroyasu's equation for predicting the time at which the spray would break up was approximately 0.3ms too early for all the tests conducted in this set of tests. The difference can be attributed to the experimental set up used.

Contrary to Karimi's findings [23], the fluctuations in the penetration were smaller at higher cylinder pressures. Karimi stated that the increased gas density and viscosity resulting from a higher cylinder pressure would increase cluster shedding. The increased density and viscosity appear to keep the main spray structure intact longer. Comparing the two images in Figure 90 below, a clear difference in the density can be seen. The image on the left had a cylinder pressure of 5 bar and the image on the right had a cylinder pressure of 20 bar; both images were captured at 1ms (after the signal was sent to the injector). The test fluid/nitrogen mixture that forms a shroud over the spray is smaller in the 20 bar test; this shows that the increased density does keep the structure together more than the 5 bar cylinder pressure.

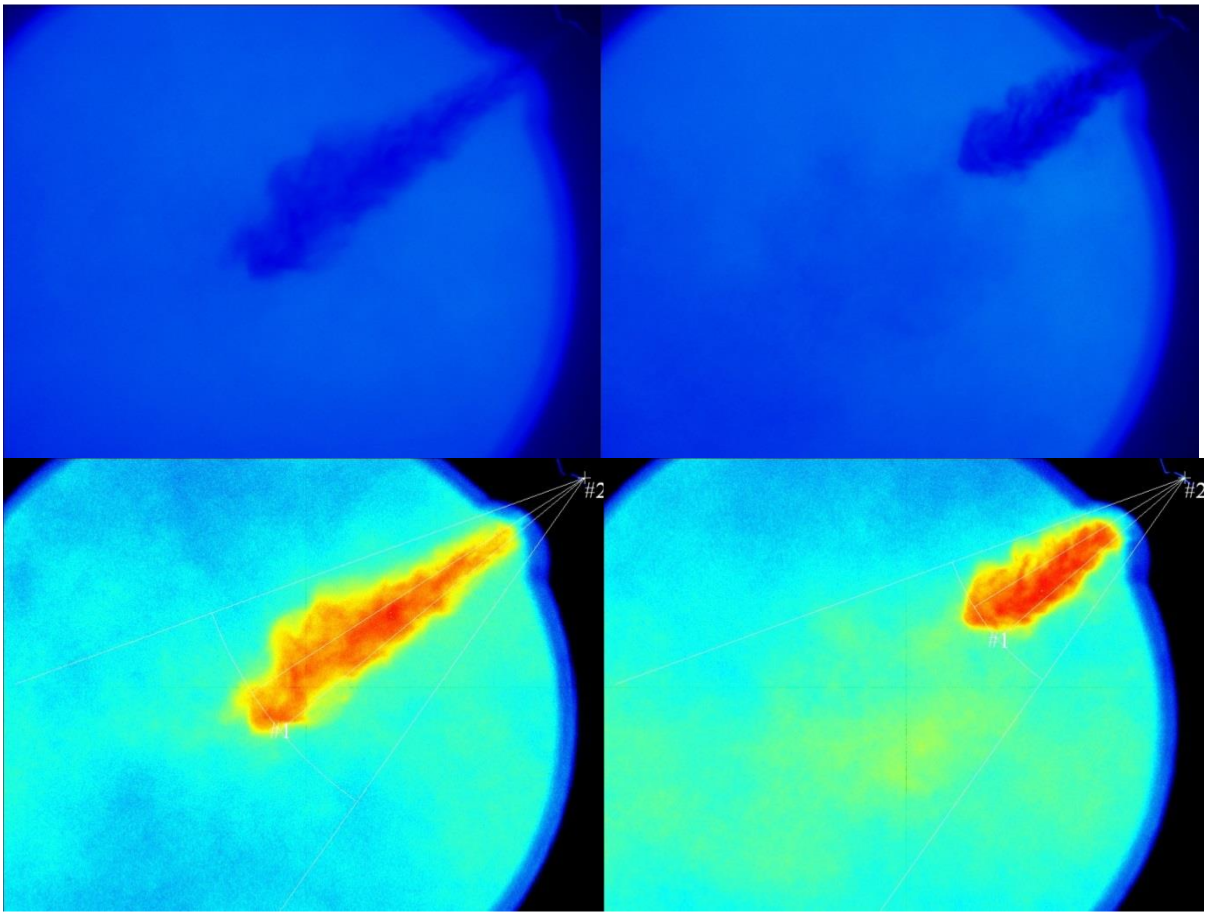

Figure 90: Comparison of spray with 5 bar (left) and 20 bar (right) cylinder pressure at 1ms.

Unlike with the tests varying the injection pressure, it can be seen in Figure 88 that all the injections for the current set of tests began at the same time. There is therefore no relation between the cylinder pressure and the injection delay. The injection delay is only influenced by the injection pressure.

Figure 91 shows the percentage difference between the test results and the models developed by Dent and Hiroyasu with an injection pressure of 780 bar and a cylinder pressure of 15 bar.

The full set of results can be seen in Figure 123 and Figure 124 in APPENDIX D – RESULTS. From the figure, it can be seen that Hiroyasu predicts the spray penetration more accurately than Dent throughout the injection. It was also noted that the accuracy of both models in predicting the spray penetration decreased as the cylinder pressure increased. Considering the average percentage difference for the whole injection event, Dent's variance increased from 26.6% with a cylinder pressure of 5 bar to 41.6% with a cylinder pressure of 20 bar. Similarly, Hiroyasu's variance increased from 22.6% to 38.9% with the same increase in cylinder pressure.

The accuracy of the models in predicting the spray penetration with atmospheric pressure did not follow the trend shown by the other tests. Dent's model showed an average variance of 46.5% and Hiroyasu 33.9%. This is higher than the variances for most of the subsequent tests. This is due to the fact that a full set of spray penetration results were not obtainable for the atmospheric pressure test as the spray quickly went beyond the frame of the camera; and the models were significantly less accurate for the earlier parts of the injection. It was also noted by Tonini et. al [39] that models that do not take into consideration the effects of cavitation in the nozzle tended to under-predict the velocity of the spray under atmospheric conditions. He concluded that nozzle cavitation plays an important role in the spray penetration under atmospheric conditions.

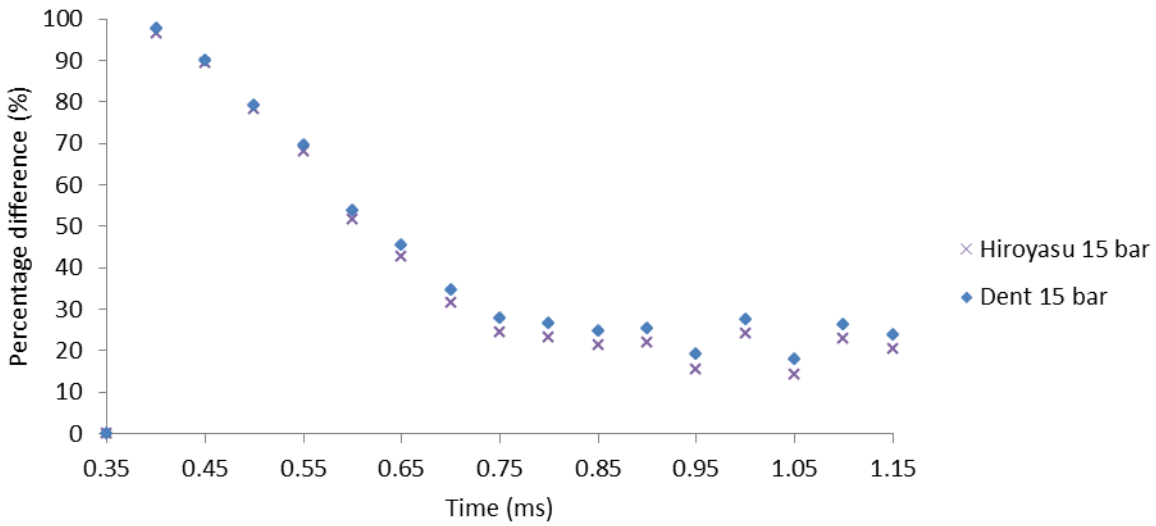

Figure 91 Percentage difference between theoretical Dent and Hiroyasu spray penetration; and test results. 780 bar injection pressure. 15 bar cylinder pressure using nitrogen.

Figure 92 below shows the variation of the cone angle with these same parameters. The cone angle (average) for the 10, 15 and 20 bar tests show that the cone angle increases with increasing cylinder pressure. With atmospheric and 5 bar cylinder pressure, the cone angles did not fit in the same trend although there was an increase in cone angle (0.8˚) when the cylinder pressure increased from atmospheric pressure to 5 bar. This can be attributed to the higher than expected velocity of the spray that results from cavitation in the nozzle.

Figure 93 shows a comparison between the average cone angle at each cylinder pressure tested and the theoretical cone angle. A comparison of the cone angle measured at each time step compared to its corresponding theoretical value can be found in Figure 137 to Figure 141 in APPENDIX D – RESULTS.

Considering Equation 2, the theoretical cone angle is proportional to the 4^{th} root of the pressure difference across the nozzle. An increase in the cylinder pressure with a constant injection pressure would result in a decrease in the pressure difference across the nozzle. However, from the experiments, it was seen that increasing the cylinder pressure increased the cone angle. This is due to the fact that the cone angle is also proportional to the 4^{th} root of the density of the gas in the spray chamber. Assuming ideal gas behaviour and constant gas temperature, the gas density is directly proportional to the pressure (increasing the gas pressure increases the gas density). Due to the large difference between the injection pressure and the cylinder pressure, changes in the cylinder pressure have a larger impact on the gas density than the pressure difference across the nozzle; the cone angle therefore increases with increasing cylinder pressure.

This increase in the cone angle can be explained as the resistance of the gas to the fluid moving in the axial direction. As the density of the gas increases, the interaction between the fluid particles and the gas particles increase. There is a larger momentum transfer between the particles and the tip of the spray is slowed down further. The fluid that is introduced into the spray chamber as the injection continues has a larger radial component as it moves in the axial direction. This tends to create a shorter, wider spray and therefore a larger cone angle, as seen in Figure 90.

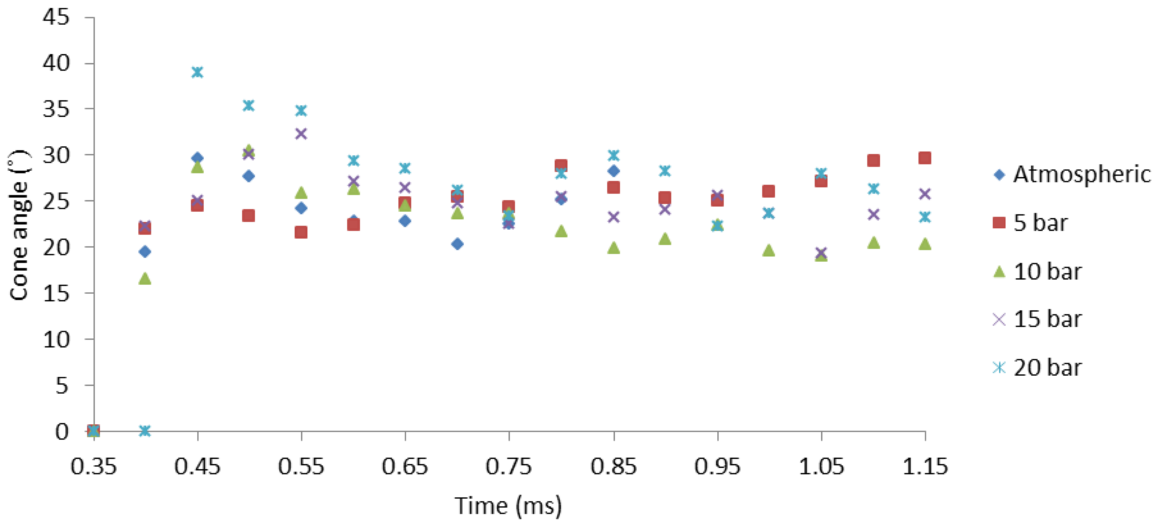

Figure 92: Cone angle vs time. 750 bar injection pressure. 0 – 20 bar cylinder pressure using nitrogen

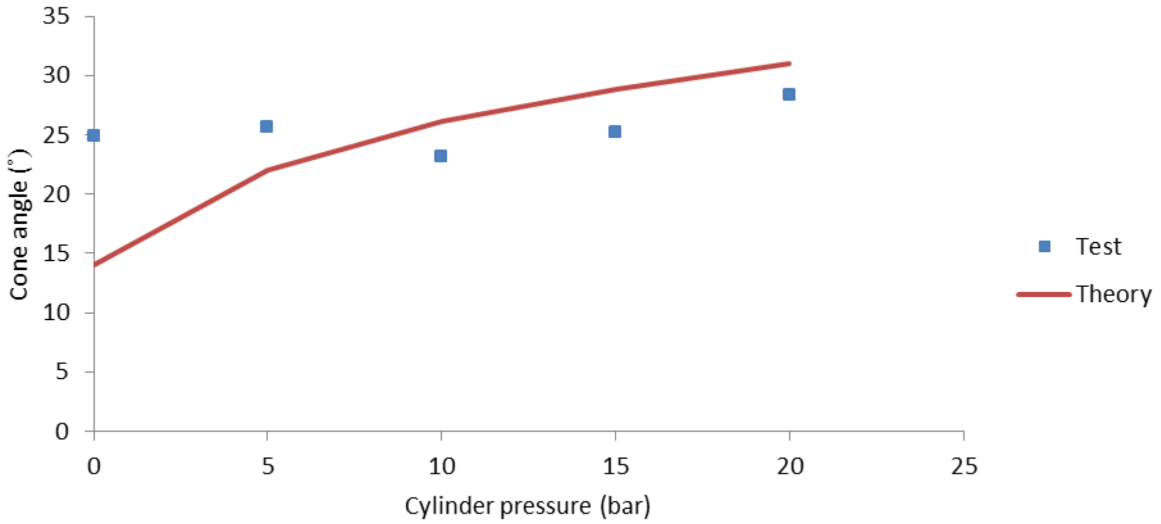

Figure 93: Average cone angle compared to theoretical cone angle. 780 bar injection pressure. Atmospheric – 20 bar cylinder pressure using nitrogen

Figure 94 and Figure 95 were obtained with the Akribis of the Inov8 Test Stand and show the firing pulse, injection rate and injection delivery vs time respectively. The tests were conducted with an injection pressure of 780 bar and cylinder pressures ranging from atmospheric pressure to 20 bar in 5 bar increments as above. It can be seen from Figure 94 that the firing pulse used for all the tests were almost identical. As with the case in the previous section, a large initial spike was needed to overcome the inertia of the needle and get it to lift. Thereafter, a smaller pulse was needed to keep the injector open and after 0.8ms, the signal to the injector was stopped so that the spring in the injector would return the needle to its original positon thus closing the injector and ending the injection process.

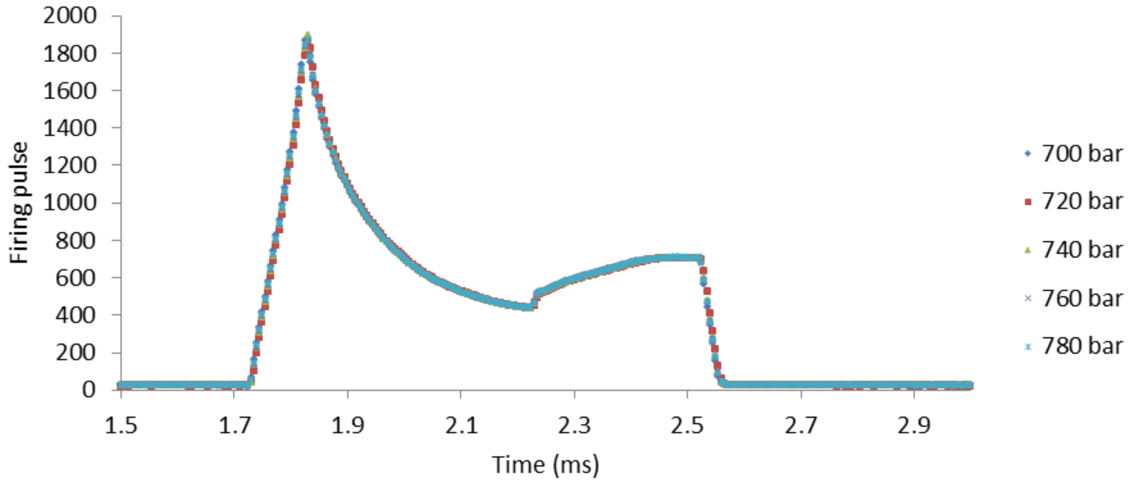

Figure 94: Firing pulse vs time. 780 bar injection pressure. Atmospheric - 20 bar cylinder pressure using nitrogen

Looking at the injection rate, it can be seen that at lower cylinder pressures, there are much larger oscillations. As the cylinder pressure is increased, the injection rate stabilizes and the graph is much smoother. As the cylinder pressure increases, the injection rate decreases. The cylinder pressure had no impact on the time at which the injection starts.

The large cone angles measured at atmospheric and 5 bar cylinder pressure can be explained by the large hesitations and spikes in injection rate (high velocity) at these pressures. After the initial spray, the fluid loses momentum (during the pause in injection) and begins to spread out radially before it is met by the secondary spray.

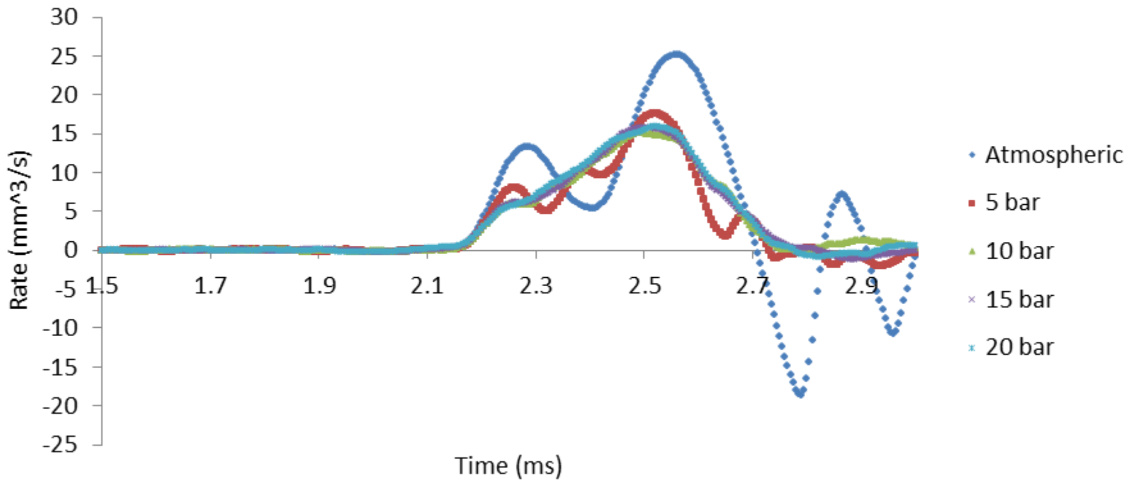

Figure 95: Injection rate vs time. 780 bar injection pressure. Atmospheric – 20 bar cylinder pressure using nitrogen

The spray hesitation discussed previously is more noticeable with a lower cylinder pressure. Figure 96 shows the average mean tip velocity vs cylinder pressure. From the figure, it can be seen that an increase in cylinder pressure results in a decrease in average mean tip velocity. The velocity decreases at a decreasing rate with a very dramatic reduction from atmospheric pressure to 5 bar (173.8m/s to 78.6m/s). The lower pressure gas has a lower density and therefore offers less resistance to the spray moving in the axial direction, thus explaining the higher velocities at lower pressures. The higher velocities mean that there is a larger flow rate out of the nozzle of the injector and this has an impact on the needle. The increased flow increases the lateral movement of the needle and thus increases the hesitation and oscillations noticed in the injection rate.

With a higher cylinder pressure, there is a lower flow rate out of the nozzle and thus less lateral movement of the needle. The reduction of the lateral movement reduces the length of the hesitation as seen in Figure 97 below. The duration of the hesitation decreases from 0.125ms to 0.015ms at 15 bar cylinder pressure; and the hesitation is completely gone when the cylinder pressure is increased to 20 bar. Although the cylinder pressure had no effect on the start of the injection, it did influence the time at which the injection stopped.

Figure 98 shows the time at the end of the injection vs the cylinder pressure. From the figure, it can be seen that an increase in the cylinder pressure results in a delay in the end of the injection. This is influenced by the velocity (flow rate) of the fluid out of the nozzle of the injector. As with the hesitation, a higher flow rate causes larger lateral movement of the needle. With the higher flow rate at the lower pressure, the needle is pulled towards the nozzle and covers the hole on its way down. At the higher cylinder pressures with the lower flow rate, the needle moved in a more axial direction and therefore the nozzle stays open longer (the needle is in a lower position before it covers the hole of the nozzle).

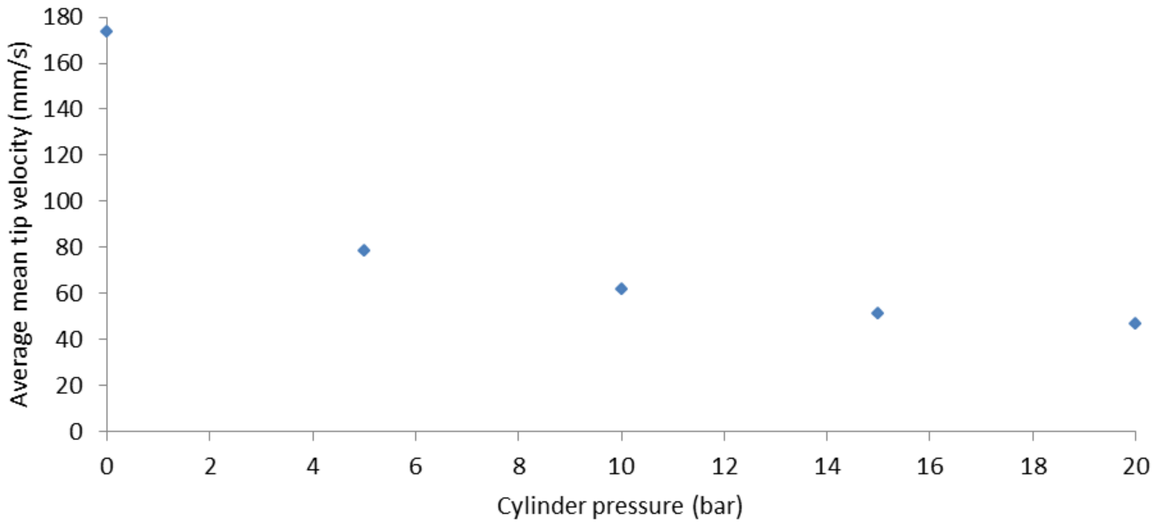

Figure 96: Average mean tip velocity vs cylinder pressure. 780 bar injection pressure. Atmospheric – 20 bar cylinder pressure using nitrogen

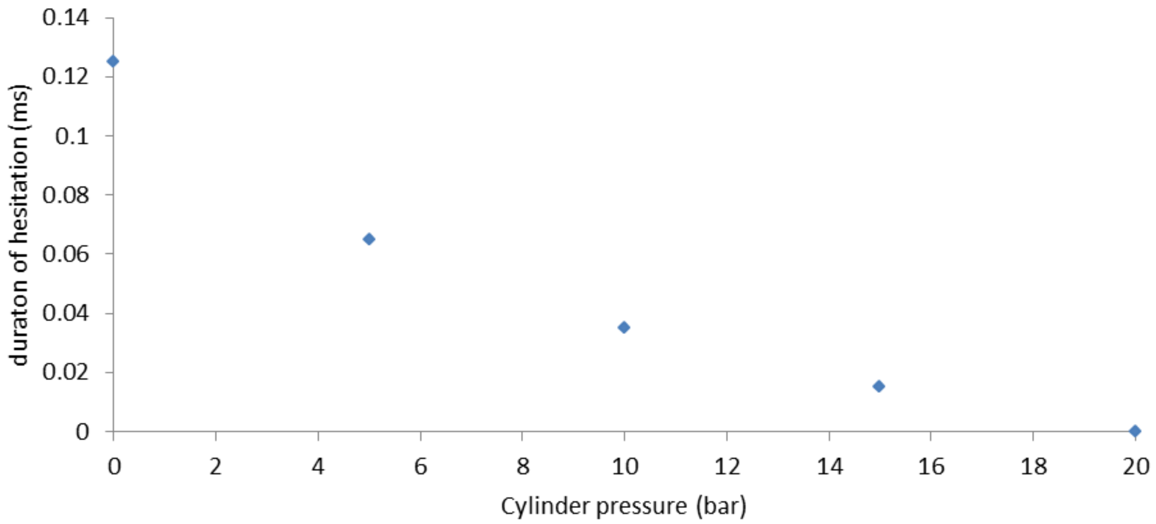

Figure 97: Duration of hesitation vs cylinder pressure. 780 bar injection pressure. Atmospheric – 20 bar cylinder pressure using nitrogen

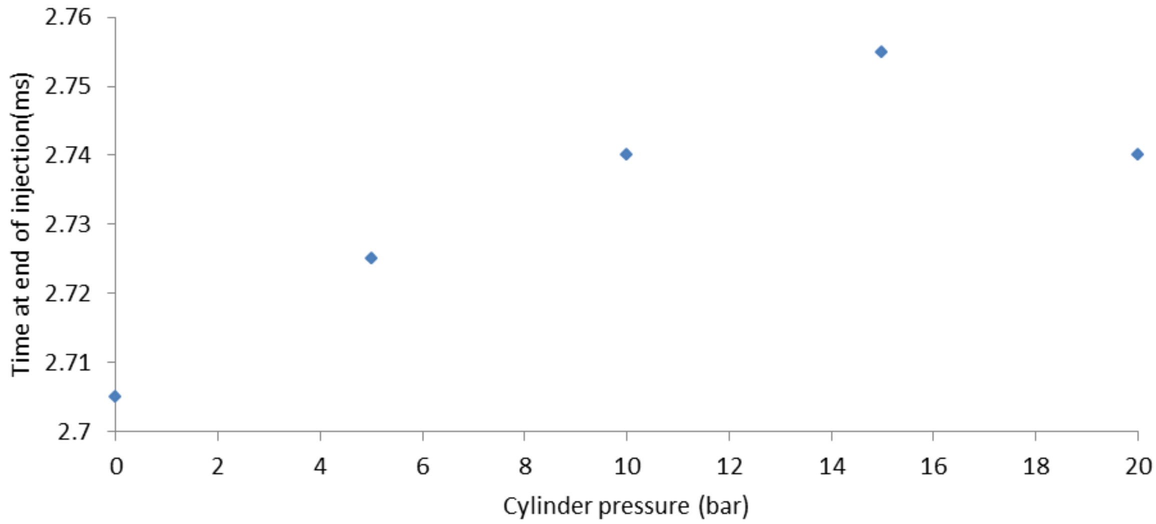

Figure 98: Time at end of injection vs cylinder pressure. 780 bar injection pressure. Atmospheric – 20 bar cylinder pressure using nitrogen

6.3. Pressure Difference

In order to determine if either the injection pressure or cylinder pressure individually, or the total pressure difference across the nozzle of the injector were more important, the following tests were conducted. Both the injection pressure and the cylinder pressure were varied while maintaining a constant difference between them. The tests were conducted with nitrogen in the spray chamber. The injection pressure was increased from 755 bar to 775 bar in increments of 5 bar, the corresponding cylinder pressure was increased from 0 to 20 bar in the same increments. The results of these tests for spray penetration are plotted in Figure 99 below. Figure 101 below shows the variation of the cone angle with these same parameters. The full set of results for these tests can be found in Table 6 in APPENDIX D – RESULTS.

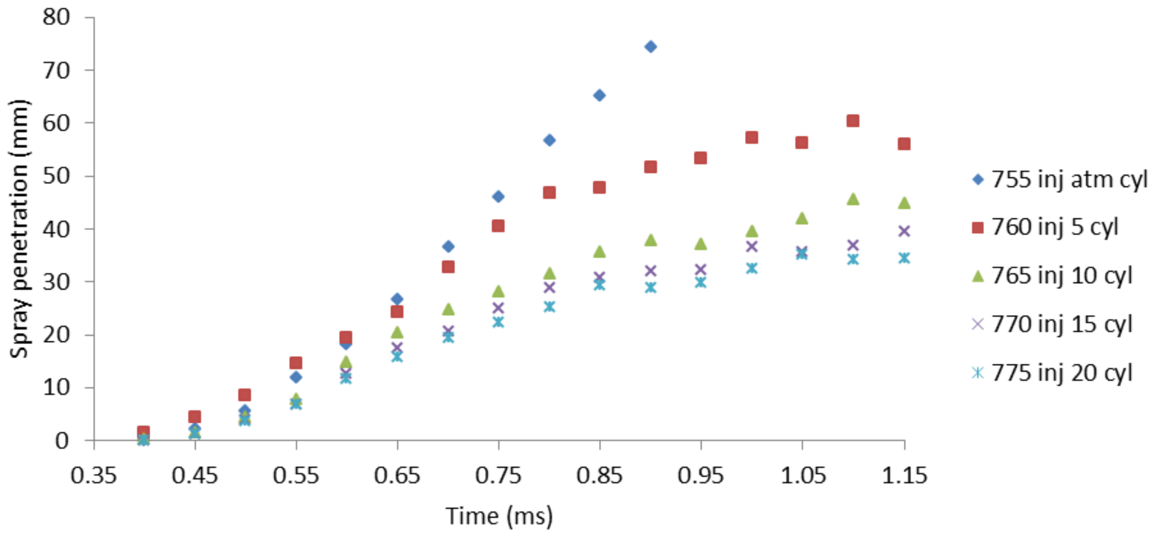

Figure 99: Spray penetration vs. time. 755 – 775 bar injection pressure. 0 – 20 bar cylinder pressure using nitrogen.

In Section 6.1 it was established that an increase in injection pressure increases the spray penetration and in Section 6.2, it was established that an increase in cylinder pressure reduces the spray penetration. From Figure 99 it can be seen that as the pressures increase, the spray penetration decreases. This means that for the pressure ranges tested, the change in cylinder pressure has a larger effect on the spray penetration than the change in injection pressure. As with the tests varying the cylinder pressure with a constant injection pressure; the difference between tests at higher cylinder pressures show smaller differences than tests with the same increments at lower cylinder pressures. There was an average difference of 27.8% in the spray penetration between the tests with 5 bar and 10 bar cylinder pressure. The average difference was only 8.4% between the tests with 15 bar and 20 bar.

The spray penetration for the test with atmospheric pressure in the cylinder increased in the same way as the test done with atmospheric pressure in the previous section. The oscillations in the spray penetration that are caused by cluster shedding decrease in magnitude as the cylinder pressure is increase. This set of tests corroborates the theory proposed in the previous section that a higher cylinder pressure (and gas density) keeps the spray structure more intact and reduces the effects of cluster shedding.

Figure 100 below shows the spray penetration test results compared to theory with an injection pressure of 760 bar and a cylinder pressure of 5 bar, the results for the other tests can be found in APPENDIX D – RESULTS. The theoretical models predict the spray penetration quite accurately between 0.85ms and 1.1ms. It was noted that as the pressures increased, the difference between the test results and theoretical results grew larger. Section 6.1 described how the accuracy of the models increased as the injection pressure increased, while Section 6.2 described how the accuracy of the models decreased with increasing cylinder pressure; this again illustrates the dominance of changes in cylinder pressure over changes injection pressure.

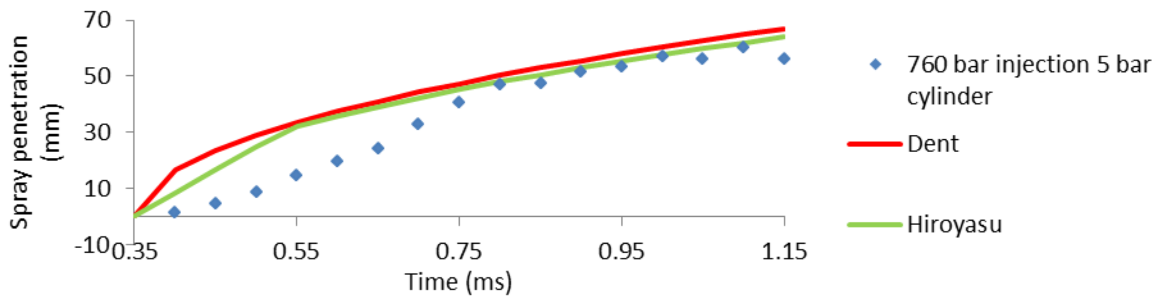

Figure 100: Spray penetration test results compared to theory. 760 bar injection pressure. 5 bar cylinder pressure using nitrogen

It has been established that increasing the injection pressure assists the fluid in passing through the nozzle thereby increasing the flow rate (injection rate) and spray penetration. Increasing the cylinder pressure has the opposite effect and hinders the flow of fluid out the nozzle. The current set of tests kept the pressure difference (driving force of the fluid) constant so there should be no increase in spray penetration as the pressures are increased. Increasing the cylinder pressure had the effect of increasing the gas density in the cylinder, so this should have reduced the spray penetration. The combined effect of raising the injection pressure and cylinder pressure was to reduce the spray penetration, even with the same pressure difference.

This demonstrates the effect of the gas density on the spray. The denser gas has more particles per unit volume and therefore there are more interactions between the droplets of injected fluid and the gas. The effects of friction are increased as the fluid moves through the gas and the momentum transfer from the moving fluid to the stationary gas is increased. This explains why the differences in spray penetration are larger later in the injection, when the penetration is more dependent on the momentum it has than the pressure difference across the nozzle.

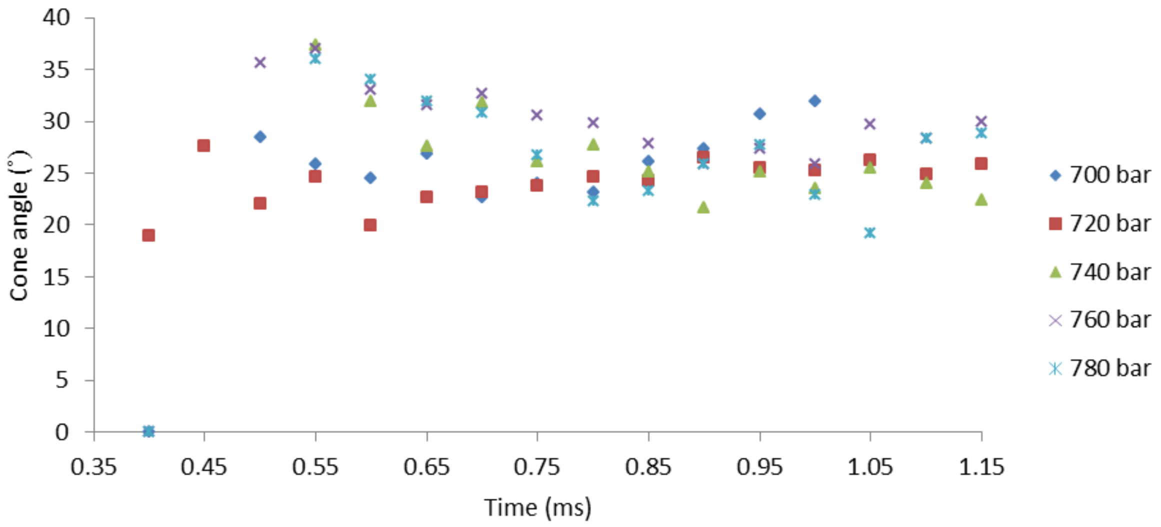

Figure 101: Cone angle vs. time. 755 – 775 bar injection pressure. 0 – 20 bar cylinder pressure using nitrogen.

Figure 101 shows the cone angle vs time for the set of tests described above. According to the theoretical model, the cone angle should increase at a decreasing rate as the pressures are increased, however, no correlation was found between the cone angle and the combinations of pressures tested. This could be due to the experimental setup.

Hiroyasu was of the opinion that the injection pressure is more important than the cylinder pressure in the earlier parts of the injection, before the spray breaks up, and the cylinder pressure becomes more important than the injection pressure after the spray has broken up. With reference to Figure 67 and Figure 88, it can be seen that at the pressures tested, the changes in cylinder pressure had a more significant impact on the spray penetration than the changes in injection pressure. The changes in the cylinder pressure represent a larger percentage of the pressure than the changes in the injection pressure, however this will always be the case as the injection pressure will always be much higher than the cylinder pressure.

Figure 102 shows a direct comparison of the spray penetration for the tests with 755 bar injection pressure and atmospheric cylinder pressure, and 760 bar injection pressure and 5 bar cylinder pressure. From the figure, it can be seen that the spray penetration for the test with the 760 bar injection pressure starts off very similar to (slightly higher than) that of the 755 bar test. Between 0.6ms and 0.65ms, the spray penetration of the 760 bar test drops below that of the 755 bar test. Similar trends can be seen when comparing two consecutive tests. This validates Hiroyasu's theory. Early on in the injection, the higher injection pressure of the second test results in a higher spray penetration, later on in the injection, the cylinder pressure has a larger impact and the higher cylinder pressure negates the effect of the higher injection pressure. This change however happens before the spray breaks up. The early phase of the injection is mostly dependent on the injection pressure (response of the injector), as it enters the air, the pressure difference across the nozzle will be the main factor to determine the spray penetration. Once the spray is further away from the nozzle, the cylinder gas properties will dominate the behaviour.

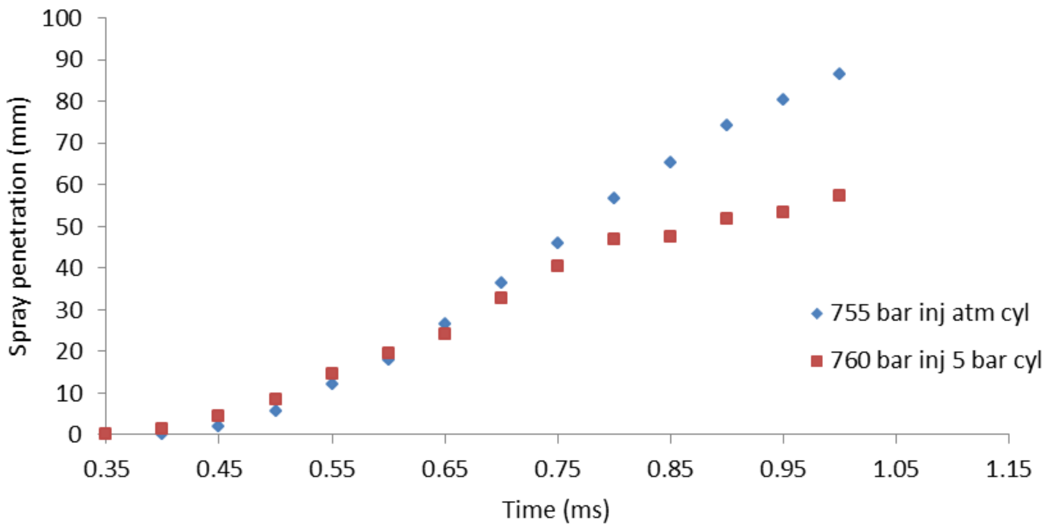

Figure 102: Spray penetration comparison. 755 bar injection pressure atmospheric cylinder pressure and 760 bar injection pressure 5 bar cylinder pressure using nitrogen

6.4. Nitrogen vs. Carbon Dioxide

The tests described in Sections 6.1, 6.2 and 6.3 were repeated with carbon dioxide in the spray chamber instead of nitrogen. The results of the tests for varying injection pressure are presented below. Figure 103 shows a plot of the spray penetration vs time with constant cylinder pressure (5 bar) and injection pressure between 700 and 780 bar.

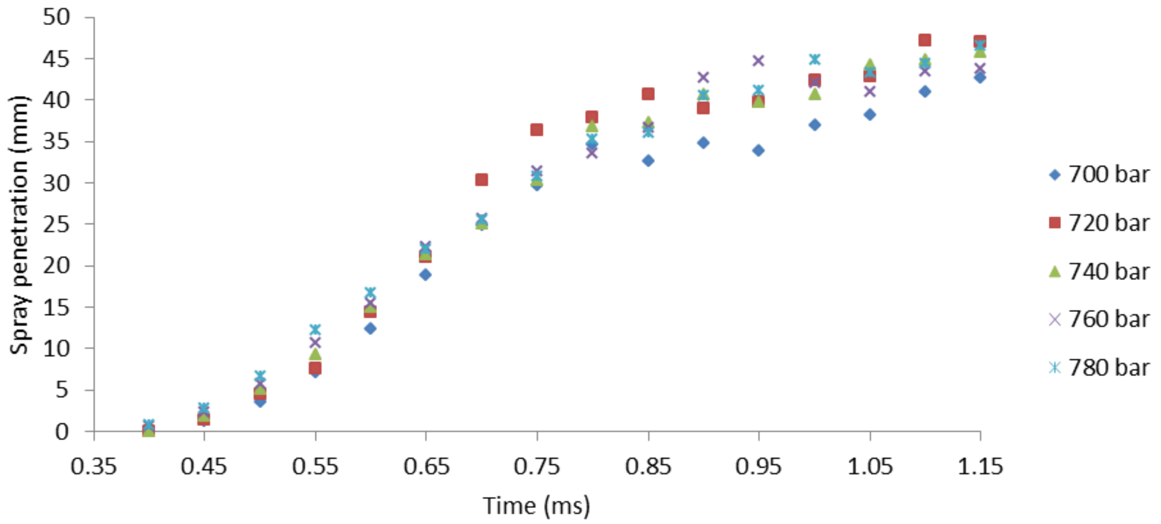

Figure 103: Spray penetration vs time. 5 bar Cylinder pressure. 700 – 780 bar injection pressure using carbon dioxide

From the figure it can be seen that the spray penetration follows the same pattern as seen in Section 6.1. An increase in injection pressure results in an increase in the spray penetration. The difference in spray penetration is smaller earlier on in the injection, but becomes larger towards the end of the injection. Comparing the difference in spray penetration for the earlier part of the injection (Figure 67) it can be seen that the injection pressure has a greater influence on the spray penetration with the carbon dioxide tests. At 0.6ms, the difference in spray penetration between tests with 700 bar and 780 bar injection pressure are 21.8% with nitrogen and 35.8% with carbon dioxide. Similar differences are seen at other times steps.

Figure 104 shows a direct comparison between the spray penetration obtained with nitrogen and carbon dioxide; with an injection pressure of 760 bar and a cylinder pressure of 5 bar. The results for the other tests can be found in APPENDIX D – RESULTS (Figure 151, Figure 152, Figure 153 and Figure 154). From the figure, it can be seen that a lower spray penetration is obtained with carbon dioxide than with nitrogen. The same is true at the other injection pressures tested. The difference is larger towards the end of the injection with an almost constant difference in the earlier parts. This is due to the difference in the densities of the gases and the effect of gas density on the momentum of the spray at the later parts of the injection. Figure 105 shows the percentage difference between the average spray penetration for nitrogen and carbon dioxide, at the various injection pressures tested, between 0.35ms and 0.75ms. With the exception of the test done at 720 bar injection pressure, the difference is almost constant. The carbon dioxide test at 720 bar resulted in a spray penetration that was larger than expected. This was due to the setup of the experiment (fluctuations in injection pressure). No correlation was found for the later part of the injection. This can be attributed to the dynamic nature of the interactions between the injected fluid and the gas in the chamber.

Comparing the results for the different gases during the later part of the injection, it can be seen that the spray penetration obtained with carbon dioxide has much smaller oscillations than the tests done with nitrogen. This means that there is less cluster shedding with the carbon dioxide. The difference in the gradients indicates that the spray has a lower velocity in the carbon dioxide.

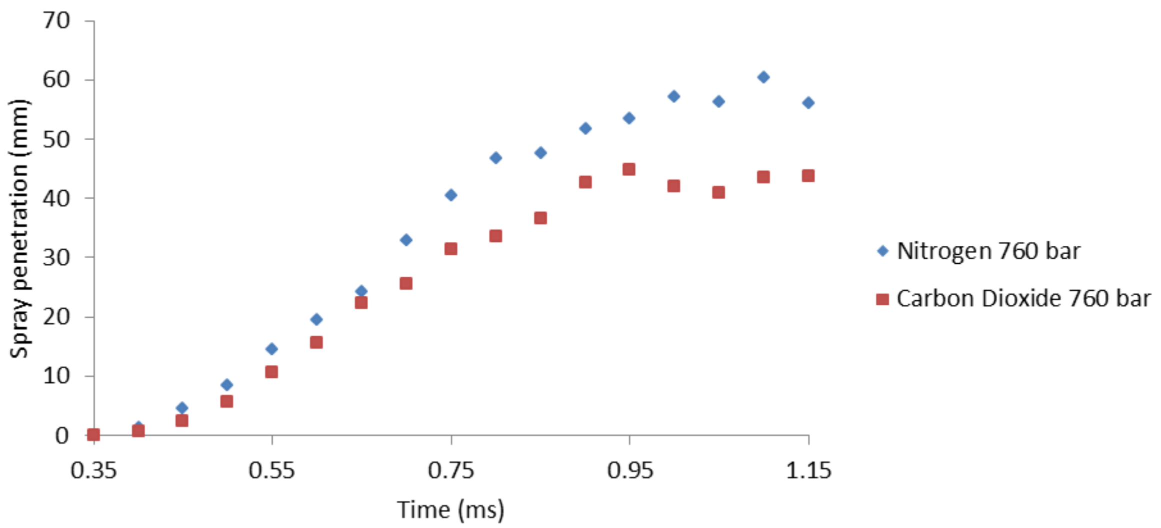

Figure 104: Spray penetration. Nitrogen compared to carbon dioxide. 760 bar injection pressure. 5 bar cylinder pressure.

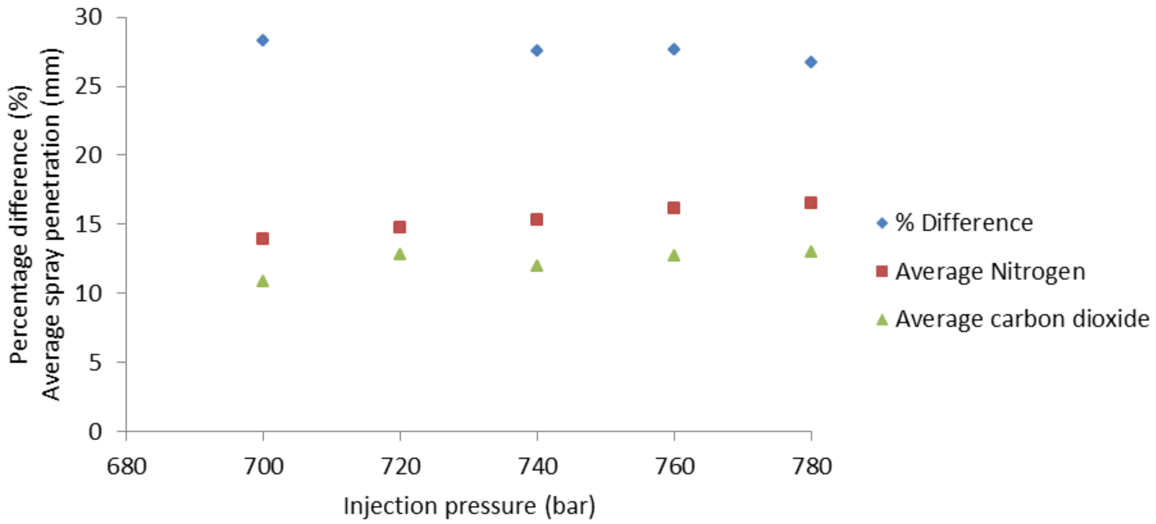

Figure 105: Percentage difference between nitrogen and carbon dioxide spray penetration. Average 0.35ms to 0.75ms.

Due to the higher molecular mass of the carbon dioxide, according to ideal gas principles, at the same pressure and temperature, carbon dioxide will have a higher density than nitrogen. Considering Equation 3, which gives the spray penetration predicted by Dent; the spray penetration is inversely proportional to the 4^{th} root of the density of the gas. This means that the spray penetration decreases at a decreasing rate as the gas density increases.

Equations 5 and 6 give the spray penetration predicted by Hiroyasu before and after the spray breaks up respectively. Equation 5 is not dependent on the density of the gas and this suggests that spray penetration before the spray breaks up is only dependent on the pressure difference across the nozzle and not on the pressure of the gas in the chamber. Equation 6 suggests that the spray penetration is inversely proportional to the 4^{th} root of the density of the gas as predicted by Equation 3.

Figure 106 shows the variation of the cone angle over time with these same parameters. As was the case with the nitrogen test, increasing the injection pressure resulted in an increase in the cone angle. The test at 720 also showed a higher than expected cone angle due to the experimental setup (fluctuations in injection pressure). Based on the difference in the density and viscosity of nitrogen and carbon dioxide and considering Equation 2 for cone angle, the average difference between the nitrogen and carbon dioxide cone angles should be 22.5%, the average experimental difference was found to be 17.3% with the carbon dioxide cone angle being larger. The difference is due to experimental set up and properties of the injector nozzle (modified nozzle and wear on the nozzle) and test fluid.

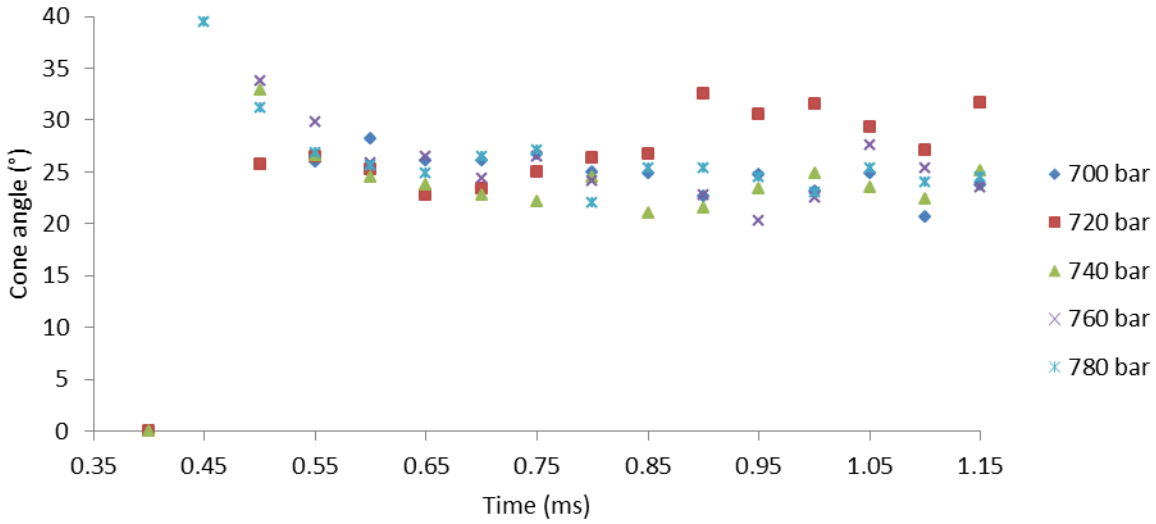

Figure 106: Cone angle vs time. 7 bar Cylinder pressure. 700 – 780 bar injection pressure using carbon dioxide

Figure 107 below shows a plot of the spray penetration vs time with a constant injection pressure of 780 bar and a cylinder pressure that varies between atmospheric and 20 bar with carbon dioxide.

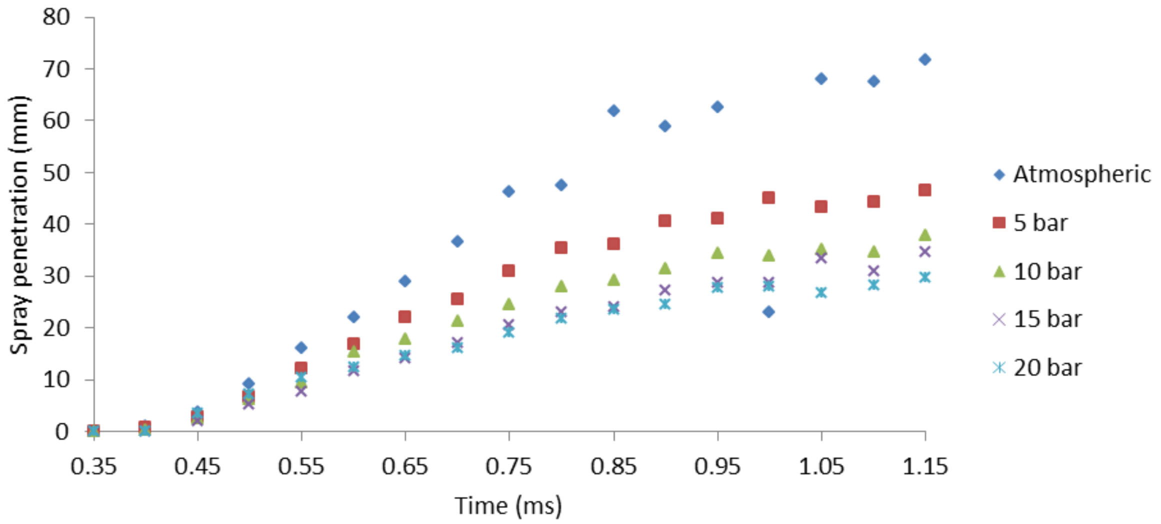

Figure 107: Spray penetration vs time. 780 bar injection pressure. Atmospheric – 20 bar cylinder pressure using carbon dioxide

From Figure 107 it can be seen that with carbon dioxide in the spray chamber, the spray penetration decreases with increasing cylinder pressure. The difference at any given time step, between two consecutive tests, decreases as the cylinder pressure increases. This is expected and was also correctly predicted by the theoretical models discussed (spray penetration decreasing at a decreasing rate with increasing cylinder pressure (density)).

Comparing Figure 107 and Figure 88 shows that a smaller spray penetration is obtained at any given pressure with carbon dioxide than with nitrogen, even tests at atmospheric pressure. The tests at atmospheric pressure were done by purging the spray chamber with the gas of interest. This is due to the higher density of the carbon dioxide. The gradients of the data sets indicate that the velocity of the spray decreases with increasing pressure.

Figure 108 shows a comparison of the spray penetration obtained with nitrogen and carbon dioxide with an injection pressure of 780 bar and a cylinder pressure of 10 bar. The results for the other tests can be found in APPENDIX D – RESULTS (Figure 160, Figure 161, Figure 162 and Figure 163). It is evident that the difference in gas density affects the spray penetration from early on in the injection. As in Figure 104 the reduced spray penetration due to the denser gas becomes apparent at 0.4ms.

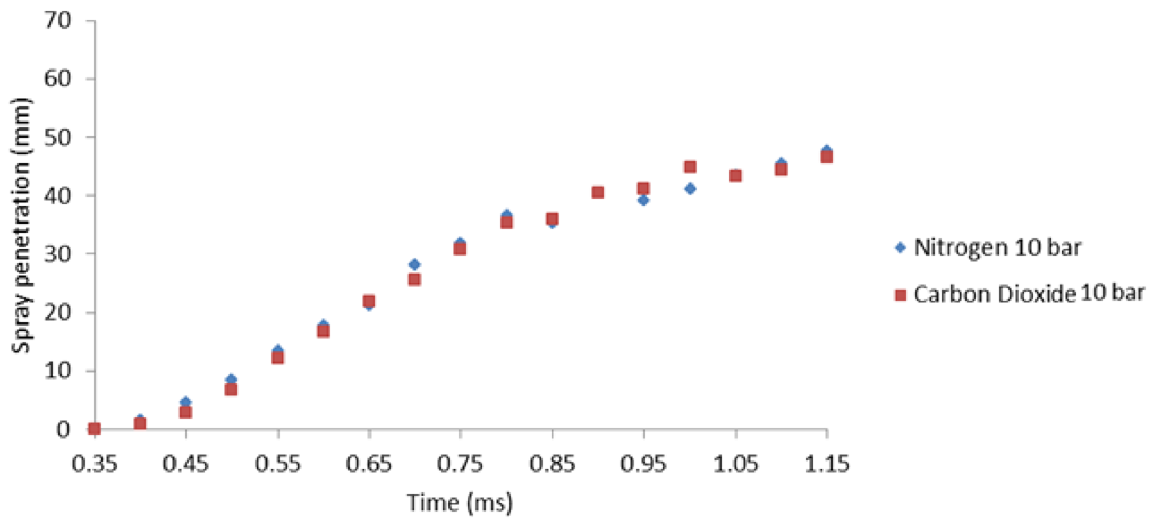

Figure 108: Spray penetration. Nitrogen compared to carbon dioxide. 780 bar injection pressure. 10 bar nitrogen 5 bar carbon dioxide cylinder pressure.

Figure 109 shows the percentage difference between the spray penetration with nitrogen and carbon dioxide at the various cylinder pressures tested. Due to the low resistance of the nitrogen at atmospheric pressure, the spray penetration grew rapidly and went beyond the frame of the camera before the end of the injection event. Due to this, the average spray penetration for that test is not a true reflection and can be disregarded. This explains the negative difference between the nitrogen and carbon dioxide tests at atmospheric pressure.

Considering the other data points, it can be seen that the difference between the two sets of tests decreases as the cylinder pressure is increased. This is due to the relationship described earlier between the spray penetration and the gas density. As the pressures are increased, the gas densities increase and the spray penetration becomes less sensitive to changes of gas density. The percentage difference in spray penetration between the two gases decreases from 29.8% at 5 bar to 12.1% at 20 bar. If higher pressures were tested, according to this trend, the differences would be even smaller until no difference is noticed.

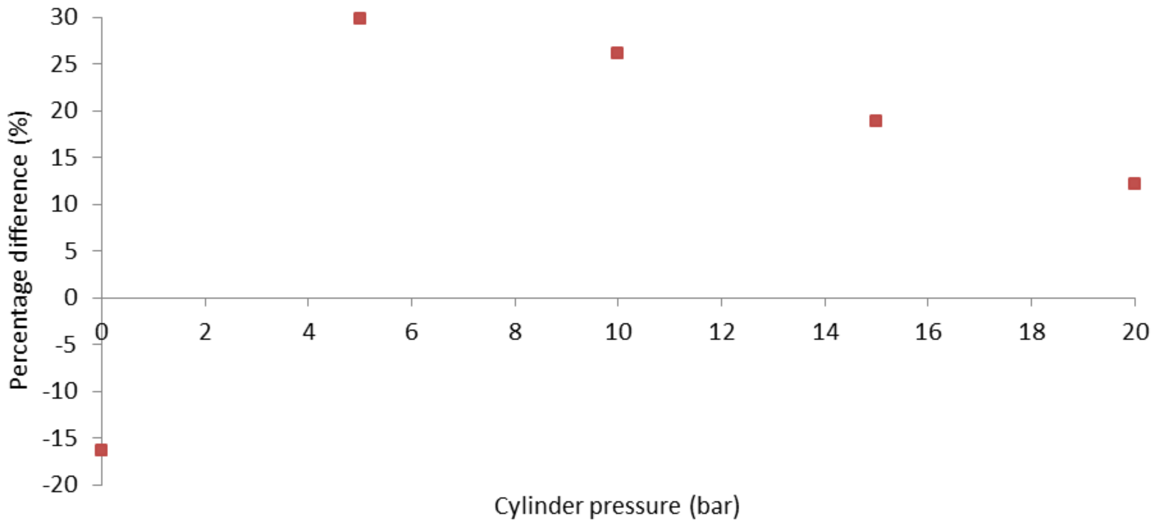

Figure 109: Percentage difference between nitrogen and carbon dioxide spray penetration. Average

To explore the effect of gas density on the spray penetration, reference is made to Figure 110. The figure compares spray penetration between nitrogen and carbon dioxide with similar gas densities. The gas densities were calculated as described in Section 5.1 assuming ideal gas behaviour. Due to the higher molecular mass of the carbon dioxide, higher densities are achieved than nitrogen at the same pressure. Figure 110 shows a comparison of the spray penetration obtained with nitrogen at 15 bar and carbon dioxide at 10 bar. Under these conditions, the density of the nitrogen would be 17.5 kg/m^3 and that of the carbon dioxide would be 18.4 kg/m^3. This represents a difference of 5.1 %. Under these conditions, although the spray penetrations are very similar, the spray penetration with nitrogen is slightly higher. The average spray penetration achieved with nitrogen at 15 bar was 21.6 mm and that of carbon dioxide at 10 bar was 21.3mm; a difference of only 1.4%. According to Hiroyasu's model, this difference would be 0.9%. The theoretical models covered in this report do not consider the viscosity of the gas when calculating the spray penetration (only cone angle).

Ideal gas behaviour predicts a negligible impact on the viscosity by changing the pressure so the effects were not of concern when using a single gas. Comparing the results of the nitrogen and carbon dioxide, the differences in viscosities of the gases would have to be considered. Nitrogen is approximately 20% more viscous than carbon dioxide and this could affect the spray structure. Based on the results of the experiments conducted, it appears as though the effect of the viscosity is negligible when compared to changes in the gas density, when considering the spray penetration.

The similarity between the spray penetration obtained with 15 bar nitrogen and 10 bar carbon dioxide shows that the spray penetration has a strong dependency on the gas density, regardless of the pressure. The difference in spray penetration between 10 and 15 bar nitrogen is 19.6% and 14.7% with carbon dioxide. Figure 111 shows the variation of average spray penetration with gas density. The figure contains results for both nitrogen and carbon dioxide at various cylinder pressures. It can be seen that the spray penetration decreases at a decreasing rate with gas density, as predicted by both Dent's and Hiroyasu's models.

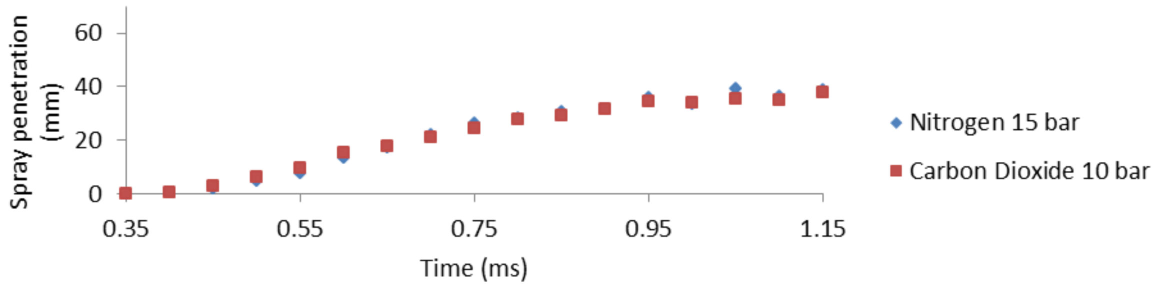

Figure 110: Spray penetration vs time. 780 bar injection pressure. 15 bar nitrogen. 10 bar carbon dioxide

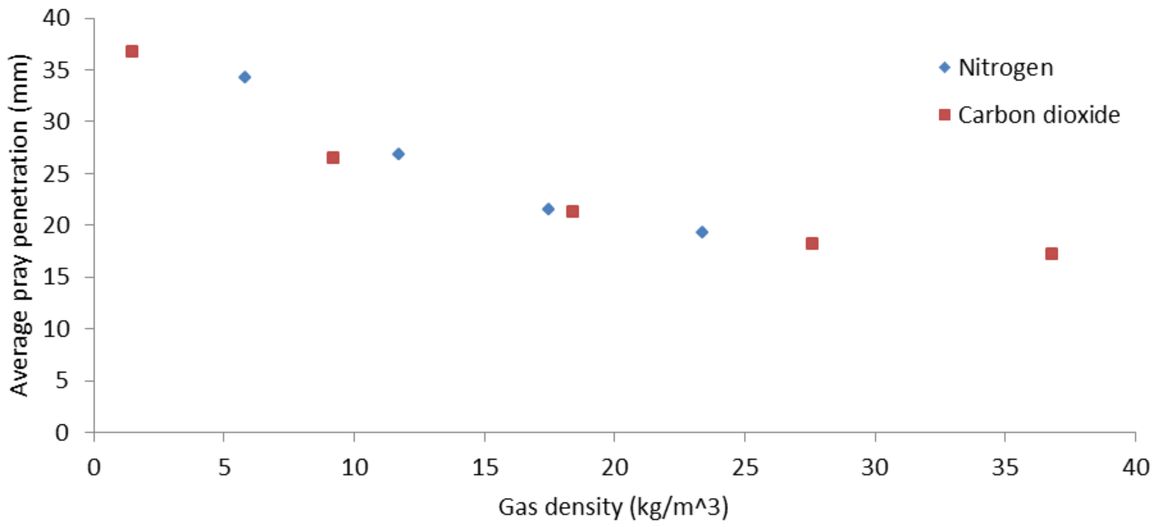

Figure 111: Average spray penetration vs. gas density. 780 bar injection pressure. Atmospheric – 20 bar cylinder pressure. Nitrogen and carbon dioxide

Figure 112 shows the changes in the cone angle with time using the same parameters. The experiments did not show a strong relationship between the cone angle and cylinder pressure. When compared to the cone angles obtained with the tests for nitrogen, the carbon dioxide cone angles were on average 9.4% larger for all the pressures tested. Figure 113 shows a comparison of the average cone angles obtained with both nitrogen and carbon dioxide. For both sets of tests, the cone angles were within a 5° range. The nitrogen cone angles were between 23.7° and 27°; and the carbon dioxide cone angles were between 25° and 30°. Analysing the theoretical models, it was discovered that the viscosity had a significant impact on the cone angle.

The cone angle is inversely proportional to the square root of the viscosity. A higher viscosity provides more resistance to the radial motion of the spray and thus results in a smaller cone angle. The change in cone angle as a result of the difference in viscosity of the gases is comparable in magnitude to the difference resulting from the change in density (10.7% and 12% respectively). The percentage differences were independent of the cylinder pressure at which they were calculated.

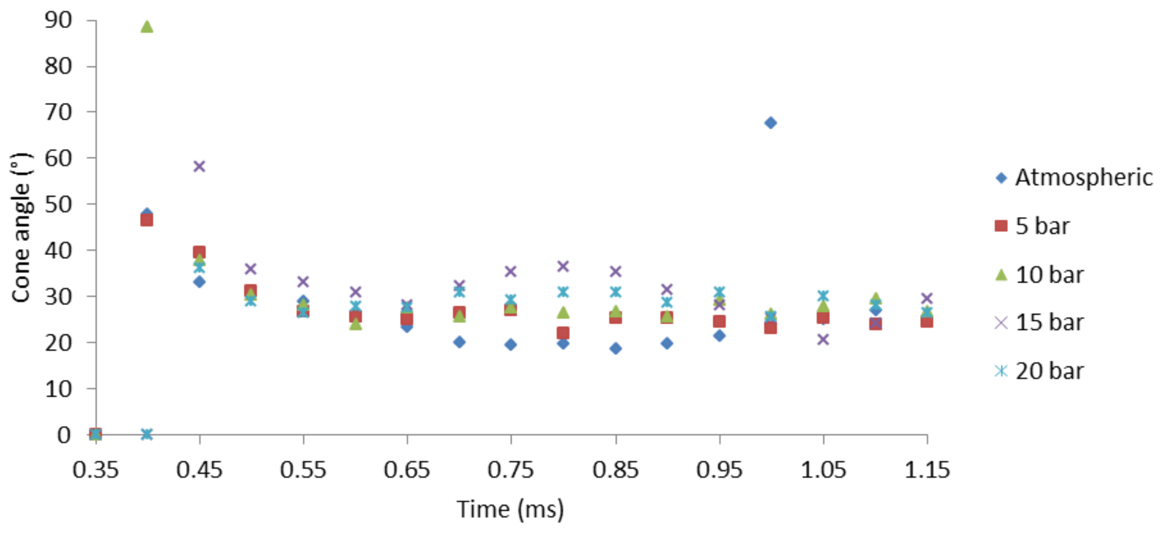

Figure 112: Cone angle vs time. 780 bar injection pressure. Atmospheric – 20 bar cylinder pressure using carbon dioxide

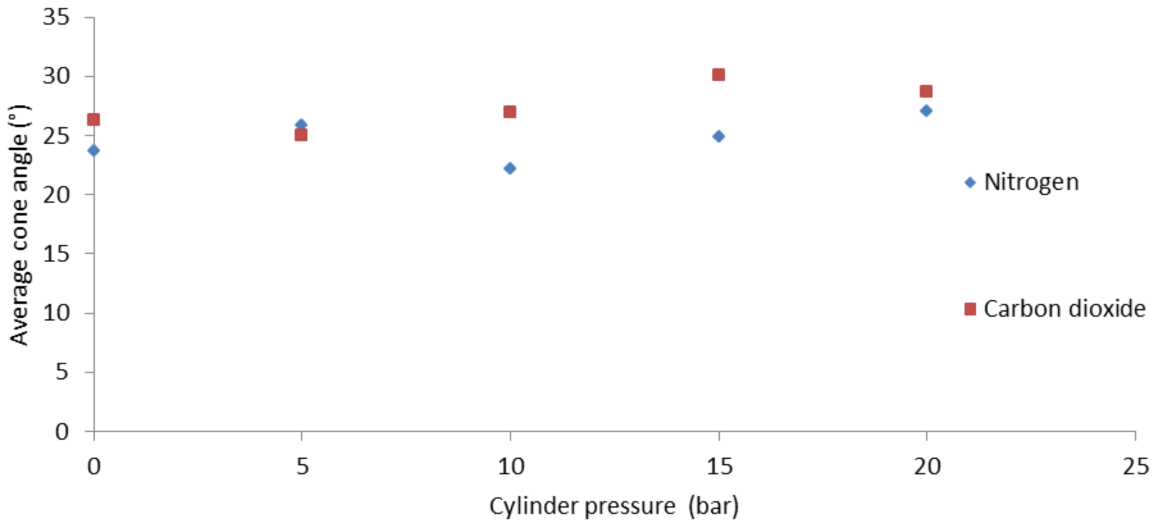

Figure 113: Average cone angle vs cylinder pressure. 780 bar injection pressure. Atmospheric – 20 bar cylinder pressure. Nitrogen and carbon dioxide.

Figure 114 shows the spray penetration vs time when a constant pressure difference (5 bar) is maintained across the nozzle of the injector while both the injection pressure and cylinder pressure are varied.

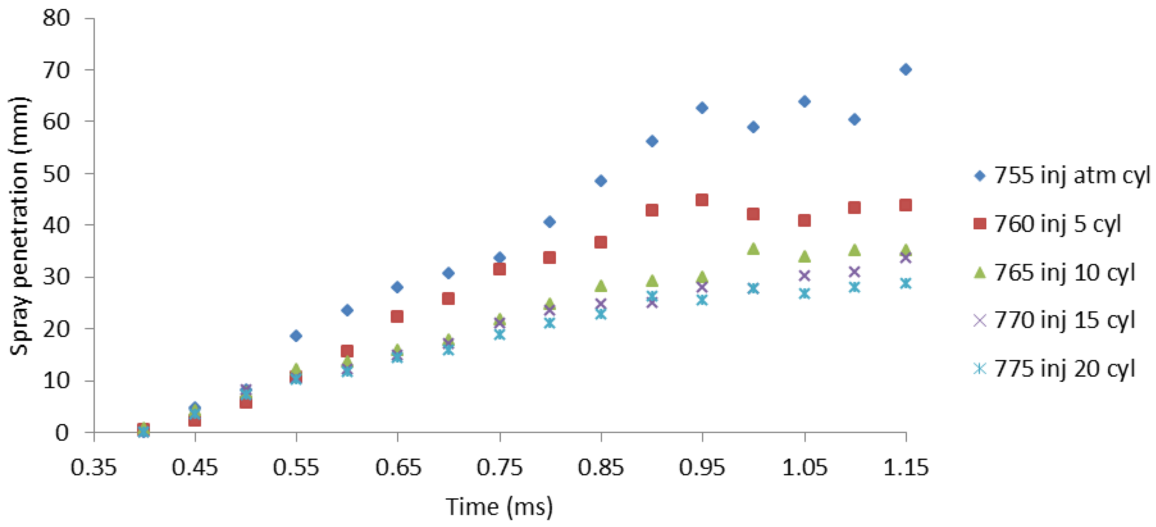

Figure 114: Spray penetration vs. time. 755- 775 bar injection pressure. Atmospheric – 20 bar cylinder pressure using carbon dioxide

From the figure, it can be seen that as the pressures increase, the spray penetration decreases. Comparing the results to Figure 99, the spray penetration for this set of tests is lower than those of the nitrogen tests. The difference between the tests at corresponding injection and cylinder pressures decreases as the pressures increase. Figure 115 shows a comparison of the results obtained for spray penetration for both sets of tests. The spray penetration is plotted against the cylinder pressure, but it should be noted that the injection pressure increases at the same rate as the cylinder pressure to maintain a constant pressure difference. The figure shows that the differences between the tests are largest at low pressures.

Reference is made to Figure 105 and Figure 109 which compare the difference in spray penetration between nitrogen and carbon dioxide tests; with varying injection pressure and cylinder pressure respectively. It was noted that a change in injection pressure had a negligible effect on the difference in spray penetration in different gases (early phase of injection). The cylinder pressure however had a noticeable influence on the spray penetration. As in this set of tests, there was a much larger difference between the two gases at lower cylinder pressures.

The data points in Figure 115 follow the same trend as those in Figure 111. The spray penetration decreases at a decreasing rate with increasing pressures. The changes in the spray penetration with nitrogen are larger than those of the carbon dioxide tests between any two consecutive tests. The higher molecular mass of the carbon dioxide shifts the graph to the left indicating that cylinder pressure has a diminishing effect on the spray penetration with increased gas density.

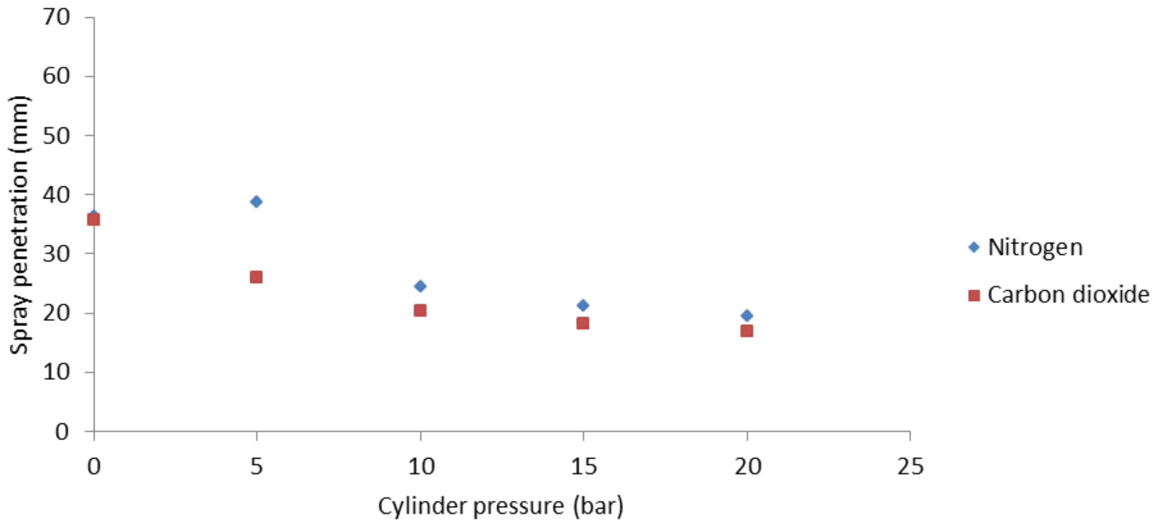

Figure 115: Average spray penetration vs cylinder pressure. Nitrogen and Carbon dioxide. 755 – 775 bar injection pressure. Atmospheric – 20 bar cylinder pressure

7. CONCLUSIONS

The results were analysed with respect to the objectives and the conclusions are presented below.

Modify the Inov8 Test Stand with a spray chamber that will allow it to be used to analyse spray patterns with a cylinder pressure of up to 20 bar.

The chamber used by Valentim [29] was retrofitted to the Inov8 Test Stand so that the unmatched precision of the data capturing system could be used to run tests with different gases and pressures (previously not possible with the Inov8 Test Stand). The set up was able to obtain consistent, accurate results, however the spray chamber was not optimal for the data capturing system of the test stand. The tip of the injector was positioned in a shadow and the chamber would quickly fill up with vapour. This meant that the geometry package of the DaVis software could not be used for data analysis, and the DaVis software was only used for data capturing. A 1 hole injector was used and the injection pressures for the experiments were kept below 800 bar to reduce the vapour and preserve the 1-hole injector. A spray chamber was designed, fabricated and certified to hold 20 bar of pressure. This spray chamber had a larger internal volume to reduce the build-up of vapour in the gas so that clearer pictures could be taken. Initial testing with the new spray chamber revealed that the injector was situated too high up to be properly captured by the camera. A minor modification was required to the spray chamber to hold the injector lower down. It was sent out for the modification and recertification and at the time when the tests were done, the modification was not completed. Due to time constraints, a full set of experiments with this new spray chamber were not possible.

Investigate the sensitivity of spray penetration and velocity to changes in injection pressure.

To determine the sensitivity of spray penetration to variations in injection pressure, tests were conducted with 5 bar nitrogen in the spray chamber and the injection pressure was varied between 700 bar and 780 bar in 20 bar increments with an injection duration of 800 µs. The spray penetration and velocity increased with increasing injection pressure. At all pressures, the spray penetration increased at an increasing rate until it broke up around 0.5ms after the injection began; thereafter the rate decreased. The effects of the changes in injection pressure were most noticeable after the spray broke up, between 0.8ms and 1.15ms there was 7mm difference between 700 bar and 780 bar. At higher injection pressures, the fluid is better vaporized and interacts more with the gas. This leads to increased cluster shedding (clusters of vaporized fluid and gas breaking away). The cluster shedding leads to fluctuations in the spray penetration and velocity. The initial acceleration of the fluid increased at an increasing rate with injection pressure. An 11.4% increase in the injection pressure resulted in a 35% increase in the acceleration for the initial phase of the injection. Increasing the injection pressure increased the force acting on the pressure shoulder of the injector and resulted in the injector opening up sooner (start of injection was earlier). The spray penetration reached 0.5mm 0.02ms earlier with a 780 bar injection pressure than it did with a 700 bar injection pressure and opened 0.01ms earlier. The cone angle of the spray increased with increasing injection pressure. Increasing the injection pressure also resulted in a higher injection rate and delivery being measured with the Akribis section of the Inov8 Test Stand.

Investigate the sensitivity of spray penetration and velocity to changes in cylinder pressure.

Determine effect of cylinder gas density on spray penetration (distance and velocity).

To determine the effect of cylinder pressure on spray penetration, tests were run with a 780 bar injection pressure and cylinder pressures varying between atmospheric and 20 bar in 5 bar increments. An increase in cylinder pressure resulted in a decrease in spray penetration. The differences in the spray penetration due to changes in cylinder pressure were noticeable earlier in the injection than the tests with changes in the injection pressure. The impact a change in cylinder pressure has on spray penetration decreases with increasing cylinder pressures (ie. changes in cylinder pressure have a diminishing effect on spray penetration). There was a 21.8% difference in spray penetration between 5 bar and 10 bar cylinder pressure and a 10.5% difference between 15 bar and 20 bar. Higher cylinder pressures resulted in a higher density cylinder gas and this kept the spray structure together for longer and reduced the effects of cluster shedding. Sprays with higher cylinder pressures had a thinner vapour/gas shroud over the liquid core. The cylinder pressure had no effect on the time at which the injection started. At low cylinder pressures (atmospheric pressure), cavitation in the nozzle plays a significant role in the velocity of the spray. Increasing the cylinder pressure has a more significant impact on the cylinder gas density than the pressure difference across the nozzle and this results in the cone angle increasing with increasing cylinder pressure. The increased density resulting from an increase in cylinder pressure provides a larger resistance to the axial flow of the spray and gives a shorter, wider spray, thus explaining a larger cone angle and smaller penetration when compared to a test with a lower cylinder pressure. The mean tip velocity of the spray decreases at a decreasing rate with increasing cylinder pressure due to increasing resistance from the gas. There was a large drop in velocity (173.8m/s to 78.6m/s) from atmospheric pressure to 5 bar. Spray hesitation was larger at lower cylinder pressures due to the increased velocity causing larger lateral movements of the needle when opening.

Investigate the relationship between spray penetration and the injection-cylinder pressure difference.

To determine if either the injection pressure or the cylinder pressure had a larger impact on the spray penetration than the overall pressure difference across the nozzle, tests were conducted while maintaining a constant pressure difference across the nozzle. The injection pressures were between 755 bar and 775 bar, and cylinder pressures between atmospheric pressure and 20 bar. Both the injection pressure and corresponding cylinder pressure were increased in increments of 5 bar. As the pressures were increased, the spray penetration decreased. This showed that the cylinder pressure had a larger effect on the spray penetration than either the injection pressure or the pressure difference across the nozzle. As with the previous tests, the cylinder pressure had a diminishing effect on the spray penetration. The increasing cylinder pressure again reduced the effects of cluster shedding. The gas density was found to be more important to the spray penetration than the pressure difference across the nozzle. The effects of the density changes were more noticeable in the later part of the injection where the pressure difference across the nozzle has less of an effect on the spray penetration. The experiments described above were repeated with carbon dioxide in the spray chamber. For all the tests, the spray penetration results followed the same trend as with nitrogen; however the spray penetration was always lower than the nitrogen counterpart at the same cylinder pressure, injection pressure and time. The difference was between corresponding tests was constant (percentage) between 0.35ms and 0.75; although the difference was more apparent in the later part of the injection, no correlation was found. During the later part of the injection, the carbon dioxide spray penetration had smaller oscillations (smoother graph) indicating that cluster shedding was less with the denser gas (due to the higher molecular mass). The spray penetration was found to decrease at a decreasing rate with increasing cylinder gas density. The difference reduced from 298% at 5 bar to 12.1% at 20 bar. The cylinder gas density was found to be more important to the spray penetration than the cylinder gas pressure. With a 5 bar difference in cylinder gas pressure, there was a difference of only 1.4% in the spray penetration due to the similarity of the densities at these pressures (5.1%). The spray had a lower velocity in the carbon dioxide compared to nitrogen and the velocity decreased with increasing cylinder pressure for both gases. The cone angle was found to be 9.4% larger on average with carbon dioxide compared to nitrogen. It was also concluded that the effect of cylinder gas viscosity on the cone angle was comparable in magnitude to the effect of gas density, and this was independent of the cylinder gas density.

Compare experimental results of spray penetration to theoretical models of Hiroyasu and Dent.

The models of both Dent and Hiroyasu were more accurate in the later parts of the injections. The models do not take into account the effects of the fluid viscosity, inertia or friction in the early stages of the injection and cannot predict the initial velocity profile of the spray. From the start of the injection, the accuracy increased rapidly until the spray broke up. In some cases, Hiroyasu's model was within 1% of the experimental results. In all cases, Hiroyasu was more accurate than Dent. The models increased in accuracy with increasing injection pressure, but decreased with increasing cylinder pressure. Dent's accuracy went from 26.6% at 5 bar to 41.6% at 20 bar while Hiroyasu went from 22.6% to 38.9% for the same cylinder pressures. The models neglect to consider the effect of cavitation in the nozzle at low cylinder pressures and tend to under predict the velocity. The model used to calculate the cone angle was accurate and was on average within 2% of the experimental cone angle.

Investigate the accuracy of Hiroyasu's equation for the time at which the spray will break up.

For the experiments conducted in the current study, Hiroyasu's model for the time at which the spray breaks up was consistently 0.3ms too early. This difference can be attributed to differences between the experimental set up used in this study and that used to develop the model. The models were developed almost 4 decades ago and the data capturing system used in the current study is more advanced (faster response, clearer images) than the technology available at that time. There have also been improvements in the components of the injection system.

Investigate Hiroyasu's theory that the injection pressure has a greater effect on spray penetration before the jet begins to breakup, and that the back pressure has a more significant impact after the jet begins to break up.

Experimental results showed that with the pressures tested, on average, changes in the cylinder pressure had a more significant impact on the spray penetration than similar changes in the injection pressure. Tests maintaining a constant pressure difference showed that the effect of changing the injection pressures was greater during the early phase of the injection; the effect of changing the cylinder pressure was greater later on in the injection. The transition happened before break up and not at break up as predicted by Hiroyasu.

8. RECOMMENDATIONS

Although the research met the objectives of the study, there were some limitations imposed on the experimental facilities. These limitations were due to budget and time constraints and the following recommendations are listed for future studies to improve upon the methods used here.

- The new pressure chamber designed for this study will be ready for testing in 2018. This chamber will provide superior images to those obtained in this study. The tip of the injector will not be in the shadow and the effect of vapour build up will be reduced. The geometry analysis package of the DaVis software will be able to analyse the spray more accurately.
- An extraction system should be designed and fitted to the spray chamber. The extraction system should separate the vapour from the gas while maintaining the pressure. The system should not introduce high velocity flows to the gas that might affect the spray pattern.
- With an extraction system in place, the bottom lid of the new spray chamber can be modified to have a window so that the axial camera of the test stand can be used. This will give better insight into the behaviour of multi-hole injectors in a pressurized environment.
- The fuel delivery system could be modified to work with DME for a better understanding of the behaviour of this fuel (a topic of interest of the School of Mechanical, Industrial and Aeronautical Engineering at The University of the Witwatersrand, Johannesburg).

BIBLIOGRAPHY

1. David Valentim. *Injector Spray Analysis and Flow Measurement.* The University of the Witwatersrand, Johannesburg. 26 August 2011
2. Clair Pelser. *Injector Spray Analysis and Flow Measurement.* The University of the Witwatersrand, Johannesburg. 26 August 2011
3. Lee Watkins. *Injector Spray Analysis and Flow Measurement.* The University of the Witwatersrand, Johannesburg. 20 August 2010
4. Curtis Murray. *Injector Spray Analysis and Flow Measurement.* The University of the Witwatersrand, Johannesburg. 15 October 2010

REFERENCES

1. Denis Gill, Josef Erhart, Ludwig Burgler, Heribert Kammerstetter, Manfred Werner. *Characterising Injection System Behaviour under Real Operating Conditions.* AVL List GmbH. AVL Pierburg Instruments Flow Technology GmbH
2. John B. Heywood. *Internal Combustion Engine Fundamentals.* Mcgraw-Hill, Inc. United States of America. 1988. ISBN 0-07-028637-X.
3. O. Bunes and P.M. Einang. *Comparing the performance of the common rail fuel injection system with the traditional injection system using computer aided modelling and simulation.* MARINTEK paper at ENSUS 2000, International Conference on Marine Science and Technology for Environmental Sustainability, Newcastle, September 2000.
4. J. Benajes, S. Molina, C. Gonzalez, R. Donde. *The role of nozzle convergence in diesel combustion.* CMT-MotoresTe´rmicos, Universidad Polite´cnica de Valencia, Camino de Vera s/n, 46022 Valencia, Spain. IstitutoTecnologiadeiMateriali e dei Processi Energetici, Consiglio Nacionaledelle Ricerche, Via R. Cozzi, 53, 20125 Milano, Italy. 20 December 2007.
5. M. Vinay Kishore. *Advanced Common Rail Injection System.* Koneru Lakshmmaiah College of Engineering, Vaddeswaram. Dept of Mechanical Engineering, Gudlavalleru Engineering College, Gudlavalleru.
6. Robert Bosch GmbH. *Diesel Fuel-Injection System Common-Rail.* Second edition, April 2005. English translation of the 3rd German edition dated: October 2004. Published by Robert Bosch GmbH, 2005. Postfach 1129, D-73201 Plochingen, Automotive Aftermarket Business Sector, Department AA/PDT5. Product Marketing, Diagnostics & Test Equipment.
7. Paolo Lino, Bruno Maione, Alessandro Rizzo. *Nonlinear modelling and control of a common rail injection system for diesel engines*. Copyright 2006 Elsevier Inc. Dipartimento di Elettrotecnicaed Elettronica, Politecnico di Bari, Via Re David 200, 70125 Bari, Italy. P. Lino et al. Applied Mathematical Modelling 31 (2007). Pages 1770–1784.
8. Sean Bennett. *Modern Diesel Technology Diesel Engines.* Delmar, Cengage Learning. 2010. ISBN-13: 978-1-4354-4044-9

9. *Common rail injection systems*. Available at http://transportation.centennialcollege.ca/oduffy/fuels/level3fuels/Common%20Rail%20injection%20systems.pdf

Last accessed 10/07/2012 18:00

10. Deanna Sclar. *Auto repair for dummies.* Second edition. Wiley Publishing Inc. Indianapolis, Indiana. ISBN: 978-0-7645-9902-6
11. Bosch. *Fuel Injectors.* Available at http://www.bosch.com.au/content/language1/html/4554.htm . Last accessed 11/07/2012, 11:25
12. T.-C. Wang, J.-S. Han, X.-B. Xie, M.-C. Lai, N. A. Henein. *Parametric Characterization of High-Pressure Diesel Fuel Injection Systems* .Vol. 125, April 2003. Mechanical Engineering Department, Wayne State University. Anthony Wayne Drive, #2123 Detroit, MI 48202. E. Schwarz, W. Bryzik. US TARDEC, Detroit, MI. Journal of Engineering for Gas Turbines and Power. Copyright 2003 by ASME.
13. *Product Data*, *Castrol Diesel Calibration Oil 4113.* January 2000 https://www.ils.co.nz/B1WebTools/assets/downloads/SKU%20TDS/101446.pdf

Last accessed 12/07/2012 12:57

14. Ivor Carroll. *Diesel Injection.* Diesel Power, The ultimate guide to diesel motoring. Presented free with issue 181 of Diesel Car. Available at http://www.fabia-vrs.com/downloads/files/injection.pdf

Last accessed 12/07/2012 13:47

15. Inov8 Technologies Ltd. *Injector Spray Analysis & Flow Measurement Stand, Operating & Maintenance Manual.*Inov8 Project no. J229A. Equipment prepared for The University of the Witwatersrand Johannesburg, South Africa. Inov* Technologies Ltd. Buckingham, UK. May 2008.
16. Steven Grover. *Injector Spray Analysis & Flow Measurement*, *Akribis Operating Manual.* The University of the Witwatersrand Johannesburg, South Africa. 2008
17. Thulasi Vijayakumar, Rajagopal Thundil Raj, Kasianantham Nathagopal. *Effect of the Injector Pressure on the Internal Flow Characteristics for Diethyl and Dimethyl Ether and Diesel Fuel Injectors.* Center for Excellence in Automotive Technology, SMBS, VIT University, Vellore, Tamil Nadu, India. 2011. UDC: 621.43.038:519.23

18. Alp Tekin Ergene, Deniz Ozde Koca, Merve Abacioglu. *Combustion characteristics of a High Pressure Fuel Injected Single Cylinder Compression-Ignition Engine, Fuelled with Diesel-Ester Blends under Various Fuel Injection Advance Angles.* Department of Mechanical Engineering, Yildiz Technical University, Besiktas, Istanbul 34349, Turkey. 08/04/2012.
19. Simón Martínez-Martínez, Fausto A. Sánchez-Cruz, Vicente R. Bermúdez and José M. Riesco-Ávila. *Liquid Sprays Characteristics in Diesel Engines*. Universidad Autónoma de Nuevo León, México. Universidad Politécnica de Valencia, Spain. Universidad de Guanajuato, México
20. David Valentim. The University of the Witwatersrand, Johannesburg. 2014
21. Steven Grover. *Injector Spray Analysis & Flow Measurement, La Vision Operating Manual.* The University of the Witwatersrand Johannesburg, South Africa. 2008
22. Ashwin. S. *Diesel Engine Fundamentals.* Posted 12/02/2009. Available at http://seminar4u.blogspot.co.za/2009/02/diesel-engine-fundamentals.html
Last accessed 17/05/2018 11:57
23. Kourosh Karimi. *Characterisation of Multiple-Injection Diesel Sprays at Elevated Pressures and Temperatures.* School of Engineering, University of Brighton. May 2007.
24. R.J.H. Klein-Douwel, P.J.M. Frijters, L.M.T Somers, W.A de Boer, R.S.G Baert. *Macroscopic diesel fuel spray shadowgraphy using high speed digital imaing in a high pressure cell.* Eindhoven University of Technology, Faculty of Mechanical Engineering, The Netherlands. 28 November 2006.
25. J. Seneschal, C. Ducottet, J.P. Schon, J.C. Champoussin, P Gucher. *Automatic system for visualization and characterization of high pressure diesel sprays.* Laboratoire Traitement du Signal et Instrumentation UMR CNRS 5516, 23 rue du docteur Paul Michelon, 42023 Saint-Etienne Cedex 02, France. Laboratoire de Mécanique des Fluides et d'Acoustique UMR CNRS 5509, ECL, 36 av. Guy de Collongue, 69134 Ecully Cedex, France. EFS, Zac du baconnet, Allée des chênes, 69700 Montagny, France. June 2003.
26. E. Delacourt, B. Desmet, B. Besson. *Characterisation of very high pressure diesel sprays using digital imaging techniques.* Laboratoire de Me´canique et Energe´tique, ENSIAME, Universite´ de Valenciennes, Le Mont Houy, 59313 Valenciennes cedex 9, France. Le Moteur Moderne, 9 rue Benoıˆt Frachon, 91127 Palaiseau, France. 9 December 2004.

27. Raul Payri, F. J. Salvador, J. Gimeno, V. Soare. *Determination of Diesel Sprays Characteristics in Real Engine In-Cylinder air Density and Pressure Conditions.* CMT – Motores Termicos, Universidad Politecnica de Valencia, Camino de Vera s/n, E-46022 Spain. Journal of Mechanical Science and Technology (KSME Int. J.), Vol. 19, No. 11, pp. 2040-2052. 2005.
28. J. Naber, D.L. Siebers. *Effects of gas density and vaporization on penetration and dispersion of Diesel sprays.* SAE Paper 960034. 1996.
29. S. Grover. *Injector Spray Analysis & Flow Measurement Stand. La Vision Operating Manual.* The University of the Witwatersrand. School of Mechanical, Aeronautical and Industrial Engineering. 2008.
30. D.J. Valentim. *Analysis of Dimethyl Ether (DME) Injection Spray Characteristics in Comparison to Diesel and Theoretically Predicted Spray Characteristics*. The University of the Witwatersrand. School of Mechanical, Aeronautical and Industrial Engineering. October 2014.
31. Omid Iskander Alimia. *Analysis of Injection Spray Patterns for Common Rail Systems.* The University of the Witwatersrand. School of Mechanical, Aeronautical and Industrial Engineering. 2011.
32. S. Grover. *A Comparison of the Performance on New and Used Common Rail Diesel Injectors.* The University of the Witwatersrand, Johannesburg. School of Mechanical, Aeronautical and Industrial Engineering. 2012.
33. Andrew Davidhazy. *Introduction to Shadowgraph and Schlieren Imaging.* Rochester Institute of Technology. 2006
34. R. Calabria and P. Massoli. *Scattering Imaging to Measure Size and Velocity of Small Particles in Dense Particle Systems.*Istituto Motori – CNR Via Marconi 8, 80125 Napoli, Italy.
35. M. Tsue, H. Hattori, A. Saito, T. Kadota. *Planer fluorescence technique for visualization of a diesel spray.* SAE Paper 922205. 1992
36. A.J. Yule, D.G. Salters. *On the distance required to atomise diesel spray injected from orifice-type nozzle.* I.Mech.E, Vol. 209. 1995
37. J. Koo, J. Martin. *Droplet size and velocities in a transient diesel fuel spray.* SAE Paper 900397. 1990.
38. M. Arai, M. Tabata, H. Hiroyasu, M. Shimizu. *Disintegrating Process and Spray Characterization of Fuel Jet Injected by a Diesel Nozzle.* SAE International. SAE paper no. 840275. 1984.

39. S. Tonini, M. Gavaises, A. Theodorakakos. *The role of droplet fragmentation in high-pressure evaporating diesel sprays.* School of Engineering and Mathematical Sciences, City University London. UK. Fluid Research Co. Athens, Greece. Industrial Engineering Department, Universita di Bergami, Italy. 28 February 2008.
40. A. Naicker. *Injector Spray Analysis and Flow Measurement*. School of Mechanical, Industrial and Aeronautical Engineering. The University of the Witwatersrand. Johannesburg. 2012
41. Prof. D. Cipolat. The University of the Witwatersrand, Johannesburg. Meeting in Johannesburg, South Africa. 21/11/2017.
42. J. C. Dent. *Basis for the Comparison of Various Experimental Methods for Studying Spray Penetration.* SAE paper 710570, SAE Trans, Vol 80, 1971.
43. H. Hiroyasu, T. Kadota and M. Arai, *Supplementary Comments: Fuel Spray Characterization in Diesel Engines.* Pp. 369-408. Plenum Press, 1980.

APPENDIX A – DATA CD

The Data CD attached contains the following:

- Flow analysis – Folder containing the data for the imaging experiments.
    - Data processing – The processed raw data obtained
        - 5 bar carbon dioxide
        - 5 bar difference carbon dioxide
        - 5 bar difference nitrogen
        - 5 bar nitrogen 02 – 5 bar cyl
        - 5 bar nitrogen
        - 780 bar carbon dioxide
        - 780 bar nitrogen
        - Hiroyasu theory
        - Nitrogen carbon dioxide
    - Raw data
        - Various folders containing raw data from the data capturing software of the Innov8 Test Stand (Flow measurement)
- Flow Measurement – Folder containing the data for the Akribis experiments.
    - Data processing
        - 5 bar – 5 bar cyl pressure, 700-780 bar inj pressure
        - 780 bar – atm-20 bar cyl pressure, 780 bar inj pressure
    - Raw data
        - Various folders containing raw data from the data capturing software of the Innov8 Test Stand (Akribis)

APPENDIX B – EXPORTING AKRIBIS DATA

The data obtained when conducting the flow measurement test using the Akribis must be exported to text files so that it can be processed later. The following procedure should be followed on the Akribis PC to export the data.

1. Open the data saved in the specified location (the data will open with Test Scope, See Figure 116 below.)

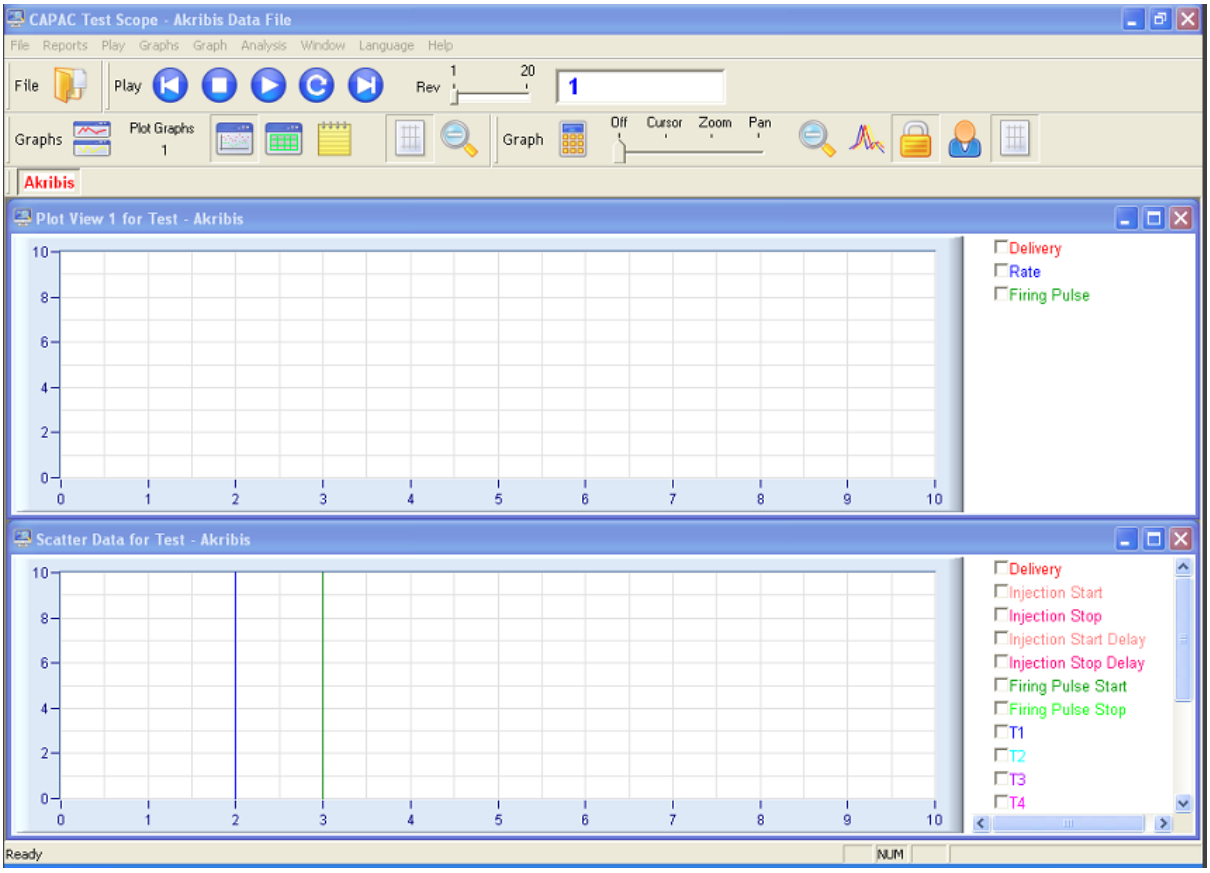

Figure 116: Test Scope

2. Go to File → Export Selected Test (See Figure 117 below)

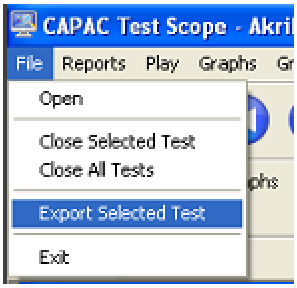

Figure 117: Export data

3. Select ‘Export Wave Forms’ (See Figure 118 blow)

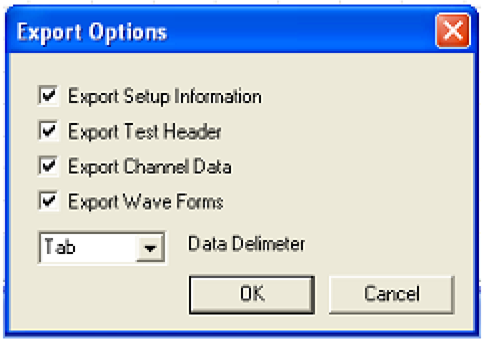

Figure 118: Export wave forms

4. Click ‘Ok’

APPENDIX C – DATA COLLECTION CODES

Spray Analysis Python Code

```
import csv


Pressure = str(input('Test pressure: '))

Dataset = str(input('Dataset: '))


Data = ''

Data2 = ''

Filename = Pressure + '_' + Dataset +'.csv'

File = open(Filename, 'w')

File.write('0.35,0.4,0.45,0.5,0.55,0.6,0.65,0.7,0.75,0.8,0.85,0.9,0.95,1.0,1.05,1.1,1.15,\n')


Time = 0.35

while Time <= 1.15:

    Timestep = str(Time)

    Path = 'C:\\Users\\andrann\\Desktop\\New folder (2)\\' + Pressure + '_bar_RP\\StephenGrover_T1=' + Timestep + '\\SumAvgRmsMinMax' + Dataset + '\\SPM-BS\\Geometry\\B00001_avg_results.txt'

    with open(Path, 'r') as handle:

        Line = handle.readlines()
```

```
        if Data == '':
            Data = Line[6][22:26]
        else:
            Data = Data + ',' + Line[6][22:26]

        if Data2 == '':
            Data2 = Line[1][19:22]
        else:
            Data2 = Data2 + ',' + Line[1][19:22]

        ##Line.close()

        Time = round(Time + 0.05,2)
        if Time == 1.0:
            Time = int(Time)
File.write(Data + '\n')
File.write(Data2)

File.close()
```

Akribis VBA Code

```
Sub Macro3()
'
' Macro3 Macro
''
For i = 1 To 20

        With ActiveSheet.QueryTables.Add(Connection:= _
            "TEXT;C:\Users\andrann\Desktop\naicker msc akribis\700b5b\Akribis_" & i & "_Delivery.txt" _
            , Destination:=Range("$A$1"))
            .Name = "Akribis_1_Delivery_1"
            .FieldNames = True
            .RowNumbers = False
            .FillAdjacentFormulas = False
            .PreserveFormatting = True
            .RefreshOnFileOpen = False
            .RefreshStyle = xlInsertDeleteCells
            .SavePassword = False
            .SaveData = True
            .AdjustColumnWidth = True
            .RefreshPeriod = 0
```

```
        .TextFilePromptOnRefresh = False
        .TextFilePlatform = 437
        .TextFileStartRow = 1
        .TextFileParseType = xlDelimited
        .TextFileTextQualifier = xlTextQualifierDoubleQuote
        .TextFileConsecutiveDelimiter = False
        .TextFileTabDelimiter = True
        .TextFileSemicolonDelimiter = False
        .TextFileCommaDelimiter = False
        .TextFileSpaceDelimiter = False
        .TextFileColumnDataTypes = Array(1)
        .TextFileTrailingMinusNumbers = True
        .Refresh BackgroundQuery:=False
    End With
    Range("B1").Select
    With ActiveSheet.QueryTables.Add(Connection:= _
        "TEXT;C:\Users\andrann\Desktop\naicker msc akribis\700b5b\Akribis_" & i & "_Firing Pulse.txt" _
        , Destination:=Range("$B$1"))
        .Name = "Akribis_1_Firing Pulse"
        .FieldNames = True
        .RowNumbers = False
        .FillAdjacentFormulas = False
```

```
    .PreserveFormatting = True
    .RefreshOnFileOpen = False
    .RefreshStyle = xlInsertDeleteCells
    .SavePassword = False
    .SaveData = True
    .AdjustColumnWidth = True
    .RefreshPeriod = 0
    .TextFilePromptOnRefresh = False
    .TextFilePlatform = 437
    .TextFileStartRow = 1
    .TextFileParseType = xlDelimited
    .TextFileTextQualifier = xlTextQualifierDoubleQuote
    .TextFileConsecutiveDelimiter = False
    .TextFileTabDelimiter = True
    .TextFileSemicolonDelimiter = False
    .TextFileCommaDelimiter = False
    .TextFileSpaceDelimiter = False
    .TextFileColumnDataTypes = Array(1)
    .TextFileTrailingMinusNumbers = True
    .Refresh BackgroundQuery:=False
End With
Range("C1").Select
With ActiveSheet.QueryTables.Add(Connection:= _
```

```
"TEXT;C:\Users\andrann\Desktop\naicker msc akribis\700b5b\Akribis_" & i &
"_Rate.txt", _
        Destination:=Range("$C$1"))
        .Name = "Akribis_1_Rate"
        .FieldNames = True
        .RowNumbers = False
        .FillAdjacentFormulas = False
        .PreserveFormatting = True
        .RefreshOnFileOpen = False
        .RefreshStyle = xlInsertDeleteCells
        .SavePassword = False
        .SaveData = True
        .AdjustColumnWidth = True
        .RefreshPeriod = 0
        .TextFilePromptOnRefresh = False
        .TextFilePlatform = 437
        .TextFileStartRow = 1
        .TextFileParseType = xlDelimited
        .TextFileTextQualifier = xlTextQualifierDoubleQuote
        .TextFileConsecutiveDelimiter = False
        .TextFileTabDelimiter = True
        .TextFileSemicolonDelimiter = False
        .TextFileCommaDelimiter = False
```

```
        .TextFileSpaceDelimiter = False
        .TextFileColumnDataTypes = Array(1)
        .TextFileTrailingMinusNumbers = True
        .Refresh BackgroundQuery:=False
    End With
    Range("D1").Select

Next i
End Sub
```

APPENDIX D – RESULTS

The final processed results are presented below.

Injection Pressure

The results for tests conducted to determine the effect of injection pressure can be found below. Table 3 is the results obtained with a constant cylinder pressure of 5 bar nitrogen with injection pressures ranging from 700 bar to 780 bar.

Table 3: Injection pressure results. 5 bar cylinder pressure. 700 – 780 bar injection pressure. Nitrogen

Time (ms)	**700 bar penetration (mm)**	**700 bar cone angle (°)**	**720 bar penetration (mm)**	**720 bar cone angle (°)**	**740 bar penetration (mm)**	**740 bar cone angle (°)**	**760 bar penetration (mm)**	**760 bar cone angle (°)**	**780 bar penetration (mm)**	**780 bar cone angle (°)**
0.35	77.8	1.5	48.6	4.3	66.7	1.5	82.1	6.0	80.0	6.8
0.40	0.8	95.3	1.1	21.8	1.2	25.2	1.4	18.9	1.9	22.0
0.45	3.3	13.6	3.6	29.7	4.0	24.5	4.5	27.6	4.7	24.5
0.50	7.2	26.2	7.5	26.2	8.4	24.4	8.5	22.0	8.29	23.4
0.55	12.3	15.2	12.9	18.0	13.7	21.3	14.5	24.6	15.2	21.6
0.60	17.0	14.2	16.9	18.7	18.1	19.4	19.4	19.9	20.7	22.4
0.65	21.6	15.2	22.6	16.6	23.6	17.8	24.2	22.7	26.0	24.7
0.70	28.0	14.4	30.4	18.2	30.7	18.5	32.8	23.1	32.1	25.5
0.75	35.1	13.4	37.5	18.3	38.1	19.6	40.4	23.7	39.7	24.3
0.80	41.4	16.7	45.5	19.9	45.9	18.9	46.8	24.6	50.3	28.8
0.85	48.0	17.9	47.6	17.3	49.4	20.2	47.6	24.2	45.8	26.4
0.90	45.5	17.6	52.1	19.1	53.8	21.3	51.7	26.5	51.9	25.3
0.95	49.9	18.4	53.4	16.9	54.3	22.0	53.4	25.5	55.9	25.1
1.00	50.6	20.5	51.1	18.3	56.4	22.4	57.2	25.2	52.3	26.0
1.05	45.7	20.2	48.5	20.8	54.0	24.0	56.3	26.2	57.6	27.1
1.10	50.9	18.2	51.4	22.2	49.2	25.0	60.3	24.9	60.3	29.4
1.15	46.9	20.7	52.2	23.3	54.3	26.1	56.0	25.8	60.9	29.6

Figure 119, Figure 120, Figure 121, Figure 122 below show the test results compared to theoretical predictions of Dent and Hiroyasu with a cylinder pressure of 5 bar (nitrogen) and injection pressures of 700 bar, 720 bar, 740 bar and 780 bar respectively.

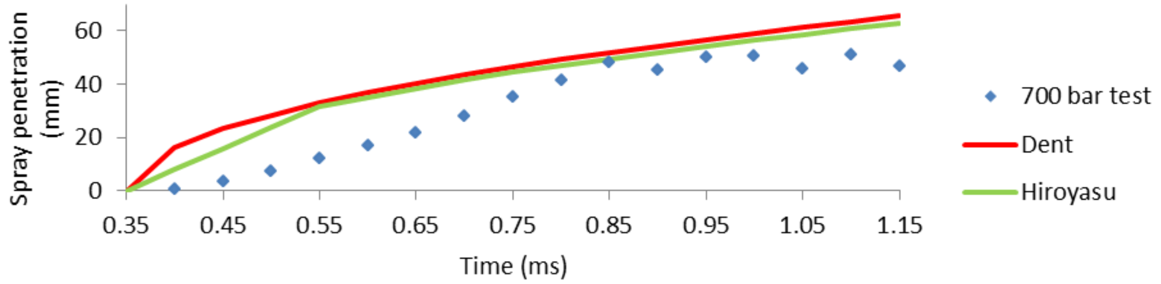

Figure 119: Spray penetration test results compared to theory. 700 bar injection pressure. 5 bar cylinder pressure using nitrogen

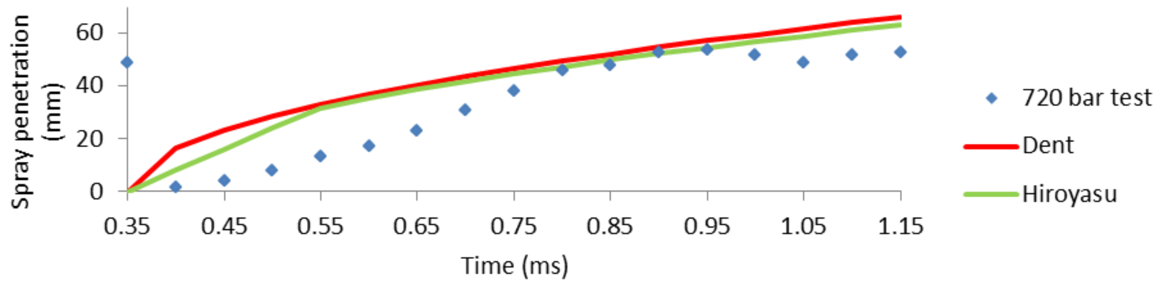

Figure 120: Spray penetration test results vs theory. 720 bar injection pressure. 5 bar cylinder pressure using nitrogen

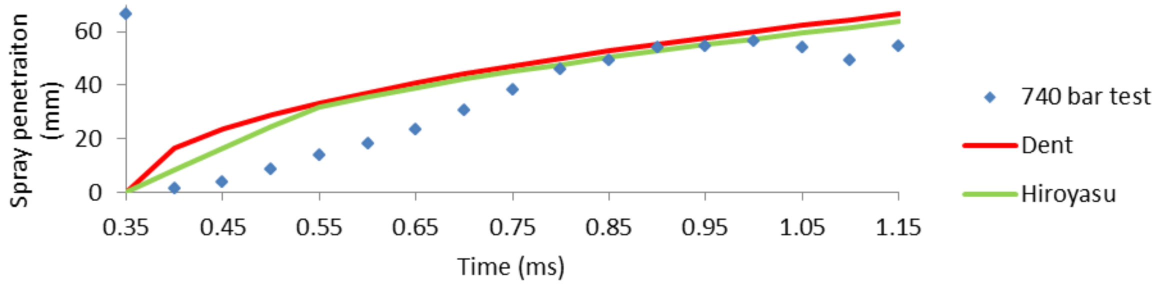

Figure 121: Spray penetration test results compared to theory. 740 bar injection pressure. 5 bar cylinder pressure using nitrogen

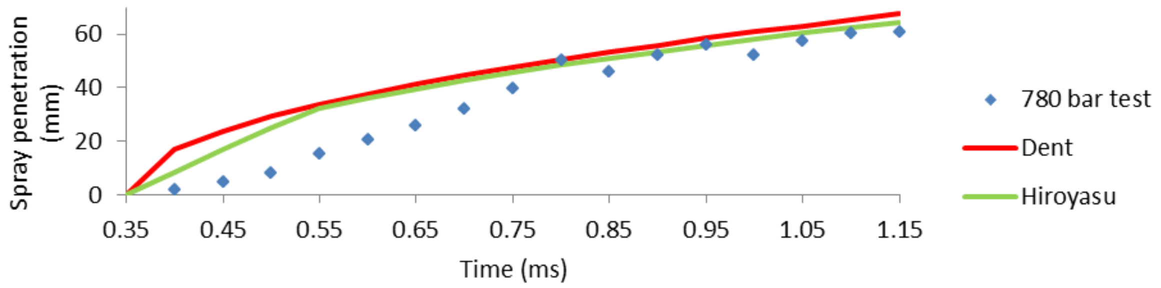

Figure 122: Spray penetration test results compared to theory. 780 bar injection pressure. 5 bar cylinder pressure using nitrogen

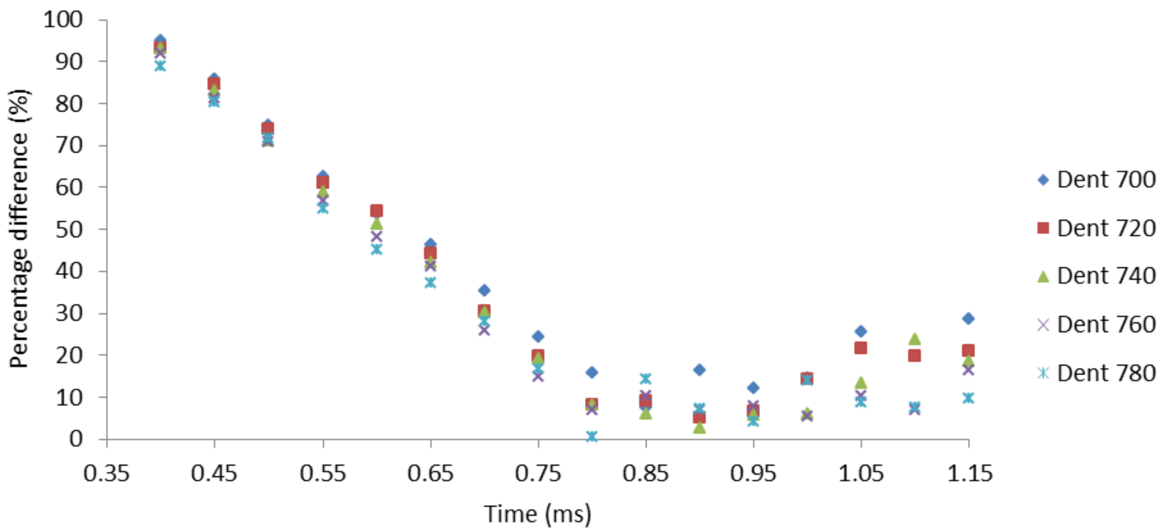

Figure 123: Percentage difference between Dent and actual results. 700 - 780 bar injection pressure. 5 bar cylinder pressure using nitrogen.

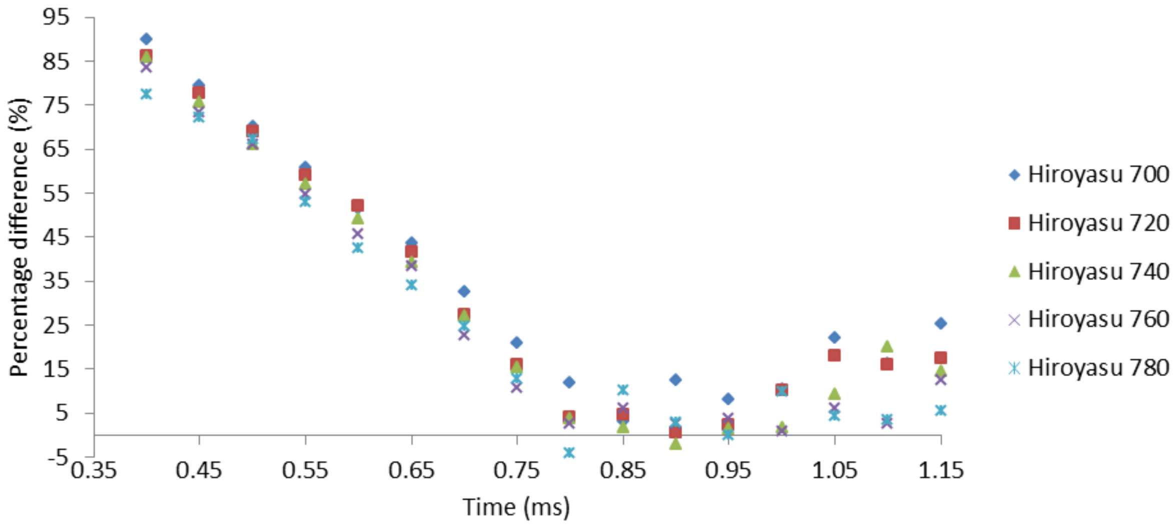

Figure 124: Percentage difference between Hiroyasu and actual results. 700 - 780 bar injection pressure. 5 bar cylinder pressure using nitrogen.

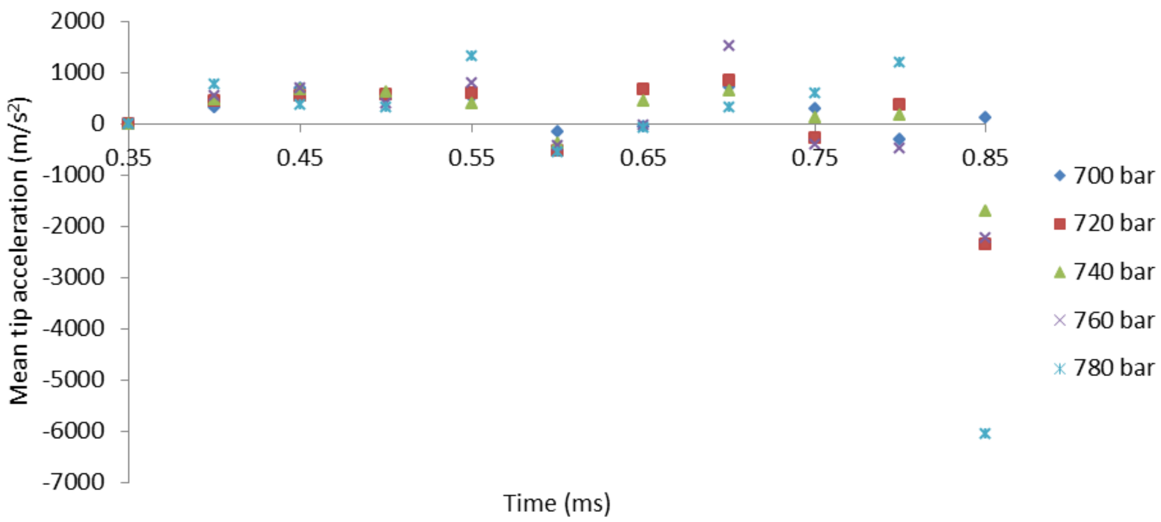

Figure 125: Mean tip acceleration. 700-780 bar injection pressure. 5 bar cylinder pressure using nitrogen

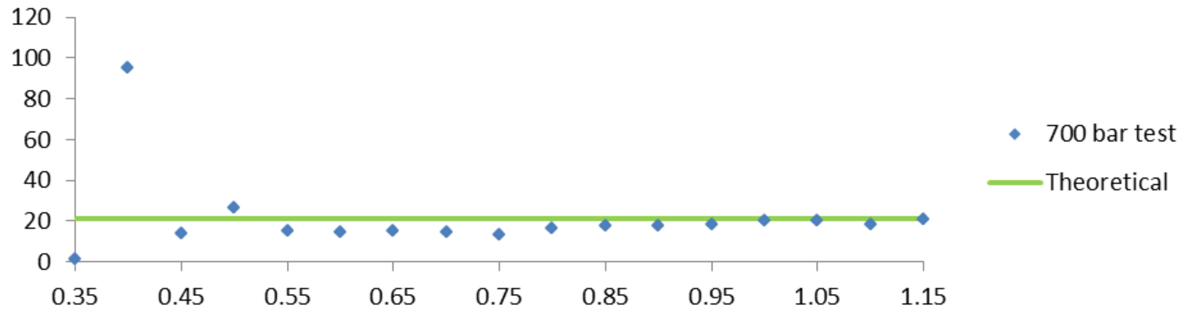

Figure 126: Cone angle test results compared to theory. 700 bar injection pressure. 5 bar cylinder pressure using nitrogen

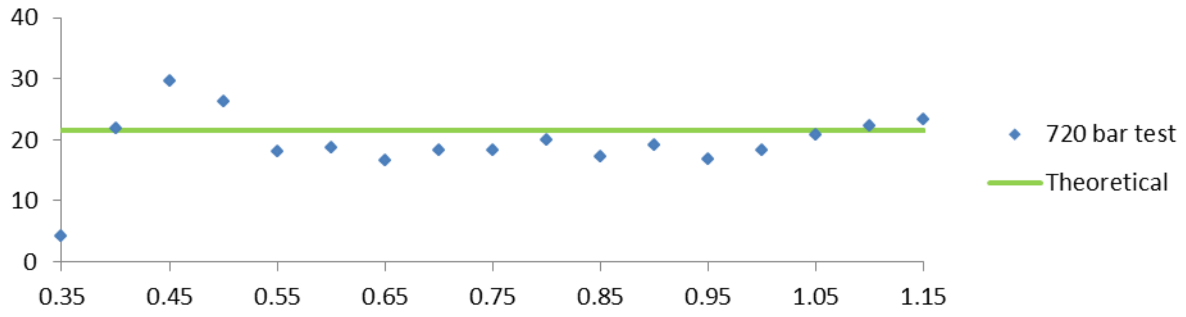

Figure 127: Cone angle test results compared to theory. 720 bar injection pressure. 5 bar cylinder pressure using nitrogen

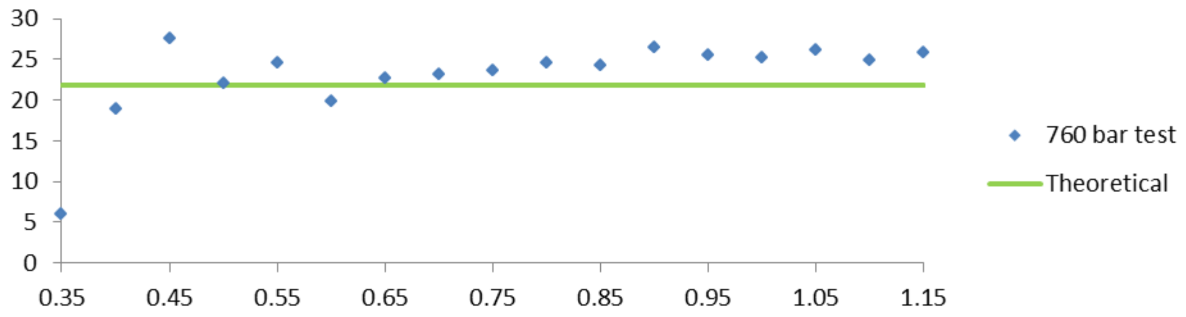

Figure 128: Cone angle test results compared to theory. 760 bar injection pressure. 5 bar cylinder pressure using nitrogen

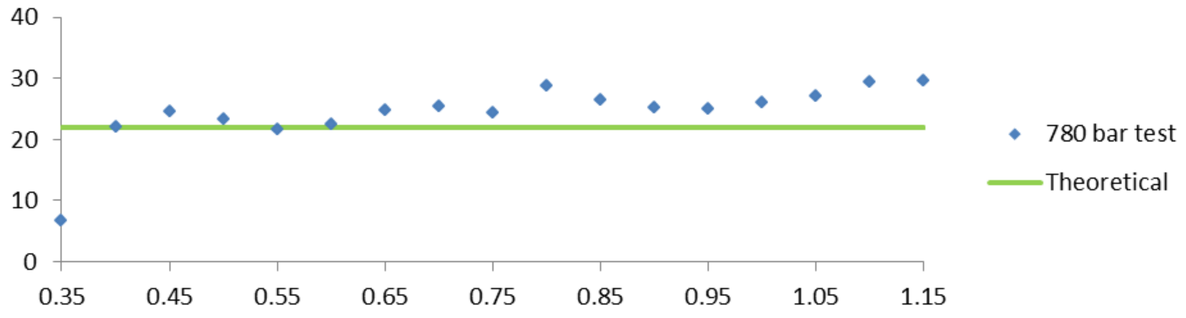

Figure 129: Cone angle test results compared to theory. 780 bar injection pressure. 5 bar cylinder pressure using nitrogen

Table 4: Injection pressure results. 5 bar cylinder pressure. 700 – 780 bar injection pressure. Nitrogen. 0.02ms time step

Time (ms)	**700 bar penetration (mm)**	**700 bar cone angle (°)**	**720 bar penetration (mm)**	**720 bar cone angle (°)**	**740 bar penetration (mm)**	**740 bar cone angle (°)**	**760 bar penetration (mm)**	**760 bar cone angle (°)**	**780 bar penetration (mm)**	**780 bar cone angle (°)**
0.35	0	0	0	0	0	0	0	0	0	0
0.37	0	0	0	0	0	0	0	0	0	0
0.39	0	0	0	0	0	0	0.2	67.9	0	0
0.41	0	0	0	0	0.4	63.7	0.5	82.2	0.7	83.5
0.43	0.6	54.4	0.7	76.0	0.7	65.4	1.2	69.4	1.3	71.9
0.45	1.0	42.2	1.2	59.5	1.8	55.5	2.1	63.5	2.2	63.1
0.47	1.8	31.2	2.1	50.2	2.5	46.1	3.1	48.2	3.6	48.7
0.49	2.7	30.1	3.1	40.2	3.8	37.6	4.4	41.6	5.0	41.8
0.51	3.8	26.5	4.5	31.9	5.23	33.0	6.4	34.6	7.2	32.1
0.53	5.3	30.6	6.4	28.6	7.1	30.4	7.8	31.8	9.6	30.6
0.55	7.0	27.9	7.8	29.6	9.0	29.7	10.3	30.7	12.1	29.8
0.57	8.6	27.5	10.1	27.1	10.8	22.1	12.6	29.4	14.2	28.9
0.59	12.2	21.1	12.6	25.4	13.5	22.5	14.8	27.1	16.3	29.6
0.61	14.5	22.5	15.3	24.6	16.3	20.8	18.2	28.0	18.3	30.4
0.63	17.6	21.9	19.2	24.8	19.2	22.4	20.3	28.7	21.2	29.4
0.65	20.1	22.2	21.9	22.1	21.7	24.5	24.3	29.1	23.7	30.5
0.67	22.7	23.7	23.8	23.8	24.0	23.7	25.2	27.3	26.8	29.6
0.69	24.9	24.0	25.2	22.4	27.1	24.2	26.5	25.5	29.0	28.0
0.71	28.0	22.6	27.4	22.0	28.6	24.5	29.2	25.1	30.4	27.6
0.73	29.5	21.9	31.1	22.1	30.8	26.9	32.1	24.1	32.5	29.4
0.75	33.5	20.5	31.5	19.3	33.7	24.8	35.5	25.7	36.8	26.9
0.77	36.1	20.0	34.9	20.9	35.7	25.6	36.9	26.2	39.7	24.9
0.79	36.7	19.3	37.1	19.5	38.6	23.1	39.9	25.5	40.9	23.6
0.81	40.4	18.3	38.6	21.0	38.8	24.7	41.3	26.9	40.2	28.4
0.83	39.9	20.5	41.5	20.5	39.8	23.1	40.7	29.4	44.8	25.9
0.85	41.8	21.2	39.9	25.2	41.9	25.4	41.4	28.4	45.8	27.2

Cylinder Pressure

The results of test conducted to determine the effect of cylinder pressure on the spray structure can be found bellow.

Table 5: Cylinder pressure results. 0 bar to 20 bar cylinder pressure. 780 bar injection pressure. Nitrogen

Time (ms)	**0 bar penetration (mm)**	**0 bar cone angle (°)**	**5 bar penetration (mm)**	**5 bar cone angle (°)**	**10 bar penetration (mm)**	**10 bar cone angle (°)**	**15 bar penetration (mm)**	**15 bar cone angle (°)**	**20 bar penetration (mm)**	**20 bar cone angle**
0.35	0	0	0	0	0	0	0	0	0	0
0.40	1.9	19.5	1.9	22.0	1.4	16.6	0.3	22.3	0	0
0.45	5.2	29.7	4.7	24.5	4.6	28.7	1.8	25.1	1.6	38.9
0.50	12.2	27.7	8.3	23.4	8.4	30.5	4.6	30.0	4.4	35.3
0.55	18.7	24.2	15.2	21.6	13.5	25.9	7.8	32.3	7.5	34.8
0.60	24.9	22.8	20.7	22.4	17.7	26.3	13.2	27.1	11.6	29.3
0.65	30.7	22.8	26.0	24.7	21.2	24.5	17.1	26.4	15.7	28.5
0.70	42.0	20.3	32.1	25.5	28.2	23.7	22.1	24.8	18.7	26.2
0.75	55.2	22.6	39.7	24.3	31.9	23.7	26.1	22.5	22.0	23.4
0.80	67.4	25.2	50.3	28.8	36.5	21.7	28.1	25.4	25.6	28.0
0.85	80.1	28.3	45.8	26.4	35.3	19.9	30.4	23.2	26.9	29.9
0.90	-	-	51.9	25.3	40.4	20.9	31.6	24.1	28.2	28.3
0.95	-	-	55.9	25.1	39.1	22.4	35.7	25.6	31.4	22.2
1.00	-	-	52.3	26.0	41.1	19.6	33.4	23.7	32.7	23.6
1.05	-	-	57.6	27.1	43.5	19.1	39.2	19.4	32.1	28.0
1.10	-	-	60.3	29.4	45.5	20.5	36.4	23.5	34.7	26.3
1.15	-	-	60.9	29.6	47.7	20.3	38.9	25.7	35.2	23.2

Figure 130,Figure 131, Figure 132, Figure 133 and Figure 134 below show the variation of spray penetration with time as well as the theoretical spray penetration; for tests with an injection pressure of 780 bar and cylinder pressures of atmospheric, 5 bar, 10 bar, 15 bar and 20 bar respectively. Nitrogen was used for these tests.

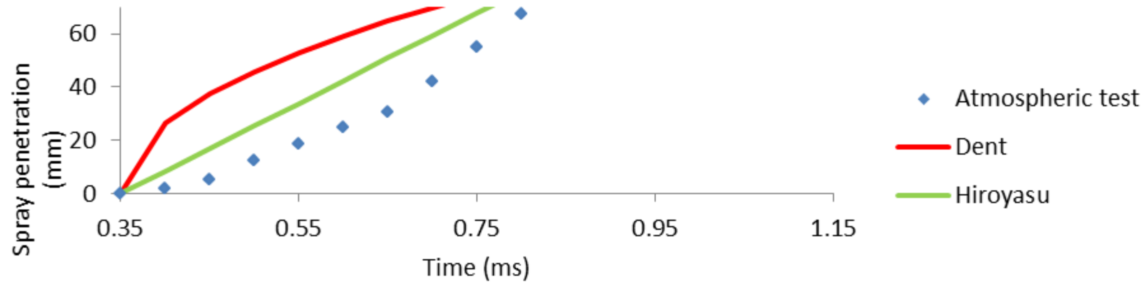

Figure 130: Spray penetration test results compared to theory. 780 bar injection pressure. Atmospheric cylinder pressure using nitrogen

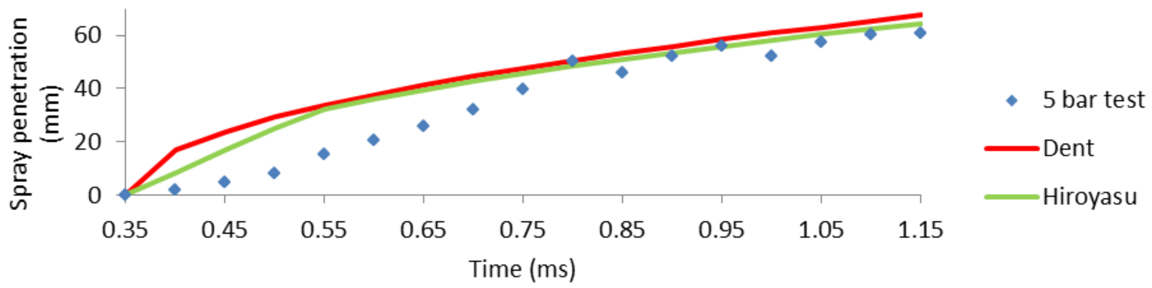

Figure 131: Spray penetration test results compared to theory. 780 bar injection pressure. 5 bar cylinder pressure using nitrogen

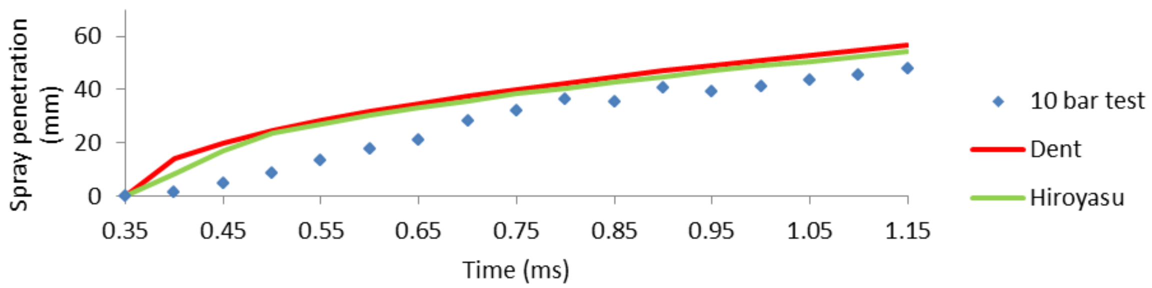

Figure 132: Spray penetration test results compared to theory. 780 bar injection pressure. 10 bar cylinder pressure using nitrogen

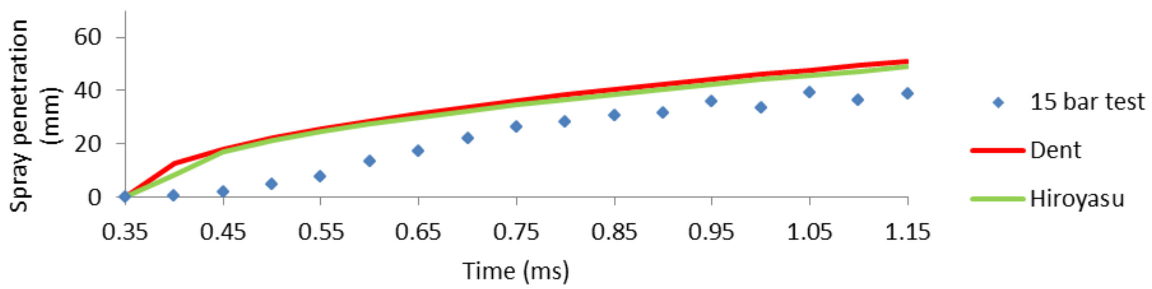

Figure 133: Spray penetration test results compared to theory. 780 bar injection pressure. 15 bar cylinder pressure using nitrogen

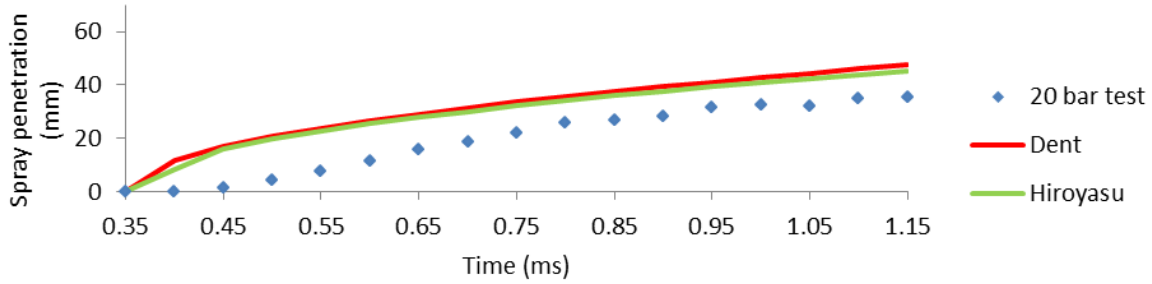

Figure 134: Spray penetration test results compared to theory. 780 bar injection pressure. 20 bar cylinder pressure using nitrogen

Figure 135 and Figure 136 show the percentage difference between the test results and theoretical results for the tests mentioned above.

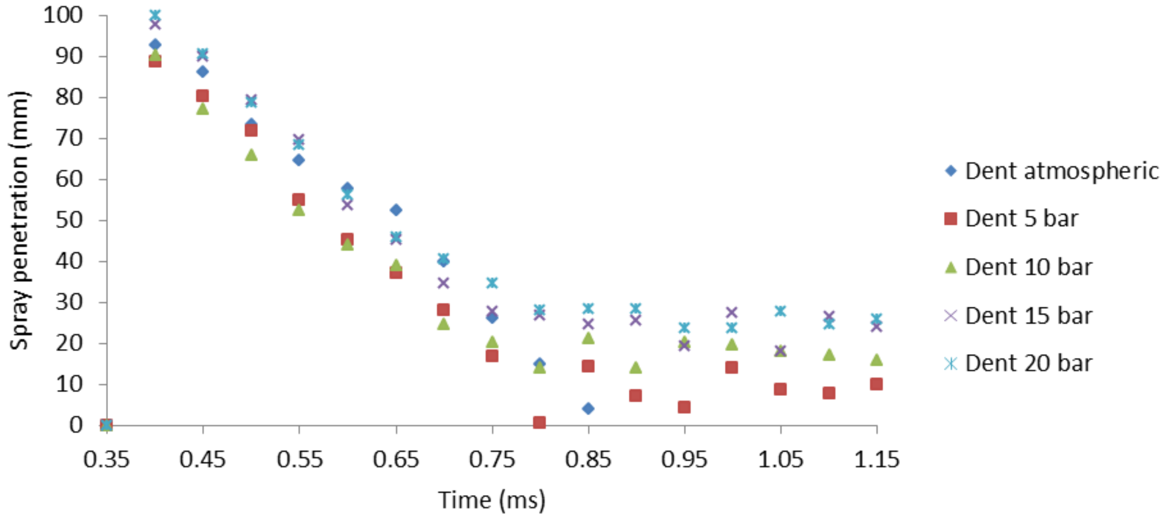

Figure 135: Percentage difference between theoretical Dent and actual results. 780 bar injection pressure. Atmospheric - 20 bar cylinder pressure using nitrogen.

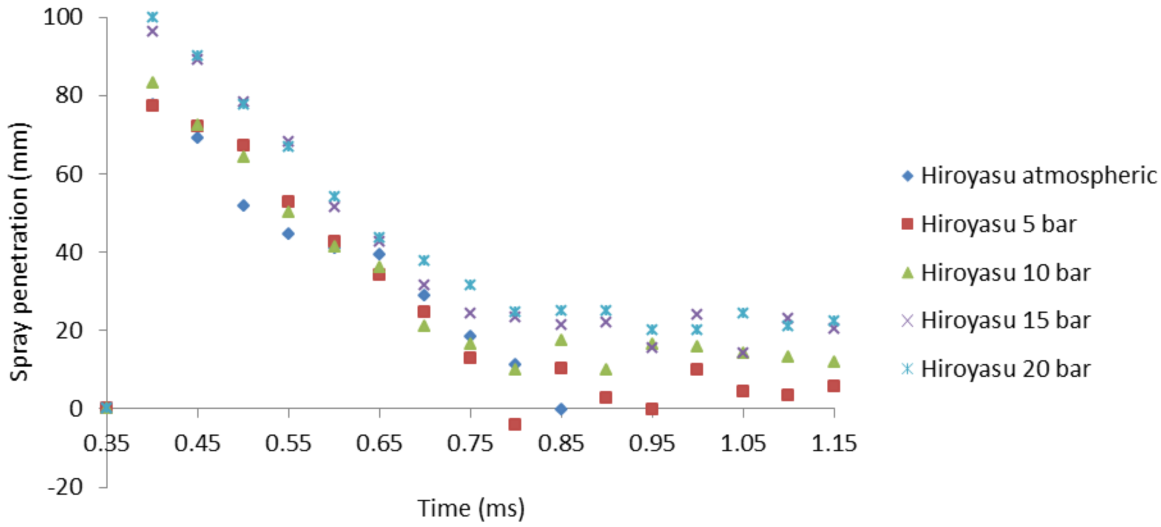

Figure 136 Percentage difference between theoretical Hiroyasu and actual results. 780 bar injection pressure. Atmospheric - 20 bar cylinder pressure using nitrogen.

Figure 137, Figure 138, Figure 139, Figure 140 and Figure 141 below show the variation of cone angle with time as well as the theoretical cone angle; for tests with an injection pressure of 780 bar and cylinder pressures of atmospheric, 5 bar, 10 bar, 15 bar and 20 bar respectively. Nitrogen was used for these tests.

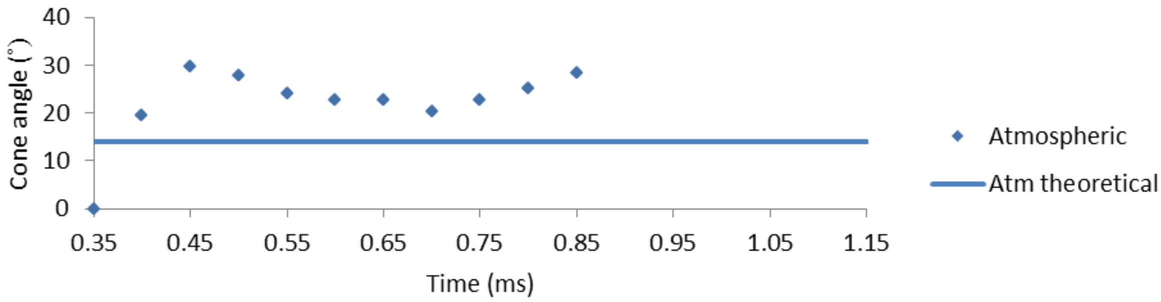

Figure 137: Cone angle test results compared to theory. 780 bar injection pressure. Atmospheric cylinder pressure using nitrogen

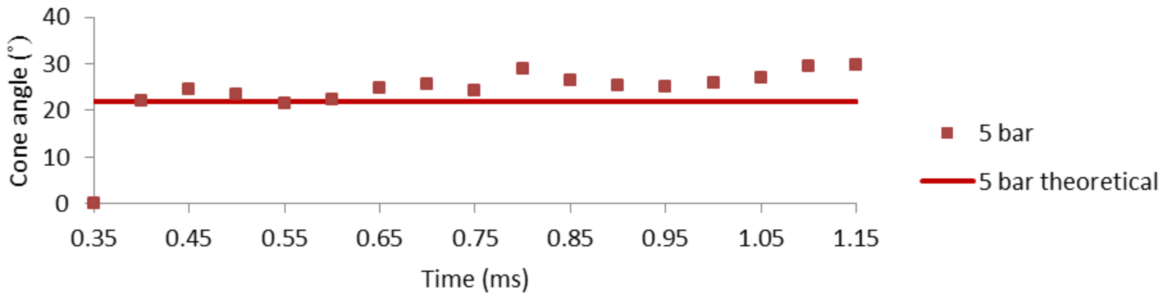

Figure 138: Cone angle test results compared to theory. 780 bar injection pressure. 5 bar cylinder pressure using nitrogen

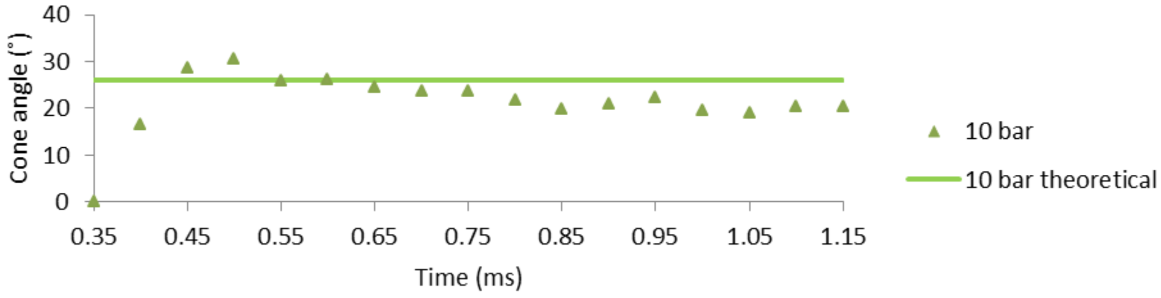

Figure 139: Cone angle test results compared to theory. 780 bar injection pressure. 10 bar cylinder pressure using nitrogen

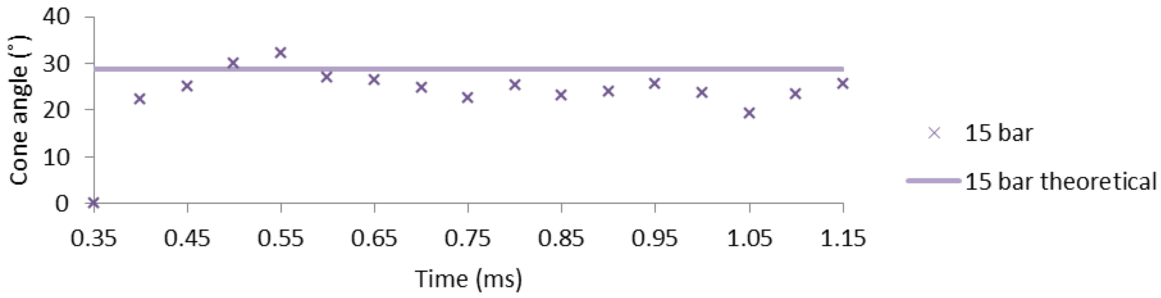

Figure 140: Cone angle test results compared to theory. 780 bar injection pressure. 15 bar cylinder pressure using nitrogen

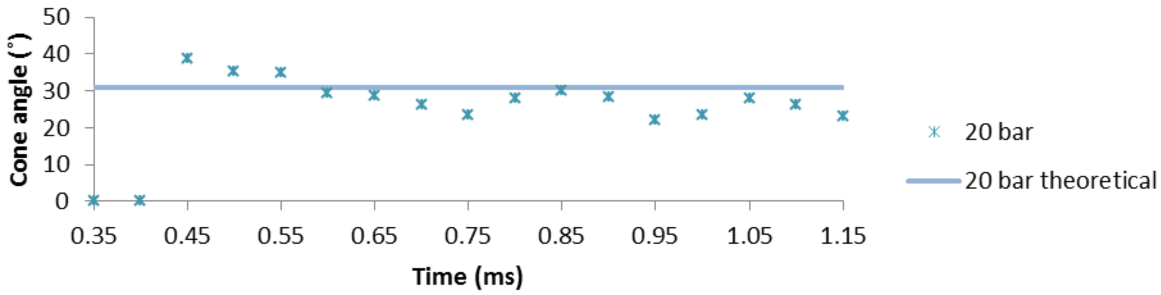

Figure 141: Cone angle test results compared to theory. 780 bar injection pressure. 20 bar cylinder pressure using nitrogen

Pressure Difference

The results of test conducted to determine if either the injection pressure or the cylinder pressure have a greater effect on the spray than the overall pressure difference, are presented below.

Table 6: Constant pressure difference results. 0 bar to 20 bar cylinder pressure. 755 bar to 775 bar injection pressure. Nitrogen

Time (ms)	755 bar injection 0 bar cylinder penetration (mm)	755 bar injection 0 bar cylinder cone angle (˚)	760 bar injection 5 bar cylinder penetration (mm)	760 bar injection 5 bar cylinder cone angle (˚)	76 bar injection 10 bar cylinder penetration (mm)	765 bar injection 10 bar cylinder cone angle (˚)	770 bar injection 15 bar cylinder penetration (mm)	770 bar injection 15 bar cylinder cone angle (˚)	775 bar injection 20 bar cylinder penetration (mm)	775 bar injection 20 bar cylinder cone angle (˚)
0.35	0	0	82.1	6	0	0	0	0	0	0
0.4	0	0	1.37	18.9	0.2	85.2	0	0	0	0
0.45	2.1	47.4	4.45	27.61	1.5	52	1.2	53.7	1.15	60.9
0.5	5.7	28.5	8.5	22	4.4	48	3.8	35.6	3.7	48.3
0.55	12	25.8	14.5	24.6	7.8	37.4	6.9	37	6.8	36
0.6	18.1	24.5	19.4	19.9	14.8	31.9	12.7	33	11.6	34
0.65	26.6	26.8	24.2	22.7	20.3	27.6	17.5	31.5	15.7	31.9
0.7	36.5	22.7	32.8	23.1	24.8	31.8	20.7	32.6	19.4	30.8
0.75	46	24	40.4	23.7	28	26.1	24.9	30.5	22.2	26.7
0.8	56.7	23.2	46.8	24.6	31.4	27.7	28.9	29.8	25.2	22.3
0.85	65.2	26.1	47.6	24.2	35.7	25.1	30.7	27.8	29.2	23.3
0.9	74.4	27.3	51.7	26.5	37.8	21.7	31.9	25.9	28.8	25.9
0.95	80.4	30.7	53.4	25.5	37.1	25.1	32.3	27.3	29.9	27.7
1	86.7	31.9	57.2	25.2	39.4	23.5	36.7	25.8	32.4	22.9
1.05			56.3	26.2	41.9	25.5	35.7	29.7	35.2	19.2
1.1			60.3	24.9	45.5	24	36.8	28.3	34.1	28.3
1.15			56	25.8	44.7	22.4	39.4	29.9	34.5	28.8

Figure 142, Figure 143, Figure 144 and Figure 145 show the test result compared to theoretical results.

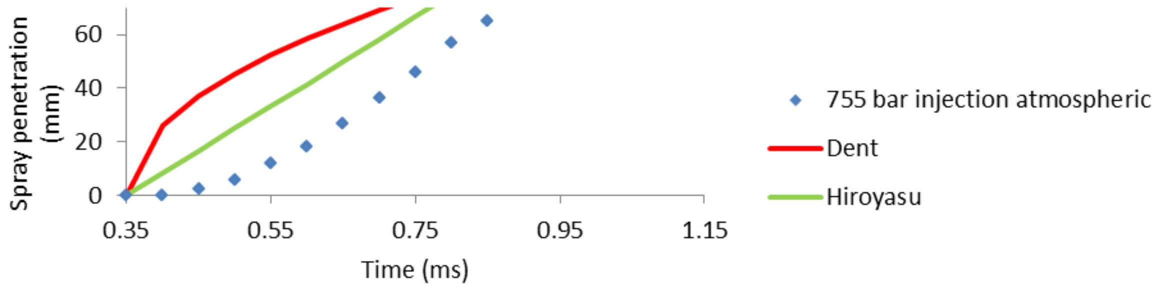

Figure 142: Test results compared to theory. 755 bar injection pressure. atmospheric cylinder pressure using nitrogen

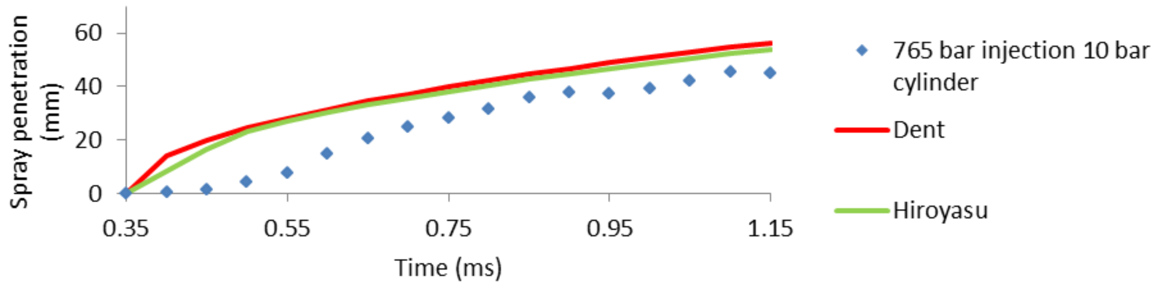

Figure 143: Test results compared to theory. 765 bar injection pressure. 10 bar cylinder pressure using nitrogen

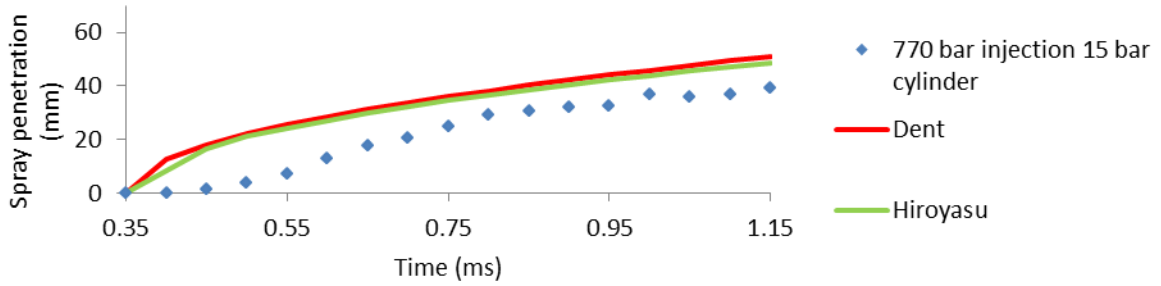

Figure 144: Test results compared to theory. 770 bar injection pressure. 15 bar cylinder pressure using nitrogen

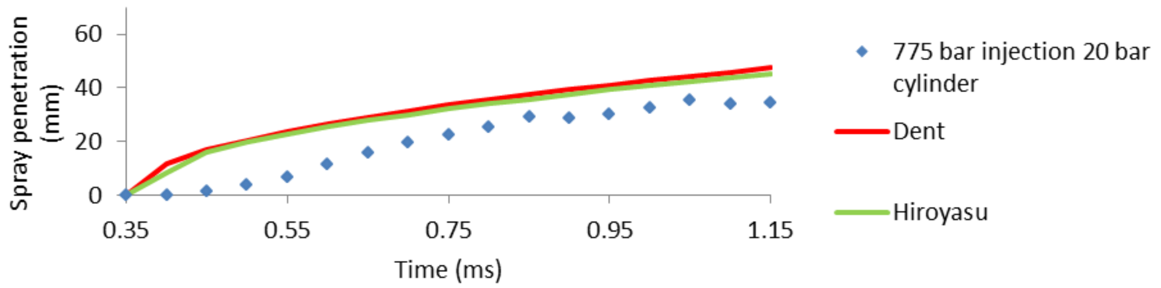

Figure 145: Test results compared to theory. 775 bar injection pressure. 20 bar cylinder pressure using nitrogen

Nitrogen Compared to Carbon Dioxide

Table 7: Injection pressure results. 5 bar cylinder pressure. 700 – 780 bar injection pressure. Carbon dioxide

Time (ms)	700 bar penetration (mm)	700 bar cone angle (˚)	720 bar penetration (mm)	720 bar cone angle (˚)	740 bar penetration (mm)	740 bar cone angle (˚)	760 bar penetration (mm)	760 bar cone angle (˚)	780 bar penetration (mm)	780 bar cone angle (˚)
0.35	0	0	0	0	0	0	0	0	0	0
0.40	0	0	0	0	0	0	0.6	46.0	0.8	46.6
0.45	1.3	42.5	1.4	45.7	1.84	47.3	2.3	41.7	2.8	39.5
0.50	3.5	44.5	4.5	25.7	5.1	32.9	5.7	33.8	6.6	31.2
0.55	7.1	26.0	7.6	26.5	9.3	26.6	10.7	29.8	12.2	26.8
0.60	12.3	28.2	14.4	25.2	15.0	24.5	15.5	25.9	16.7	25.6
0.65	18.8	26.1	21.0	22.7	21.4	23.8	22.3	26.5	21.9	24.9
0.70	24.9	26.1	30.3	23.4	25.0	22.8	25.6	24.4	25.5	26.5
0.75	29.7	26.7	36.3	25.0	30.3	22.1	31.4	26.5	30.8	27.1
0.80	34.6	25.0	37.9	26.3	36.8	24.5	33.6	24.1	35.3	22.0
0.85	32.6	24.8	40.7	26.7	37.3	21.0	36.6	52.9	36.0	25.4
0.90	34.8	22.6	39.0	32.5	40.6	21.5	42.7	22.8	40.5	25.4
0.95	33.9	24.7	39.8	30.5	39.8	23.4	44.7	20.3	41.1	24.5
1.00	36.9	23.1	42.3	31.5	40.7	24.9	42.0	22.5	44.9	23.0
1.05	38.2	24.9	42.8	29.3	44.2	23.5	40.9	27.6	43.3	25.3
1.10	41.0	20.6	47.2	27.1	44.8	22.4	43.4	25.4	44.4	24.0
1.15	42.7	23.7	47.0	31.7	45.8	25.1	43.8	23.5	46.6	24.5

Figure 146, Figure 147, Figure 148, Figure 149 and Figure 150 below show the test results compared to theoretical predictions of Dent and Hiroyasu with a cylinder pressure of 5 bar (carbon dioxide) and injection pressures of 700 bar, 720 bar, 740 bar, 760 bar and 780 bar respectively.

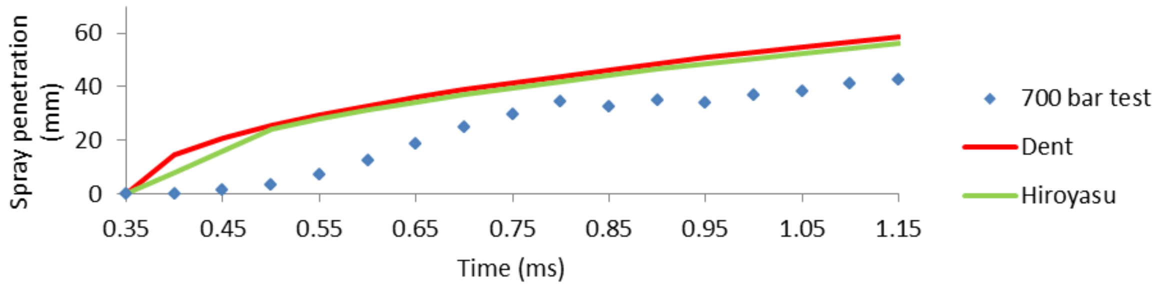

Figure 146: Spray penetration test results compared to theory. 700 bar injection pressure. 5 bar cylinder pressure using carbon dioxide

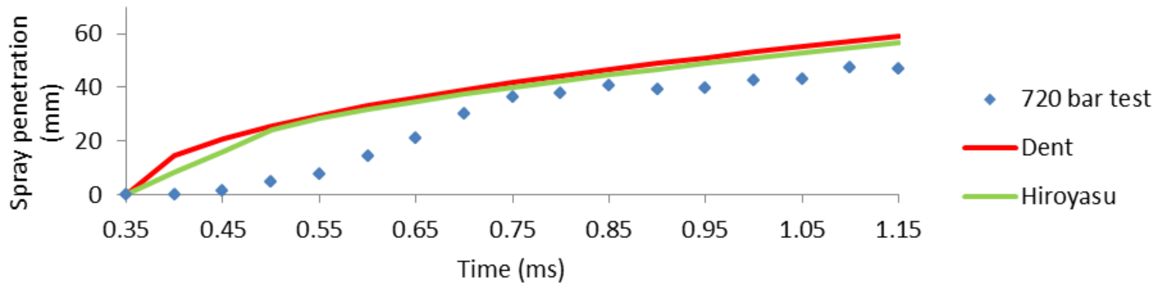

Figure 147: Spray penetration test results compared to theory. 720 bar injection pressure. 5 bar cylinder pressure using carbon dioxide

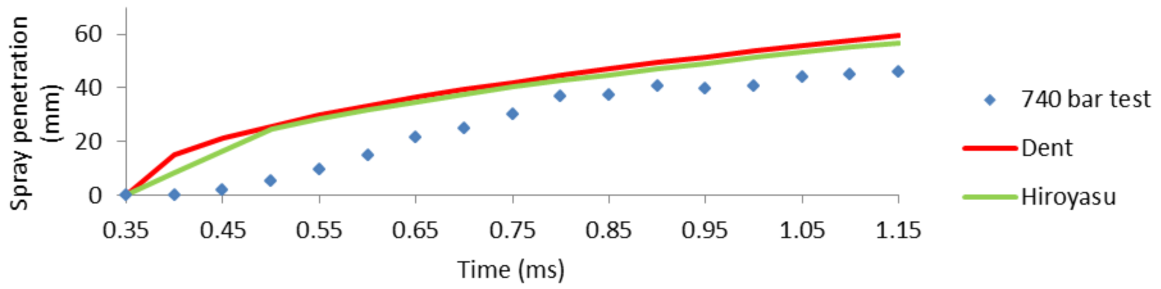

Figure 148: Spray penetration test results compared to theory. 740 bar injection pressure. 5 bar cylinder pressure using carbon dioxide

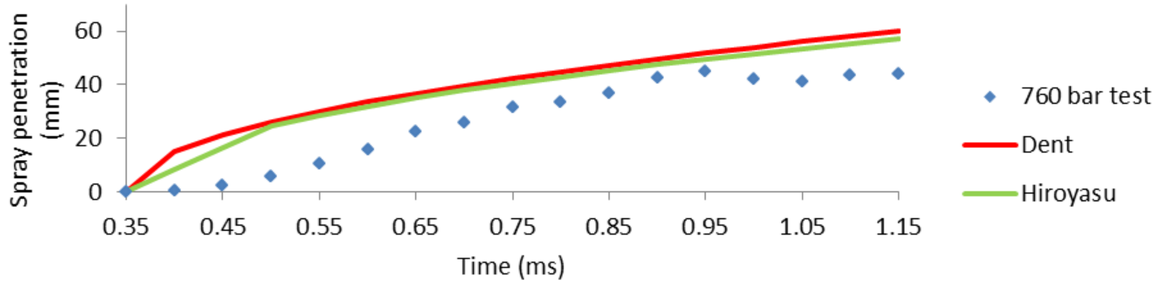

Figure 149: Spray penetration test results compared to theory. 760 bar injection pressure. 5 bar cylinder pressure using carbon dioxide

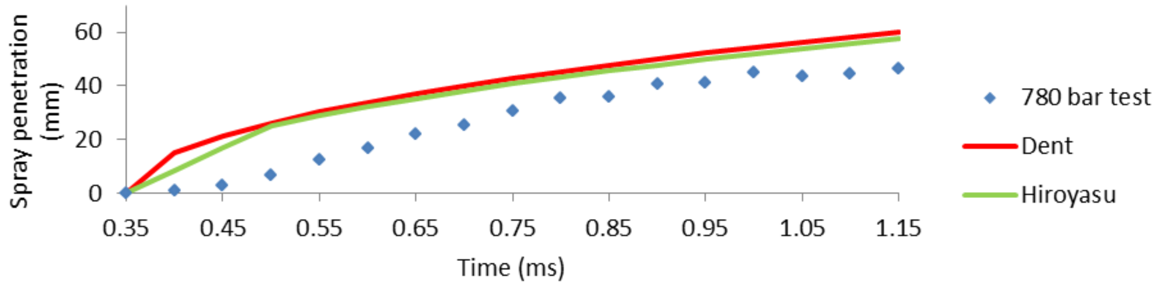

Figure 150: Spray penetration test results compared to theory. 780 bar injection pressure. 5 bar cylinder pressure using carbon dioxide

Figure 151, Figure 152, Figure 153 and Figure 154 show a comparison between the spray penetration at injection pressures of 700 bar, 720 bar, 740 bar and 780 bar respectively with a cylinder pressure of 5 bar.

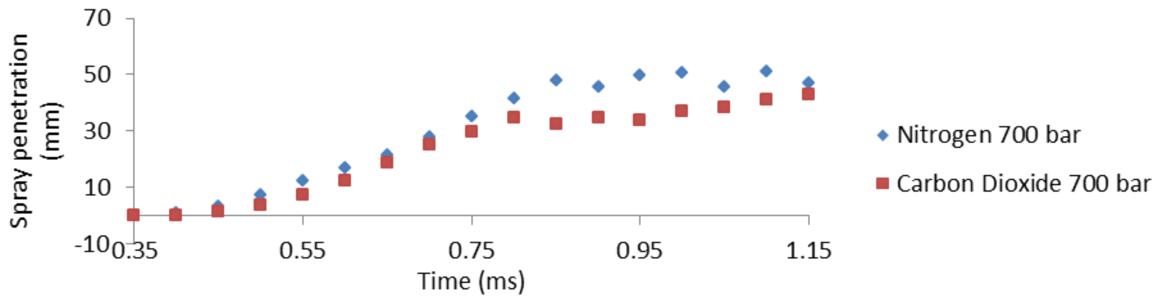

Figure 151: Spray penetration. Nitrogen compared to carbon dioxide. 700 bar injection pressure. 5 bar cylinder pressure.

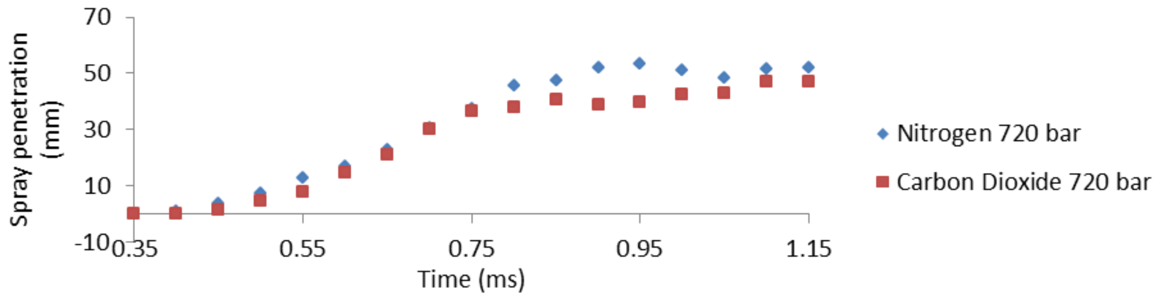

Figure 152: Spray penetration. Nitrogen compared to carbon dioxide. 720 bar injection pressure. 5 bar cylinder pressure.

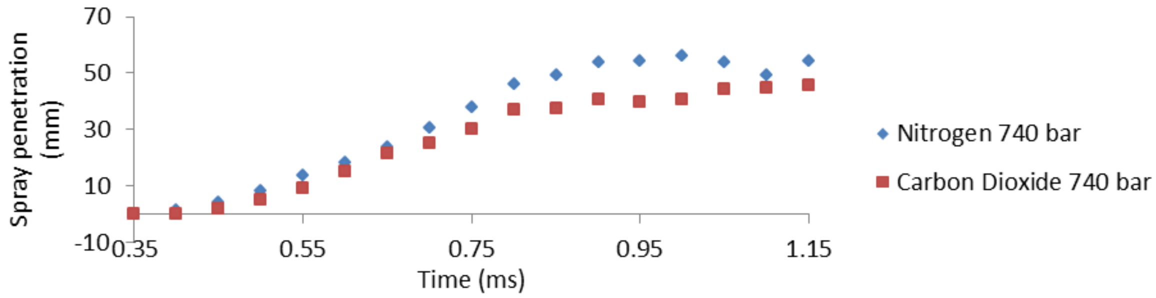

Figure 153: Spray penetration. Nitrogen compared to carbon dioxide. 740 bar injection pressure. 5 bar cylinder pressure.

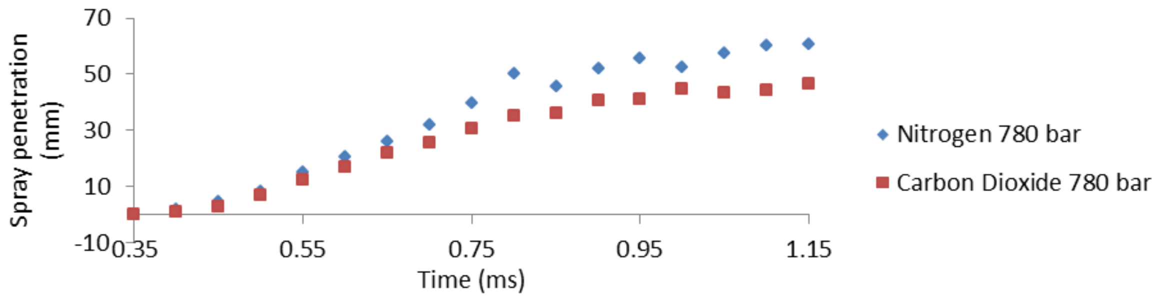

Figure 154: Spray penetration. Nitrogen compared to carbon dioxide. 780 bar injection pressure. 5 bar cylinder pressure.

Table 8: Cylinder pressure results. 0 bar to 20 bar cylinder pressure. 780 bar injection pressure. Carbon dioxide

Time (ms)	**0 bar penetration (mm)**	**0 bar cone angle (°)**	**5 bar penetration (mm)**	**5 bar cone angle (°)**	**10 bar penetration (mm)**	**10 bar cone angle (°)**	**15 bar penetration (mm)**	**15 bar cone angle (°)**	**20 bar penetration (mm)**	**20 bar cone angle (°)**
0.35	0	0	0	0	0	0	0	0	0	0
0.40	0.9	47.9	0.8	46.6	0.3	88.4	0	0	0	0
0.45	3.7	33.2	2.8	39.5	2.6	37.9	1.9	58.3	3.4	36.3
0.50	9.2	31.1	6.6	31.2	6.1	30.3	5.1	35.9	7.1	28.9
0.55	16.1	28.9	12.2	26.8	9.5	28.2	7.6	33.2	10.3	26.3
0.60	21.9	25.8	16.7	25.6	15.3	23.8	11.6	30.9	12.4	27.8
0.65	29.0	23.4	21.9	24.9	17.7	27.6	14.2	28.1	14.7	27.5
0.70	36.6	20.1	25.5	26.5	21.2	25.7	17.1	32.4	16.1	30.9
0.75	46.2	19.5	30.8	27.1	24.4	27.5	20.4	35.3	19.1	29.3
0.80	47.5	19.7	35.3	22.0	27.9	26.4	22.9	36.4	21.8	30.9
0.85	61.8	18.7	36.0	25.4	29.3	26.8	24.1	35.3	23.4	30.8
0.90	59.0	19.8	40.5	25.4	31.3	25.7	27.2	31.5	24.5	28.7
0.95	62.7	21.5	41.1	24.5	34.3	29.1	28.8	28.1	27.6	30.9
1.00	22.9	67.6	44.9	23.0	33.9	26.1	28.8	25.3	27.9	25.5
1.05	68.1	25.1	43.3	25.3	35.2	27.7	33.3	20.6	26.6	30.1
1.10	67.5	27.0	44.4	24.0	34.7	29.6	31.0	24.2	28.2	28.2
1.15	71.7	24.6	46.6	24.5	37.9	26.7	34.6	29.5	29.8	26.5

Figure 155, Figure 156, Figure 157, Figure 158 and Figure 159 below show the variation of spray penetration with time as well as the theoretical spray penetration; for tests with an injection pressure of 780 bar and cylinder pressures of atmospheric, 5 bar, 10 bar, 15 bar and 20 bar respectively. Nitrogen was used for these tests.

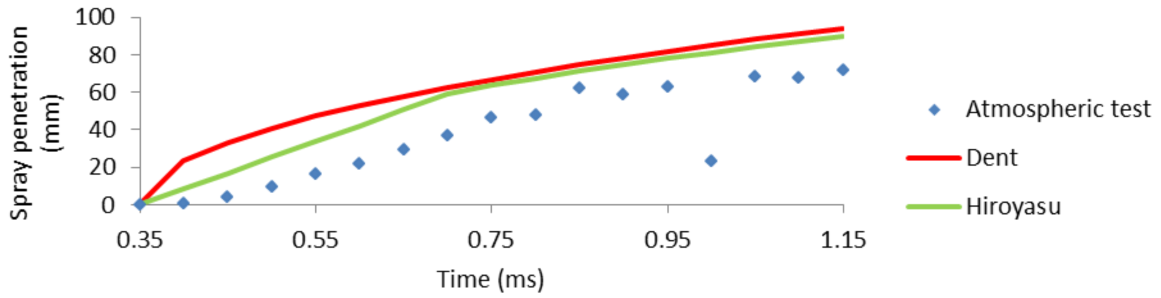

Figure 155: Spray penetration test results compared to theory. 780 bar injection pressure. Atmospheric cylinder pressure using carbon dioxide.

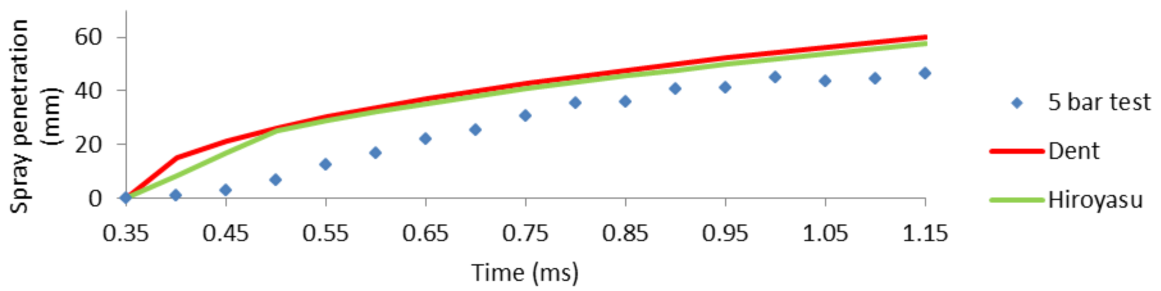

Figure 156: Spray penetration test results compared to theory. 780 bar injection pressure. 5 bar cylinder pressure using carbon dioxide

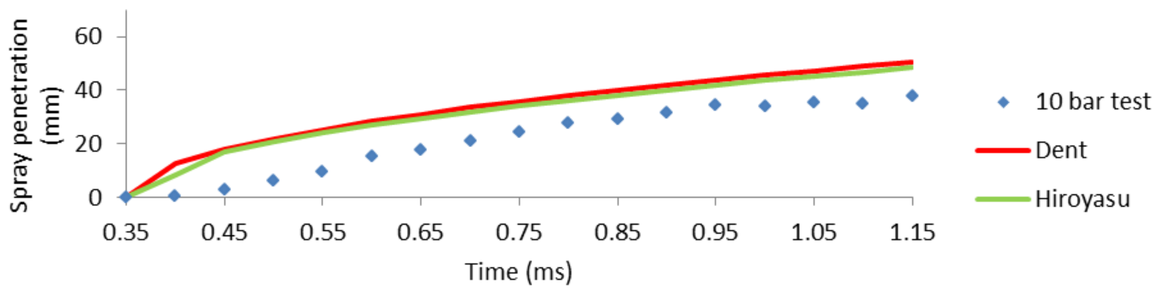

Figure 157: Spray penetration test results compared to theory. 780 bar injection pressure. 10 bar cylinder pressure using carbon dioxide

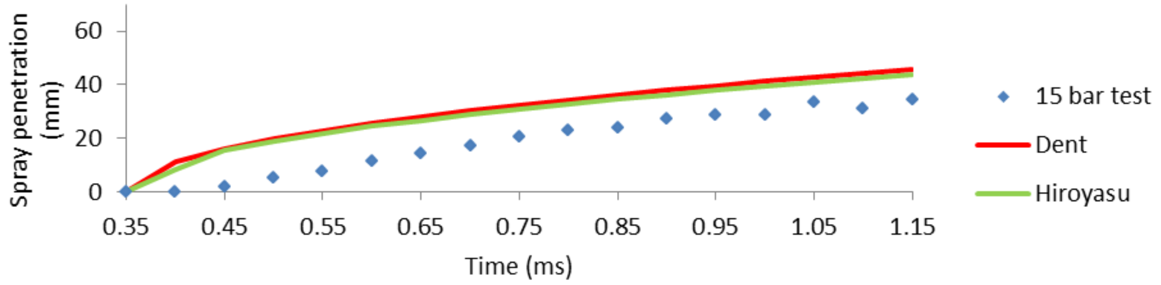

Figure 158: Spray penetration test results compared to theory. 780 bar injection pressure. 15 bar cylinder pressure using carbon dioxide

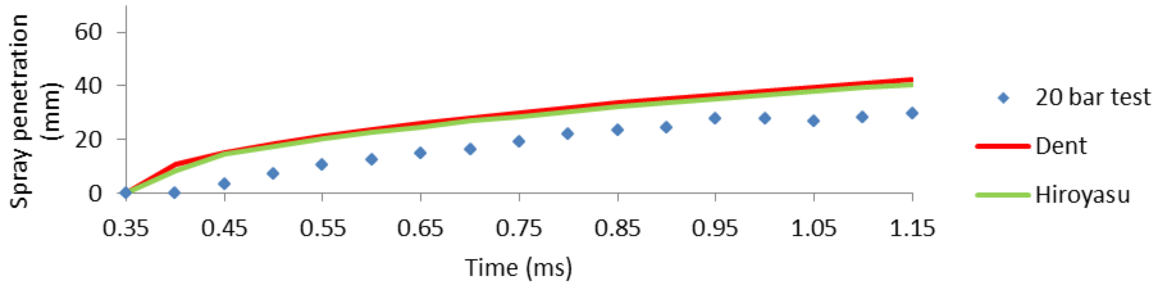

Figure 159: Spray penetration test results compared to theory. 780 bar injection pressure. 20 bar cylinder pressure using carbon dioxide

Figure 160, Figure 161, Figure 162 and Figure 163 below show a comparison on the measured spray penetration between nitrogen and carbon dioxide with an injection pressure of 780 bar and cylinder pressures of atmospheric, 5 bar, 15 bar and 20 bar respectively.

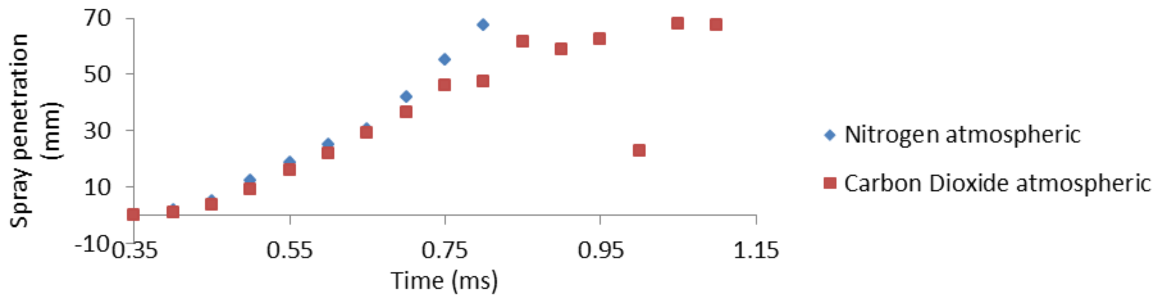

Figure 160: Spray penetration. Nitrogen compared to carbon dioxide. 780 bar injection pressure. Atmospheric cylinder pressure.

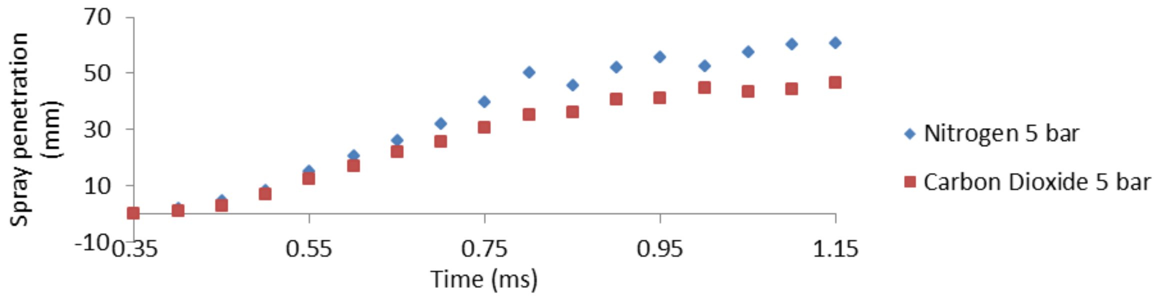

Figure 161: Spray penetration. Nitrogen compared to carbon dioxide. 780 bar injection pressure. 5 bar cylinder pressure.

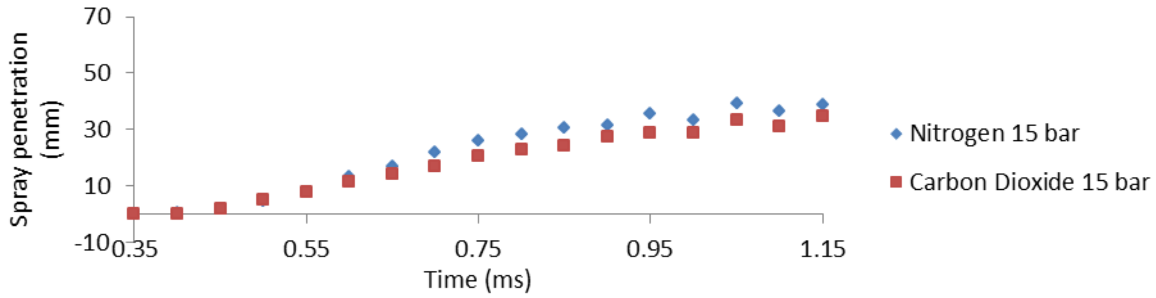

Figure 162: Spray penetration. Nitrogen compared to carbon dioxide. 780 bar injection pressure. 15 bar cylinder pressure.

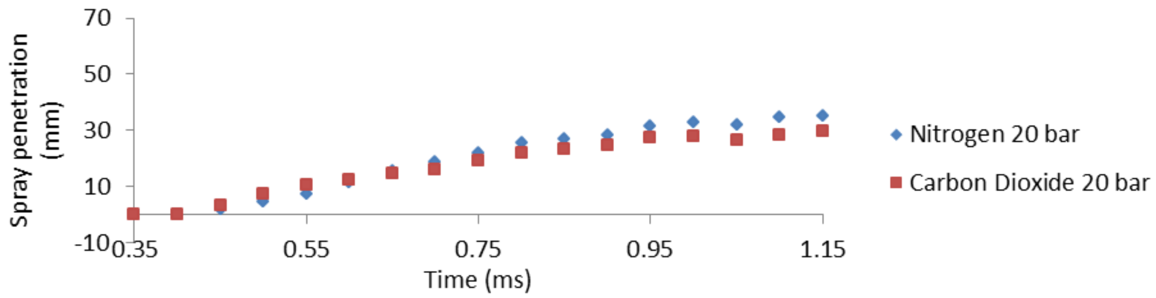

Figure 163: Spray penetration. Nitrogen compared to carbon dioxide. 780 bar injection pressure. 20 bar cylinder pressure.

Table 9: Constant pressure difference results. 0 bar to 20 bar cylinder pressure. 755 bar to 775 bar injection pressure. Carbon dioxide

Time (ms)	**755 bar injection 0 bar cylinder penetration (mm)**	**755 bar injection 0 bar cylinder cone angle (˚)**	**760 bar injection 5 bar cylinder penetration (mm)**	**760 bar injection 5 bar cylinder cone angle (˚)**	**76 bar injection 10 bar cylinder penetration (mm)**	**765 bar injection 10 bar cylinder cone angle (˚)**	**770 bar injection 15 bar cylinder penetration (mm)**	**770 bar injection 15 bar cylinder cone angle (˚)**	**775 bar injection 20 bar cylinder penetration (mm)**	**775 bar injection 20 bar cylinder cone angle (˚)**
0.35	0	0	0	0	0	0	0	0	0	0
0.40	0	0	0.6	46.0	0.7	81.7	0	0	0	0
0.45	4.7	44.8	2.3	41.7	4.2	37.0	3.4	34.5	3.4	35.5
0.50	8.1	34.2	5.7	33.8	7.7	33.1	8.1	29.5	7.1	29.7
0.55	18.6	34.8	10.7	29.8	12.1	26.1	10.3	29.5	10.2	27.8
0.60	23.4	41.2	15.5	25.9	13.6	31.5	12.2	31.6	11.5	29.2
0.65	28.0	41.4	22.3	26.5	15.8	32.4	14.9	29.4	14.3	31.6
0.70	30.6	42.8	25.6	24.4	17.7	35.7	17.0	31.3	15.9	32.8
0.75	33.7	45.5	31.4	26.5	21.8	32.8	21.1	28.4	18.9	29.5
0.80	40.5	42.2	33.6	24.1	24.8	31.5	23.6	31.9	20.9	29.6
0.85	48.5	44.6	36.6	52.9	28.1	28.6	24.7	30.1	22.8	28.5
0.90	56.1	40.0	42.7	22.8	29.2	31.5	25.0	35.2	26.1	23.5
0.95	62.7	43.3	44.7	20.3	29.9	30.1	28.0	33.0	25.4	28.9
1.00	58.9	41.0	42.0	22.5	35.3	27.4	27.7	29.8	27.6	26.4
1.05	63.9	43.0	40.9	27.6	34.0	28.9	30.1	32.0	26.6	30.0
1.10	60.3	40.3	43.4	25.4	35.2	26.5	30.8	27.7	28.0	30.8
1.15	70.1	42.5	43.8	23.5	35.2	30.9	33.7	26.5	28.7	30.8

Figure 164, Figure 165, Figure 166, Figure 167 and Figure 168 below show the test results compared to the theoretical predictions for tests done with a constant pressure difference of 5 bar (carbon dioxide).

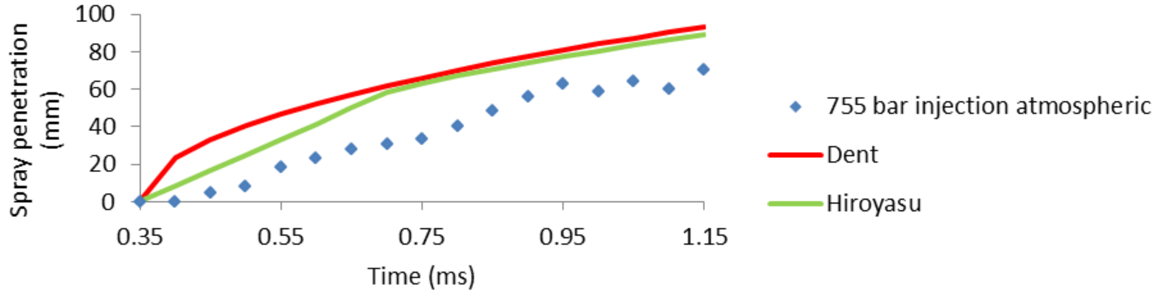

Figure 164: Test results compared to theory. 755 bar injection pressure. Atmospheric cylinder pressure using carbon dioxide

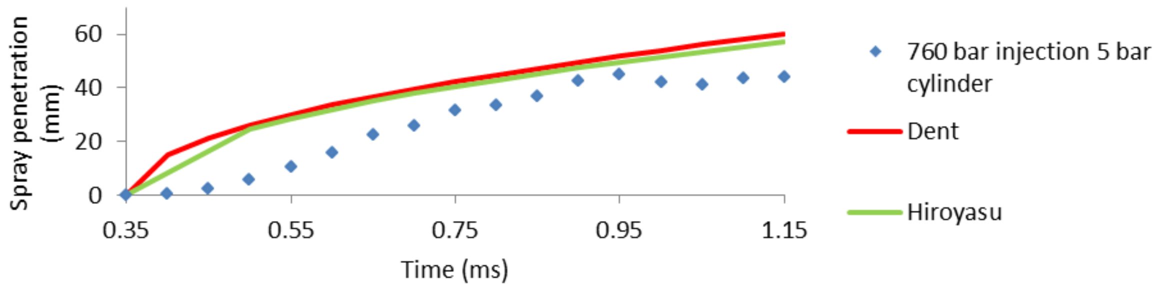

Figure 165: Test results compared to theory. 760 bar injection pressure. 5 bar cylinder pressure using carbon dioxide

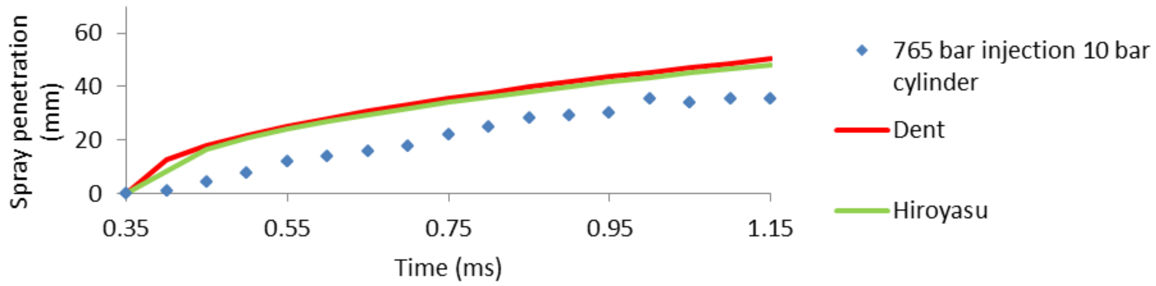

Figure 166: Test results compared to theory. 765 bar injection pressure. 10 bar cylinder pressure using carbon dioxide

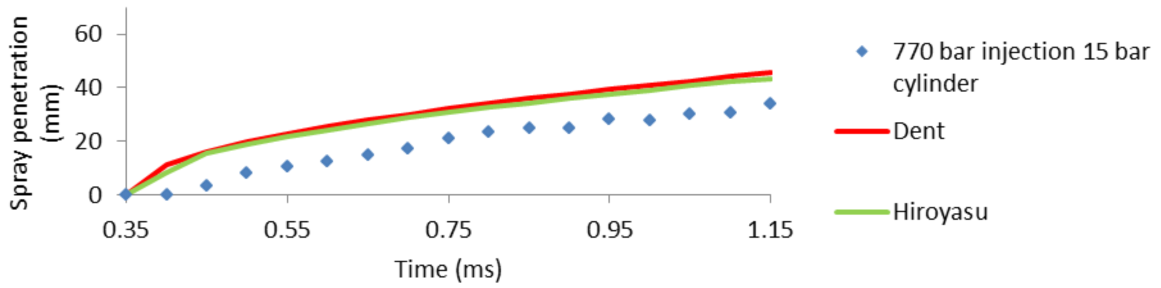

Figure 167: Test results compared to theory. 770 bar injection pressure. 15 bar cylinder pressure using carbon dioxide

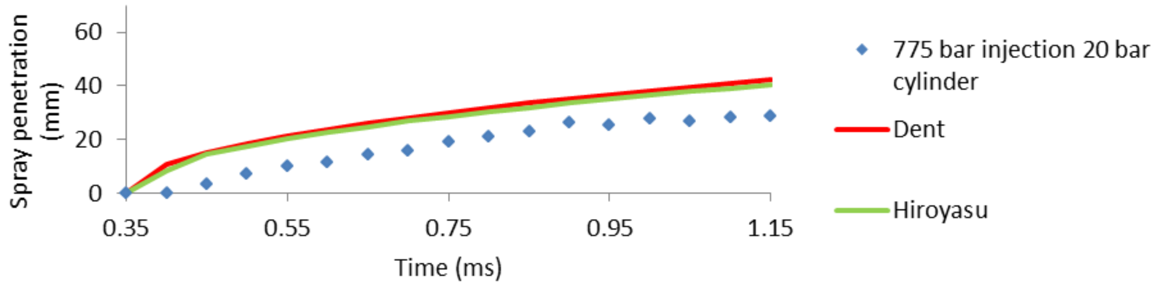

Figure 168: Test results compared to theory. 775 bar injection pressure. 20 bar cylinder pressure using carbon dioxide

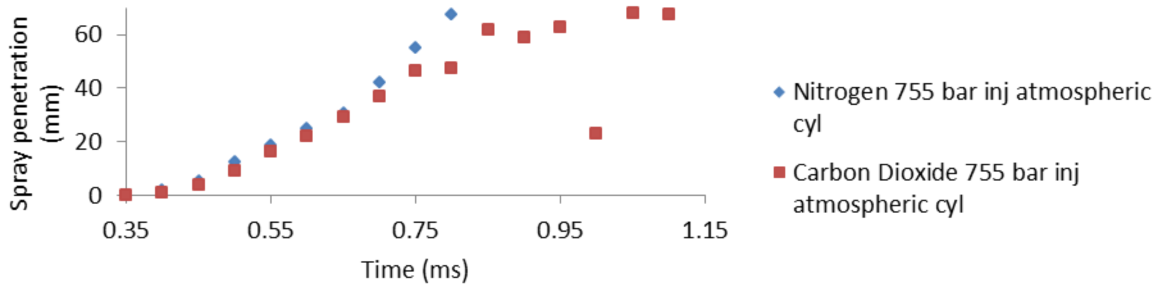

Figure 169: Spray penetration. Nitrogen compared to carbon dioxide. 755 bar injection pressure. Atmospheric cylinder pressure.

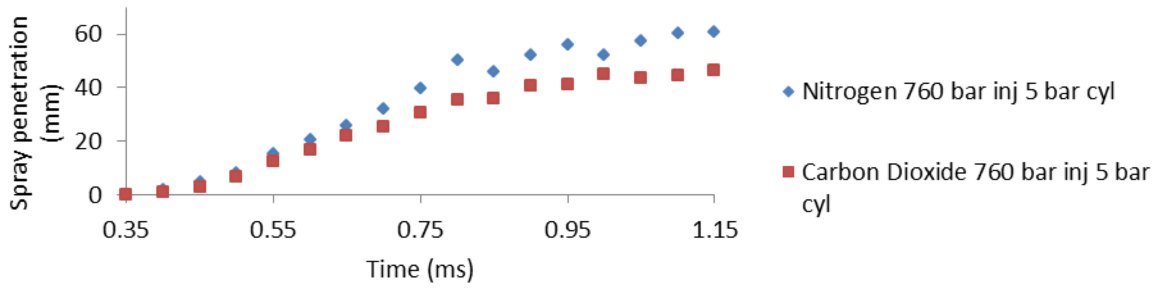

Figure 170: Spray penetration. Nitrogen compared to carbon dioxide. 760 bar injection pressure. 5 bar cylinder pressure.

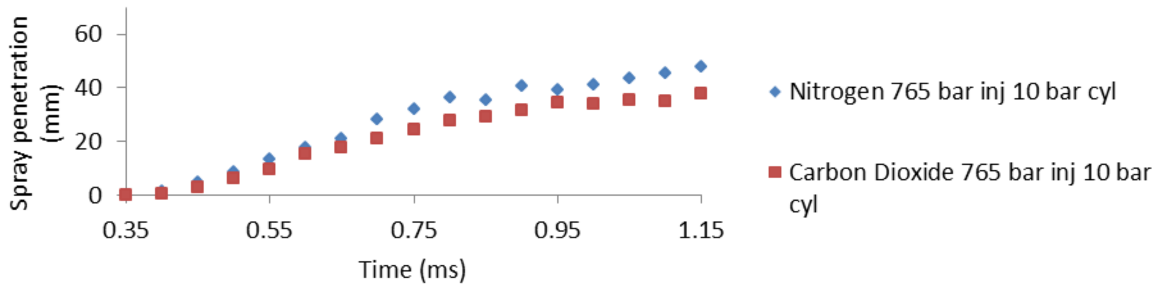

Figure 171: Spray penetration. Nitrogen compared to carbon dioxide. 765 bar injection pressure. 10 bar cylinder pressure.

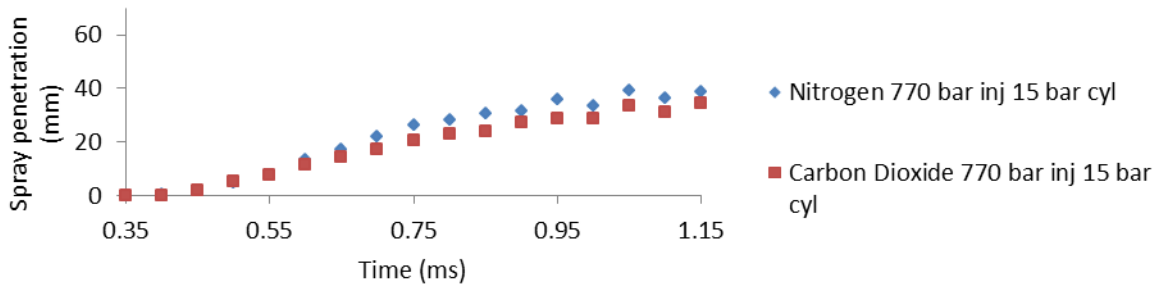

Figure 172: Spray penetration. Nitrogen compared to carbon dioxide. 770 bar injection pressure. 15 bar cylinder pressure.

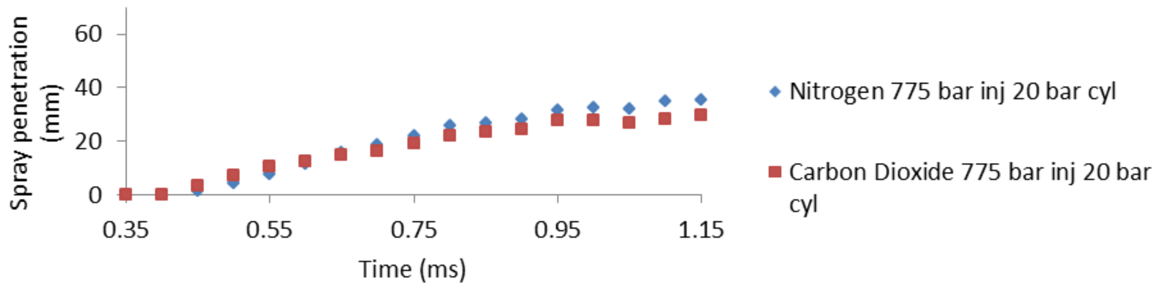

Figure 173: Spray penetration. Nitrogen compared to carbon dioxide. 775 bar injection pressure. 20 bar cylinder pressure.

APPENDIX E – SPRAY CHAMBER DESIGN

SCHOOL OF MECHANICAL, INDUSTRIAL & AERONAUTICAL ENGINEERING

RESEARCH PROJECT

Masters project report

Project title: Spray Chamber Design
Project supervisor: Prof. D. Cipolat
Date: 23/11/2017
Student: Andran Naicker
Student number: 317465

1. INTRODUCTION

1.1. Background

Experiments are to be conducted to analyse the behaviour of fuel being sprayed from an injector into an environment with varying pressures. The existing system holds the injector in a shadow and fills up with vapour too quickly to use the analysis software. A new pressurizedspray chamber must therefore be designed.

1.2. Task Statement

The task is to design a pressurizedinjector spray chamber.

1.2.1. Task as given

Design a spray chamber for the Inov8 Test Stand capable of holding 20 bar.

1.2.2. Task as understood

The task is to design a new spray chamber that will allow the effects of back pressure on spray characteristics to be investigated. The spray chamber will have to be able to safely contain a pressure of 20 bar. The spray chamber must also have windows to that the high speed camera can capture images of the spray; and for the various light sources to illuminate the spray. The chamber will have to hold the injector in a suitable position so that clear images can be captured. The chamber will have to have attachment points for compressed gas supply as well as a purging system and pressure relief valve. There will have to be an access panel so that the windows can be cleaned from the inside and a system to drain the injected test fluid. The spray chamber must in no way affect the characteristics of the injector spray. The new spray chamber must be a direct replacement for the current spray chamber and must not affect the functions of the Inov8 Test Stand.

1.3. Literature Review

The spray chamber must be designed using the same principles as a pressure vessel.

1.3.1. Pressure vessel failure

The most common cause of failure of pressure vessels is corrosion. If moisture is allowed to collect in the pressure vessel, this could lead to corrosion. Corrosion could also occur if the pressure vessel is used to contain corrosive substances. Corrosion may cause pitting or grooving; if this occurs on a large area of the pressure vessel, it results in a reduction of the material thickness. The reduction of the plate thickness means that the pressure vessel will be highly stressed, even under normal operating conditions. The more stressed the material is, the faster it will corrode until the pressure vessel ruptures. [4]

Pressure vessels can also fail due to excessive stress. If the pressure vessel is subjected to repeated stresses that exceed its limits, it may fail due to fatigue. Pressure vessels used to contain compressed gasses are subjected to rapid pressure fluctuations. If the pressure vessel is not allowed to expand and contract with temperature variations, it can experience large stresses that might also lead to failure. [4]

Regular inspection of the pressure vessel, including the inside surfaces can significantly reduce the risk of failure. If moisture is allowed to collect in the pressure vessel, this could lead to corrosion. Safety valves and other devices that are not functioning properly could result in pressure vessel failure. If the safety valve is adjusted to high, the pressure vessel might be subjected to pressures higher than the design pressure and this will result in failure. [4]

Defects in the material that were not identified during fabrication could lead to the failure of the pressure vessel. Inferior workmanship could also result in failure. Poor welding may look acceptable on the surface, but could contain slag, too much porosity or have a lack of penetration.[4]

Inspection openings on the pressure vessel are essential to ensure that the internal surfaces can be inspected. Regular inspections of the internal surfaces can significantly reduce the risk of failure. Removable heads or cover plates may be used instead of inspection openings as long as they are large enough to allow thorough inspections of the internal surfaces to be conducted. Openings should be places at the ends of the pressure vessel so that a light source placed on one end will illuminate all the internal surfaces. It is important to ensure that the inspection openings are able to function after installation i.e. the pressure vessel must not be installed in such a way that the openings are blocked. [4]

All pressure vessels are required to have a system to protect from being over pressured. This is usually in the form of a pressure relief valve that is set to the design pressure of the pressure vessel.

1.3.2. Pressure vessel standards

Pressure vessels are usually structures with complex geometries and are required to function under various loading conditions. Pressure vessels are therefore governed by a set of standards and codes to ensure that they are able to perform their function safely [1]. One of the most widely used set of standards for high strength steel alloys is from the American Society of Mechanical Engineers (ASME) [1]:

$$\sigma_{allowable} = min\left(\frac{S_y}{1.5} ; \frac{S_{ut}}{2.14}\right) \quad \text{Equation 1}$$

Where:

$\sigma_{allowable}$	Allowable stress
S_y	Yeild Strength
S_{ut}	Ultimate tensile strength

Another widely used standard is the European Standard for Unfired Pressure Vessels, EN13445 [1]:

$$\sigma_{allowable} = min\left(\frac{S_y}{1.5} ; \frac{S_{ut}}{2.4}\right) \quad \text{Equation 2}$$

Where:

$\sigma_{allowable}$	Allowable stress
S_y	Yeild Strength
S_{ut}	Ultimate tensile strength

Comparing Equation 1and Equation 2, it can be seen that the European Standard will result in a more conservative design and therefore a safer pressure vessel [1].

1.3.3. Market analysis

There are no pressure vessels on the market that can be used for the desired purpose. One will therefore have to be designed and manufactured.

2. PRODUCT REQUIREMENTS AND SPECIFICATIONS

The spray chamber must comply with the following requirements, constraints and criteria.

2.1. Requirements

1. The spray chamber must contain a pressure of 20 bar.
2. The spray chamber must have windows for the high speed camera and lights of the test stand.
3. The spray chamber must hold the injector in place.
4. The spray chamber must have at least one access panel.
5. The spray chamber must have a large enough volume to not fill up with vapour and obscure the images.

2.2. Constraints

1. The spray chamber must fit within the test stand.
2. The spray chamber must not affect normal operation of the test stand.
3. The location of the windows of the spray chamber must correspond to the location of the camera and lights.
4. The spray chamber must comply with the ASME design codes.

2.3. Criteria

1. The spray chamber must be safe.
2. The spray chamber must have minimal stress concentrations.
3. The spray chamber must be easy to maintain.
4. The spray chamber must be easy to manufacture.
5. The spray chamber must not interfere with the fuel jets.
6. The windows must allow the camera to have a clear view.
7. The windows must allow sufficient light into the chamber.

3. DESIGN DEVELOPMENT

Conceptual designs will be developed and selected for further development.

3.1. Concept Generation

The follow conceptual designs will be considered for further analysis.

3.1.1. Round chamber

The first concept is a round chamber with flat plates on either end. The plates will be removable so that there will be access to the inside of the chamber.

3.1.2. Rectangular chamber

The second concept is a box made by joining together 6 flat plates. The plates on the top and/or bottom will be removable so that there will be access to the inside of the chamber.

3.1.3. Rectangular box, rounded edges

The third concept is a combination of the first two concepts. The chamber will be rectangular, but it will have rounded edges on 4 sides. The plates on the top and/or bottom will be removable so that there will be access to the inside of the chamber.

3.2. Concept Selection

Table 10 below shows the comparison between the three concepts that were generated. Each of the criteria from section 2 was given a value and each concept was given a score for each of the criteria.

Table 10: Spray chamber concept selection

Concept	**Round chamber**	**Rectangular chamber**	**Rectangular chamber, round edges**
Safe (/20)	20	10	15
Minimal stress concentrations (/15)	15	5	10
Easy to maintain (/10)	10	5	7.5
Easy to manufacture (/10)	10	5	7.5
Must not interfere with jets (/15)	5	15	10
Clear view for camera (/15)	5	15	15
Allow in sufficient light (/15)	5	15	15
Total (/100)	70	70	80

From the table, it can be seen that concept 3 with a score of 80/100, would provide the best solution. Table 11 below shows how the scores in Table 10 were calculated.

Concept 1 would be the least stressed design and also the easiest to manufacture and maintain. However, it would be difficult to fit the large windows needed onto this design. Concept 2 would have been the most difficult to manufacture and maintain, however, it would allow large windows to be fitted. Concept 3 was the best compromise between the concepts.

Due to these factors, concept 3 will be developed further in greater detail.

Table 11: Concept evaluation

Concept	**Round chamber**	**Rectangular chamber**	**Rectangular chamber, round edges**
Safe	A round pressure vessel is the safest	A rectangular pressure vessel has more points at which failure can occur	The rounded edges makes the pressure vessel safer
Minimal stress concentrations	The round sides means there are no stress concentrations	Many corners, therefore lots of stress concentrations	The rounded edges minimise the stress concentrations.
Easy to maintain	The round surfaces are easy to inspect for irregularities.	There are many corners and therefore inspections and cleaning is more difficult	Number of corners is reduced and therefore easier to inspect and clean
Easy to manufacture	Simple geometry is easy to manufacture	Lots of welding required	More complex bending is required but not as much welding
Must not interfere with jets	Smaller cross sectional area	Large cross sectional area	Medium cross sectional area
Clear view for camera	Difficult to install large windows	Large windows can be fitted.	Large windows can be fitted
Allow in sufficient light	Difficult to install large windows	Large windows can be fitted	Large windows can be fitted

4. DESIGN EVALUATION

The spray chamber will be made out of high strength steel. It will be rectangular so that large windows can be fitted and it will have rounded edges to reduce stress concentrations. There will be a pressure relief valve that will be set to 20 bar to prevent the spray chamber being over pressured. The spray chamber will have flat plates on the top and bottom. One or both of the plates will be removable so that the internal surfaces can be inspected and cleaned. There will be a valve of to drain any injected test fluid. There will also be attachment points for the injector (on the top plate) and an inlet for the compressed nitrogen. The chamber will have a pressure gauge so that the internal pressure can be monitored. There will also need to be a purging system so that the pressure in the chamber can be safely released.

The spray chamber will be broken up into the different parts as described above and each part will be analysed in detail below.

5. Box design

5.1. Box Literature Review

The box of the spray chamber can be modelled as a rectangular box. Ignoring the rounded edges in the analysis will result in a more conservative design.

5.1.1. Methods of analysis

There are two broadly accepted mechanical models for calculating the strength of a rectangular pressure vessel. These are the rigid frame model and the plate model [2].

The rigid frame model involves finding the distributed moment on a ring element of unit length of the pressure vessel using the rigid frame theory of mechanics of materials [2].

The plate method analyses each wall of the pressure vessel as a plate using methods derived from the theory of elastic plates [2].

By combining these two methods using the principle of superposition, we can obtain a set of formulae that analyses the side walls of the pressure vessel as plates, while taking into consideration the interaction between the plates [2].

The side walls of the pressure vessel can be modelled as seen in Figure 174 below.

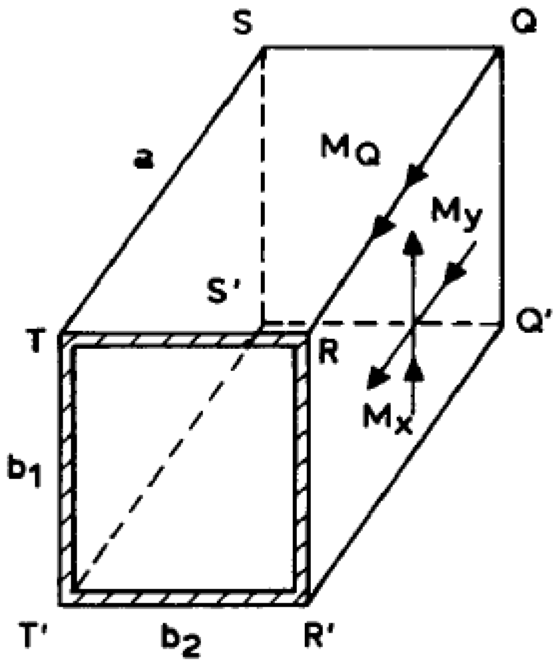

Figure 174: Pressure vessel side walls [2]

If each plate is analysed individually as seen in Figure 175 below, the moments acting on the pressure vessel can be found.

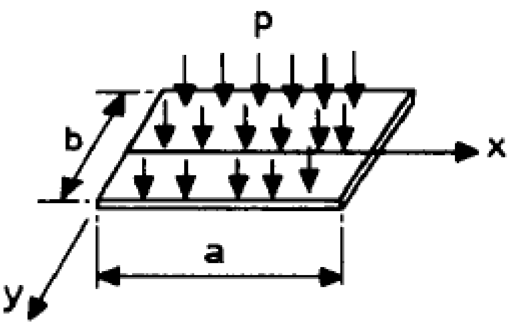

Figure 175: Single wall of pressure vessel [2]

The maximum moments will act at the centre of the plates and can be found using Equation 3 and Equation 4 [2]:

$$M_{xi}^{p} = \frac{4pa^2}{\pi^3} \sum_{m=1,3,\ldots}^{\infty} \frac{(-1)^{(m-1)/2}}{m^3} \left[1 - \frac{1}{cosh\alpha_{mi}} - \frac{\alpha_{mi} tanh\alpha_{mi}}{2cosh\alpha_{mi}} (1 - \mu)\right]$$ Equation 3

$$M_{yi}^{p} = \frac{4pa^2}{\pi^3} \sum_{m=1,3,\ldots}^{\infty} \frac{(-1)^{(m-1)/2}}{m^3} \left[\frac{\alpha_{mi} tanh\alpha_{mi}}{2cosh\alpha_{mi}} (1 - \mu) 1 - \frac{\mu}{cosh\alpha_{mi}} + \mu\right]$$ Equation 4

Where

M^{p}_{xi}	Bending moment due to pressure about the x-axis
M^{p}_{yi}	Bending moment due to pressure about the y-axis
p	Internal pressure
a	Plate length
μ	Poisson’s ratio

The variable α can be found using Equation 5 below [2]

$$\alpha_{mi} = \frac{m\pi b_i}{2a}$$ Equation 5

Where:

b	Plate width

The plates will also experience a bending moment due to the interactions with the neighbouring plates. These moments can be found using Equation 6 and Equation 7 [2].

$$M_{xi}^{M} = \sum_{m=1,3,...}^{\infty} \frac{(-1)^{(m-1)/2}}{2cosh\alpha_{mi}} E_m[2\mu + (1-\mu)\alpha_{mi}tanh\alpha_{mi}]$$ Equation 6

$$M_{yi}^{M} = \sum_{m=1,3,...}^{\infty} \frac{(-1)^{(m-1)/2}}{2cosh\alpha_{mi}} E_m[2 - (1-\mu)\alpha_{mi}tanh\alpha_{mi}]$$ Equation 7

Where

M^{M}_{xi} Bending moment due to other plates about the x-axis

M^{M}_{yi} Bending moment due to other plates about the y-axis

The constant E_m can be found using Equation 8 below [2]:

$$E_m = \frac{4pa^2}{\pi^3 m^3}\left(\frac{2tanh\alpha_{m1} + 2tanh\alpha_{m2}}{-\alpha_{m1} + \alpha_{m1}tanh^2\alpha_{m1} - tanh\alpha_{m1} - \alpha_{m2} + \alpha_{m2}tanh^2\alpha_{m2} - tanh\alpha_{m2}} + 1\right)$$ Equation 8

The total bending moment on a plate about the x-axis can be found by adding Equation 3 and Equation 6. Similarly, the total moment about the y-axis can be found by adding Equation 4 and Equation 7 [2].

The maximum stress on the plate can be found using Equation 9 [3]:

$$\sigma_{max} = \frac{6M_{max}}{t^2}$$ Equation 9

Where:

σ_{max} Maximum stress at the centre of the plate

M_{max} Maximum moment acting on the plate

t Plate thickness

By setting the maximum stress equal to the allowable stress in Equation 9, the required plate thickness can be found.

The method of analysis outlines above ignores the effect of the top and bottom plates as it was developed for pressure vessels with heights that are much greater that the lengths. In a pressure vessel with a smaller aspect ratio (< 2), these plates will support much of the load induced by the internal pressure. The model therefore produces a pressure vessel that is very conservative and therefore much safer. [3]

5.2. Box Product Requirements and Specification

The box of the spray chamber will have to comply with the following list of requirements, constraints and criteria.

5.2.1. Requirements

1. The box will have to contain 20 bar of pressure
2. The box must have attachment points for the injector, pressure relief valve, nitrogen inlet valve, purge valve and test fluid drain valve
3. The box must have an access panel

5.2.2. Constraints

1. The box must fit in the test stand
2. The box must not interfere with the normal operation of the test stand.
3. The location of the windows of the spray chamber must correspond to the location of the camera and lights.
4. The spray chamber must comply with the ASME design codes.

5.2.3. Criteria

1. The box must be safe.
2. The box must have minimal stress concentrations.
3. The box must be easy to maintain.
4. The box must be easy to manufacture.
5. The box must not interfere with the fuel jets.
6. The window openings must allow the camera to have a clear view.
7. The windows openings allow sufficient light into the chamber.

5.3. Box Design Development

The existing box is 285 x 285 x 355mm. The new box should have the same length and depth so that the position relative to the lights and camera are unchanged. This will also ensure that there is no interference with the injector spray. The longer the box, the larger the stresses the box will be subjected to. The length should therefore be kept to a minimum. Previous experimentation with the rig showed that the spray penetration rarely exceeds 100mm even at maximum injection pressure [5]. A box with a length three times that (300mm) of the maximum spray penetration should be sufficient to ensure that there is no interference. The four corners of the side walls will have a 50mm fillet (outside radius). This will ensure that there is sufficient space to fit the windows. There will be a flange on both the top and bottom of the spray chamber (refer to Figure 176); the top and bottom lids (Figure 177) will be bolted to these flanges and sealed with gaskets.

5.3.1. Material

The material used for the spray chamber must be of pressure vessel quality. The material must also be locally available. The material must be able to handle very large cyclical stresses. It will not be exposed to large temperature fluctuations. Based on these requirements, the material chosen is a carbon steel plate for moderate and low temperature service; ASTM A516 Grade 60. The properties of the selected material can be seen in Table 12 below.

Table 12: Spray chamber material properties [9]

Density	7.85 g/cc
Ultimate tensile strength	450-585 MPa
Tensile yield strength	240 MPa
Modulus of elasticity	200 GPa
Poissons ratio	0.29
Shear modulus	80 GPa

5.3.2. Spray chamber analysis

The spray chamber will be analysed with a safety factor of 2 (with respect to the yield strength). This will ensure that the spray chamber meets the criteria of the pressure vessel design codes, and it will result in a safe spray chamber. The bending moments on the side walls were calculated using the model described in section 5.1.1. Using the maximum bending moment calculated and setting the maximum stress equal to the maximum allowable stress, the minimum plate thickness was found to be 25.66mm. The tensile forces that the chamber will be subjected to only require a plate thickness of 3.9mm. The chamber will therefore fail in bending before it fails in tension.

Using the next largest standard size i.e. 30mm, an FEA analysis was performed on the spray chamber. From Figure 178, it can be seen that the stresses in the spray chamber are very low (49 MPa) compared to the maximum allowable stress of 120 MPa. This is due to the conservative nature of the model used. An FEA analysis was performed using a plate thickness of 25mm. The stresses can be seen in Figure 179 below. From the figure, it can be seen that the maximum stress would be 96.5 MPa. An FEA analysis was conducted on a spray chamber with a wall thickness of 20 mm. The stresses can be seen in Figure 180. From the figure, it can be seen that the maximum stress would be 138 MPa. This is higher than the allowable stress in the spray chamber. The chamber will therefore be made with a wall thickness of 25mm.

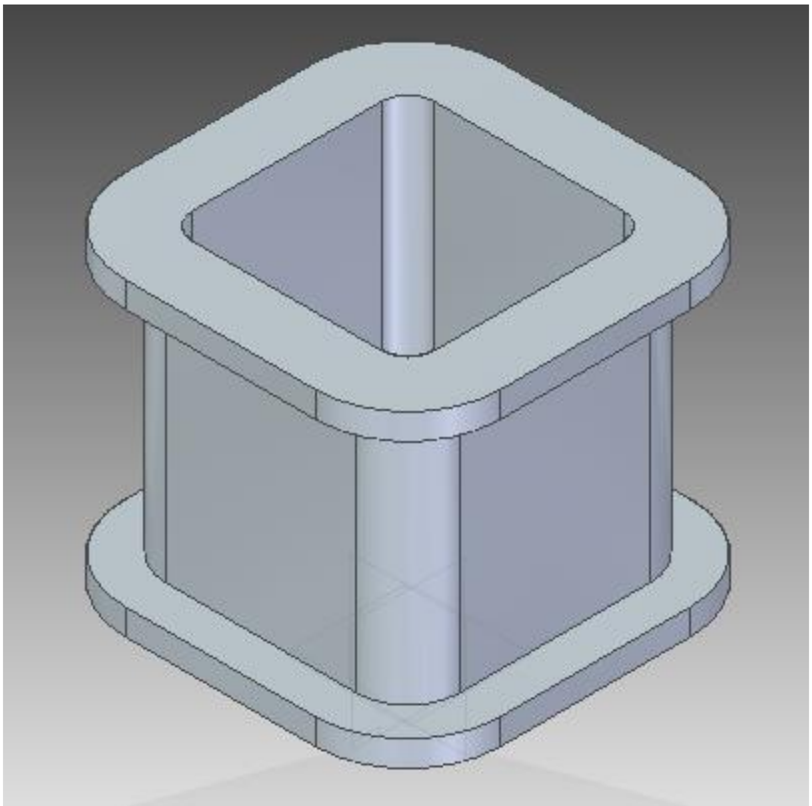

Figure 176: Spray box

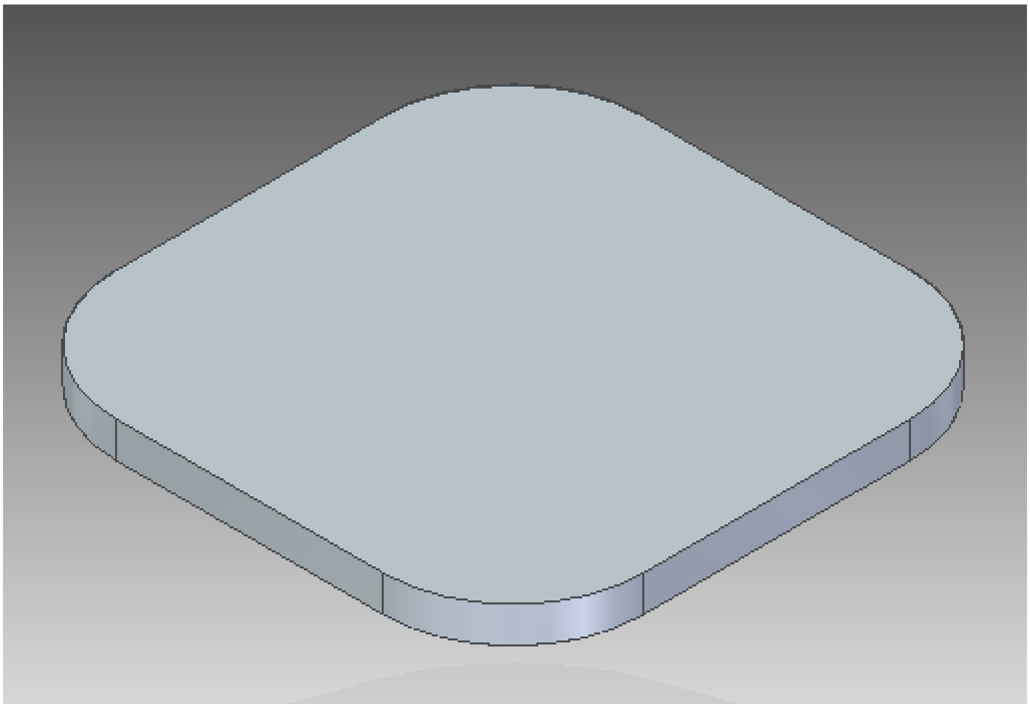

Figure 177: Lid

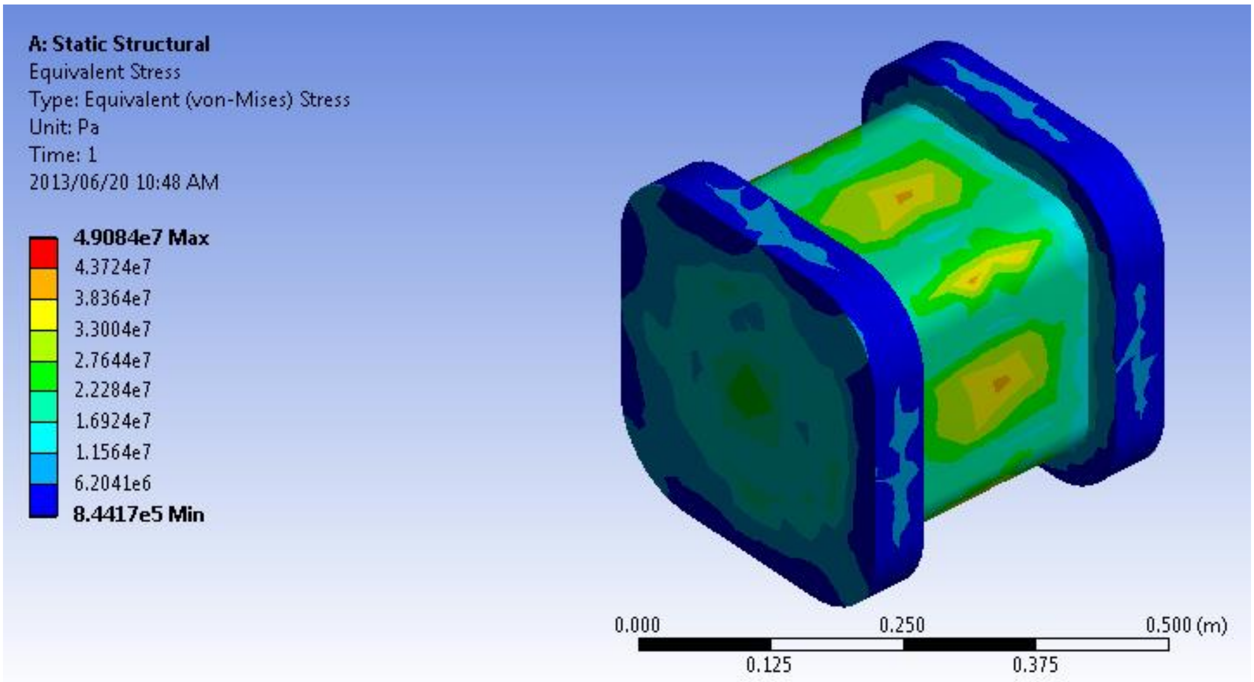

Figure 178: Stress 30mm

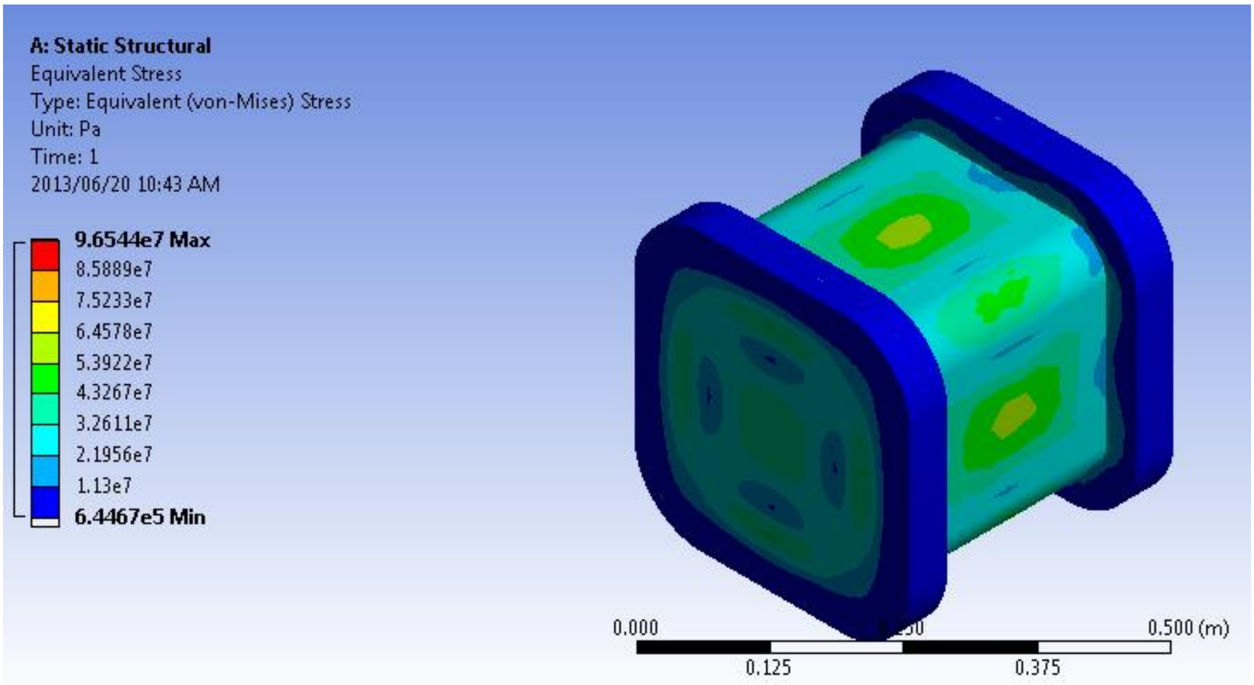

Figure 179: Stress 25mm

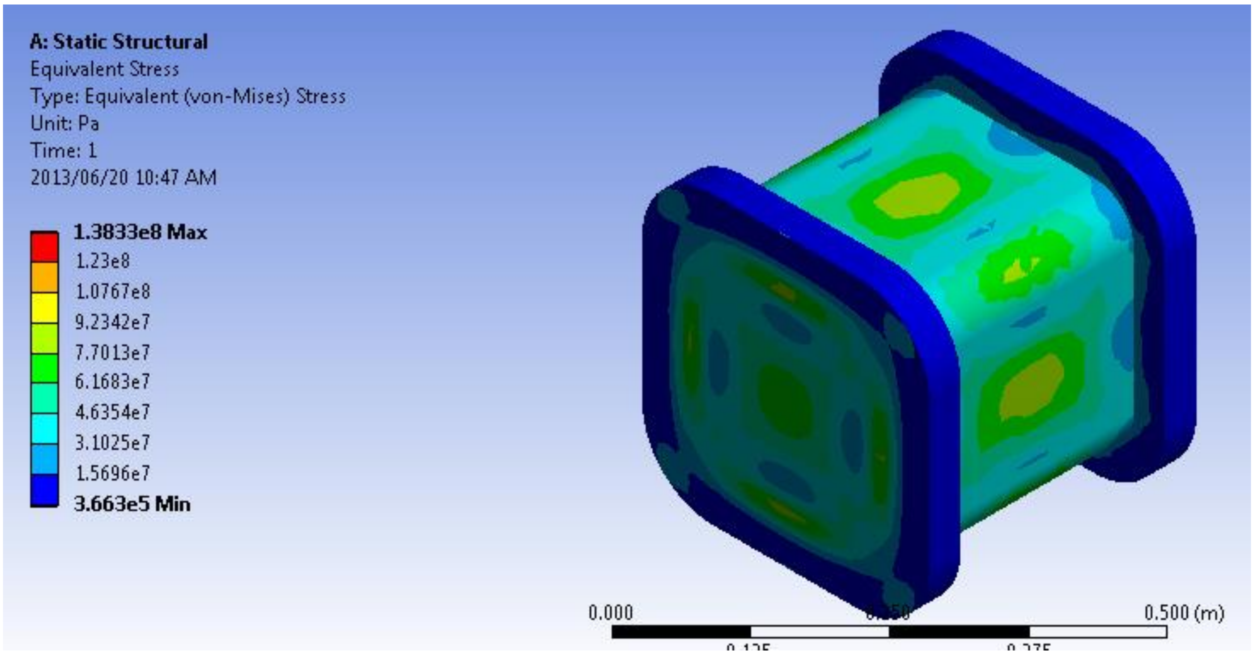

Figure 180: Stress 20mm

Windows

The sides of the box will be machined as seen in Figure 181 below. The windows will be supported from the inside by a thin strip of material.

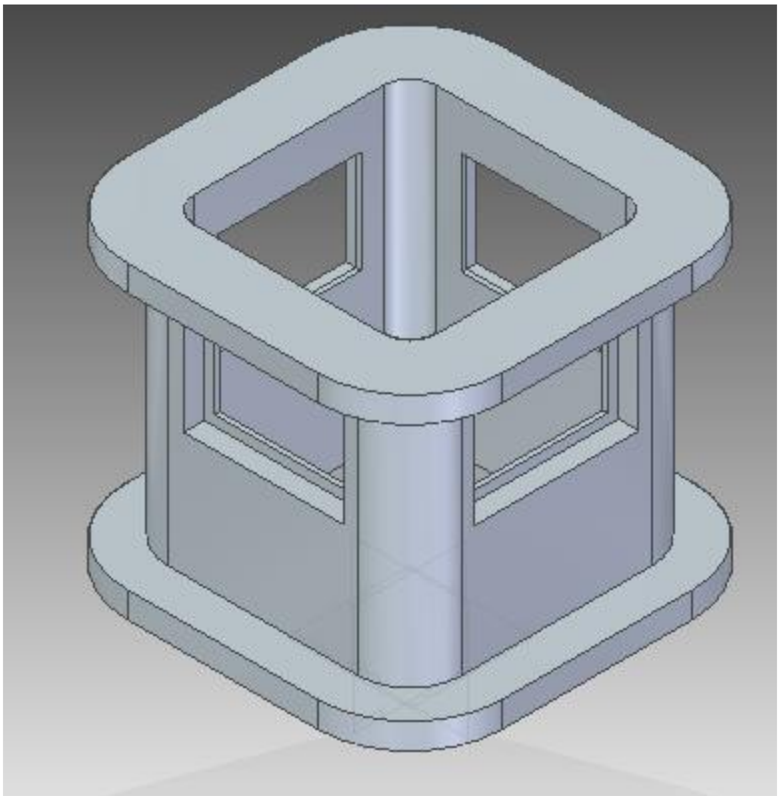

Figure 181: Box with window holes

Window Flange

The windows will be held in place by flanges made of the same material as the spray chamber. The flanges will be bolted to the spray chamber box and will overlap the sides of the window by 10mm all around seen in Figure 182 below.

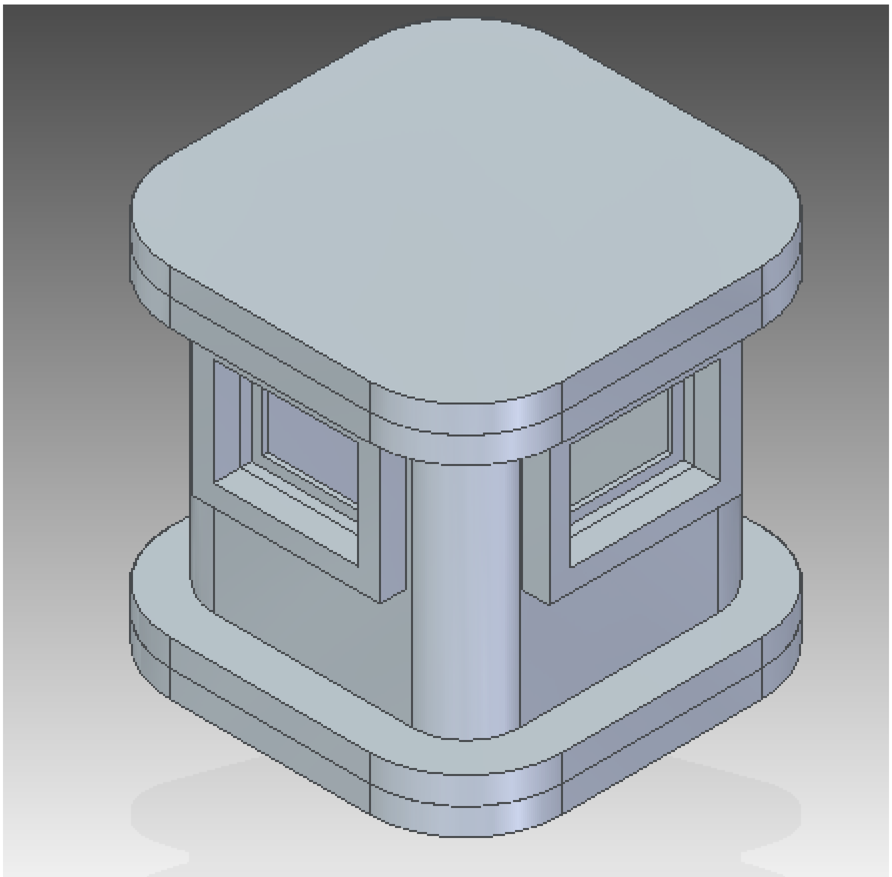

Figure 182: Box with window flange

Lids

The top lid will have to be modified to hold the injector in place. In the original setup, the injector is held 30.9mm below the top of the window. The injector will be fixed in the same relative position with the pressurized spray chamber.

The lid will have a hold drilled through the centre. A piece of round bar will be machined as seen in Figure 183 below to hold the injector. This round bar will then be welded to the inside of the lid.

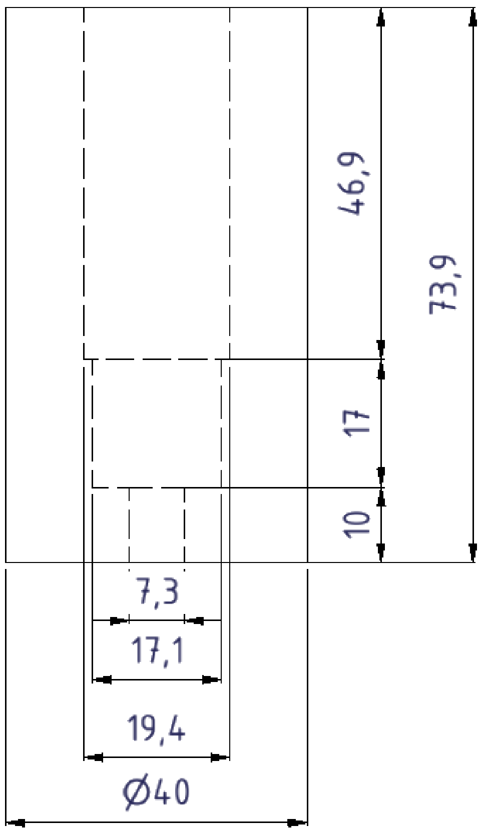

Figure 183: Injector holder

5.3.3. Welding analysis

The flanges for the lids on the top and bottom of the box will be welded to the main body of the box. Figure 184 below shows the welds that will be used. There will be a large butt weld (red) between the plates of the flange and box; and a fillet weld (blue) all around the outside corner.

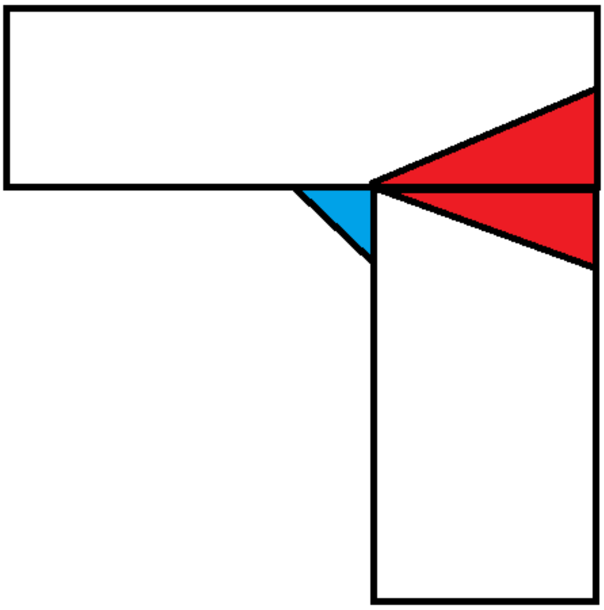

Figure 184: Lid flange welds

Butt weld

The butt weld will be in tension when the spray chamber is pressurized. The stress on the weld can be calculated using Equation 10 [8].

$$\sigma = \frac{F}{hl} \quad \text{Equation 10}$$

Where:

σ – Stress in the weld

F – Force the weld is subjected to

h – Weld throat

l – Length of the weld.

With a weld throat of 25mm and the weld going all the way around the spray chamber, the stress is fund to be 7.05 MPa. The reinforcements on the butt weld must be machined smooth to reduce stress concentrations [8].

Choosing an electrode with an AWS number of E60xx, the permissible stress in the weld is $0.60S_{y.}$ The chosen electrode has a yield strength of 345 MPa [8] and therefore the permissible stress in the weld is 207 MPa. The stress in the weld is 29 times less than the permissible stress and it will therefore be safe.

Fillet weld

With a plate thickness of 25mm, the minimum fillet weld size is 10mm [8]. The fillet weld is subjected to both tensile and shear forces. The maximum shear stress in the weld can be found using Equation 11 [8] and the maximum tensile stress can be found using Equation 12 below.

$$\tau = \frac{1.196F}{hl} \qquad \text{Equation 11}$$

$$\sigma = \frac{0.623F}{hl} \qquad \text{Equation 12}$$

With a weld throat of 10mm and the weld going all the way around the spray chamber; the maximum shear stress is found to be 21.08MPa, while the maximum tensile stress is 4.39 MPa. The maximum allowable stresses can be seen in Table 13 below.

Table 13: Maximum allowable stresses on fillet welds [8]

Strength Level of Weld Metal (EXX)	60*	70*	80	90*	100	110*	120
Allowable shear stress on throat, ksi (1000 psi) of fillet weld or partial penetration groove weld							
$\tau =$	18.0	21.0	24.0	27.0	30.0	33.0	36.0
Allowable Unit Force on Fillet Weld, kip/linear in							
†$f =$	12.73h	14.85h	16.97h	19.09h	21.21h	23.33h	25.45h
Leg Size h, in	Allowable Unit Force for Various Sizes of Fillet Welds kip/linear in						
1	12.73	14.85	16.97	19.09	21.21	23.33	25.45
7/8	11.14	12.99	14.85	16.70	18.57	20.41	22.27
3/4	9.55	11.14	12.73	14.32	15.92	17.50	19.09
5/8	7.96	9.28	10.61	11.93	13.27	14.58	15.91
1/2	6.37	7.42	8.48	9.54	10.61	11.67	12.73
7/16	5.57	6.50	7.42	8.35	9.28	10.21	11.14
3/8	4.77	5.57	6.36	7.16	7.95	8.75	9.54
5/16	3.98	4.64	5.30	5.97	6.63	7.29	7.95
1/4	3.18	3.71	4.24	4.77	5.30	5.83	6.36
3/16	2.39	2.78	3.18	3.58	3.98	4.38	4.77
1/8	1.59	1.86	2.12	2.39	2.65	2.92	3.18
1/16	0.795	0.930	1.06	1.19	1.33	1.46	1.59

*Fillet welds actually tested by the joint AISC-AWS Task Committee.

†$f = 0.707h\ \tau_{all}$.

From the table, it can be seen that with a E60xx electrode, the maximum shear stress is 124 MPa and the maximum tensile stress per unit length is 87,67h N/mm. The tensile stress per unit length the fillet weld is subjected to is found to be 109.8 N/mm. A stronger electrode will therefore have to be used; E80xx.

The box will be manufactured from sheet steel. The sheet will be bent to form the main body of the box. The exposed sides will have to be welded together to for a strong air tight bond. The edges of the plate will be back-gouged on both sides and welded using a butt weld in each side as seen in red in Figure 185 below.

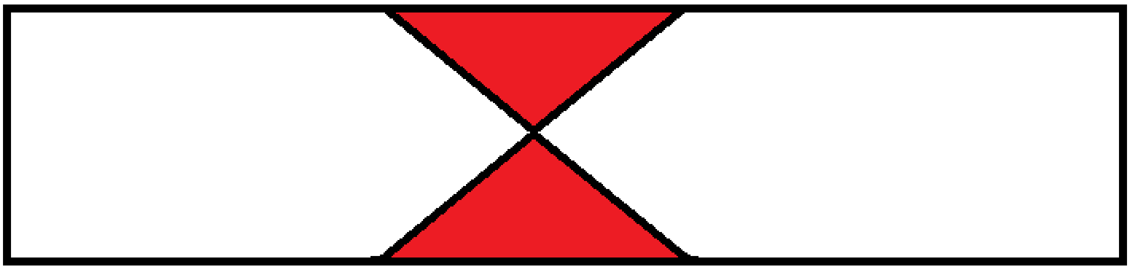

Figure 185: Butt weld on box

The stresses on the weld can be determined as before. The stress is found to be 28.2 MPa and the weld will therefore be safe.

The weld will be down the length of the main body of the box. To ensure maximum strength, the weld will be made down a portion of the box that is not on a bend or window. The weld must also not be located where the bolts for the window flange will be. The position of the butt weld can be seen in Figure 186 below.

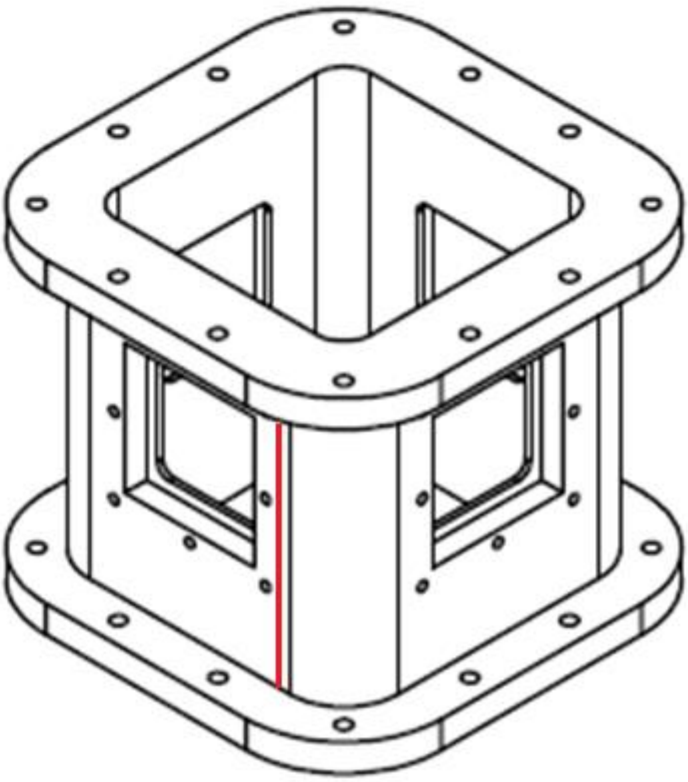

Figure 186: Position of butt weld on box

5.3.4. Bolt analysis

The top and bottom lids, as well as the window flanges will be fixed to the spray chamber with bolts.

Lid bolts

The top and bottom lids will be secured to the spray chamber with 12 bolts and nuts each. Grade 9.8, M12x75 bolts will be used. These bolts have the following properties:

Proof strength: 650 MPa

Tensile strength: 900 MPa

Yeild strength: 720 MPa

As seen in Table 14 below.

Table 14: Bolt grade properties [7]

Property Class	Size Range, Inclusive	Minimum Proof Strength,† MPa	Minimum Tensile Strength,† MPa	Minimum Yield Strength,† MPa	Material	Head Marking
4.6	M5–M36	225	400	240	Low or medium carbon	4.6
4.8	M1.6–M16	310	420	340	Low or medium carbon	4.8
5.8	M5–M24	380	520	420	Low or medium carbon	5.8
8.8	M16–M36	600	830	660	Medium carbon, Q&T	8.8
9.8	M1.6–M16	650	900	720	Medium carbon, Q&T	9.8
10.9	M5–M36	830	1040	940	Low-carbon martensite, Q&T	10.9
12.9	M1.6–M36	970	1220	1100	Alloy, Q&T	12.9

The bolt stiffness can be found using Equation 13[7].

$$k_b = \frac{A_d A_t E}{A_d l_t + A_t l_d}$$ Equation 13

Where:

A_t – The tensile stress area, 84.3 mm^2 for an M12 bolt as seen in [7]

Ad – The cross sectional area of the bolt at the shank

E – Young's modulus

l_t – length of the threaded section between the nut face and thread run out

l_d – length of the unthreaded section of the bolt

As seen in Figure 187 below.

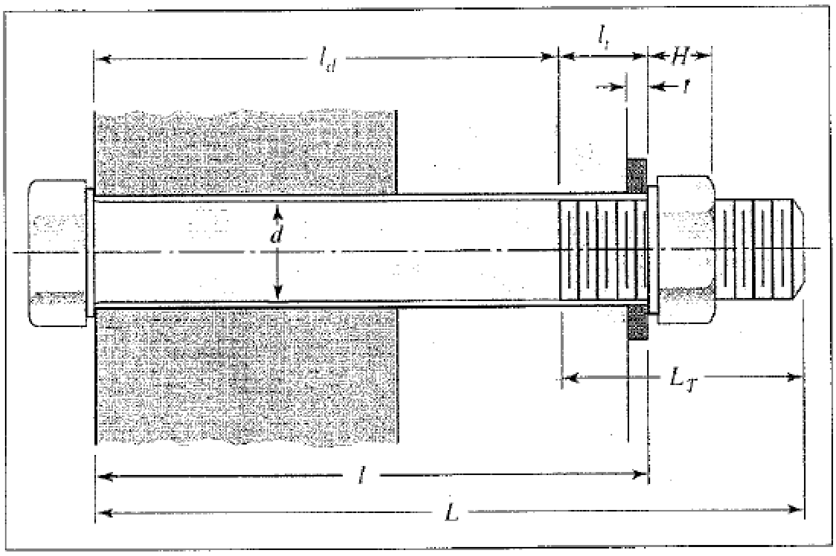

Figure 187: Geometry and notation of a bolted joint [7]

Table 15: Standard bolt dimensions [7]

Nominal Major Diameter d mm	Coarse-Pitch Series Pitch p mm	Tensile-Stress Area A_t mm²	Minor-Diameter Area A_r mm²	Fine-Pitch Series Pitch p mm	Tensile-Stress Area A_t mm²	Minor-Diameter Area A_r mm²
1.6	0.35	1.27	1.07			
2	0.40	2.07	1.79			
2.5	0.45	3.39	2.98			
3	0.5	5.03	4.47			
3.5	0.6	6.78	6.00			
4	0.7	8.78	7.75			
5	0.8	14.2	12.7			
6	1	20.1	17.9			
8	1.25	36.6	32.8	1	39.2	36.0
10	1.5	58.0	52.3	1.25	61.2	56.3
12	1.75	84.3	76.3	1.25	92.1	86.0
14	2	115	104	1.5	125	116
16	2	157	144	1.5	167	157
20	2.5	245	225	1.5	272	259
24	3	353	324	2	384	365
30	3.5	561	519	2	621	596
36	4	817	759	2	915	884
42	4.5	1120	1050	2	1260	1230
48	5	1470	1380	2	1670	1630
56	5.5	2030	1910	2	2300	2250
64	6	2680	2520	2	3030	2980
72	6	3460	3280	2	3860	3800
80	6	4340	4140	1.5	4850	4800
90	6	5590	5360	2	6100	6020
100	6	6990	6740	2	7560	7470

k_b is found to be 370.21 x 10^6 N/m.

The stiffness of the member can be found using Equation 14 [7].

$$k_m = \frac{0.5774\pi E d}{2\ln\left(5 \times \frac{0.5774l+0.5d}{0.5774l+2.5d}\right)}$$ Equation 14

Where:

d – Diameter of the bolt

l – Grip length

The grip length included the thickness of the washers, which can be found in Table 16 below.

Table 16: Washer dimensions [7]

Washer Size*	Minimum ID	Maximum OD	Maximum Thickness	Washer Size*	Minimum ID	Maximum OD	Maximum Thickness
1.6 N	1.95	4.00	0.70	10 N	10.85	20.00	2.30
1.6 R	1.95	5.00	0.70	10 R	10.85	28.00	2.80
1.6 W	1.95	6.00	0.90	10 W	10.85	39.00	3.50
2 N	2.50	5.00	0.90	12 N	13.30	25.40	2.80
2 R	2.50	6.00	0.90	12 R	13.30	34.00	3.50
2 W	2.50	8.00	0.90	12 W	13.30	44.00	3.50
2.5 N	3.00	6.00	0.90	14 N	15.25	28.00	2.80
2.5 R	3.00	8.00	0.90	14 R	15.25	39.00	3.50
2.5 W	3.00	10.00	1.20	14 W	15.25	50.00	4.00
3 N	3.50	7.00	0.90	16 N	17.25	32.00	3.50
3 R	3.50	10.00	1.20	16 R	17.25	44.00	4.00
3 W	3.50	12.00	1.40	16 W	17.25	56.00	4.60
3.5 N	4.00	9.00	1.20	20 N	21.80	39.00	4.00
3.5 R	4.00	10.00	1.40	20 R	21.80	50.00	4.60
3.5 W	4.00	15.00	1.75	20 W	21.80	66.00	5.10
4 N	4.70	10.00	1.20	24 N	25.60	44.00	4.60
4 R	4.70	12.00	1.40	24 R	25.60	56.00	5.10
4 W	4.70	16.00	2.30	24 W	25.60	72.00	5.60
5 N	5.50	11.00	1.40	30 N	32.40	56.00	5.10
5 R	5.50	15.00	1.75	30 R	32.40	72.00	5.60
5 W	5.50	20.00	2.30	30 W	32.40	90.00	6.40
6 N	6.65	13.00	1.75	36 N	38.30	66.00	5.60
6 R	6.65	18.80	1.75	36 R	38.30	90.00	6.40
6 W	6.65	25.40	2.30	36 W	38.30	110.00	8.50
8 N	8.90	18.80	2.30				
8 R	8.90	25.40	2.30				
8 W	8.90	32.00	2.80				

k_m is found to be1.93 x 10^9 N/m.

The endurance limit of the bolt is found using Equation 15 [7].

$$S_e = \frac{1}{k_f}(0.566 - 9.68 \times 10^{-5} S_{uc})S_{uc} \quad \text{Equation 15}$$

Where:

S_e – Endurance limit

k_f – Bolt stress concentration factor (found in Table 17 below)

S_{uc} – Ultimate compressive strength (equal to the Ultimate tensile strength)

Table 17: Bolt stress concentration factor [7]

Metric Grade	K_f		
	Rolled Threads	Cut Threads	Fillet
3.6 – 5.8	2.2	2.8	2.1
6.6 – 10.9	3.0	3.8	2.3

The endurance limit of the bolt is found to be 143.66 MPa.

The bolt preload is found using Equation 16 [7] below.

$$F_i = 0.75\, F_p \qquad \text{Equation 16}$$

F_p can be found using Equation 17 [7] below.

$$F_p = A_t S_p \qquad \text{Equation 17}$$

Where S_p is the proof strength of the bolt.

F_i is found to be 41.09 x 10^3 N.

The factor of safety for the bolted joint can be found using Equation 18 [7] below.

$$n_f = \frac{2NS_e(S_{ut}A_t - F_i)}{CP_{total}(S_{ut} + S_e)} \qquad \text{Equation 18}$$

Where:

N – Number of bolts

P_{total} – Total force acting on the joint.

$$C = \frac{k_b}{k_b + k_m}$$

C = 0.16

P_{total} = 165.675 x 10^3 N

The factor of safety on the bolted joint is therefore 4.33.

The factor of safety with respect to the separation of the plates, which would lead to a leak can be found using Equation 19 [7] below.

$$n_o = \frac{NF_i}{P_{total}(1-C)}$$ Equation 19

This safety factor is found to be 3.54.

The torque required to tighten the bolt is found using Equation 20 [7].

$$T = kF_i d$$ Equation 20

Where:

K – a constant found in Table 18 below.

Table 18: Bolt condition [7]

Bolt Condition	K
Non-plated, black finish	0.3
Zinc-plated	0.2
Lubricated	0.18
Cadmium-plated	0.16

The required torque will be 98.62 N.m.

Window flange bolts

The window flange bolts were analysed using the same methodology used for the analysis of the lid bolts.

The window flanges will be secured using 8 M8x45, grade 9.8 bolts.

The flange bolts will not be fastened with nuts, instead, the body of the spray chamber will be drilled and tapped. The bolted section will therefore have to be analysed as a cap screw.

The grip length is found using Equation 21 [6] below.

$$l_{grip} = t_{washer} + t_1 + h \qquad \text{Equation 21}$$

Where:

t_1 – Thickness of the flange

$$h = \begin{cases} \frac{t_2}{2} & t_2 < d \\ \frac{d}{s} & t_2 \geq d \end{cases}$$

The grip length would then be 31.3 mm.

The stiffness of the bolt can be found with Equation 22 [6] below.

$$k_{cap\ screw} = \frac{A_t E}{L_T} \qquad \text{Equation 22}$$

Where L_T is equal to the grip length.

The bolt stiffness was calculated to be 233.87 x 10^6 N/m

The member stiffness is 1.36 x 10^9 N/m

This would make the parameter C = 0.147.

With a stress concentration factor of 3 from Table 17, the endurance limit is 143.66 MPa and the bolt preload is 17842.5 N.

With 8 bolts per flange, the factor of safety is 5.39 and the factor of safety against separation is 3.98.

The torque required is 28.55 Nm.

5.3.5. Windows

The following was used by the supplier of the windows in order to calculate the thickness of the windows for the desired application. Refer to **APPENDIX – A** for an email from the supplier.

DESIGN OF PRESSURE WINDOWS

Calculation of thickness of optical windows used in vacuum or pressure applications

The maximum stress S_{max} on a uniformly loaded window is given by:

$S_{max} = (K . D^2 . P) / (4 . T^2)$ *and also* $S_{max} = F_a / SF$ *(See Safety Factor Box)*

and then solving for thickness T

$T = D.\sqrt{(SF . K / 4)} . \sqrt{(P / F_a)}$ *(CIRCULAR WINDOWS)*

$T = L .\sqrt{(SF . K / 2)} . \sqrt{(P / (F_a . (1 + R^2)))}$ *(RECTANGULAR WINDOWS)*

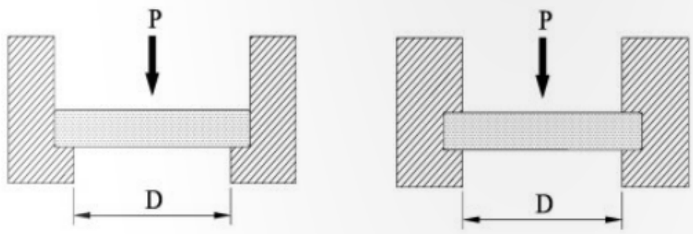

Unclamped, S_{max} at centre — Clamped, S_{max} at edge

DEFINITIONS

S_{max}	=	Maximum stress
SF	=	Safety Factor
F_a	=	Apparent Elastic Limit
K	=	Empirical Constant
D	=	Unsupported Ø for circular window
L,W	=	Length & Width for rectangular window
R	=	L / W
T	=	Thickness of window
P	=	Load per unit area

CLAMPED

Circular Window (Safety Factor of 4 & K_c = 0.75)

$T = 0.866 D \sqrt{(P / F_a)}$

Rectangular Window (Safety Factor of 4 & K_c = 0.75)

$T = 1.23 L \sqrt{(P / (F_a . (1 + R^2)))}$

UNCLAMPED

Circular Window (Safety Factor of 4 & K_u = 1.125)

$T = 1.06 D \sqrt{(P / F_a)}$

Rectangular Window (Safety Factor of 4 & K_u = 1.125)

$T = 1.50 L \sqrt{(P / (F_a . (1 + R^2)))}$

CONSTANT K

The value of **K** depends on the method of support, upon the force introduced in clamping and upon the brittle / ductile character of the window material involved.

Empirically, a **K** value of 0.75 is found suitable for most optical crystals when the perimeter is clamped, and a value 50% greater when unclamped.

K_c = 0.75
K_u = 1.125

6. DESIGN SPECIFICATIONS

6.1. Manufacture

6.1.1. Box

The box will be made from a 25mm sheet of the specified steel. The sheet will be cut to the required dimensions (975.6x250mm). The sheet will then be bent to obtain the required radii for the four corners. The two edges of the plate will then be chamfered and butt welded together. The four windows (100x100mm) will be cut with 10mm fillets. The windows will then be machined 10mm all around, 20mm deep to create a recess for the window to fit into. The 8mm bolt holes will then be drilled at tapped for the M8 bolts that will hold the window flanges in place.

The flanges for the lid will then be cut out of a sheet of the same material and the holes (12mm) will be drilled as per the drawing. The inner edge of the flange and the body of the box will be chamfered at 30º and butt welded. The flanges will be welded to the body of the box using a 10mm fillet weld around the outside corner. Both the butt weld and fillet weld can be seen in Figure 184.

6.1.2. Injector holder

The injector holder will be turned on a lathe to the dimensions indicated in the drawing.

6.1.3. Top and bottom lids

The lids will be cut out of the same 25mm thick steel. The 12mm bolt holes will then be drilled as indicated in the corresponding drawing. The top lid will have a 19.4mm hole drilled in the centre to accommodate the injector.

6.1.4. Window flanges

The window flanges will be cut out of 25mm thick sheet steel. The 8mm holes will then be drilled as per the drawing.

6.2. Engineering Drawings

The following are the engineering drawings for the spray chamber and all components to be manufactured.

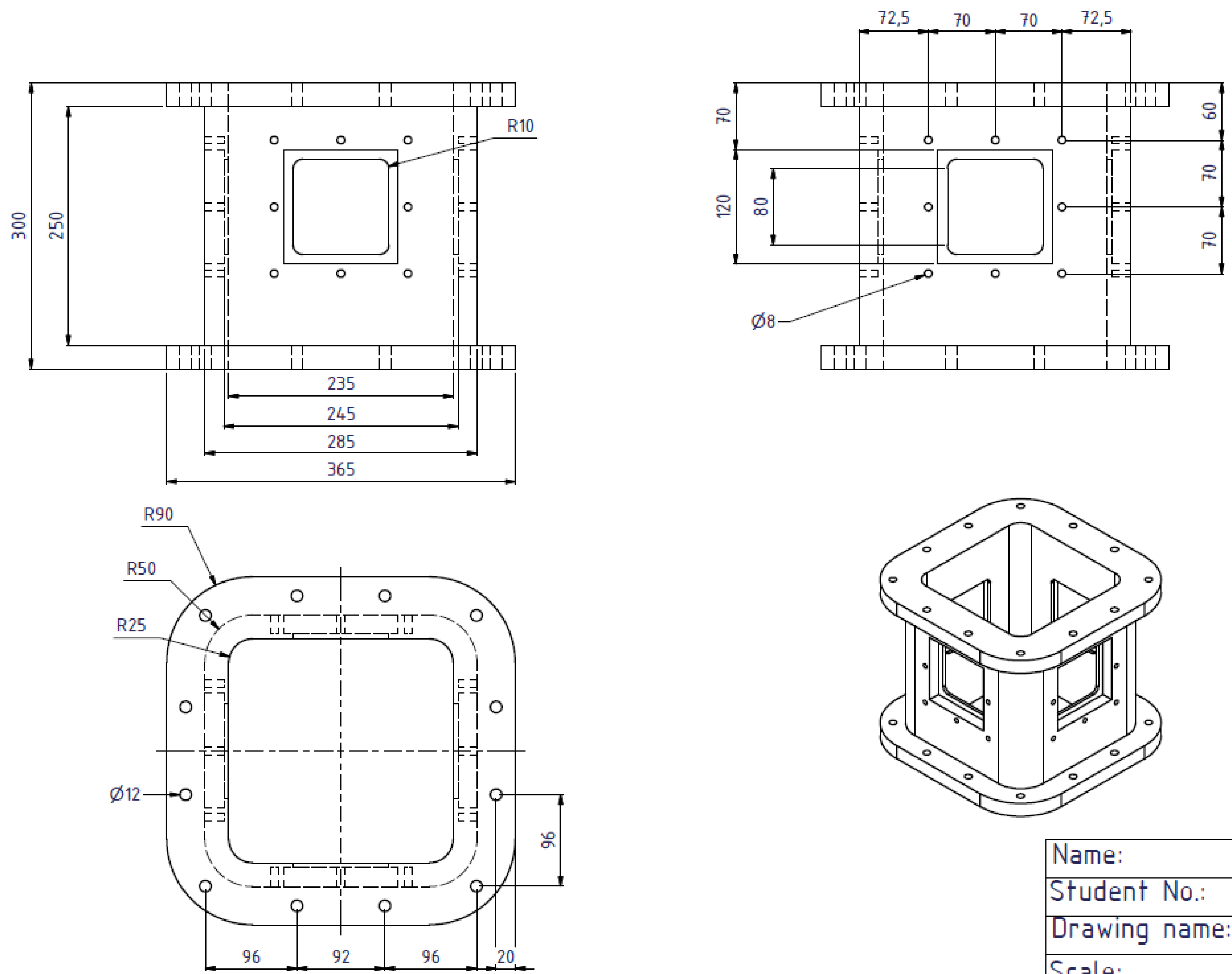

Name:	Andran Naicker	
Student No.:	317465	
Drawing name:	Box	
Scale:	1 : 4	
Date:	12/02/2014	

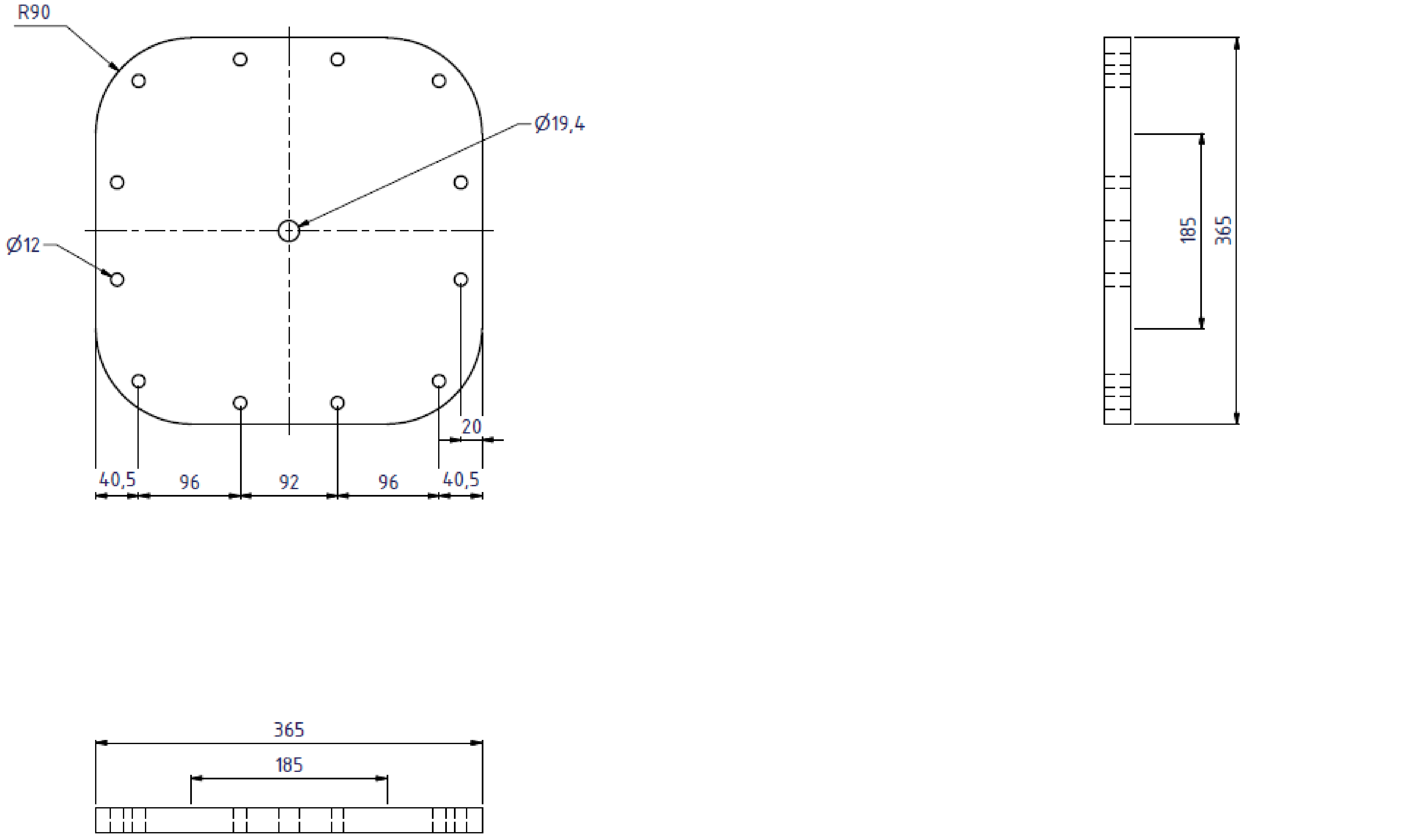

Name:	Andran Naicker	
Student No.:	317465	
Drawing name:	Top Lid	
Scale:	1 : 4	
Date:	12/02/2014	

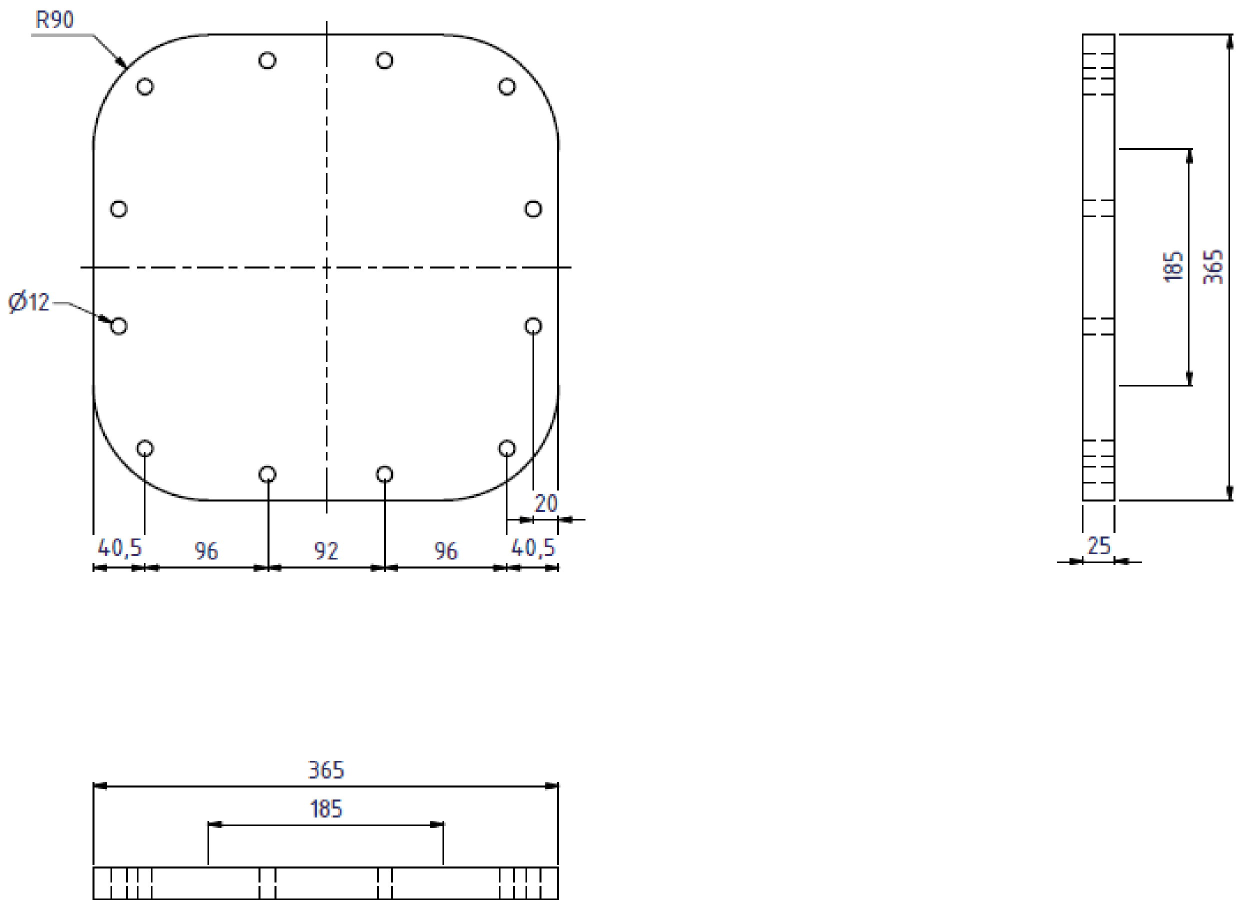

Name:	Andran Naicker	
Student No.:	317465	
Drawing name:	Bottom Lid	
Scale:	1 : 4	
Date:	12/02/2014	

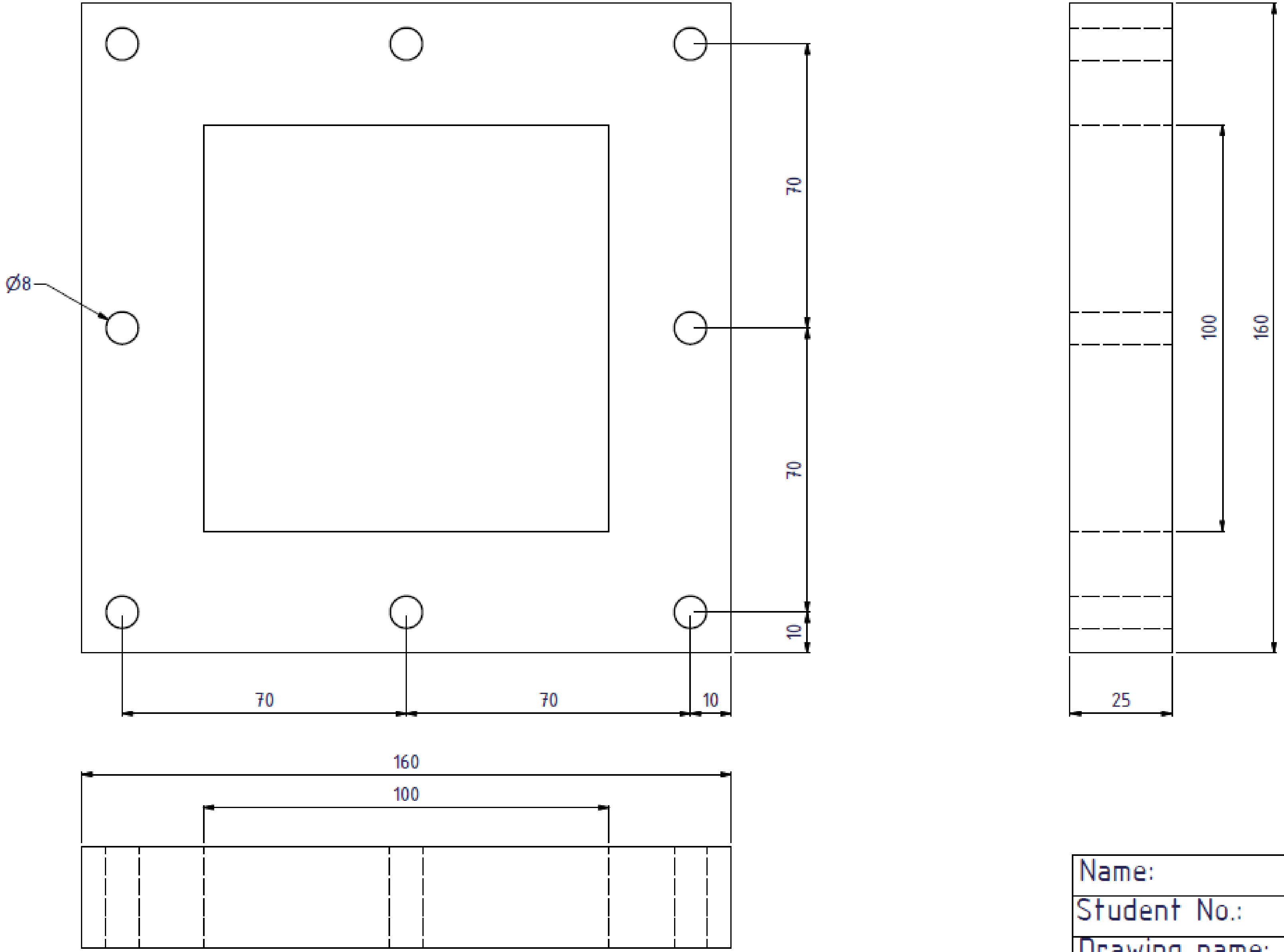

Name:	Andran Naicker
Student No.:	317465
Drawing name:	Window Flange
Scale:	1 : 1
Date:	12/02/2014

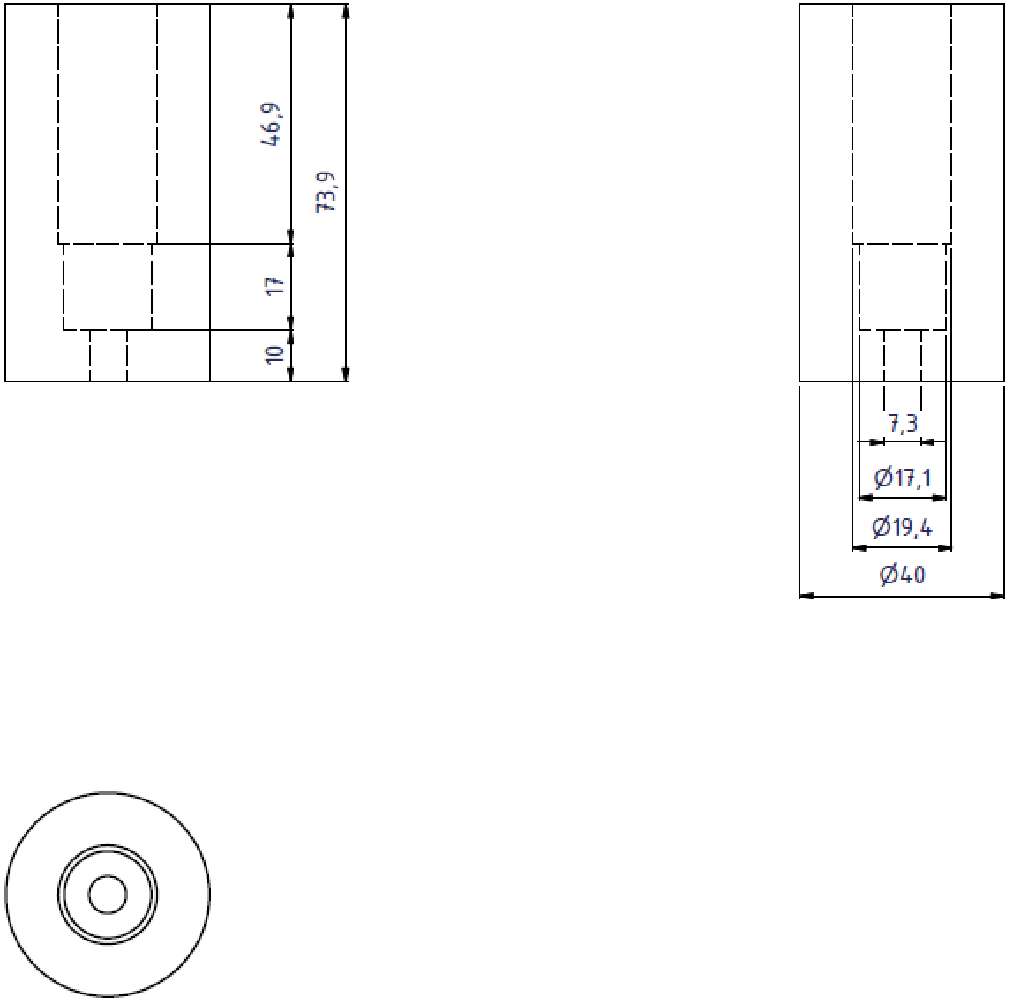

Name:	Andran Naicker
Student No.:	317465
Drawing name:	Injector Holder
Scale:	1 : 1
Date:	12/02/2014

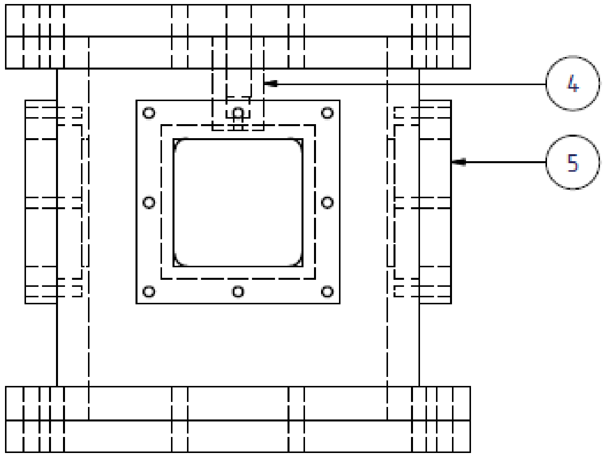

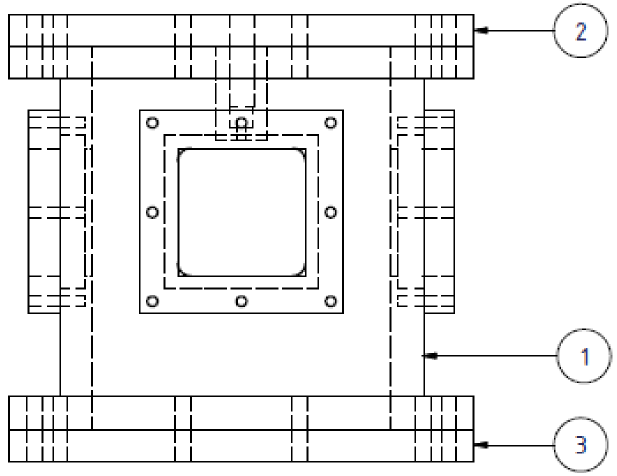

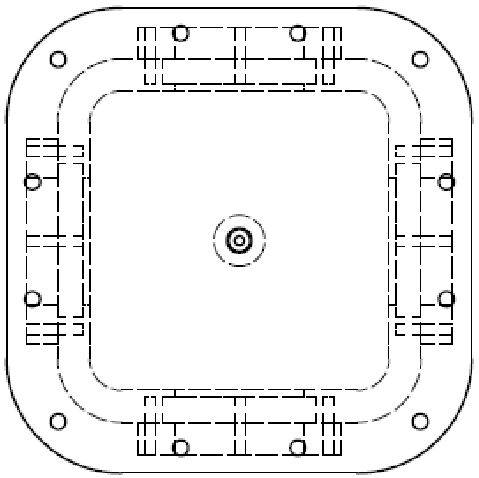

5	Window flange	Default	4 off
4	Injector holder	Default	1 off
2	Bottom lid	Default	1 off
2	Top lid	Default	1 off
1	Box	Default	1 off
Item	Description	Material	Remarks

Top and bottom lid secured to box using M12x75 grade 9.8 bolts, M12 nuts and M12 washers

Window flanges secured to box using M8x45 grade 9.8 bolts and washers.

Name:	Andran Naicker
Drawing name:	Assembly
Scale:	1 : 4
Date:	12/02/2014

6.3. Assembly

The injector holder will be lined up with the hole on the top lid and welded in place with a 10mm fillet weld.

A gasket will then be placed on the top flange on the box, the holes on the top lid will be lined up with the holes of the flange (with the injector holder inside the spray chamber). They will then be fastened together with 12 M12 bolts using washers and the corresponding nuts. The nuts must be torque to 98.62 N.m. The same process must be repeated for the bottom lid.

The gaskets must then be placed in the recess for the windows (on the box). The glass window will then be placed gently in the recess ensuring that it sits flush. The window flange must then be placed on the window and the bolt holes lined up with those on the box. The window flange will then be fastened to the box with 8 M8 bolts and washers. The bolts must be torque to 28.55 N.m. The same process must be repeated for all the windows.

The spray chamber must then be pressure tested. The test certificates can be found in APPENDIX B – SPRAY CHAMBER CERTIFICATES.

6.4. Cost Analysis

The following quotations were received for the manufacturing of the spray chamber and supply of all the needed components.

The spray chamber will cost R 37 653.00 to manufacture.

The quartz glass windows will cost R29 457.60 with shipping.

The valves and pressure gauge will cost R12 217.32

This brings the total cost of the spray chamber R79 327.92.

P O Box 75282
Lynnwood Ridge
0040
South Africa
Tel.: +27 (12) 349 5191
+27 (12) 349 5190

E-mail: info@marmit.co.za

MEASURING INSTRUMENTS TECHNOLOGY (MIT) (Pty) Ltd

Manufacturers, exporters and importers of photonic components, instruments and systems

To	:	Metso	Date	:	12 February 2014
Attn.	:	Andan Naicker	Pages	:	Cover +

QUOTATION

Dear Andan

Thank you for your valued enquiry.

1. I can get you BK 7 windows as follows:

BK7 glass flat window, size 120.0x120.0+0.0/-0.25mm, thickness 27.0+/-0.5mm (thick to keep 20 bar pressure difference), both sides SQ 40-20s/d, SF lambda/10 per inch @633nm, parallelism <3arcmin, bevels ~0.5mm x45deg.

Q'ty	Description		Unit ZAR	Price	VAT	Total
4	27 mm	Uncoated	R 6,460.00	R 25,840.00	R 3,617.60	R 29,457.60

The expected delivery/lead time is 8 – 10 weeks A.R.O.

UV Fused silica material is also available – the required thickness is 29 mm. Pricing on request.

PLEASE NOTE:

1. All quoted prices exclude VAT, or as explicitly indicated.
2. Prices may change, errors and omissions excepted.
3. Freight and clearance costs are estimated at an additional R2950.00 (excl. VAT) for the batch.
4. Prices were calculated at the current exchange rate of R15.20 for 1 Euro and are subject to exchange rate fluctuations.
5. This quote is valid for 30 days.
6. Payment terms: Pre-payment with order.

I trust that you will find this quote acceptable and look forward to your response accordingly.
Please do not hesitate to contact me any time for further assistance or information.

Best Regards

M. Hengstberger

Margie Hengstberger

HYDRO OIL COOLING AND ENG (PTY) LTD

P.O. BOX 3251
VANDERBIJLPARK
1900
(REG. No. 1984/002191/07)

GENERAL ENGINEERING AND HEAT EXCHANGER SPECIALISTS
TEL: (016) 986 1172/3/4 FAX : (016) 986 1175
E mail : info@hydroc.co.za
Website www.hydroc.co.za

Our Ref.: HJK/lvm/20599/2014C 18 February 2015

METSO

ATTENTION: MR. ANDRAN NAICKER

Dear Sir,

OUR QUOTATION NO. : Q20599/2014C

RE: PRESSURE VESSEL

We thank you for your valued enquiry and are pleased to submit our quotation as follows:

MANUFACTURE AND SUPPLY

One only pressure vessel in accordance with your sketches

NOTE: Metso to supply the following free of charge to HOC:

1. Windows
2. Pressure gauge
3. Pressure relief valve
4. Air relief valve
5. Inlet valve
6. Gaskets

PRICE: **R37 653.00 each**

PRICE BASIS

1. The price excludes VAT
2. The price excludes Government approved inspection
3. The price excludes design, design approval and drawing work
4. The price excludes transport
5. The price includes pressure test certificate (HOC witness)
6. **The price is valid for 30 days from date of quote only**

<u>TERMS OF PAYMENT</u>: To be discussed

<u>DELIVERY</u>: 3 – 4 weeks from receipt of your official order

We trust that the above quotation meets with your approval and remain at your service for any further information you may require.

Yours faithfully,
HYDRO OIL COOLING & ENG.,

<u>MR. HJ KARSTEN</u>

ESTIMATOR

VESSCON
SEPRITE
THE SEPARATOR THAT SEPARATES THE MEN FROM THE BOYS

P.O. BOX 13355, NORKEM PARK, 1631.
KEMPTON PARK, GAUTENG, SOUTH AFRICA
Land line Phone +27 (11) 972-6788 ~ & ~ Wireless +27 (11) 972-0989
E-MAIL ADDRESS **john@vesscon.co.za**

ESTIMATE

DATE: **February 25, 2014**
ESTIMATE # **6328-A-2**
OTHER REF #

MASTER FABRICATORS OF ALL MANNER OF AIR, GAS AND STEAM PERIPHERALS.

PIPE INSTALLATIONS FOR ALL MEDIUMS.

CARBON STEELS.

STAINLESS STEELS.

ALUMINIUM.

SUPPLYING INDUSTRY WITH LOCALLY MANUFACTURED PRODUCTS OF DISTINCTION.
OPENING NEW AVENUES OF TRADE PREVIOUSLY NOT POSSIBLE THROUGH INNOVATIVE DESIGN AND MANUFACTURING TECHNIQUES.

PUTTING SOUTH AFRICA ON THE MAP AS A GOOD RELIABLE SOURCE OF SECONDARY PRODUCTS.

"ONCE A CUSTOMER, ALWAYS A CUSTOMER"

BILL TO:
Name: **ANDRAN NAICKER**
Company Name: **METSO MINERALS**
Street Address
City, ST ZIP Code
Phone

YOUR ORDER # TBA
ENQUIRED BY ANDRAN NAICKER

SEND TO:
Name: **ANDRAN NAICKER**
Company Name: **METSO MINERALS**
Street Address
City, ST ZIP Code
Phone

UNIT	UNIT TYPE	DESCRIPTION	RATE	AMOUNT
		VESSEL		
1	EACH	UNIT PER YOUR SKETCHES	R 66,385.00	R 66,385.00
1	LOT	GLASS SUPPLIED	R 0.00	R 0.00
1	LOT	FINAL MACHINING	R 6,500.00	R 6,500.00
		THIS IS ESTIMATE # 6328-A-2 (THIS IS FULL PENETRATION WELDS OFFER).		R 0.00
				R 0.00
				R 0.00
		MANUFACTURED TO ONE OR ALL OF THE FOLLOWING;		R 0.00
		ASME VIII (LATEST EDITION)		R 0.00
		PD 5500 (LATEST EDITION)		R 0.00
		SANS 347 (LATEST EDITION)		R 0.00
				R 0.00
				R 0.00
				R 0.00
				R 0.00
				R 0.00
		DELIVERY TWO TO THREE WORKING DAYS (EX WORKS)		R 0.00
		30% DEPOSIT REQUIRED WITH THIS ORDER.		R 0.00
		100% PAYMENT WILL BE REQUIRED UPON DELIVERY.		R 0.00
				R 0.00
		PER YOUR REQUEST OF 24/02/2014		R 0.00
				R 0.00
				R 0.00
				R 0.00

SUBTOTAL	R 72,885.00
VAT RATE	14.00%
TOTAL VAT	R 10,203.90
DISCOUNT OFFERED	5%
TOTAL DUE	**R 83,088.90**
DISCOUNT AMOUNT OFFERED	**R 4,154.45**
AMOUNT LESS DISCOUNT AMOUNT OFFERED. CONDITIONS FOR DISCOUNT MUST BE	**R 78,934.46**

Should you need clarification on any item. Please do not hesitate to contact the compiler.

YOUR TERMS ARE (PRICE SHOWN IN **"TOTAL DUE"** LESS ANY **"DISCOUNT OFFERED"**) SUBJECT TO ANY NOTES BELOW.
NOTES; **DISCOUNT MAY ONLY BE TAKEN IF PAYMENT IS MADE WITHIN 4 (FOUR) WORKING DAYS.**
DELIVERY PERIOD SUBJECT TO ANY NOTES BELOW.
NOTES; **DELIVERY IS SUBJECT TO PRIOR ORDER, WORKLOADING, OR ANY DELAYS IMPOSED BY ANY OTHERS.**
VALIDITY PERIOD SUBJECT TO ANY NOTES BELOW IS (30 DAYS).
NOTES; **VALIDITY SHOWN WILL STRICTLY BE ADHERED TO.**
Should you wish to order please will you fax an order to e- mail to john@vesscon.co.za

Please note that the above Estimate is given in good faith using the information at hand at the time of estimation. It is important to note that we can not be asked to carry the cost of omissions or errors on your behalf or our *behalf*. Please check that we have covered all bases as you require.

THANK YOU FOR YOUR ENQUIRY!

Compiled by:- John Cheetham

ESTIMATE

P.O. BOX 13355, NORKEM PARK, 1631.
KEMPTON PARK, GAUTENG, SOUTH AFRICA
Land line Phone +27 (11) 972-6788 ~ & ~ Wireless +27 (11) 972-0989
E-MAIL ADDRESS john@vesscon.co.za

SEPRITE
THE SEPARATOR THAT SEPARATES THE MEN FROM THE BOYS

DATE: February 26, 2014
ESTIMATE # 6328-A-3
OTHER REF #

MASTER FABRICATORS OF ALL MANNER OF AIR, GAS AND STEAM PERIPHERALS.

PIPE INSTALLATIONS FOR ALL MEDIUMS.

CARBON STEELS.

STAINLESS STEELS.

ALUMINIUM.

SUPPLYING INDUSTRY WITH LOCALLY MANUFACTURED PRODUCTS OF DISTINCTION.
OPENING NEW AVENUES OF TRADE PREVIOUSLY NOT POSSIBLE THROUGH INNOVATIVE DESIGN AND MANUFACTURING TECHNIQUES.

PUTTING SOUTH AFRICA ON THE MAP AS A GOOD RELIABLE SOURCE OF SECONDARY PRODUCTS.

"ONCE A CUSTOMER, ALWAYS A CUSTOMER"

BILL TO:
Name: ANDRAN NAICKER
Company Name: METSO MINERALS
Street Address
City, ST ZIP Code
Phone

YOUR ORDER # TBA
ENQUIRED BY ANDRAN NAICKER

SEND TO:
Name: ANDRAN NAICKER
Company Name: METSO MINERALS
Street Address
City, ST ZIP Code
Phone

UNIT	UNIT TYPE	DESCRIPTION	RATE	AMOUNT
		VESSEL		
1	EACH	3/4" 800# FCS GLOBE VALVE SCREWED OR SOCKET WELD	R 833.00	R 833.00
1	EACH	3/4" BSP CARBON STEEL PRESSURE RELIEF VALVE SET AT 35 BAR	R 9,993.00	R 9,993.00
1	EACH	63mm GLYCERINE FILLED PRESSURE GAUGE. 0 - 4 mPa WITH CALIBRATION CERTIFICATE.	R 455.00	R 455.00
				R 0.00
				R 0.00
				R 0.00
		MANUFACTURED TO ONE OR ALL OF THE FOLLOWING;		R 0.00
		ASME VIII (LATEST EDITION)		R 0.00
		PD 5500 (LATEST EDITION)		R 0.00
		SANS 347 (LATEST EDITION)		R 0.00
				R 0.00
				R 0.00
				R 0.00
				R 0.00
				R 0.00
				R 0.00
		DELIVERY TWO TO THREE WORKING DAYS (EX WORKS)		R 0.00
		30% DEPOSIT REQUIRED WITH THIS ORDER.		R 0.00
		100% PAYMENT WILL BE REQUIRED UPON DELIVERY.		R 0.00
				R 0.00
		PER YOUR REQUEST OF 24/02/2014		R 0.00
				R 0.00
				R 0.00
				R 0.00

SUBTOTAL	R 11,281.00
VAT RATE	14.00%
TOTAL VAT	R 1,579.34
DISCOUNT OFFERED	5%
TOTAL DUE	R 12,860.34
DISCOUNT AMOUNT OFFERED	R 643.02
AMOUNT LESS DISCOUNT AMOUNT OFFERED. CONDITIONS FOR DISCOUNT MUST BE	R 12,217.32

Should you need clarification on any item. Please do not hesitate to contact the compiler.

YOUR TERMS ARE (PRICE SHOWN IN **"TOTAL DUE"** LESS ANY **"DISCOUNT OFFERED"**) SUBJECT TO ANY NOTES BELOW.
NOTES; **DISCOUNT MAY ONLY BE TAKEN IF PAYMENT IS MADE WITHIN 4 (FOUR) WORKING DAYS.**
DELIVERY PERIOD SUBJECT TO ANY NOTES BELOW.
NOTES; **DELIVERY IS SUBJECT TO PRIOR ORDER, WORKLOADING, OR ANY DELAYS IMPOSED BY ANY OTHERS.**
VALIDITY PERIOD SUBJECT TO ANY NOTES BELOW IS (30 DAYS).
NOTES; **VALIDITY SHOWN WILL STRICTLY BE ADHERED TO.**
Should you wish to order please will you fax an order to e- mail to john@vesscon.co.za

Please note that the above Estimate is given in good faith using the information at hand at the time of estimation. It is important to note that we can not be asked to carry the cost of omissions or errors on your behalf or our *behalf*. Please check that we have covered all bases as you require.

THANK YOU FOR YOUR ENQUIRY!

Compiled by:- John Cheetham

7. CONCLUSIONS

A spray chamber was required to conduct experiments with the Inov8 Test Stand to simulate engine back pressures. The pressure chamber was required to simulate pressures of up to 20 bar without affecting the normal operation of the test stand.

- A square pressure chamber was designed with the same internal dimensions as the existing spray box. The spray chamber was built out of 25mm thick steel plate with top and bottom lids that were bolted to the spray chamber. There were four 27mm thick quartz glass windows on the four sides of the chamber. The windows were held in place with bolted flanges and would not have any effect on the camera used for the experiments. An injector holder was attached to the top lid to hold the tip of the injector in line with the windows.
- FEA analysis showed that the spray chamber was strong enough to hold 20 bar of pressure. After construction, the pressure chamber was tested and certified for 20 bar of pressure. The test certificates can be found in APPENDIX B – SPRAY CHAMBER CERTIFICATES.

8. REFERENCES

1. A.Th. Diamantoudis, Th. Kermanidis. *Design by Analysis Versus Design By Formula of High Strength Steel Pressure Vessels: A Comparative Study*. Laboratory of Technology and Strength of Materials, Department of Mechanical Engineering and Aeronautics, University of Patras, Patras 26500, Greece. 1 June 2004.
2. Ying-Zheng Guo & Zhao-Jing Zeng. *The Six-Plate Analytical Method for Rectangular Pressure Vessels of Finite Length.* Department of Mathematics and Mechanics, Southeast University, Nanjing 210096, People's Republic of China. Department of Mechanical Engineering, Nanjing University of Chemical Technology, Nanjing 210009, People's Republic of China. 20 June 1997.
3. Ying-Zheng Guo & Zhao-Jing Zeng. *A New Mechanical Model for Rectangular Structures Subjected to Internal Pressure.* Department of Mathematics and Mechanics, Southeast University, Nanjing 210096, People's Republic of China. Department of Mechanical Engineering, Nanjing University of Chemical Technology, Nanjing 210009, People's Republic of China. 24 Jan 1990.
4. Robert Chuse. *Pressure Vessels. The ASME Code Simplified.* Fifth edition. McGraw-Hill Book Company. 1954. ISBN 0-07-010872-2
5. Andran Naicker. *Injector Spray Analysis and Flow Measurement.* The University of the Witwatersrand, Johannesburg. 22/08/2012.
6. Thomas H. Brown, Jr. IMark's Calculations for Mechanical Design. The McGraw-Hill Companies. 2005. ISBN 0-07-143689-8
7. Mr. T. Frangakis. *Power Screws and Bolt Design.* MECN 2002. Mechanical Engineering Design class notes. 2009.
8. Richanrd G. Budynas, J. Keith Nisbett. *Shighley's Mechanical Engineering Design, Ninth Edition.* The McGraw-Hill Companies Inc. 2011. ISBN 978-0-07-352928-8
9. ASTM A16 Grade 60. Available at http://www.matweb.com/search/DataSheet.aspx?MatGUID=9e4158972bfb4b22b378690d12b9ee17 Last accessed 15/05/2013, 11:58.

APPENDIX – A

RE: Quatz glass

sales to: andran.naicker 13/02/14 11:02 AM

From: "sales" <sales@marmit.co.za> Show Details

History: This message has been replied to.

1 attachment

0212PressureWindows.png

Hi Andran
I have had the following feedback from me manufacturer:

The Apparent Elastic Limit (Fa) is 64500000 for BK7 glass and 55000000 for UVFS

The formulas to be used for the calculations are as per the attachment.
As you can see there is a safety factor of 4, and another factor derived from the clamping method and the shape of the window.

On re-calculation the minimum safety thickness for BK7 glass window should be 16.0+/-0.5mm and for UVFS window 17.0+/-0.2mm.

Are you in agreement with this ?

Let me know whether the windows will be suitable for your application.

Best Regards

Margie Hengstberger
Measuring Instruments Technology (MIT)
Pretoria South Africa
Tel: +27 12 349 5191
Fax: +27 12 349 5190
Cell: +27 82 784 2011
margie@marmit.co.za
"We are now on the CSIR Campus" Blg 33

APPENDIX B – SPRAY CHAMBER CERTIFICATES

H.O.C. & Engineering
HYDRO OIL COOLING & ENGINEERING (Pty) Ltd
(Reg. No: 1984/002191/07)

SAIW IIW ISO3834 Part 2

Heat Exchanger Specialists and General Engineering

4 Michelin Street NW7 PO Box 3251 Vanderbijlpark 1900 Tel: (016) 986-1172/3/4 Fax: (016) 986-1175
Web Site: www.hocengineering.co.za E-Mail: info@hydroc.co.za

Pressure Test Certificate

PRESSURE TEST CERTIFICATE NUMBER:	10364
HOC PROCESS NUMBER:	6227
HOC JOB NUMBER:	H11972
EQUIPMENT / JOB DESCRIPTION:	NEW EXPERIMENT CHAMBER
CUSTOMER:	UNIVERSITY OF THE WITSWATERSRAND
CUSTOMER ORDER NUMBER:	3456263 /3455523
DRG / SPECIFICATION NUMBER:	
CODE OF MANUFACTURE:	
ITEM TESTED:	WITS CHAMBER

DESCRIPTION	SHELL SIDE		TUBE SIDE	
POSITION TESTED	HORIZONTAL		HORIZONTAL	
TEST PRESSURE (KPA)	3000(NITROGEN)			
WATER TEMPERATURE (C)				
CHLORIDES				
DURATION OF TEST (MIN)	30			
PRESSURE GAUGE NUMBER		J71480-1		
CALIBRATION CERT NUMBER		P1003539		
CALIBRATION DATE		19/02/2016		
PRESSURE GAUGE RANGE		0-10MPA		

ACCEPTED BY:	RESPONSIBLE PERSON	SHELL SIDE	TUBE SIDE	DATE SIGNED
H.O.C:				2016-08-30
CUSTOMER:				2016-08-30
AUTHORISED INSPECTION AUTHORITY (THIRD PARTY):				2016-08-30

REMARKS:

PREPARED BY:	D. VERMEULEN, M. JOUBERT	FORM:	HOC-QAF.38 PRESSURE TEST CERTIFICATE
REVIEW DATE:	2016-08-03	REVISION NUMBER:	06
ISSUE DATE:	2016-08-03	NEXT REVIEW DATE:	2018-08-03

CERTIFICATE OF CALIBRATION

SA GAUGE

sanas
Calibration Laboratory
Lab No. 245

Certificate No P1003539

"The South African National Accreditation System (SANAS) is a member of the International Laboratory Accreditation Cooperation (ILAC) Mutual Recognition Arrangement (MRA). This arrangement allows for the mutual recognition of technical test and calibration data by member accreditation bodies worldwide. For more information on the arrangement please consult www.ilac.org"

Calibration of a	:	Pressure Gauge
Manufacturer	:	SA Gauge
Description	:	3 A 100 D 12B 0-10 MPa
Model No	:	N/A
Serial No	:	J71480-1
Calibrated for	:	Hydro Oil Cooling & Engineering (Pty) Ltd
Address	:	4 Michelin Street, NW7 Vanderbijlpark
Job Card No	:	J1211672
Temperature	:	22 ± 2 °C
Calibration Date	:	19-02-2016
Issue Date	:	19-02-2016
Re-calibration Date	:	19-02-2017
Calibrated by	:	**Dinesh Betchan** ....
Checked by	:	Riaan Reinach ....

This certificate is issued without alteration and in accordance with the conditions of accreditation granted by SANAS. The results reflected in the certificate is a correct record of the measurements made at the time of calibration. Subsequently the accuracy will depend on factors such as care exercised in handling the instrument and the frequency of use. Recalibration should be performed after a period so chosen to ensure that, under normal circumstances, the instrument accuracy remain within the desired limits. The accuracies of all measurements were traceable to the national measurement standards of South Africa , unless otherwise noted. Copyright of this certificate is owned jointly by SA Gauge and SANAS and may not be reproduced other than in full, except with prior written approval of SA Gauge and SANAS. The reported expanded uncertainty is based on a standard uncertainty multiplied by a coverage factor k = 2 providing a level of confidence of approximately 95%, the uncertainty of measurement has been estimated in accordance with the principles defined in the GUM, Guide to Uncertainty of Measurement, ISO, Geneva, 1993"

SANAS Authorized Technical Signatory
Dinesh Betchan

SA Gauge (Pty) Ltd
P. O. Box 22369
Glenashley
4022
RSA
Tel: +27 (031) 5792216-7-8
Fax: +27 (031) 5792301

8 Beechfield Crescent
Springfield Park
Durban
Email: sanas@sagauge.com
Website: www.sagauge.com
(Pty) Ltd 2003/017040/07

1. LABORATORY STANDARDS AND EQUIPMENT USED:

Asset No	Standards or Equipment	Serial Number	Certificate Number	Expiry Date
2-19	THA2 - SUPCO	405-096-0025	77735	31-07-2016
2-11	Beta 321	9043060	S20160112-2	12-01-2017

2. PROCEDURE

2.1 The UUT was calibrated in accordance with procedure 2-01 and the manufacturers recommendation if available.
2.2 The UUT was set to zero prior to calibration.
2.3 The results as reflected on this certificate were entered directly on PC during the execution of the calibration.
2.4 UUT resolution: 0.2 MPa

3. RESULTS

3.1 PRESSURE

UUT Display (MPa)	Applied Pressure (As Found) (MPa)		Applied Pressure (As Left) (MPa)	
	Upward	Downward	Upward	Downward
0	0	0	0	0
2	1.989	1.980	1.989	1.980
4	3.986	3.978	3.986	3.978
6	5.992	5.980	5.992	5.980
8	7.979	7.969	7.979	7.969
10	9.982	N/a	9.982	N/a

3.2 REPEATABILITY

UUT Display (MPa)	Applied Pressure (MPa)	
	Upward	Downward
6	5.992	5.980
6	5.986	5.979
6	6.002	5.994

Uncertainty of measurement: ± 0.07 MPa

4. NOTES

4.1 Results were entered directly onto the PC.

End of certificate

SANAS Authorized Technical Signatory

SA GAUGE

CERTIFICATE OF CALIBRATION

sanas Calibration Laboratory
Lab No. 245

Certificate No P1006072

"The South African National Accreditation System (SANAS) is a member of the International Laboratory Accreditation Cooperation (ILAC) Mutual Recognition Arrangement (MRA). This arrangement allows for the mutual recognition of technical test and calibration data by member accreditation bodies worldwide. For more information on the arrangement please consult www.ilac.org"

Calibration of a	:	Pressure Gauge
Manufacturer	:	SA Gauge
Description	:	3 A 100 G 12B 0-4 MPa
Model No	:	N/A
Serial No	:	J1214489-1
Calibrated for	:	Hydro Oil Cooling & Engineering (Pty) Ltd
Address	:	4 Michelin Street, NW7 Vanderbijl Park
Job Card No	:	J1214489
Temperature	:	22 ± 2 °C
Calibration Date	:	30-06-2016
Issue Date	:	30-06-2016
Re-calibration Date	:	30-06-2017
Calibrated by	:	**Dinesh Betchan** ....
Checked by	:	Riaan Reinach ....

This certificate is issued without alteration and in accordance with the conditions of accreditation granted by SANAS. The results reflected in the certificate is a correct record of the measurements made at the time of calibration. Subsequently the accuracy will depend on factors such as care exercised in handling the instrument and the frequency of use. Recalibration should be performed after a period so chosen to ensure that, under normal circumstances, the instrument accuracy remain within the desired limits. The accuracies of all measurements were traceable to the national measurement standards of South Africa , unless otherwise noted. Copyright of this certificate is owned jointly by SA Gauge and SANAS. The reported expanded uncertainty is based on a standard uncertainty multiplied by a coverage factor k = 2 providing a level of confidence of approximately 95%, the uncertainty of measurement has been estimated in accordance with the principles defined in the GUM, Guide to Uncertainty of Measurement, ISO, Geneva, 1993'

SANAS Authorized Technical Signatory
Dinesh Betchan

Intertek
Date: 26/8/2016
ZA - 0019

SA Gauge (Pty) Ltd
P. O. Box 22369
Glenashley
4022
RSA
Tel: +27 (031) 5792216/7/8
Fax: +27 (031) 5792301

8 Beechfield Crescent
Springfield Park
Durban
Email: sanas@sagauge.com
Website: www.sagauge.com
(Pty) Ltd 2003.017040/07

Certificate No P1006072

1. LABORATORY STANDARDS AND EQUIPMENT USED:

Asset No	Standards or Equipment	Serial Number	Certificate Number	Expiry Date
2-19	THA2 - SUPCO	405-096-0025	77735	31-07-2016
2-03	PRESSURE MODULE	P903670	73279	30-11-2017
2-08	M2001 READOUT	9043104	n/a	n/a

2. PROCEDURE

2.1 The UUT was calibrated in accordance with procedure 2-01 and the manufacturers recommendation if available.
2.2 The UUT was set to zero prior to calibration.
2.3 The results as reflected on this certificate were entered directly on PC during the execution of the calibration.
2.4 UUT resolution: 0.1 MPa

3. RESULTS

3.1 PRESSURE

UUT Display (MPa)	Applied Pressure (As Found) (MPa)		Applied Pressure (As Left) (MPa)	
	Upward	Downward	Upward	Downward
0	0	0	0	0
1	1.0027	0.9975	1.0027	0.9975
2	2.0043	2.0012	2.0043	2.0012
3	3.0076	3.0048	3.0076	3.0048
4	4.0059	N/a	4.0059	N/a

3.2 REPEATABILITY

UUT Display (MPa)	Applied Pressure (MPa)	
	Upward	Downward
2	2.0043	2.0012
2	2.0032	2.0005
2	2.0049	2.0020

Uncertainty of measurement: ± 0.04 MPa

4. NOTES

4.1 Results were entered directly onto the PC.

End of certificate

SANAS Authorized Technical Signatory

Intertek
Reviewed: L Wilkinson
Initials:
Date: 28/9/2016
ZA-1046

DLM

Over Pressure Protection; Flow, Level &
Density Measurement; Automation & Control
1 Angus Crescent , Longmeadow Business Estate East,
Modderfontein
PO Box 758, Isando 1600
Tel: +27 (0) 11-457 0500
Fax: +27 (0) 11-608 4999
www.dlm.co.za

IZANDRA TRADING (PTY) LTD

CERTIFICATE OF PRESSURE SETTING

This is to certify one valve supplied against

Customer Order No *IZ4791*

Invoice Number *11004576*

Invoice/Test Date *2016/11/10*

Valve Pneumatically Set To Relieve At

2400 kPa Gauge

Make Of Valve *BAILEY SAFETY RELIEF VALVE*

Figure Number *707VSL*

Inlet *20mm BSP SCREWED MALE*

Outlet *20mm BSP SCREWED FEMALE*

Record Number *44953*

Serial Number *5GB1-1610-058747*

Customer Tag No *N/A*

QA

STEPHEN DLAMINI
WORKSHOP MANAGER

MARTIN ELS
QUALITY ASSURANCE MANAGER

Set pressure verification testing performed in accordance with instructions in the applicable Operation and Maintenance Manual. This Safety Valve should only be used in accordance with the applicable operating instructions and within the application specifications of the purchase order.

NOTE: ALWAYS CHECK THE SET PRESSURE BEFORE INSTALLATION.

INTERNATIONAL
INSTITUTE OF WELDING

Having satisfied the requirements of the IIW Manufacturer Certification Scheme according to ISO 3834

Company: **Hydro Oil Cooling and Engineering (Pty) Ltd**

The Unit: Fabrication Workshop

Located in: 4 Michelin Street, Vanderbijlpark

is certified in accordance with

SANS ISO 3834 Part 2

For the product(s): Refurbishment and fabrication of pressure equipment, heat exchangers and oil coolers for the petrochemical and power generation industries

with the scope of work stated in the attached Schedule

Certificate number and revision status: ZA-088 – Rev. 0

First Issue date: 2015/07/22

Current issue date: 2015/07/22

Date of expiry: 2018/07/21

ANBCC Governing Board Representative

Sean Blake

SAIW Certification South Africa

Scheme Manager

Herman Potgieter

This Certificate is subject to the rules established by IIW for the certification of Companies

IIW Manufacturer Certification Scheme

SCHEDULE

Extent of validity of IIW Certificate N° ZA-088 Rev. 0

Product standard(s):

BS/PD 5500 EN/ISO 13445

Alternative Standard(s) (refer to ISO 3834 – 5)

ASME VIII

Welding process (ISO 4063)		**Parent material groups (ISO/tr 15608)**
(MMA)	111	1, 2, 8
(MIG/MAG)	135	
(GTAW)	141	
(SAW)	121	

Responsible Coordination Personnel:

Name	**Qualification**	**Job function and level*****
C. A. van der Merwe	Boiler Maker	RWC (Specific)
H. Vermeulen	ISO 9001	QC (Basic)

*** The level must be stated in order to comply with ISO 14731

ANBCC Governing Board Representative

Sean Blake

Scheme Manager

Herman Potgieter

The standards and documents referred in the certificate and schedule are those valid at the time of certification

INTERNATIONAL INSTITUTE OF WELDING

Having met the education and training requirements of IIW Guideline "International Welding Inspection Personnel" and by examination having satisfied the requirements of the Examination Board of the IIW Authorised National Body

Ryan Kurt Wyngard

Date of birth: 16/08/1978

is hereby awarded the diploma of

INTERNATIONAL WELDING INSPECTOR

STANDARD LEVEL

Date: 18/03/2016

Diploma Nº ZA-IWIP-S00588

Chairman of ANB Examination Board

TZ Joubert

Head of Training

S Blake

IIW Authorised National Body

SAIW CERTIFICATION SOUTH AFRICA

This diploma is subject to the rules concerning its use and misuse
See overleaf

SAIW
CERTIFICATION

Having met the education and training requirements of
SAIW Certification and by examination having
satisfied the requirements of the
Governing Board of SAIW Certification

Ryan Kurt Wyngard

780816 5228 08 0
Identity Number

is hereby awarded the diploma in

Senior Welding Inspector

Level 2

11 December 2015	Pass	6215
Date	Result	Diploma Number

Chairperson
SAIW Certification Governing Board

Manager
Qualification and Certification

TÜV Rheinland Inspection Services (Pty) Ltd

This is to certify that

Whitey van der Merwe
5101025024085

has successfully completed the

INTERNAL AUDITOR WORKSHOP: ISO 9001:2008

held at

TÜV Offices, Centurion

on

05-07 July 2011

IQA 1102 / 02

Facilitator

TÜVRheinland®
Precisely Right.

TÜV Rheinland Inspection Services (Pty) Ltd

This is to certify that

C.A van de Merwe

ID number 510102 5024 08 5

has successfully completed the workshop

IMPLEMENTING ISO 9001:2008 IN A SERVICE INDUSTRY

held at

TÜV Rheinland, Pretoria

on

28-30 June 2011

Certificate Number IMP11/05

Facilitator

TÜVRheinland®
Precisely Right.